TECHNISCHE UNIVERSITÄT MÜNCHEN

Professur für Holztechnologie

Development of a numerical method for the strength prediction of timber

Ani Khaloian-Sarnaghi

Vollständiger Abdruck der von der Ingenieurfakultät Bau Geo Umwelt der Technischen Universität München zur Erlangung des akademischen Grades eines

Doktor-Ingenieurs

genehmigten Dissertation.

Vorsitzender: Prof. Dr. Ernst Rank

Prüfer der Dissertation: 1. Prof. Dr.-Ing. Jan-Willem van de Kuilen

2. Prof. Dr.-Ing. habil. Fabian Duddeck

3. Prof. Dr. Andrea Frangi, ETHZ/Schweiz

Die Dissertation wurde am 29.10.2019 bei der Technischen Universität München eingereicht und durch die Ingenieurfakultät Bau Geo Umwelt am 17.02.2020 angenommen.

Abstract

One of the important steps, before timber boards can be used as lamellas in glued laminated timber and wood composites is strength grading. Grading is generally done visually (based on the visible parameters on the surface of the boards) or by machine (by measurement of the dynamic modulus of elasticity (MoE_{dyn}) and some kind of knot assessment algorithm). Machine grading is the faster and more accurate of the two methods. As access to the actual density for measurement of MoE_{dyn} may be impossible in some conditions, this grading method may face problems in strength prediction. Therefore, the modern tools with more advanced computerized methods may be good replacements for providing better strength predictions. By having access to the database of more than 25,000 different wood samples, including different soft/hardwood species, tested in tension/bending, the step is provided for back engineering of the data and development of a digital grading tool for wood.

The aim of this research is to develop a simple reconstruction process and an advanced numerical method with minimum input parameters, which can output parameters that may increase the prediction accuracy and quality. Therefore, after reconstruction of the geometrical model of the boards solely based on surface information of the knots, the model is used in the finite element analysis to extract the numerical parameters for tensile strength predictions.

Before the boards can be used for the virtual tensile tests, a structural model of wood needs to be created to represent the variation of the fibers around the knots/natural features and to provide information about the global/local fiber pattern in boards. This is an important step to define the variation of the local anisotropic material directions in wood. In this thesis, fluid dynamic methods are used to resemble the fiber pattern in wood and to predict its anisotropy. The modeled boards are then used in the virtual tensile tests to predict the stress developments. Due to the heterogeneous structure of wood, stress distribution is not uniform in this material and higher stresses are developing around the natural features. To overcome the problem of predicting the interacting stress concentration factors in 3D-anisotropic and heterogeneous space, three mathematical equations are provided that consider the geometrical aspects of knots as well as the average and maximum stresses that are developing in timber.

Additionally, the process of stress-wave-propagation and MoE_{dyn} measurement is virtually modeled. This is done by using the average density of each set of species as input parameter, which reduces the dependency of the measurements on the actual density of the samples and can be used in different physical conditions for strength prediction of any wood sample.

In the end, all the numerical parameters are used in a non-linear multiple regression analysis and a model is provided for virtual tensile strength prediction of wood. The quality of the predictions is on the same level or higher than any recently available grading method. Therefore, a digital grading machine is provided in this research based on the surface image of timber.

Zusammenfassung

Die Festigkeitssortierung ist ein wichtiger Schritt, bevor Holzbretter als Lamellen in Brettschichtholz und Holzwerkstoffen verwendet werden können. Gewöhnlich erfolgt die Sortierung visuell (basierend auf den auf der Brettoberfläche sichtbaren Parametern) oder maschinell (durch Messung des dynamischen Elastizitätsmoduls (MoE_{dyn}) und einen Algorithmus zur Bestimmung der Ästigkeit), wobei die maschinelle Sortierung die schnellere und genauere der beiden Methoden ist. Allerdings erweist sich diese Methode der Festigkeitsbestimmung oftmals als problematisch, da auf die zur Messung des E-Moduls benötigte Dichte unter bestimmten Bedingungen nicht immer zugegriffen werden kann. Eine gute Alternative für bessere Festigkeitsvorhersagen könnten deshalb moderne Tools mit fortschrittlicheren computergestützten Methoden bieten. Durch Zugriff auf eine Datenbank mit über 25000 verschiedenen Holzproben, einschließlich zug-/biegegeprüften Nadel- und Laubholzarten, ist eine Nachkonstruktion (Reverse-Engineering) der Daten sowie die Entwicklung eines digitalen Holzsortierungstools möglich.

Ziel dieser Studie ist die Entwicklung eines einfachen Rekonstruktionsverfahrens sowie einer fortschrittlichen Berechnungsmethode, die mit wenigen Inputparametern Outputparameter mit besserer Vorhersagegenauigkeit und Qualität liefert. Nach Rekonstruktion eines geometrischen Modells lediglich basierend auf den Oberflächeninformationen der Äste wird dieses Modell in der Finite-Elemente-Analyse zur Ermittlung der numerischen Parameter für die Bestimmung der Zugfestigkeit eingesetzt.

Vor der virtuellen Zugprüfung der Bretter muss zunächst ein Strukturmodell des Holzes entworfen werden, um die Faservariation im Bereich der Äste / natürliche Merkmale darzustellen und um Informationen zum globalen/lokalen Faserverlauf in den Brettern zu erhalten. Dies ist ein wichtiger Schritt um die Schwankung der lokalen anisotropen Materialrichtungen im Holz zu bestimmen. In der vorliegenden Arbeit werden fluiddynamische Methoden verwendet, um den Faserverlauf im Holz nachzubilden und dessen Anisotropie vorherzusagen. Die modellierten Bretter werden dann in virtuellen Zugprüfversuchen zur Bestimmung des Spannungsverlaufs verwendet. Aufgrund der heterogenen Holzstruktur ist die Spannungsverteilung in diesem Material nicht gleichmäßig und es entwickeln sich höhere Spannungen im Bereich der Äste. Anhand von drei mathematischen Gleichungen, die die geometrischen Astaspekte sowie die im Holz entstehenden mittleren und maximalen Spannungen berücksichtigen, soll das Problem der Vorhersage interagierender Spannungskonzentrationsfaktoren im dreidimensionalen anisotropen und heterogenen Raum gelöst werden.

Des Weiteren wird ein Verfahren zur Messung der Spannungswellenausbreitung und des E-Moduls virtuell modelliert. Dabei dient die mittlere Dichte einer jeden Holzartengruppe als Inputparameter, wodurch die Abhängigkeit der Messungen von der tatsächlichen Dichte der Proben reduziert wird; dieses Verfahren kann dann unter unterschiedlichen physikalischen Bedingungen für die Festigkeitsbestimmung jeglicher Holzproben verwendet werden.

Schließlich werden alle numerischen Parameter in einer nichtlinearen multiplen Regressionsanalyse verwendet und ein Modell für die virtuelle Zugfestigkeitsvorhersage von Holz erstellt. Die Vorhersagequalität ist auf demselben Niveau oder höher wie das jeglicher aktuell verwendeter Sortierverfahren. In dieser Studie wird somit eine digitale Sortiermaschine basierend auf dem Holzoberflächenbild vorgestellt.

Acknowledgements

In particular, I would like to thank my doctoral supervisor, Prof. Jan-Willem van de Kuilen for his constant support and for giving me the opportunity to participate on diverse and very interesting tasks within the scope of my doctoral research at his chair. The numerous opportunities he offered helped me to develop my scientific, as well as my personal skills. The trust he put on me as well as the freedom he created to work with different groups and students made a fruitful working atmosphere. His words in the beginning of my PhD "A COMPUTER CAN NOT MAKE YOU CRAZY" made it easier to handle problems and difficult situations. Thanks for all your time you invested for the discussions and thanks for providing the opportunities to present my research in different international conferences.

Furthermore, I thank my colleagues, Andriy Kovryga and Andreas Rais, for their scientific and mental supports and for their help regarding the database.

Especial thanks to Wolfgang Gard from TU Delft and Jan Kirschke from the Department of Diagnostic and Interventional Neuroradiology for helping me with the CT-scans and evaluation of the images.

Thanks to my colleagues Zhouyan Xia, Petra Jakobsen and Andrea Berger-James for their encouragements during my thesis and being the supports with language editing.

Thanks to my colleagues in the Mechanics Group for always being there and supporting me in this way.

My gratitude to Carmen Sandhaas for all her scientific, technical and mental supports and to Philipp Dietsch for being my mentor.

I further thank Prof. Duddeck for giving me the possibility to create the Material Group and discuss the recent material developments with researchers of diverse fields. Thanks to my colleagues from the Chair of Metal Structures for providing me with the software and my colleagues from the chairs of Computational Mechanics, Computation in Engineering, Structural Analysis, Physics and the Department of Diagnostic and Interventional Neuroradiology for all their help and support.

I also thank my running and archery trainers for being this positive. Thanks for teaching me to be tough and to start a positive competition and go for my goal beside helping the others. Thanks for showing me that the word "can't" does not exist in this world and that success needs effort.

Thanks to all my friends for their encouragements.

Last but not least, I would like to especially thank my family, Evelyne, Hamlet, Sevana and Aren for giving me the opportunity to go for higher education this far away, for always being beside me, supporting me, and encouraging me. Thanks for your open ears to listen, to laugh and to cry with me, for your all positive energies to make me goal oriented and to show me to be, to think and to act positively. Your continuous support strengthened me in different steps of my life. I am not used to marathons, but with all your help and support, this marathon got much simpler for me.

Nomenclature

$f_{t,\alpha}$	Strength under an angle α
$f_{t,o}$	Strength under an angle 0
$f_{t,90}$	Strength under an angle 90
σ_{ij}	Stresses in different orthotropic directions
ε_{ij}	Strains in different orthotropic directions
C_{ijkl}	Compliance matrix
D_{ijkl}	Stiffness matrix
E_i	Modulus of elasticity
G_i	Shear modulus
v_{ij}	Poisson ratios
P	Density
$\vec{v}$	Velocity vector in three spatial directions
u, v, w	The velocities in three spatial directions
$\tilde{v}$	Viscosity like variable (Sparlat Allmaras variable
$\hat{v}$	Kinematic viscosity
μ	Constant Newtonian viscosity
u^*	Friction velocity
p	Pressure
d_i	Damage parameter
$F_{t/c,0/90}$	Failure criteria
K	Stress concentration factors
c	Distance from the center of the hole to the nearest edge of the panel
a	Radius of hole
h	Thickness of plate
ψ	Semi-stream function
A_{knot}	Knot area
A_{total}	Cross sectional area of the board
$A_{projected}$	Projected knot area
ω_0	Natural frequency
λ	Wave length
l	length of the specimen
M	Mass matrix
F	Force
t	Time
$\ddot{u}$	Acceleration
$I^{(i)}$	Internal force vector

L	Longitudinal material direction of wood fibers
R	Radial material direction of wood fibers
T	Tangential material direction of wood fibers
α, β, γ	Rotational angle of the fibers in three coordinate directions
θ	Fiber angle
φ	Angle of the annual rings
∇	Divergence operator
Δ	Laplacian operator

Abbreviations

CT	Computed Tomography
UMAT	User defined material model
SCF_i	Stress Concentration Factors
MoE	Modulus of Elasticity
MoE_{dyn}	Dynamic modulus of elasticity
TKAR	Total Knot Area Ratio
DEB	Single knot or DIN Einzellast Brett (DIN 4074. (2012))
DAB	Knot cluster or DIN Astansammlung Brett (DIN 4074. (2012))
IP	Indicating parameter
CC_i	Center to center distance
Freq.	Frequency
FEM	Finite element method
CoV	Coefficient of variation
R^2	Coefficient of determination

List of Figures

List of Tables

Table of Content

Chapter 1 Introduction

1.1 Background and motivation

Safety of timber structures depends on many factors from which one of the initial and most important steps is the assignment of correct strength grade. The quality of timber can be assessed for structural and/or appearance purposes. Strength grading of timber is generally performed based on visual or machine grading methods (EN 14081-1), based on which timber is allocated to different strength classes to which the mean and characteristic values of the mechanical and material properties are assigned (EN 338). In contrast to the visual grading method, which is based on the visual inspections, machine strength grading is based on using large variation of non-destructive technologies, allowing the measurement of knottiness parameters, density and eigenfrequency. For this kind of grading, statistical relationships are used between the parameters of non-destructive measurements and the mechanical properties. Prediction parameters, used in a regression analysis are named as indicating parameters (IPs). Utilized statistical methods are based on single or multiple regression analysis (especially in a linear form), which analyze the relation of prediction parameters (the variables or outputs of different measurement methods) to the strength.

As knots are the main strength governing parameters, there have been increasing interests in modeling wood with its imperfections during the last decades in order to predict the strength and failure of the material numerically, using higher and more advanced technologies. First tries for modeling of these characteristics and the resulted local fiber deviation in wood are going back to several decades, starting with the researches of Bodig and Goodman over the years 1969 to 1980s (Goodman and Bodig 1980). By developing the flow-grain analogy, a two-dimensional finite element model of the grain dislocations and flow around knots have been generated. By application of this analogy, and by usage of finite element method, mathematical models have been developed for prediction of the macrostructural, tensile and fracture behavior of the material (Cramer and Goodman 1986, Goodman and Bodig 1978, 1980, Phillips et al. 1981). In 1982, 2D models have been developed and they have been used to predict stress distributions around knots in the LT-plane (Cramer and Goodman 1982). In 1987, by a detailed look on the post-yielding behavior of the wooden material, its failure has been modeled using the maximum stress theory and Tsai-Wu's yielding criterion (Zandbergs and Smith 1987). In 1997, a new model of wood has been created by assuming fibers to be oriented such that the principal stresses during growth of the tree coincide with the fiber orientation (Mattheck 1997). In his model, Von-Mises criterion was considered as a yielding criterion for wood. In 2001, the 2D flow-grain analogy was extended to a 3D model, which enabled to describe the knot's geometries in a more accurate way (Foley 2001). A mathematical expression has been provided in this paradigm to predict geometry of the growth layers in the vicinity of knots in RL-plane. This model has been used later by several researchers for more detailed structural analysis (Hackspiel 2010, Lukacevic and Füssl 2014, Lukacevic et al. 2015). In 2012, wood material model was extended by consideration of more accurate rotations for fibers in the vicinity of knots (Guindos and Guaita 2013). In 2013, a study has been performed; comparing the models, based on flow-grain analogy, and principal stresses (Lang and Kaliske 2013). Results of this study have shown that fiber orientation around a round knot is similar for both models. Another model has been created in 2013, which predicted fiber orientation based on streamlines and equipotential lines. A 2D layer-wise meshing procedure has been applied in this model, which has shown the fiber deviation around knots (Jenkel and Kaliske 2013, Jenkel 2016). Although different studies have been performed for improving the prediction quality of fiber deviation around knots, but the geometry of wood is more complicated in

reality, when considering complete non-uniform shapes of the knots. Focus of this thesis is on the main species that are used for engineered wood products, such as spruce or Douglas fir (Rais et al. 2014a,b). These species contain many non-uniform knots and imperfections, which can not be neglected for structural applications. Such defects are the main strength governing parameters under tension and may influence the mechanical behavior of the engineered wood products. Detailed investigation of the developed models for wood showed that less attention is paid on effects of knot amounts and their clusters in boards and in engineered wood products. These features are believed to highly influence the uniformity of the fiber pattern in wood. For using wood as an engineered product, its mechanical properties should satisfy the requirements. Extreme grain deviation can be a severe strength-reducing characteristic of timber (Kuisch et al. 2012). Up to now, machine or visual grading are being used for the grading of wood, which may lead to some measurement errors (such as measurement errors after frequent measurements during visual grading or inaccurate usage of density in machine grading). In this study, a new method is provided for strength prediction of boards using more advanced computational approaches. The database in the Department of Wood Technology of Technical University of Munich contains enormous information about knots and their geometrical configurations beside the material and mechanical properties of different wood samples and species. These data provide the basis for this thesis. The recent method suggests an approach for geometrical reconstruction of timber boards based on surface information of knots (Khaloian Sarnaghi and Van de Kuilen 2019a) that are obtained from visual grading (Stapel and Van de Kuilen 2013, 2014a, 2014b). Based on different stress analyses on the reconstructed models (Khaloian Sarnaghi and Van de Kuilen 2019a,b) mathematical approaches are provided for tensile strength prediction of timber boards.

1.2 Objective of this thesis

By describing the problems in the previous sub-chapter, the objective of this thesis is to provide a method to be able to automatize the strength grading process of timber and to predict the tensile strength virtually, using a computer-based approach. For this reason, the model needs to be formulated in a way to cover the natural scatter of timber by considering variations in amount of imperfections in boards and their geometrical configurations. Therefore, knots with sharp angles, edge knots, combination of different knot shapes (conical/cylindrical) in a board, and knots that are appearing on multiple surfaces need to be considered as possible geometrical configurations for knots. Moreover, existence of both dead and live knots in a same board is a possibility to be analyzed in the developed model. As dead/live knots are characterized by the kind of connections to their bulk material, separate options need to be provided in the developed method to distinguish between these cases and to overcome the problems that may occur during prediction of the local fiber deviation and correspondingly the stress distribution pattern. This is especially important in cases of complex geometrical knot configurations and knot clusters. Therefore, information about this connection behavior, beside the geometrical configuration of knots, may help for better predictions. In addition, the critical locations that may cause crack initiation and failure of the material need to be predicted.

To reduce human measurement errors that are arising from the visual grading procedure, an automatized computer method needs to be developed to reconstruct the boards with the minimum cost and based on the surface information of knots. The method needs to cover the recognition of knots, as the main strength governing parameters. Due to anisotropic nature of wood, the method needs to cover possible rotation of the coordinate directions for prediction of the deviation of the material properties from the global coordinate direction, which could represent the natural flow of fibers in timber. Additionally, the developed method needs to be sensitive enough to cover the natural scatter of timber, and to be applicable to different wood species. Similar to the parameters that are obtained from visual- and machine-based approaches for strength grading of timber, focus of this thesis is on extraction of parameters that are obtained by implementing numerical approaches that may improve the quality of

predictions compared to the currently available methods. To investigate capabilities of the developed virtual approach for strength predictions, the method is going to be used for a scatter of softwood and hardwood timber boards, and is going to be generalized to a species independent model.

1.3 Scope of the thesis

This thesis covers a range of numerical analyses for mechanical representation of wood, its grading and strength prediction process. Therefore, discussions about five different topics are categorized in five chapters, where each process is defined and explained separately as follows:

- Board reconstruction and the linkage to the database (Chapter 2)

In this part of the thesis, a complete reconstruction method is presented. Reconstruction is done based on the measured knot data over the surfaces of the boards, which is stored in a database in the Department of Wood Technology of Technical University of Munich. In this chapter, a short introduction about the database and the knot registration method is available as well. By programming an automatic link to the database and by analyzing the data, the required board can be geometrically reconstructed with the 3D full representation of defects and imperfections.

- Development of a method for fiber prediction (Chapter 3)

In this chapter, a method is developed to predict fiber pattern around natural defects of wood, such as knots and knot clusters. As wood is an anisotropic material (with L-R-T planes), its material properties are not homogeneous along the board. These properties are varying based on the deviation of fibers, which are influencing the mechanical properties correspondingly. Due to strong variation of the structure of different wooden species, especially when comparing softwoods to hardwoods, focus of this part of the thesis is to develop a method to generalize the prediction of fiber pattern for different wood species in order to cover these variations.

- Stress Concentration factors (SCFs) (Chapter 4: summary of the paper "**Strength prediction of timber boards using 3D FE-Analysis**")

Focus of this chapter is to develop numerical parameters that can correlate to the strength properties and can represent the mechanical behavior of timber. Due to heterogeneous nature of wood, defects and imperfections are not uniformly shaped and spaced in this material. Shapes of these features, their orientations and their rotations are relatively random, when generalizing the model to a species-independent one. For this reason, the stress distribution in wooden boards is not uniform, and peak stresses are developing around these natural features. In this chapter a mathematical method is developed for prediction of the stress concentration factors in a 3D anisotropic and heterogeneous space. For this reason, three mathematical equations are provided for calculation of the SCFs by considering the actual and the projected knot areas as well as the stresses that are developing around knots and in knot-free board regions, which are discussed and explained separately.

- Virtual Dynamic Modulus of Elasticity (MoE_{dyn}) (Chapter 4: summary of the paper "**Tensile strength prediction of softwood glulam lamellas using virtual vibration technique**")

Similar to the approach for calculation of the dynamic modulus of elasticity in laboratory as well as in daily practice in sawmills, a virtual method is developed in this part of the thesis to predict the velocity of a stress wave after its complete round of traveling forth and back through board. By predicting velocity of the stress wave after passing through the heterogeneities in a board, the frequency and finally the dynamic modulus of elasticity are being estimated numerically. To keep simulations independent of

the density variation among boards (as measurement of density may not be accurate, especially in wet conditions), the average density of each wood species is used as input data for numerical analysis. Therefore, the velocity, and correspondingly the frequency, are calculated solely based on the average density of each species. The MoE_{dyn} can be updated later by the actual density values, if this parameter is available. This process is explained in details in this chapter.

- Strength prediction, scatter analysis and validation of the model) (Chapter 4: summary of the paper "**An advanced virtual grading method for wood based on surface information of knots**")

In this part of the thesis, numerical parameters that have been obtained from previously defined steps are used in statistical regression analyses for prediction of tensile strength. Results of the single and multiple linear and nonlinear regression analysis are presented here.

Similar analyses are performed during this step for parameters that are obtained from experimental measurements. Both sets of results are compared and the numerical method is validated. A mathematical equation is provided in the end to represent the non-linear relation of the parameters and to predict tensile strength.

Finally, after validating the model, the model is used to predict the tensile strength of two small groups of medium dense European hardwoods. Prediction results are compared to the actual strength values from tensile tests.

- Chapter 5 includes the summary and concluding remarks of the thesis.

Following flow chart describes the structure of the thesis with its individual steps. Appendix 3 contains all papers that are published for this thesis.

Figure 1-1: Flow-chart of the thesis.

Chapter 2 General information about mechanics of wood, database and virtual board reconstruction

2.1 Anatomical structure of wood

Wood is a natural material with complex structure. The structure of wood is affecting its mechanical behavior and is determining its material properties in a 3D space. These variations are not only found in between species, but also among different samples of one specimen. Variations are increasing, when comparing softwoods to hardwoods.

Different softwood and hardwood species are studied in this thesis to be able to develop a numerical model for strength prediction of wood by considering its natural scatter. Species that are analyzed here are softwood species, spruce and Douglas fir, and hardwood species, beech, ash and maple. Introduction about the anatomic view of different wood species is kept short in this chapter to cover only the aspects, relevant for the understanding of this thesis. An accurate description can be found in (Kollmann and Cote 1984, Dinwoodie 1981).

Growth rings in wood have two different zones. A zone, which is created in the early season, includes cells with larger diameters and thinner cell walls that allow transportation of the nutrients. This part is lighter in color and is called the earlywood. In the second part that develops in the later seasons of the year, the growing of cells slows down, which results in development of cells that are smaller in diameter. Therefore, density of these main zones strongly vary from each other, which also affects the mechanical behavior of wood in total. The majority of softwood volume is made of longitudinal tracheid cells, which provide the mechanical support and enable fluid transport. In the radial direction, from the pith (center of the stem) to the bark, another type of cells are growing, which are called Parenchyma rays. These cells are the nutrient storages and they reinforce wood in radial direction. (Burgert and Eckstein 2001, Burgert et al. 2002).

Depending on the research question and the required level of calculation, different scales need to be considered for analysis. These scales vary by considering the level of analysis from stem to the annual ring effects, cell wall consideration, or consideration of cell wall constituents (cellulose, hemi-cellulose and lignin). In this thesis, analyses are performed from micro- to macro-level by considering the fiber pattern and its deviation in a micro-structural level, to the effects of knots, testing of boards and prediction of failure in macro-level.

2.2 Knots and imperfections in the material

2.2.1 General information about knots

A knot is defined as part of the branch that is enclosed by the natural growth of the tree (Staab 1999). Depending on the configuration of knots inside wood, knots can be categorized into two groups: live knots or dead knots (Figure 2-1). A live knot is referred to a knot, where the cambium of the branch is mixed with the cambium of the trunk. Therefore, fibers of the trunk expand in the branch by growing of the tree (Fink et al. 2012, Kretschmann 2010). In contrast to this group, a dead knot refers to a dead branch in the trunk, where the trunk continues to grow and to cover the branch. Therefore, the structure seems to be more non-uniform in this case (as the fibers do not expand into the knot) and the connection to the bulk material may get lost. As live knots are integrated in their bulk material, the growth rings tend to turn toward the main axis of the knot. This situation affects the strength of this material strongly,

as wood is strongest in the longitudinal fiber direction. Conditions are slightly different in case of dead knots. In such cases, fibers continue to go around knots without being connected to the knot.
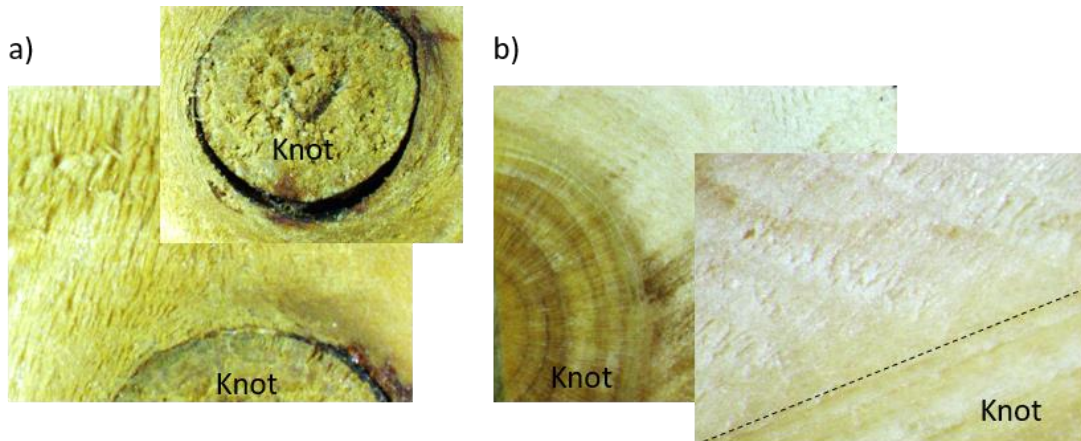
Figure 2-1: Representation of the dead knot (a) and live knot (b) and the integration of the fibers around them.

2.2.1.1 Knottiness

Knottiness is defined by measuring visible growth characteristics, such as knots, on the surfaces of wood. This parameter is used in European standards for strength grading of timber. Based on the strength class of timber, material parameters are being assigned to the structural timber element (EN 338 (2016)). Knottiness can be determined visually or by machine (EN 14081-1 (2016)). In a timber board, knottiness can be defined by considering the total knot area ratio (TKAR) or a single knot area ratio (DEB and DAB) (DIN 4074 (2012)), as presented in next chapters of this thesis. Machine grading can be performed based on a surface scanning system such as WoodEye or an X-Ray system (Microtec, LuxScan). Non-destructive measurements are being used in this grading method to predict the mechanical properties. This is done generally by measurement of eigenfrequency and density to predict dynamic modulus of elasticity in combination with knot parameters (Stapel and Van de Kuilen 2013).

2.2.1.2 Density

Density is another grade determining parameter for timber. Although the correlation between the clear wood density and the strength and stiffness parameters is relatively strong, providing a good parameter for predictions (Fosile 1971), but the correlation between this parameter and the strength reduces for case of timber with multiple natural features (Oscarsson 2014).

2.2.2 Natural fiber pattern in wood

Natural fiber orientation is an important parameter, affecting the mechanical properties of wood by causing deviations in orthotropic directions. Spiral grain orientation in logs is getting more significant if timber is sawn from these logs. The rotation of fibers or their natural deviations around natural imperfections are causing significant reductions in strength, which needs to be considered accurately for structural applications. Therefore, transformation of the local fiber deviation to the global direction and consideration of the orthotropic fiber rotation may help to get a more accurate estimation about the strength of this material.

An empirical equation for the prediction of timber strength under uniformly deviating fiber angle was provided by Hankinson (Equation (2-1)) (Hankinson 1921).

$$f_{t,\alpha} = \frac{f_{t,0} \cdot f_{t,90}}{f_{t,0}\sin^2\alpha + f_{t,90}\cos^2\alpha} \tag{2-1}$$

where $f_{t,\alpha}$ is the strength under an angle α. $f_{t,0}$ is the strength parallel to the fiber direction, and $f_{t,90}$ is the strength in perpendicular to the fiber direction.

This equation helps to estimate the global strength reduction due to the deviation of fibers. However, for more complex cases, such as a timber with multiple knots and strong local fiber deviations (without exact information about the local fiber angle), this equation may underestimate the material strength. More advanced computer-based simulation approaches are replacing the analytical solutions in such conditions.

Several studies experimentally considered the effects of knots on the structural and mechanical behavior of timber (Eberhardsteiner 2002, Fink and Köhler 2012, Stübi 2001 (the more recent ones)). Some studies also considered the failure mechanisms and local failure development in the location of knots (Buksnowitz 2010, Fink et al. 2012). Few studies (Frese 2016) consider the knot effects by applying local reduction in the stiffness properties of the material. Different studies (Foley 2001, Hofstetter et al. 2009, Guindos and Guaita 2013, Lukacevic and Füssl 2014) numerically considered fiber deviations around these natural features as well.

As failure in softwood is generally initiating in the vicinity of knots, especially under tensile loading conditions, a more accurate consideration of these features may lead to better approximations regarding the prediction of strength and stiffness of timber.

2.3 Anisotropic structure of wood

Anisotropy means that the properties of wood are varying in different material directions. However, the structure of wood is such, that its material properties can be assumed to follow three main orthotropic directions. These directions are defined as the longitudinal direction (L) which is aligned along the fiber direction, radial (R) and tangential (T) directions in the transverse direction of the fibers, aligned normal and tangential to the growth rings, respectively.

Stiffness and strength properties of wood are strongly dependent upon the geometrical direction that they are obtained from. Therefore, for representation of the elastic behavior of wood, nine different material parameters are required (explained below). Additionally, strength properties in each coordinate direction, under different loading conditions, are required to approximate the mechanical behavior of wood in numerical analysis.

Under short loading times and moderate stress conditions, wood can be relatively well treated by applying a linear elastic constitutive law, explained in the following equation:

$$\sigma_{ij} = C_{ijkl} . \varepsilon_{kl} \tag{2-2}$$

Equation (2-2) links the stresses to the strains. The linear elastic behavior of wood can be described by considering three moduli of elasticity (E_L, E_R, E_T), three shear moduli (G_{LR}, G_{LT}, G_{RT}), and three Poisson's ratios (v_{LR}, v_{LT}, v_{RT}). As the fibers are mainly oriented in the longitudinal direction, a relatively high degree of anisotropy exists between the properties of *L* and *R, T* directions. This high anisotropy level can be observed, if comparing the moduli of elasticity and the shear moduli in the three main material coordinate directions (EN 338 2016, Kretschmann 2010, Bodig and Jayne 1993).

Further than the elastic properties, directional dependency can be represented by the strength anisotropy as well. Wood has the highest strength in its longitudinal direction (EN 338 2016, Bodig and Jayne 1993).

$$E_L : E_R : E_T \approx 20 : 1.6 : 1$$

$$G_{LR} : G_{LT} : G_{RT} \approx 10 : 9.4 : 1$$

Compliance matrix for an orthotropic material can be presented as follows:

$$
\begin{bmatrix}
\varepsilon_{LL} \\
\varepsilon_{RR} \\
\varepsilon_{TT} \\
\gamma_{LR} \\
\gamma_{LT} \\
\gamma_{RT}
\end{bmatrix}
=
\begin{bmatrix}
\dfrac{1}{E_L} & \dfrac{-v_{RL}}{E_R} & \dfrac{-v_{TL}}{E_T} & 0 & 0 & 0 \\[2ex]
\dfrac{-v_{LR}}{E_L} & \dfrac{1}{E_R} & \dfrac{-v_{TR}}{E_T} & 0 & 0 & 0 \\[2ex]
\dfrac{-v_{LT}}{E_L} & \dfrac{-v_{RT}}{E_R} & \dfrac{1}{E_T} & 0 & 0 & 0 \\[2ex]
0 & 0 & 0 & \dfrac{1}{G_{LR}} & 0 & 0 \\[2ex]
0 & 0 & 0 & 0 & \dfrac{1}{G_{LT}} & 0 \\[2ex]
0 & 0 & 0 & 0 & 0 & \dfrac{1}{G_{RT}}
\end{bmatrix}
\cdot
\begin{bmatrix}
\sigma_{LL} \\
\sigma_{RR} \\
\sigma_{TT} \\
\sigma_{LR} \\
\sigma_{LT} \\
\sigma_{RT}
\end{bmatrix}
\qquad (2\text{-}3)
$$

where *R, T*, and *L* represent the radial, tangential, and longitudinal directions of wood respectively. E_i is the modulus of elasticity, G_{ij} is the shear modulus, and v_{ij} is the Poisson's ratio.

The compliance matrix should be symmetric. This results in:

$$
v_{RL} = v_{LR}\frac{E_R}{E_L} \qquad\qquad v_{TL} = v_{LT}\frac{E_T}{E_L} \qquad\qquad v_{TR} = v_{RT}\frac{E_T}{E_R} \qquad\qquad (2\text{-}4)
$$

The material matrix (inverse of the compliance matrix) for an orthotropic material can be represented as:

$$
\begin{bmatrix}
\sigma_{LL} \\
\sigma_{RR} \\
\sigma_{TT} \\
\sigma_{LR} \\
\sigma_{LT} \\
\sigma_{RT}
\end{bmatrix}
=
\begin{bmatrix}
\dfrac{E_L(1-v_{RT}v_{TR})}{k} & \dfrac{E_L(v_{RT}v_{TL}+v_{LR})}{k} & \dfrac{E_L(v_{RL}v_{TR}+v_{TL})}{k} & 0 & 0 & 0 \\[2ex]
\dfrac{E_R(v_{LT}v_{TR}+v_{LR})}{k} & \dfrac{E_R(1-v_{LT}v_{TL})}{k} & \dfrac{E_R(v_{LR}v_{TL}+v_{TR})}{k} & 0 & 0 & 0 \\[2ex]
\dfrac{E_T(v_{LR}v_{RT}+v_{LT})}{k} & \dfrac{E_T(v_{LT}v_{RL}+v_{RT})}{k} & \dfrac{E_T(1-v_{LR}v_{RL})}{k} & 0 & 0 & 0 \\[2ex]
0 & 0 & 0 & G_{LR} & 0 & 0 \\[2ex]
0 & 0 & 0 & 0 & G_{LT} & 0 \\[2ex]
0 & 0 & 0 & 0 & 0 & G_{RT}
\end{bmatrix}
\cdot
\begin{bmatrix}
\varepsilon_{LL} \\
\varepsilon_{RR} \\
\varepsilon_{TT} \\
\gamma_{LR} \\
\gamma_{LT} \\
\gamma_{RT}
\end{bmatrix}
$$

and

$$
k = 1 - v_{RT}v_{TR} - v_{LR}v_{RL} - v_{LT}v_{TL} - v_{LR}v_{RT}v_{TL} - v_{RL}v_{TR}v_{LT}
$$

The material matrix should be positive definite i.e. $\varepsilon^T.D.\varepsilon > 0$ (the material resists deformations). This leads to the following restrictions:

$$
1 - v_{RT}v_{TR} - v_{RL}v_{LR} - v_{LT}v_{TL} - v_{LR}v_{RT}v_{TL} - v_{RL}v_{TR}v_{LT} > 0
$$

$$
1 - v_{RT}v_{TR} > 0
$$

$$
1 - v_{RL}v_{LR} > 0
$$

$$
1 - v_{LT}v_{TL} > 0
$$

Mostly, the global coordinate directions and the orthotropic directions of wood are not completely aligned to each other. Therefore, the global coordinate directions need to be rotated and be transformed to the orthotropic direction of wood. This is an important transformation that needs to be considered for wood, as small deviation of fibers may result in a considerable stiffness reduction under different conditions.

As both systems are orthogonal, two angles that are representing the angle of fibers and the angle of annual rings are in general enough for connecting both coordinate directions. However, as three angles are linked together based on the following equation, third angle needs to be defined as well for the second transverse direction to represent the global transformation.

$$\cos^2 \theta + \cos^2 \phi + \cos^2 \varphi = 1 \tag{2-5}$$

In Equation (2-5), θ represents the fiber angle and φ represents the angle of annual rings. Therefore, a three-dimensional rotation of the coordinate system is possible through Figure 2-2 (Bodig and Jayne 1993):

	L	R	T
X₁	cosθ	-sinθsinφ	sinθcosφ
X₂	0	cosφ	sinφ
X₃	-sinθ	-sinφcosθ	cosθcosφ
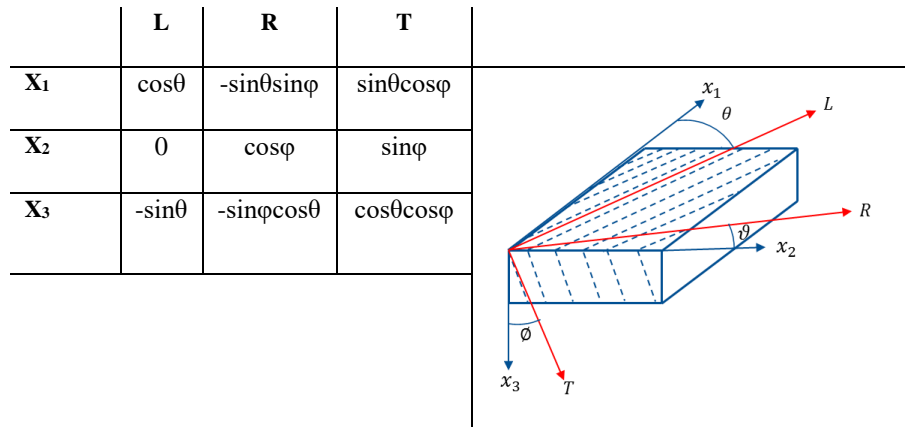
Figure 2-2: Geometrical and material coordinate directions in wood (Bodig and Jayne 1993).

2.4 Finite element modeling and failure analysis

Finite element analysis has been widely used in different engineering applications, to describe wood from micro-level to macro-level. Wood is a material with anisotropic failure and combined ductile and brittle failure behavior under different loading configurations. Different pre-defined models exist in commercial software for describing the failure of composite materials. Hill criterion (Dias et al. 2010), Hoffman criterion (Van der Linden et al. 1994, Xu et al. 2009), Tsai-Wu criterion (Li et al. 2018) with single-surface isotropic failure criteria are generally used for describing the failure behavior, which cannot capture the single failure modes. Hashin criteria (Hashin 1980, Maimí 2006) is another possibility for fiber composites, which gives the opportunity for defining separate failure modes for defining the failure in fiber or matrix directions under tension or compression.

In this thesis, continuum damage mechanics (CDM) is used to describe the anisotropic damage behavior of wood (Sandhaas 2011). The introduction is kept relatively simple in this part, to only give an overview about this method. A full description about this method can be found in (Sandhaas 2011). CDM approach has been widely used in the previous studies (Cofer et al. 1999) for modeling of the impact loads, bending in timber (Khennane et al. 2014), dowel joints (Sandhaas 2011, Khelifa et al. 2016) and aerospace applications (Lee 2015, Lopes 2009, Maimí et al. 2008, Matzenmiller et al. 1995, Valipour et al. 2014). This method is able to describe and identify brittle failure modes in tension and shear as well as nonlinear elastic failure modes in compression, combined in one 3D constitutive model for wood (Sandhaas 2011). The constitutive model was developed as a user material (UMAT) and implemented in ABAQUS/Standard in Sandhaas (2011). The model has been slightly further developed in this thesis to cover its applicability for different numerical applications and to reduce the numerical errors.

Eight different failure criteria have been defined that calculate the linear and nonlinear relativity of maximum stresses to the strength of the material for initiation of the brittle and ductile failure behavior under tension and compression (Sandhaas 2012).

Criterion I:

$$F_{t,0}(\sigma) = \frac{\sigma_L}{f_{t,0}} \le 1 \quad \text{if } \sigma_L \ge 0 \tag{2-6}$$

Criterion II:

$$F_{c,0}(\sigma) = \left| \frac{-\sigma_L}{f_{c,0}} \right| \le 1 \quad \text{if } \sigma_L < 0 \tag{2-7}$$

Criteria III / IV:

$$F_{t,90R/T}(\sigma) = \frac{\sigma_{R/T}^2}{f_{t,90}^2} + \frac{\sigma_{LT/LR}^2}{f_v^2} + \frac{\sigma_{RT}^2}{f_{roll}^2} \le 1 \quad \text{if } \sigma_{R/T} \ge 0 \tag{2-8}$$

Criteria V-VIII:

$$F_{c,90R/T}(\sigma) = \left| \frac{-\sigma_{R/T}}{f_{c,90}} \right| \le 1 \quad \text{if } \sigma_{R/T} < 0 \tag{2-9}$$

$$F_{vR/T}(\sigma) = \frac{\sigma_{LT/LR}^2}{f_v^2} + \frac{\sigma_{RT}^2}{f_{roll}^2} \le 1 \tag{2-10}$$

By reaching one of the failure criteria, damage starts to evaluate and the stiffness of elements is being reduced until a complete material failure is reached. Definition of state variables gives the opportunity to keep track of the loading history during the analysis. The basic constitutive equation for damage model is presented in Equation (2-11). This model represents the reduction of element stiffness by implementation of the failure mechanism during the numerical procedure.

$$\sigma_{ij} = (1-d)D_{ijkl}\varepsilon_{kl} \tag{2-11}$$

Parameter "d" in Equation (2-11) equation shows the isotropic damage of the material. This procedure is slightly more complex for wood, as nine different damage parameters need to be considered to represent anisotropic failure of wood. Damage parameters are presented as follow:

- $d_{t,0}$ = damage in tension parallel to the fiber direction
- $d_{c,0}$ = damage in compression parallel to the fiber direction
- $d_{t,90R}$ = damage in tension perpendicular to the fiber direction, radial direction (LT-plane)
- $d_{c,90R}$ = damage in compression perpendicular to the fiber direction, radial direction
- $d_{t,90T}$ = damage in tension perpendicular to the fiber direction, tangential direction (LR-plane)
- $d_{c,90T}$ = damage in compression perpendicular to the fiber direction, tangential direction
- d_{vR} = damage in longitudinal shear, LT-plane
- d_{vT} = damage in longitudinal shear, LR-plane
- d_{roll} = damage in rolling shear, RT-plane

The material matrix for wood, by considering damage parameters is presented in Equation (2-12) (Sandhaas 2012).

$$
\begin{bmatrix} \varepsilon_{LL} \\ \varepsilon_{RR} \\ \varepsilon_{TT} \\ \gamma_{LR} \\ \gamma_{LT} \\ \gamma_{RT} \end{bmatrix} =
\begin{bmatrix}
\dfrac{1}{(1-d_0)E_{LL}} & \dfrac{-v_{RL}}{E_{RR}} & \dfrac{-v_{TL}}{E_{TT}} & 0 & 0 & 0 \\[2mm]
\dfrac{-v_{LR}}{E_{LL}} & \dfrac{1}{(1-d_{90R})E_{RR}} & \dfrac{-v_{TR}}{E_{TT}} & 0 & 0 & 0 \\[2mm]
\dfrac{-v_{LT}}{E_L} & \dfrac{-v_{RT}}{E_R} & \dfrac{1}{(1-d_{90T})E_{TT}} & 0 & 0 & 0 \\[2mm]
0 & 0 & 0 & \dfrac{1}{(1-d_{vR})G_{LR}} & 0 & 0 \\[2mm]
0 & 0 & 0 & 0 & \dfrac{1}{(1-d_{vT})G_{LT}} & 0 \\[2mm]
0 & 0 & 0 & 0 & 0 & \dfrac{1}{(1-d_{roll})G_{RT}}
\end{bmatrix}
\cdot
\begin{bmatrix} \sigma_{LL} \\ \sigma_{RR} \\ \sigma_{TT} \\ \sigma_{LR} \\ \sigma_{LT} \\ \sigma_{RT} \end{bmatrix}
\qquad (2\text{-}12)
$$

In this thesis, in addition to the state variables, a separate parameter is defined that follows status of the elements (presented by a value between one and zero; zero meaning inactive element in the calculation). As damage is a parameter between zero and one (one representing full failure), the status parameter is analyzing possible failure modes in each time increment. As soon as the damage parameter in any of the elements is reaching its limit, the status of this parameter is being changed by flagging the integration points of the elements for deletion. In case of multiple integration points, the element is deleted only when all the integration points are flagged for deletion. By deletion of the element, all the stresses in that specific element are set to zero and the element no longer continues to contribute to the overall strain energy of the model. Therefore, by deletion of the elements, the failed elements are being deactivated from the analysis, which results in a uniform load transfer through the model. This process is comparable to what happens in tests from the point of view of no energetic contribution of the failed elements on failure of overall sample.

2.5 Knot modeling process

2.5.1 Knots and knot geometries

Knots are considered as weak points in wood and may influence initiation and propagation of cracks. Therefore, having accurate information about knots, their properties and their geometrical configurations in boards may lead to more accurate predictions, especially when considering the mechanical behavior of this material.

Generally, knots can be categorized in the following groups (according to the database in the Department of Wood Technology in TUM):

- Live knots (which are connected to the bulk material)
- Dead knots (which have a partial contact or no contact to their bulk material)
- Holes
- Conical-shaped knots (which are visible mainly on one surface of the board, or they produce a point on the second surface of the board that they are reaching, based on the location of the pith).

Based on the location of pith (center of tree) and based on the cutting pattern of the boards, knots may have different geometries and they may be visible on multiple surfaces of a board. A knot can generally cover up to three surfaces. However, in very rare cases, it is also possible that four surfaces of a board are covered by a knot. Possible knot geometries and the surfaces on which they may be visible are presented in Figure 2-3. These different configurations are assigned to seven subgroups (shown in Figure 2-3). Therefore, numerical analysis can be performed by considering exact locations and geometries of knots, based on which homogenization of the material may be reduced and a more accurate view about the development of stresses in this material can be extracted.

Conical knots, pith in the middle
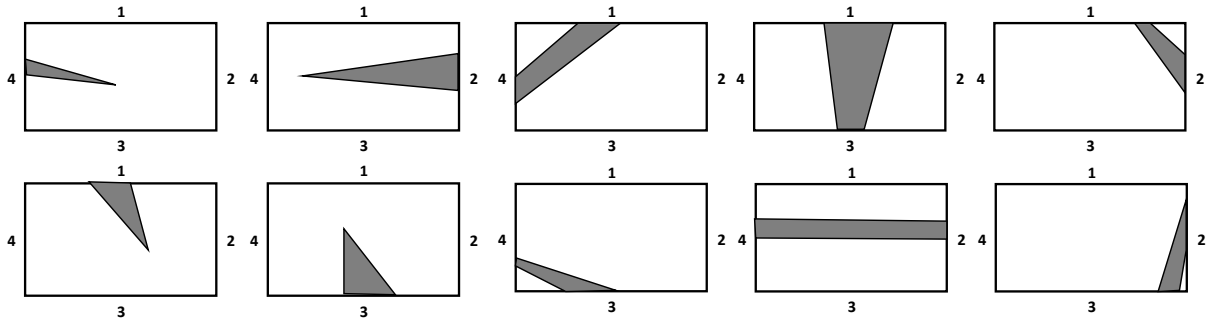
Conical or cylindrical knots on two surfaces

Corner knots on two surfaces
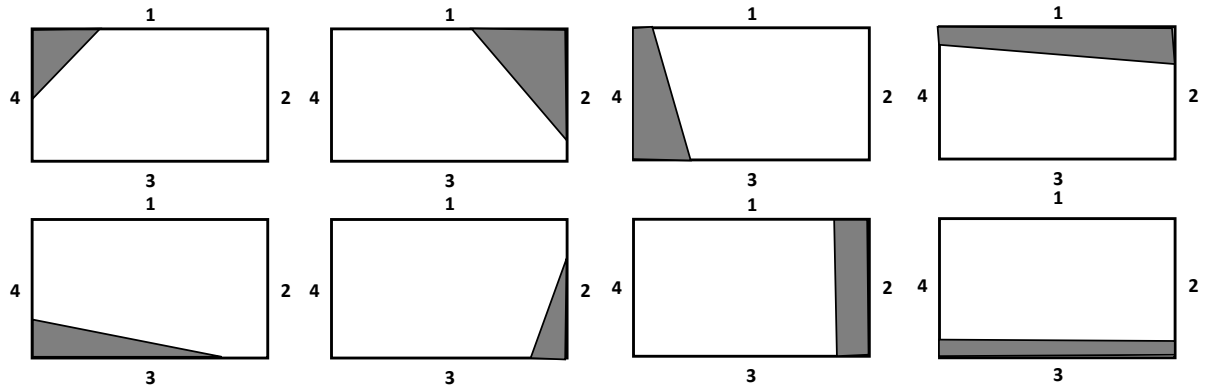
Corner knots covering three surfaces

Conical or cylindrical knots on three surfaces
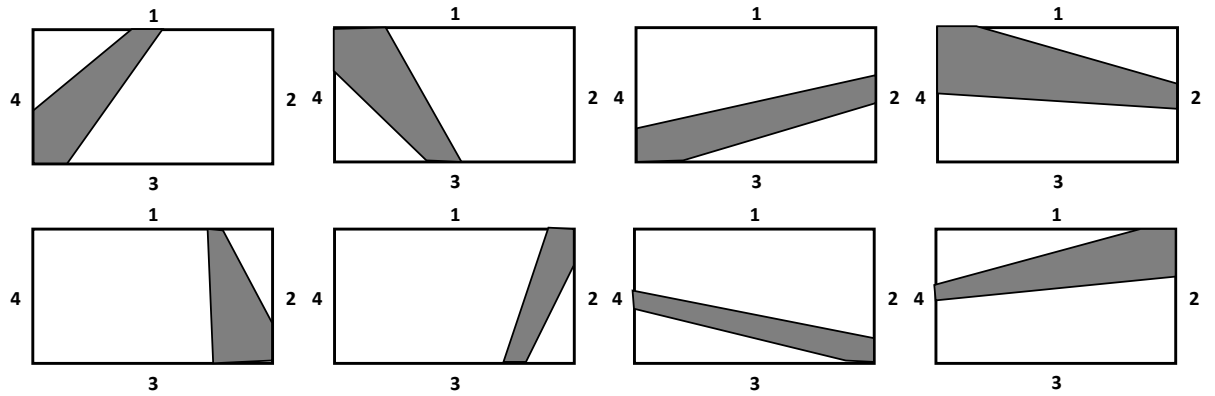
Conical knots creating a point on one surface
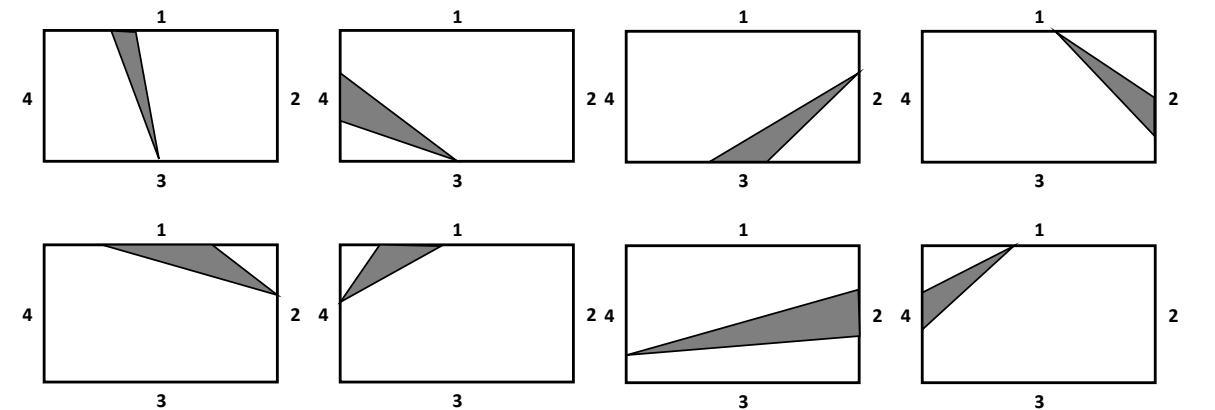
Corner conical knots creating point on a surface or in the middle
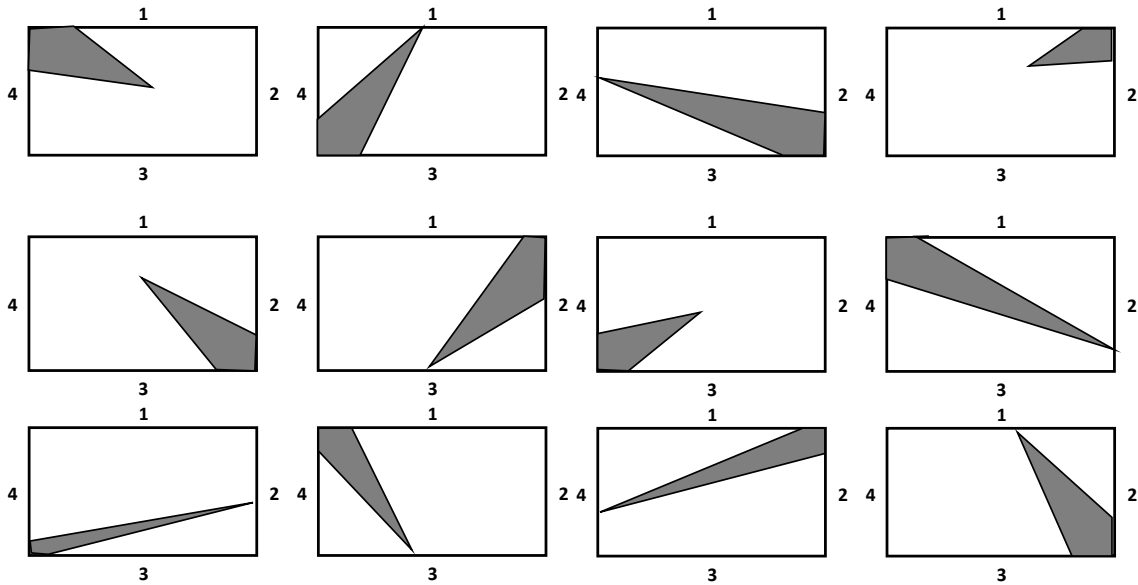
Figure 2-3: Knot shapes, registered in database as a basis for numerical models.

2.5.2 Representation of the knots in the database

All boards are visually graded and knot parameters are registered in a database in the Department of Wood Technology of TUM before performing any tests. Knot registration includes information about the geometrical shapes, sizes and locations of the knots in a single or in a cluster form. Eigenfrequency, density and moisture content of the boards are also measured beside the knot parameters. Additionally, dynamic Modulus of Elasticity (MoE_dynamic) of each sample, which is a strong predictor of strength, is calculated and is registered in the database. Registered data in the database can be accessed any time for numerical analysis. Material parameters, such as strength and static modulus of elasticity are another set of parameters that are being measured and registered in the database after performing of the physical tests (tension or bending). Therefore, a complete set of information, regarding most required parameters for representing the initial material and mechanical behavior of the boards is available. By having access to the database, which includes samples of different wooden species and more than 15000 boards (including more than 10000 softwood specimens and more than 5000 different hardwood specimen), focus of the first part of this thesis is to transform this stored data of the database to virtual geometrical model of the boards automatically. Therefore, reconstruction in this thesis is done solely based on the surface information of the knots.

Visual grading and knot registration methods have been further developed over time to cover the scatter that is required for 3D full representation of the boards. Therefore, registered knot data in the database and the number of parameters to describe these features have been changed over time by new developments. Uniform registration method could simplify the required numerical process for developing a method for 3D board reconstruction. However, this non-uniformity requires development of a standard approach that covers such data variation and scatter. Visual knot assessment and its registration are performed in two different ways. Thus, any possible deviation in registration methods needs to be considered in the developed approach to cover the scatter and to present the most accurate geometrical reconstruction, which is closer to the actual board conditions.

Knot measurements for visual assessment are performed based on one of the following both approaches:

- The standard method (chapter 2.5.2.1)
- The extended method (chapter 2.5.2.2)

For both registration methods, a global Cartesian coordinate system is assigned on the lower left corner of the boards. Based on this global coordinate, locations and surface shapes of the knots are registered in the database (Figure 2-4).
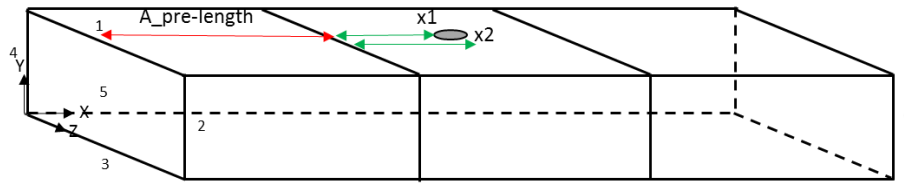
Figure 2-4: The position of the global coordinate system and numbering of the surfaces for visual and numerical knot position registrations. Green arrow shows the x-coordinate based on the local measurements in the test length, and red arrow shows the transformation to the global coordinate system.

The x-axis of the global coordinate system is always directed in the longitudinal direction of the board, parallel to the fibers. Knots are mainly measured along the test length of the samples, which is an area involved in the tests for measurement of the strength (including a length, which is 9 times width of the boards) (EN 408 (2010)). However, the dynamic modulus of elasticity based on stress wave transformation requires information about the full length of the boards. The x-coordinate for some cases is registered based on the longitudinal distance from the local coordinate system, located in the beginning of the test length area, whereas for some other cases it is based on the global coordinate system. If the x-coordinate is based on the test length of the board (x=0 is in the beginning of the test length), the additional length to the beginning of the board (A-pre_length in Figure 2-4), needs to be taken into account for accurate representation of the x-coordinate based on the global coordinate system of the board. If the data is registered based on the global coordinate system, this measured value can be taken directly as the x-value, without any need for modifications.

The y- and z-directions are measured perpendicular to the x-direction. The y-direction is representing the location of the knot in the depth of the board, whereas the z-direction represents the knot location across the width of the board. These coordinates are represented in Figure 2-5.
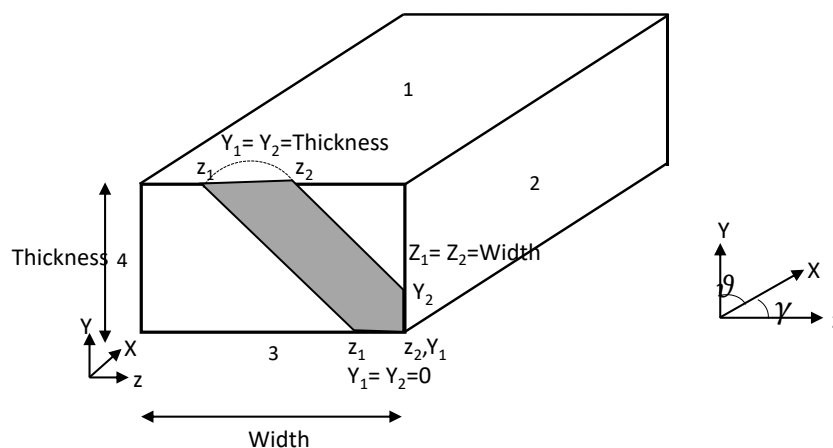
Figure 2-5: Registration of y and z-coordinates of the knots. The numbers 1, 2, 3, and 4 are representing the four surfaces of the board.

Depending on the location of the center (pith) of the tree, some knots may only create a single point on one surface or internally in the board. Therefore, as shown in Figure 2-6, only one value of y and z-coordinate may be enough in such cases, to represent the location of the point. Thus, the point location can be represented by its single coordinates x, y, and z. If the point is directly on the surface, the location

can be presented by its x and z coordinates, as y=0 in this case. In contrast to these knot types, if center of the tree is located outside of the board, areas of circular or elliptical shapes may appear on the surfaces that are covered by knot, and the beginning and ending point of the knot area on each surface need to be taken into account (Figure 2-5).
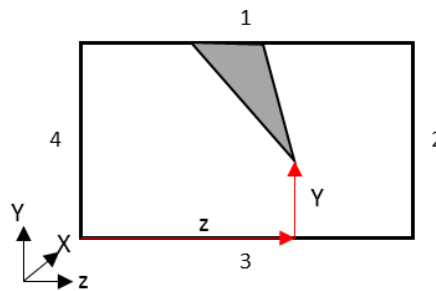
Figure 2-6: Coordinates of a point in the cases where the knot is creating a point inside the board.

Beside the coordinates, the maximum and minimum diameters of knots (shown in Figure 2-7) are registered, which are giving an overview about the form and the direction of the elliptical surfaces on each surface.
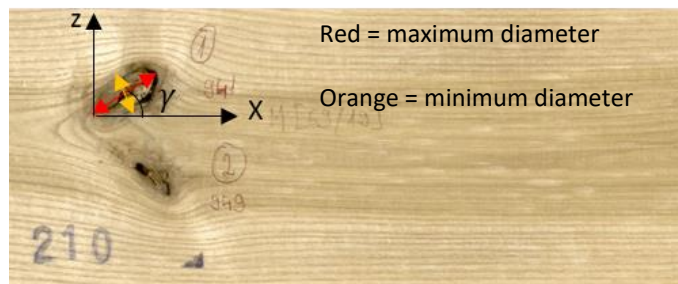
Figure 2-7: Maximum and minimum diameters of the knots.

2.5.2.1 Data, based on the standard registration method

In the standard registration method, knots are registered based on the following data:

- The y-coordinates at the beginning and ending position of the knot on the surfaces where the knot appears
- The z-coordinates at the beginning and ending position of the knot on the surfaces where the knot appears
- Maximum diameter of the knot
- Minimum diameter of the knot
- Estimated center of gravity of the knot volume as the x-coordinate

Center of gravity of each knot volume is used for representation of the x-coordinate of each knot in this registration method. Therefore, information about exact coordinates of the beginning and ending position of the knot areas in the x-direction is missing and estimations are required for knot reconstruction. Based on the registered data regarding the maximum and minimum diameters of the knot, an approximation can be made to predict these coordinates for reconstruction of the geometrical model of the boards. Data regarding the y- and z-coordinates of the knots are registered as explained before. However, it is not specified whether the angle of an ellipse with respect to the longitudinal axis is positive or negative.

2.5.2.2 Data, based on the extended registration method

Previous knot registration method is exchanged with the extended registration method to be able to overcome the problems that may occur during standard registration method. Problems in the previous

15

method may especially occur due to representation of the x-coordinate of the knots as the center of gravity of each knot volume, which may cause data inaccuracies. The extended method is the modified standard method, which takes into account more parameters for knot representation over the surfaces. Thus, knots are represented more accurately in this method and 3D full reconstruction of the boards is more straightforward, using this method. Following information about knots can be found in the database for this registration format:

- The x-coordinates at the beginning and ending position of the knot area on the surfaces where knot is appearing
- The y-coordinates at the beginning and ending position of the knot area on the surfaces where knot is appearing
- The z-coordinates at the beginning and ending position of the knot area on the surfaces where knot is appearing
- Maximum diameter of the knot
- Minimum diameter of the knot
- Knot center location on each surface
- Angle γ, which shows the angle of the rotation of a knot over the surface of the board compared to the principal axis of the board (shown in Figure 2-7)

Therefore, accuracy of the data registration in the extended method is increased, and the required data for geometrical reconstruction of the boards can be extracted. Angle of rotation of each knot can be calculated by knowing exact position of the knots. Therefore, additional information can be provided about degree of rotation of the knot from its straight configuration.

Table 2-1 summarizes the parameters of an example board that are registered in the database. In this table, sample number represents the number or an ID of the board of interest. Knot number is a counter starting at x=zero and shows the total amount of knots that are existing in the board. Repetition of the same number in this column shows number of the surfaces that each knot is appearing on. Surface number is the number of the surface, which is occupied by each knot for a board. The y_ or z_dir1 and _dir2 are the starting and ending positions of the knots on the specified surfaces, respectively. The x-dir. is a representation for the center of the knot in x-direction. Distance to the center shows an approximate center of the knot from the edge of the board. This value is not necessarily required for reconstruction, as the knot axis can be approximated by averaging the location of the knot in y_ or z_dir1 and z_dir2. Additionally, the thickness, width and the length of each board is measured and registered in the database, which are important parameters for reconstruction but are not presented in this table.

Another set of parameters that are available in the database but are not considered for reconstruction process are the density, moisture content and eigenfrequency values, which are used for calculation of the MoE_{dyn}.

Center of knot is especially important in case of knots with conical shapes, where starting point of the knot is on a surface or in the board internally and therefore, a point is being created over the surface or inside the board (as presented in Figure 2-3 for knots that are creating a point on a surface). The program needs to be able to analyze the database based on the given board number in order to figure out some possible knot configurations that a knot can have and to reconstruct each board separately. In this thesis, numerical simulations are run for two sets of softwood species and three sets of hardwood species, among thousands of samples in the database, to be able to cover the natural scatter of wood, to verify the robustness of the modeling approach (as discussed in chapters 3 and 4), and to generalize the model to a species-independent one.

Table 2-1: Registered parameters in a single board (extended method)

Sample number	Knot number	Center in z-dir. (mm)	Center in y-dir. (mm)	Surface number	y or z_dir.1 (mm)	y or z-dir.2 (mm)	Minimum diameter (mm)	Maximum diameter (mm)	x-dir. (mm)	Distance to the center (mm)	Direction of angle γ
1241	1	65	4	1	50	28	20	23	1815	39	-
1241	2	65	4	1	133	100	22	35	1913	115	-
1241	3	-	-	1	86	79	7	7	2177	83	-
1241	3	-	-	3	61	64	2	3	2184	63	-
1241	4	-	-	1	46	39	6	7	2293	43	-
1241	4	-	-	3	49	55	5	6	2300	52	L
1241	5	-	-	1	50	42	8	9	2378	46	-
1241	5	-	-	3	51	57	5	6	2371	54	-
1241	6	-	-	1	100	75	22	28	2549	86	-
1241	6	-	-	3	66	75	9	13	2533	69	R
1241	7	-	-	2	8	11	3	5	2199	9	-
1241	7	-	-	3	98	116	5	18	2199	106	-
1241	8	65	4	3	68	75	4	12	1843	72	L
1241	9	-	-	3	8	40	17	32	2551	25	-
1241	9	-	-	4	34	1	32	33	2563	16	-

2.6 Three-dimensional numerical modeling of boards

2.6.1 General

The generalized reconstruction method in this thesis is based on estimation of the coordinate directions and it covers the representation of both registration methods. Therefore, it is possible to compare and validate the simulation results with the measured data, independent of the knot registration method that is used for reconstruction. For this reason, PYTHON is used to create the link to the data of the database and PYTHON in combination with ABAQUS CAE (Simulia 6.14) are used for the 3D reconstruction and finite element analysis.

Location, orientation and shape of the knots together with the surfaces that may be occupied by each knot need to be analyzed for the reconstruction process. For this reason, 15 possible surface combinations, showing possible knot configurations need to be analyzed. These possible surface configurations (presented in Figure 1s of paper 3) include:

- Four single surfaces occupied by knot
- Six double surfaces occupied by knot
- Four configurations, where the knot is occupying three surfaces
- One configuration for the case, where the knot covers four surfaces

Separate plane and axis of rotation are defined for each knot based on which center of the knot can be predicted and material properties of the knots can be assigned to each knot volume separately. This is an important step especially in the case of live knots.

Based on the type of each knot in a real board, similar conditions may be implemented for numerical simulations. In case of the live knots, a surface contact may be defined between the knot area and the wooden bulk material, which makes it possible to analyze friction and movement of the knot with respect to its bulk material under different loading conditions. Additionally, by applying different material properties to the knots, influence of material differences on the load transfer and distribution of the stresses may be checked. In case of holes, simple holes are modeled during the reconstruction process. In case of dead knots, only part of the knot is connected to the bulk material. However, in order to make simplifications in the modeling process and to reduce the computational costs (by reducing the number of elements and preventing the contact regions), knots are modeled as holes in virtual tensile analysis. Later in this thesis (sub-chapter 2.6.2.2), the difference in modeling knots as solid volumes or holes and variation of the material properties are checked and discussed. It is shown that this simplification is possible for wood under tension. Similarly, this simplification does not have a considerable influence on the results of the numerical analysis in case of dead knots. This is due to a weak connection of the dead knot volume to its bulk material. Conical shaped knots are modeled in the same way during the numerical simulations. A comparison for modeling of these different types of knots is presented in Figure 2-11.

The developed reconstruction method enables reconstruction of the test length as well as the full length of the boards, based on the type of the analysis that is going to be performed. Different accuracy levels are required for the model considering the type of the analysis. As an example, for virtual prediction of the dynamic modulus of elasticity, complete knot information over the full length of the boards is required. In contrast to this case, tensile analysis requires only information about the test length of the boards for tensile strength predictions.

Simulations are run for 102 spruce boards, 150 Douglas fir boards, 200 beech and 14 ash and maple boards. For the spruce, beech, ash and maple boards, knots are registered based on the extended registration method, whereas, for the Douglas fir boards, knots are registered based on the standard registration method. The boards are strongly different in wood qualities (Khaloian Sarnaghi and Van de Kuilen 2019c); a general phenomenon relating to the "knottiness" of wood.

2.6.2 Geometrical model

The reconstruction process needs to be generalized in order to cover the natural scatter of the boards. Additionally, this process needs to be capable of handling the differences in data registration methods and it needs to process the necessary data and check its accessibility for reconstruction. Therefore, the program needs to be established in a way to cover different possible aspects for analyzing surfaces of the boards. In the first step, entire surfaces of the boards are being analyzed one after each other to check possibility of each surface to be occupied by part of a knot. After analyzing the surfaces and based on the surface information of knots (regarding the coordinates and the geometrical position of each knot), the possibility for development of cylindrically-shaped knots is being analyzed. Later, by extraction of the dimensions of the knots over each surface, correct diameters are being assigned to each knot. If the knot has a circular shape on a board surface, consideration of the direction for diameter assignment is not important (as one diameter is enough for representation of a circle). However, if the knot has an elliptical shape, correct diameter has to be assigned in a correct direction to get a realistic rotation in the knot geometry. This process is performed separately for each knot along the board.

In the second step, a similar procedure is being performed for all knots to check the possibility of having a knot with a conical shape. If the knot has a conical shape, it is being checked if the cone is complete in the geometry or not. Therefore, it is necessary to be checked whether the knot is making a point on a surface or in the board internally. Another option is that the cone is passing through the board and it does not have a completed conical shape in the board. After completing the geometrical categorization of all knots along the board, a separate axis of rotation is being defined for each knot, by finding the center of each knot. The reconstruction process is presented schematically in Figure 2-8.
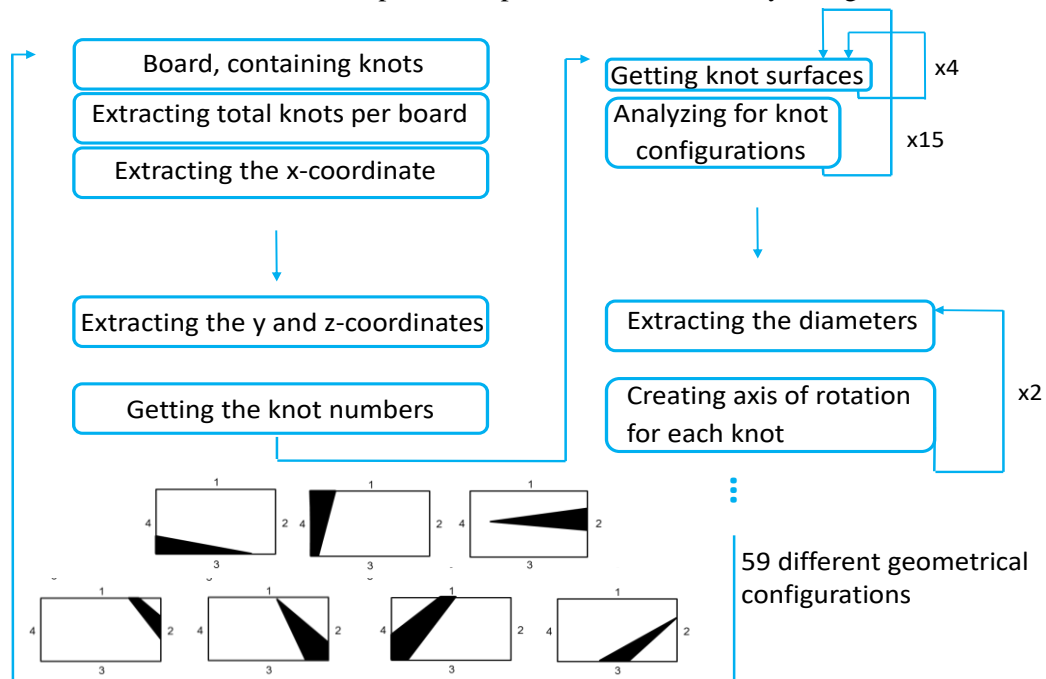
Figure 2-8: Schematic view of the reconstruction process.

Number of the loops that the program needs to run to analyze each knot configuration is presented with x4, x15 and x2 in Figure 2-8. As shown in this figure, each knot can cover maximum four surfaces of a board. Although this condition is very rare, but it is seen for some species like pine or beech with relatively big knots. In general, 59 different geometrical configurations can be presented numerically, as summarized in seven groups, presented in Figure 2-8.

As mentioned before, the reconstruction process is done by creating a matrix over the accessed information of the database. Dimensions of the matrix are filled first based on the columns and then based on the rows, as described in the next sub-chapters.

2.6.2.1 Column-wise

Number of the columns of the total matrix is equal to the number of the parameters that are presented in Table 2-1. This data shows the required data for presenting the boards, their dimensions and positions of the knots in the boards. Number of the columns has a constant value of 12 for all the boards, as shown in Table 2-1.

2.6.2.2 Row-wise

Number of the rows of the final matrix is the result of the summation of the total number of the surfaces, covered by each knot and for all tested boards. Therefore, the three parameters that need to be defined, are explained here as x, y, and z. This is schematically and mathematically presented in Figure 2-9 and Equation (2-13), respectively.
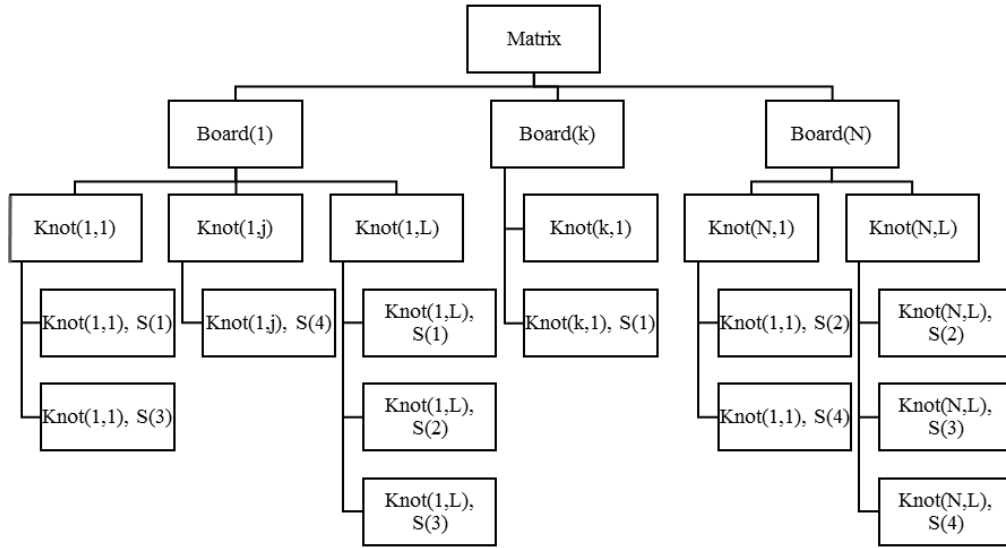
Figure 2-9: Example schematic representation of the matrix of the database and Equation 2-13.

Figure 2-9 represents an example matrix, containing data of three boards. First board contains three knots, which are visible on two, one and three surfaces, respectively. Parameter S(i) in this figure represents the surface number which is covered by that specific knot. This can be a value between one and four, as a knot can be covered by maximum four surfaces. The surface numbers are shown in Figure 2-4. Same explanation is valid for boards k and N in Figure 2-9.

$$T \subseteq R^3$$
$$T = \left\{1 \leq x \leq 4; 1 \leq y \leq L; 1 \leq z \leq N\right\}$$

(2-13)

In Equation (2-13), parameter x represents total number of the surfaces in a board, which a knot can cover. Parameter y represents the total number of the knots in each board (with L as the total knot number). Parameter z represents the total number of boards, which are tested and stored in the database and need to be simulated (with N as the total board number). T_{total} is then the sum of T as a function of x, y, z.

By extracting the data of each board from the matrix of the stored data, total number of the knots in each board is found and the surfaces that may be covered by each knot (as shown in Figure 2-3) are analyzed automatically. Dimensions of the knots are extracted for each surface and the geometrical model of the board is estimated based on the extended-method, or by estimation of the x-coordinate from the knot center of gravity and diameter, based on the standard-registration method (to be found in chapter 2.5.2). This data is then transferred to ABAQUS, and the geometrical model is reconstructed automatically by considering all the knots. Knots may have different possible geometries, different angles and positions.

An example model for a geometrically reconstructed board is presented in Figure 2-10. This figure represents an example of a spruce board with relatively uniform knot shapes. Knots are measured and presented in the test length of the boards in this case. Figure 2-10a,b,c shows an extended view of the knots over the board, to make the visualization of their configurations and rotations possible. Figure 2-10d is the final front view of the board with knots.
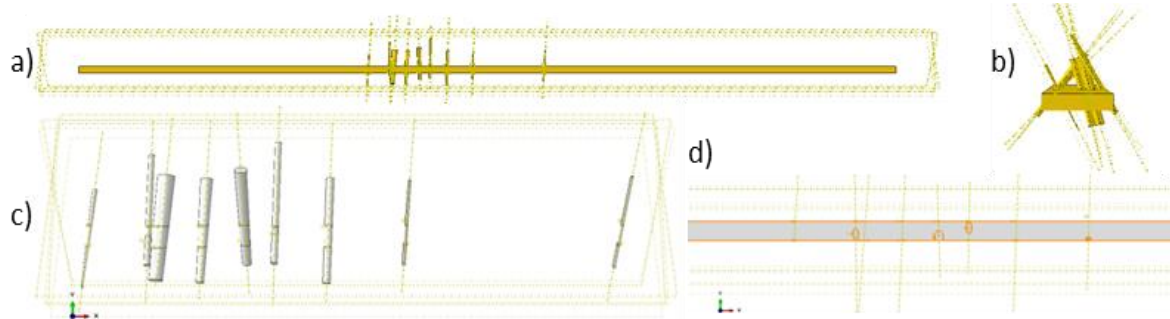
Figure 2-10: Geometrical reconstruction of an example spruce board. a) front view with the center part of board (test length) for which knots are measured, b) side view, c) representation of only knots, d) representation of the board with the knots and solid geometries with different configurations and properties.

Sensitivity analysis is performed to cover possible errors during the reconstruction process, which may be resulted due to possible measurement and registration errors in the database over many years. For this reason, an error term is added to the program randomly, which randomly variates dimensions of the knots with ±5mm (Khaloian Sarnaghi and Van de Kuilen 2019a). Although this error term may cause small deviations in the geometry of knots, but it is relatively small to influence the numerical results during the numerical analysis.

As mentioned before, wooden boards, modeled during this thesis are qualitatively different and some may contain up to 90 knots. Therefore, defining solid geometries for knots (that increases the number of the elements) and application of contact in the numerical model may considerably increase the calculation time. In the first step, influence of modeling knots as holes and outcome of this approach on stresses are analyzed numerically. For this reason, knots are initially modeled as solid volumes with contact and relatively fine mesh in the knot area for prediction of the stress transfer. Later, these features are modeled as holes with relatively fine mesh around the holes to provide a good stress distribution. Boards are modeled under a tensile stress of 10 MPa. Two knots are selected for this analysis. One knot is the knot with the total maximum stress in the board, whereas the second knot is selected completely randomly. Paths are defined, crossing the clear wood, knot boundaries and the knot, along the center of the knot. The results are compared on the knot boundaries and are shown in Figure 2-11.
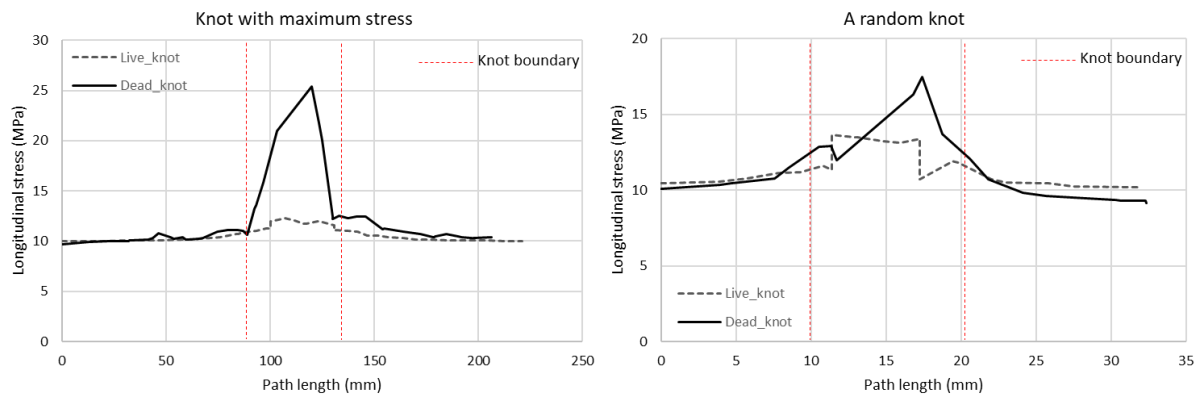
Figure 2-11: Comparison of defining the knot as a solid volume (live knot) or a hole (dead knot).

The knot with the maximum stress is the one with an approximate diameter of 40 mm. Second random knot is a relatively small and circular shaped knot with a diameter of an approximately 10 mm. It is

shown on the knot boundaries of the random knot (shown with red lines in Figure 2-11) that the stress paths are slightly deviating from each other; however, the paths are relatively similar until they reach the knot boundaries. This deviation is stronger for case of the knot with the maximum stresses, as these are generally locations with more complicated geometrical patterns, where the stress singularities are higher. However, the stress paths until the knot boundaries are relatively similar in these cases as well. As the main point of interest in this thesis is the stresses that are developing till the knot boundaries for calculation of the stress concentration factors (described later in Paper 1 of this thesis), definition of knots as holes simplifies the numerical procedure and reduces the calculation time. Therefore, knots are modeled as holes for the next steps of this thesis.

2.6.3 Interacting stress concentrations

Amount of the geometrical imperfections and knots in wood is different from one species to the other. Existence of many knot clusters is also not unexpectable in especially softwood species. Therefore, stresses that are developing around each of these features may be influenced by the other ones. For this reason, considering interaction of the stresses in a 3D space is an important step in solving the problems during this thesis. The localized stress increase around the geometrical features such as holes, radii, or notches is an important parameter for different materials that need to be considered especially for structural applications. Calculation of these localized high stresses as a single parameter is important for prediction of different short and long-term material behavior. For a single circular hole in an infinitely thin element under uniaxial tension, this factor can be calculated as presented in Equation (2-14).

$$K = \frac{2 + (1 - \frac{d}{H})^3}{1 - (\frac{d}{H})} \tag{2-14}$$

where K is the stress concentration factor, d is the diameter of a hole, and H is the width of the panel (Pilkey WD and Pilkey DF 2008).

The same factor in a semi-infinite element, under a uniaxial loading condition is calculated based on Equation (2-17). In such a case, the load carried by the section between the edge of the panel and the hole is presented as Equation (2-15) (Mindlin 1948).

$$P = \sigma.c.h\sqrt{1 - (\frac{a}{c})^2} \tag{2-15}$$

where σ is the applied uni-axial stress to the isotropic plate (see also Figure 2-12), c is the distance from the center of the hole to the nearest edge of the panel, h is the thickness of the plate, and a is the radius of the hole.

Analytically, stresses can be calculated based on the Equation (2-16).

$$\sigma_{analytical} = \frac{\sigma.c.h\sqrt{1 - (\frac{a}{c})^2}}{1 - (\frac{a}{c})} \tag{2-16}$$

$$K = \frac{\sigma_{max}}{\sigma_{analytical}} \frac{\sigma_{max}(1 - (\frac{a}{c}))}{\sigma\sqrt{1 - (\frac{a}{c})^2}} \tag{2-17}$$

In a similar way, the stress concentration factors (K) around the elliptical hole can be calculated using Equation (2-18) (Durelli et al. 1952).

$$K = 1 + 2\sqrt{\frac{a}{r}}$$

(2-18)

where a is the major radius of the ellipse and r is the radius of curvature of the notch.

In contrast to a single notch condition, multiple notches influence the stress criteria of each other. Therefore, interaction of the stress concentration may result in a reduction or an increase in amount of the total stress concentration factor. A 2D plate with multiple notches of different sizes and shapes, and interacting stress concentrations is presented in Figure 2-12. Such interacting stress concentrations may occur in different structural applications, such as aerostructures, due to the design of multiple features such as holes or radii for specific applications or during the repairing procedure. These features may be assigned close to each other and may cause interaction of the stresses, depending on the loading conditions. Heterogeneities in wood are distributed non-uniformly through the material. These features are influencing both strength and the material properties of this material. As shown in Figure 2-12, such condition with non-uniform geometrical shapes and inconsistent center-to-center (CC_i) distance, is naturally seen for wood. As the material itself is non-homogeneous, wrong considerations of additional multiple holes for joints and connections without considering the effects of interacting stress concentrations may lead to unexpected failure and increased fatigue of the structure. Interaction of the stress concentrations may lead to an increase in the stresses, compared to the single notch conditions.
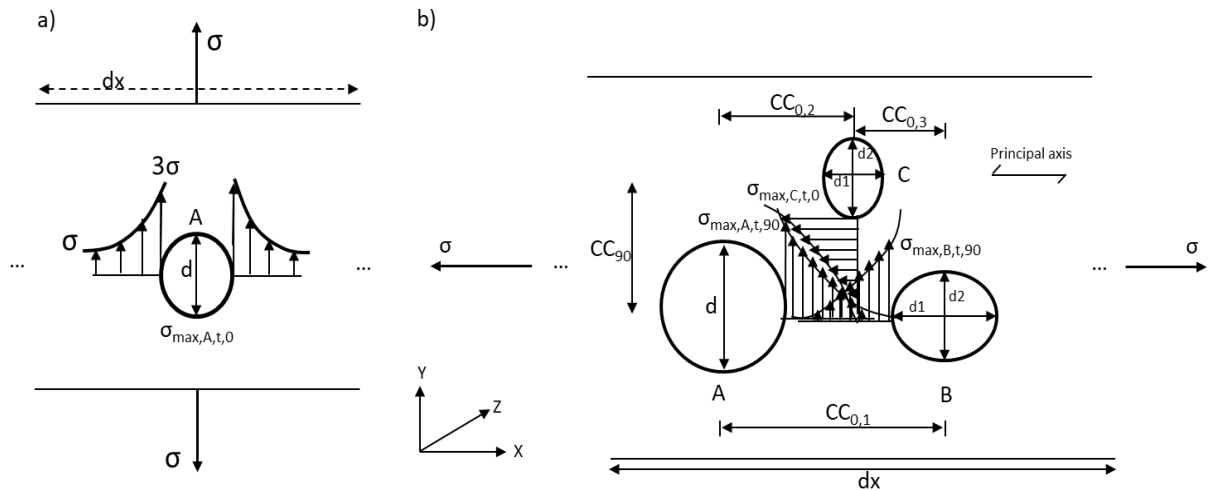
Figure 2-12: Stress concentration: a) single notch with development of stresses around, b) multiple notches and the interacting stress concentrations (close look on a specific length dx of an example board).

Numerous studies considered influences of the multiple features under specific loading conditions on development of the interacting stresses. Majority of these studies analyzed stress interactions in between these features that are located relatively close to each other, mostly for aerostructural applications. Such conditions seem to be more common in this engineering field. Ling (1968) performed the first studies regarding the interacting stress concentration factors of two circular holes in a plate. According to Peterson (Pilkey WD and Pilkey DF 2008), multiple effects of the stress concentration factors are the product of all single factors, presented in Equation (2-19):

$$K_t = K_1 . K_2$$

(2-19)

where K_1 and K_2 are the two stress concentration factors of two geometrical features. This factor can also be calculated by considering root sum squares of the single parameters, according to the Equation (2-20).

$$K_t = \sqrt{K_1{}^2 + K_2{}^2}$$

(2-20)

or by considering K_t as :

$$K_t = K_1 \sqrt{K_2}$$

(2-21)

with $K_1 \geq K_2$ (Whitley 2013).

However, the interaction Equations (2-19) to (2-21) are limited to two combined features in a 2D plane. These conditions can be more complex for 3D cases with more than two combined features, especially when the geometrical features/holes may have combination of circular and elliptical shapes. This is the case for wood with knots, which needs to be deeply analyzed. An example plate with interaction of the stresses in 2D space is presented in Figure 2-12. As shown in this figure, higher stresses are developing around each of these geometrical features compared to the bulk material. However, at the central location of this example, combination of the stress concentrations is shown, which may result in an increase in the total stress concentration factor to a value higher than three times the normal stresses.

Missing information about stress interactions in between multiple and non-uniform geometrical features in a 3D space, especially for anisotropic materials, motivated this thesis for development of a method for calculation of the stress concentration factors in wood. Details of these methods are discussed in Chapter 4 and in Paper 1 (Khaloian Sarnaghi and Van de Kuilen 2019a).

Chapter 3 Prediction of the fiber pattern: Flow-induced fiber patterns in complex 3D heterogeneous space as a representation for microstructure of wood

3.1 General

As shown before, knots are the main strength governing parameters. These natural defects are causing local fiber deviation in wood, which is affecting the uniform flow of the stresses in timber. By reconstructing the full 3D model of the timber boards, based on the knot information on the surfaces of the boards, fiber distribution is predicted in the material based on the concepts of fluid dynamic analysis. Due to the large scatter of different wooden species, regarding the number and geometrical configuration of knots, application of laminar flow may lead to underestimations in prediction of the fiber deviation around these geometrical complications. This condition can be seen more frequently at the locations of knot clusters or in hardwood species with more complex fiber pattern. In this thesis, concepts of the Spalart-Allmaras method are applied for the CFD analysis. Validation of the predicted fiber pattern is done, using the CT-scan images of timber boards. Based on the CT-scan data, optimum flow condition is found for prediction of wood fibers. The flow in this case should allow transition of the laminar flow to a turbulent one without development of a very thick turbulent region. A turbulent region with large vortices is an unrealistic condition for wood. Additionally, effect of the up-flow and down-flow on prediction of the fiber patter is analyzed and is validated with the CT-scan data. Validation of this step is done for five spruce boards and over 15 surface-cuts in the boards, based on which fiber pattern is validated not only on the surfaces of the boards, but also in timber boards internally. Velocity vectors at each specific location along the boards may provide information about the rotational angles of the coordinate directions at that location. Based on this information, a method is provided for prediction of the local orthotropic directions of timber for strength predictions. Confirmation of the numerical results by the CT-scan data shows the strength of this numerical approach for prediction of the fiber pattern and for stochastic distribution of the material properties in timber.

3.2 Introduction to fiber prediction in wood

Complex fiber pattern of the hardwood species and complex knot clusters in softwood species that are considered in this thesis are analyzed and the mathematical approach, which is provided for prediction of the fiber pattern in wood (Goodman and Bodig 1978) is further developed. In this thesis, Computational Fluid Dynamic (CFD) analysis is used for prediction of fiber direction and correspondingly for estimation of the anisotropic properties of wood.

Since the main fluid transport is occurring in growing cells, an actual fluid flow exists around knots when cells are growing (Goodman and Bodig 1978, Jenkel and Kaliske 2013, Baño et al. 2010, Hu et al. 2017). Based on the concepts of the flow-grain analogy (Phillips et al. 1981, Cramer and Goodman 1982), the stream-lines of laminar flow have been generally used in different studies to represent the fiber pattern in wood in 2D (Cramer and Goodman 1986, Goodman and Bodig 1978, Zandbergs and Smith 1987, Foley 2001) and 3D (Hackspiel et al. 2014, Lukacevic and Füssl 2014, Guindos and Guaita 2013, Lang and Kaliske 2013, Jenkel 2016).

Additionally, a study in 2013 (Lang and Kaliske 2013) concentrated on comparing the models, based on flow-grain analogy and principal stresses, which showed that the results around a round knot in both

models are corresponding well to eachother. Another model in 2013 considered the streamlines and equipotential lines for prediction of fiber orientation based on a 2D layer-wise meshing procedure (Jenkel 2016). Although different studies aimed on prediction of the fiber deviation around knots, but missing information about the influence of geometrical complications on flow pattern, and the optimum flow conditions for performance of better predictions is covering contents of this part of the thesis. As discussed previously, some wooden species, such as Douglas fir, have up-to 90 knots, which are creating complex geometrical conditions for the numerical analysis. Accumulation of knots in specific locations in timber boards are creating challenging conditions, which are changing the uniformity of the fiber deviation, and are causing small turbulence in the pattern. Therefore, the concepts of the flow-grain analogy and the usage of stream lines of laminar flow (Phillips et al. 1981, Cramer and Goodman 1982) is developed further in this study to represent the fiber pattern in wood and to cover the natural scatter of this material. Applying the streamlines of the laminar flow in complex conditions may underestimate the fiber deviations around the imperfections. Therefore, small turbulent viscosity is expected in such locations, which allows for flow separation. However, an optimized flow solution needs to be extracted, before a complex and thick vortex zone is developed in the model, as this is an unrealistic condition for wood.

CFD analysis has been used in many studies for analyzing effects of the obstacles on the stream function of a flow, for different structural conditions and applications (Ouro et al. 2017, Chatterjee et al. 2010, Wang et al. 2013, Bao et al. 2010, Zdravkovich 1987, Burghardt et al. 2005, Bent 2003). The current model aims in covering a scatter of geometrical imperfections for a scatter of wood species, to provide a more realistic solution for the prediction of fiber deviation, which may improve the quality of strength prediction of timber.

Among possible approaches that are currently used for geometrical reconstructions, CT-scanning is the most common approach especially for biomedical applications (Wong et al. 2017, De Backer et al. 2010, Contro et al. 2004, Inthavong et al. 2014, Hambli 2013, Maquer et al. 2014, Pistoia et al. 2002, Kowalczyk 2010). As shown in previous chapters, knots are causing local fiber deviation in wood. Therefore, they are considered as the governing parameters for tensile strength of timber. These features are complicating the geometrical structure of this material. Therefore, besides the cellular structure of the boards, detailed information of the knots is important for both reconstruction and more accurate predictions. CT-scan images are used in this thesis for the validation of fiber profile.

Philips Ingenuity 128 multidetector computed tomography scanner (Philips Healthcare, Best, Netherlands) with 0.3x0.3x0.8mm^3 spatial resolution using a high resolution reconstruction kernel (YB), 120kVp and 200mAs is used for CT scanning of the wooden boards. The resolution in this case is 5 cm. Afterwards, MicroDicom 2.7.9 and RadiAnt DICOM Viewer 4.2.1 are used as the visualization software for the CT-scan images and analyzing the DICOM files. A CT-scan of an example spruce board with its different views and respectively the reconstructed board is shown in Figure 3-1. A knot cluster is also marked in this figure as an example. This location creates a complicated combination of features and influences the global fiber pattern of wood. It is shown in the figure that the global fiber pattern of this sample strongly deviates from the assumption of uniform laminar flow estimations.

For this part of the thesis, Python (2.7.3) and ABAQUS/CFD (Simulia, 6.14-2) are used as the tools for the geometrical reconstruction and the CFD analysis for fiber predictions. Numerical analyses are performed for 253 different wood samples to visualize the variations based on the knot shapes and material properties.
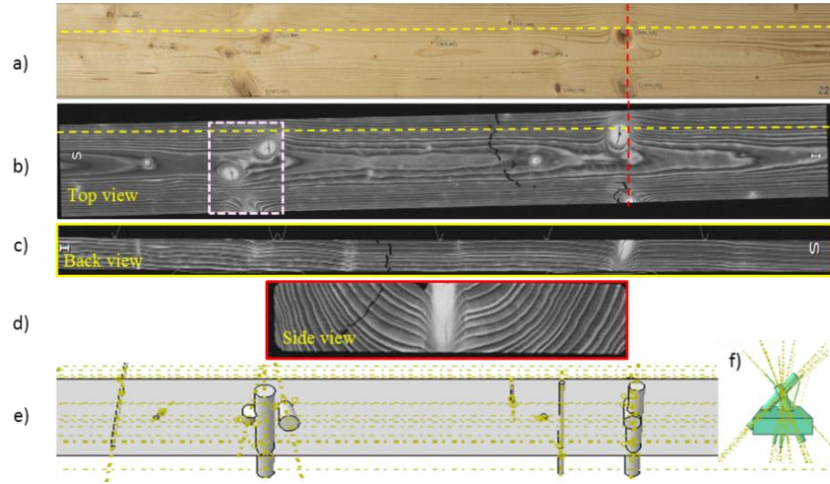
Figure 3-1: CT-scan of an example spruce board with its different views. Yellow and red dotted paths show the locations, where cuts are made for visualization of the board along its thickness and the width. Pink dotted rectangle shows the location of a knot cluster.

CT-scanning of wood and the density map of this material enables to extract an entire information about the geometrical view of the boards, locations of the knots and distribution of the fiber around imperfections. As shown in Figure 3-1, knots are generally observed as circles or ellipses with higher densities on the surfaces of the boards. These high-density points in softwood species are creating clusters that are influencing the fiber profile of the boards. In contrast to softwoods, hardwood species have fewer and well-spaced knots whereas, their fiber profiles are more complicated with more non-uniform pattern. Therefore, a realistic condition needs to be provided to cover the scatter of different samples and to be able to represent the fiber pattern in wood.

By having the opportunity for segmentation of the CT-scan data, the fiber information on different coordinate directions and locations in wood and around knots can be extracted, which is used later for validation of the modeling approach.

In total 50 boards are randomly selected among the numerically considered samples to check the relation between the drag pressure and tensile strength, as a possible IP for strength predictions.

3.3 Theory and Methods

3.3.1 Numerical simulations

Fluid is modeled as Newtonian, incompressible and isothermal material, with constant viscosity and density. By neglecting the body forces acting on the fluid over the flow, the generalized Navier-Stokes momentum equation (Rabbani et al. 2016, Rabbani et al. 2018) can be written as:

$$\rho(\frac{\partial \vec{v}}{\partial t} + \vec{v}\nabla\vec{v}) = -\nabla p + \mu\Delta\vec{v} \qquad (3\text{-}1)$$

where ρ is the density, $\vec{v}$ is the velocity vector in three spatial directions, μ is the constant Newtonian viscosity, ∇ is the divergence operator, and Δ is the Laplacian operator.

By satisfying the mass conservation requirement, Equation (3-2) can be obtained.

$$\nabla\vec{v} = 0 \qquad (3\text{-}2)$$

For laminar flow, Equations (3-1) and (3-2) should be solved for u, v, w (the velocities in three spatial directions), and for p (the pressure) which are coupled and non-linear.

To consider small fluctuations in fluid, time-averaged conditions for the velocity, pressure, shear stresses, etc. are considered. Therefore, the velocity components are represented as follows:

$$\begin{cases} u(x,y,z,t) = \overline{u} + u'(x,y,z,t) \\ v(x,y,z,t) = \overline{v} + v'(x,y,z,t) \\ w(x,y,z,t) = \overline{w} + w'(x,y,z,t) \end{cases} \tag{3-3}$$

Parameters $\overline{u}$, $\overline{v}$, $\overline{w}$ in Equation (3-3) denote the time averaged velocities, whereas the " ' " denotes the fluctuations about the time averaged qualities, which is the deviation of the quantity from its average value. Therefore, mean value of the fluctuation is zero (Equations (3-4) and (3-5)).

$$\overline{u} = \lim_{T \to \infty} \frac{1}{T} \int_0^T u \, dt \tag{3-4}$$

$$\overline{u}' = \lim_{T \to \infty} \frac{1}{T} \int_0^T (u - \overline{u}) \, dt = \overline{u} - \overline{u} = 0 \tag{3-5}$$

By considering continuity for the left side of the Equation (3-1) and by replacing the velocity components with the modified components, including the time averaged and fluctuation parts, the momentum equation in the longitudinal fiber direction of wood, representing the mainstream direction "x", takes the form:

$$\overline{u}\frac{\partial \overline{u}}{\partial x} + \overline{v}\frac{\partial \overline{v}}{\partial y} + \overline{w}\frac{\partial \overline{w}}{\partial z} = -\frac{\partial \overline{p}}{\partial x} + \frac{\partial}{\partial x}(\mu\frac{\partial \overline{u}}{\partial x} - \rho\overline{u}'^2) + \frac{\partial}{\partial y}(\mu\frac{\partial \overline{u}}{\partial y} - \rho\overline{u'v'}) + \frac{\partial}{\partial z}(\mu\frac{\partial \overline{u}}{\partial z} - \rho\overline{u'w'}) \tag{3-6}$$

where $-\rho\overline{u}'^2$, $-\rho\overline{u'v'}$, and $-\rho\overline{u'w'}$ are the turbulent stresses. The vector sum is taken as representative for expected main fiber direction around the defects.

Large amount of natural defects and knot clusters in especially softwood species are causing more difficult flow conditions compared to the species with few and well-spaced knots. Therefore, the streamlines of laminar flows cannot describe the fiber pattern of the natural scatter in wood. However, development of extreme vortices are also unrealistic for wood, as fiber patterns in this material are never developing thick vortex layer. Therefore, the two-equation turbulent models, such as $K - \omega$ or $K - \varepsilon$, are not realistic expressions for the fiber distributions in wood.

Focus of this part of the thesis is to allow flow separation. Therefore, slightly modified Spalart Allmaras turbulence method (Spalart and Allmaras 1994) (Equation (3-7)) is used to let transition of the flow from laminar to turbulent, and to consider small fluctuations around the geometrical complications and knot clusters in timber boards without letting the development of the thick vortex layer in the model. Therefore, the production term (the first term in the right side of the Equation (3-7)) is kept relatively small by reducing the influence of the parameter, representing the magnitude of vorticities (Equation (3-10)).

$$\frac{d}{dt}\int_V \rho\widetilde{v}\,dV + \int_S \rho\widetilde{v}(\vec{v} - \vec{v}_m).\vec{n}\,dS = \int_V \rho c_{b1}\widetilde{S}\widetilde{v}\,dV - \int_V \rho c_{w1}f_w(\frac{\widetilde{v}}{d})\,dV +$$
$$\int_V \frac{\rho(1 + c_{b2})}{\sigma}\nabla.\{(v + \widetilde{v})\nabla\widetilde{v}\}dV - \int_V \frac{\rho c_{b2}}{\sigma}(v + \widetilde{v})\nabla.\nabla\widetilde{v}\,dV \tag{3-7}$$

In Equation (3-7), V is the arbitrary control volume with surface area of S. Nu- tilde ($\widetilde{v}$) is a viscosity like variable (Sparlat Allmaras variable) (Ferziger and Peric 2002, Aupoix and Spalart 2003, Spalart and Allmaras 1994). $\vec{n}$ is the normal vector to the surface S. $\vec{v}_m$ is the velocity of a moving mesh, and $\vec{v}$ is the velocity vector. The rest of the parameters of this equation are described in Equation (3-8)-(3-11), with the following constants: c_{b1}=0.1355, c_{b2}=0.622, c_{v1}=7.1, σ=0.6667, c_{w2}=0.3, c_{w3}=2, κ=0.41, c_{v2}=5,

and $c_{w1} = \frac{c_{b1}}{K^2} + \frac{1+c_{b2}}{\sigma}$ (ABAQUS 6.14c). Therefore, this method solves five equations for the analysis including four equations of the laminar flow and one extra equation for local viscosity, which provides a more realistic condition for the description of fiber pattern in wood compared to laminar flow. Thus, a very small eddy viscosity of 1e-05 is applied to the CFD analysis.

The f_w and turbulent eddy viscosity are computed using Equation 3.8:

$$f_w = g\left(\frac{1+c_{w3}^6}{g^6+c_{w3}^6}\right)^{\frac{1}{6}} \qquad\qquad g = r + c_{w2}(r^6 - r) \qquad\qquad r = \frac{\tilde{v}}{\tilde{S}\kappa^2 d^2} \tag{3-8}$$

$$\mu = \rho\tilde{v}f_{v1}$$

with:

$$\hat{v} = \tilde{v}f_{v1} \qquad\qquad f_{v1} = \frac{X^3}{X^3 + c_{v1}^3} \qquad\qquad X = \frac{\tilde{v}}{\hat{v}} \tag{3-9}$$

In this equation, μ is the molecular dynamic viscosity. The caret over the kinematic viscosity ($\hat{v}$) is inserted, to create a difference between the viscosity and velocity terms.

In Equation (3-7):

$$\tilde{S} = S + \frac{\tilde{v}}{\kappa^2 d^2}f_{v2} \qquad\qquad \text{with} \qquad f_{v2} = 1 - \frac{X}{1 + Xf_{v1}} \tag{3-10}$$

where:

$S = \sqrt{2R_{ij}R_{ij}}$ is the magnitude of vorticity (Corona et al. 2018), which is kept close to zero, and d is the distance of each point to the closest wall.

Additionally, we have:

$$R_{ij} = \frac{1}{2}\left(\frac{\partial u_i}{\partial x_j} - \frac{\partial u_j}{\partial x_i}\right) \tag{3-11}$$

By neglecting extreme vorticity development for wood and by covering big ranges of fluid domains (Re in Equation (3-12) (Pettersson et al. 2006, Franco et al. 2006)) with smooth transition in between, this method provides more reasonable conditions for prediction of fiber pattern in wood, especially in complex geometrical regions.

$$\text{Re} = \frac{\rho v d}{\mu} \tag{3-12}$$

Reynolds number in Equation (3-12) is a dimensionless number with d as the characteristic dimension (diameter), ρ is the mass density, v is the velocity, and μ is the dynamic viscosity.

However, it needs to be mentioned that the concepts of laminar flow and flow-grain analogy may still be sufficient for prediction of the fiber distribution in samples with few and well-spaced knots, where knots have more uniform geometrical shapes (Equation (3-13)). Therefore, timber boards in this thesis are categorized into two groups.

- Boards with few and well-spaced knots
- Boards with knot clusters

To be able to assign correct fluid model for predictions, the distances between knots need to be analyzed first. By considering different conditions for geometrical configuration of the knots and by analyzing influences of these features on deviation of fibers, the limit is chosen as follows:

$$d = \frac{1}{10}(y, z) \parallel d = \frac{1}{100}(x) \tag{3-13}$$

where x, y, and z are representing the global spatial coordinates of the boards, and d is the distance between knots in three spatial coordinate directions. Therefore, if the knots in a board are well-spaced, having a relative distance larger than the limit presented in Equation (3-13) in each direction, laminar flow can be used for the CFD analysis. If any of the limitations is not valid anymore for the distances between knots, the one-equation Spalart-Allmaras method is used for numerical simulations. Turbulent methods are preferred to be used For hardwood species with more complex fiber pattern, although they may have only few and well-spaced knots. The algorithm is schematically presented in Figure 3-2.
FC3D4 (ABAQUS 6.14b) elements are used for CFD analysis in this thesis. To prevent unsteady solutions due to the mesh refinement, convergence tests are performed to find the optimum mesh size for the boards. Non-uniform mesh is used by applying finer mesh around the obstacles and coarsening the mesh further away from them. Therefore, more detailed information can be extracted about the rotational behavior of the fluid after passing the obstacles.
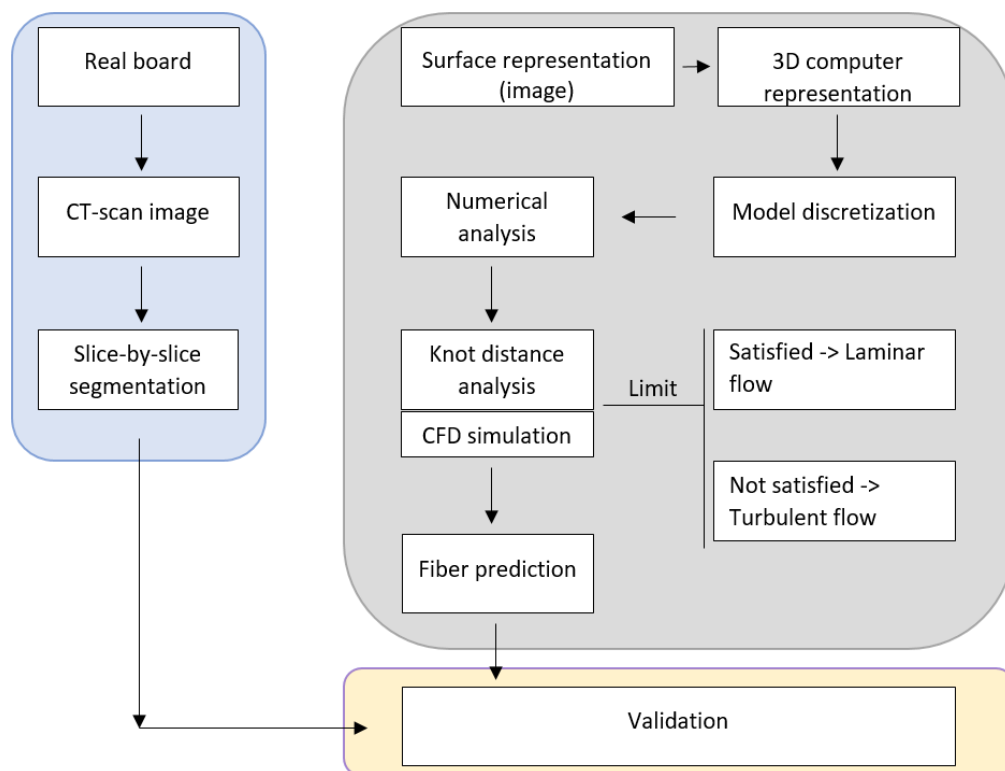
Figure 3-2: The schematic representation of the algorithm for the CFD analysis for predicting the fiber deviations.

3.3.2 Mesh sensitivity analysis

Three mesh resolutions are analyzed to check the mesh-resolution convergence. For this reason, the velocity map is plotted over two different paths along the width of the boards (Figure 3-3). The first path represents velocity variation in a clear-wood part of the board, whereas the second one represents velocity variation at a location with knot. This case is checked for velocities in x- and in y-directions. As shown in Figure 3-3, refining the mesh especially close to knot regions is resulting in smaller velocity variations, away from walls. This is in agreement with the theoretical expression of Equation (3-14),

where by increasing the mean velocity, the viscous sub-layer gets thinner, until a nearly flat profile is obtained (Chatterjee et al. 2010).

$$y = \delta_{sublayer} = \frac{5v}{u^*}$$

(3-14)

In Equation (3-14), u^* is the friction velocity.

Similar conditions are visible for knot boundaries, regarding the linear reduction and then increase of the velocities. In Figure 3-3b, the velocities are presented in transverse direction. These components have very small values, which are corresponding well with the actual conditions in wood. Fiber profile in wood contains mainly the x-component and is relatively small in the third direction. Comparing Figure 3-3b.1 and Figure 3-3b.2, an inverse behavior can be seen for the velocity variation. This is due to the fact that the knot causes an upstream and downstream flow, directly before and after the knot area respectively. Inverse components are activated to make the flow constant on the location away from the knot after passing this region.
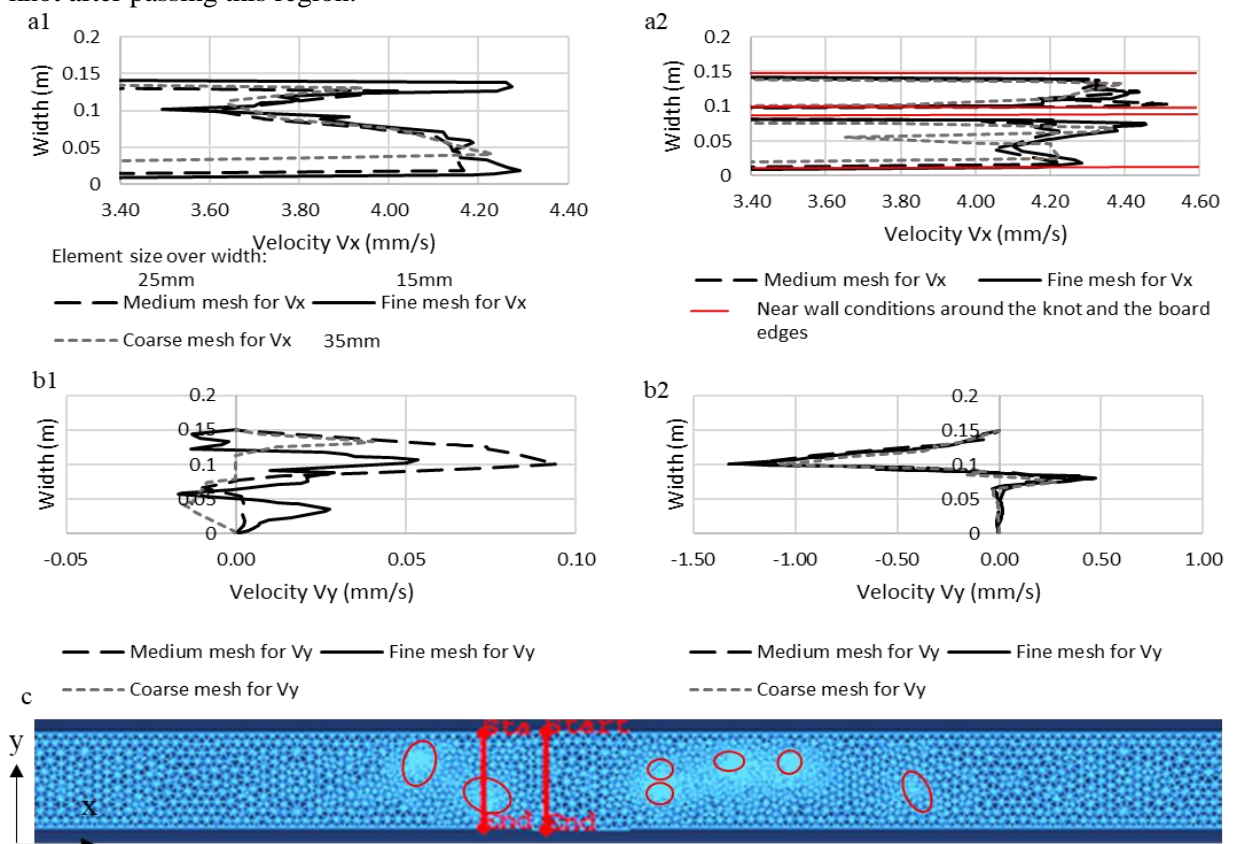
Figure 3-3: Effect of mesh refinement on the velocity in x and y directions of a spruce board. a) V_x, b) V_y. 1) The path along the clear wood part of the board, 2) the path along a location containing the knot. The red lines in the last figure show the locations of the paths in the clear-wood part and close to the knot through which the velocities are analyzed. The red lines in Figure 3-3a.2 show the locations of the wall conditions with zero velocities and respectively the linear slight increase and decrease of the velocities around that. The middle two red lines here show the locations, where the boundaries of the knot are located. The red circles in part (c) are the position and shape of the knots.

Dirichlet boundary conditions are used for the inlet, and velocities in ranges of $1 < v < 10$ mm/s, describing the fiber flow in wood, has been applied to the boards to analyze the influence of flow speed on estimation of the fiber pattern in wood. Higher velocities are causing stronger flow attack to the obstacles and are causing development of more complex vortices with a thicker vortex layer, which is not realistic for wood (Figure 3-4, with a fine mesh described in Figure 3-3). Therefore, flow speed is kept relatively small (4 mm/s). No-slip conditions are applied on the cones geometry, enforcing no-slip

along the knots. Walls of the domain are also set with no-slip conditions. Sensitivity analysis is performed to be able to represent the fiber pattern on the boundary of boards and to analyze the velocity field development along this region. For this reason, the width and the thickness of the boards are modeled 2mm larger than the actual dimensions, to be able to represent the stream function especially around edge knots. This dimensional variation is not used later for solid analysis and definition of the material anisotropic directions (Chapter 4).
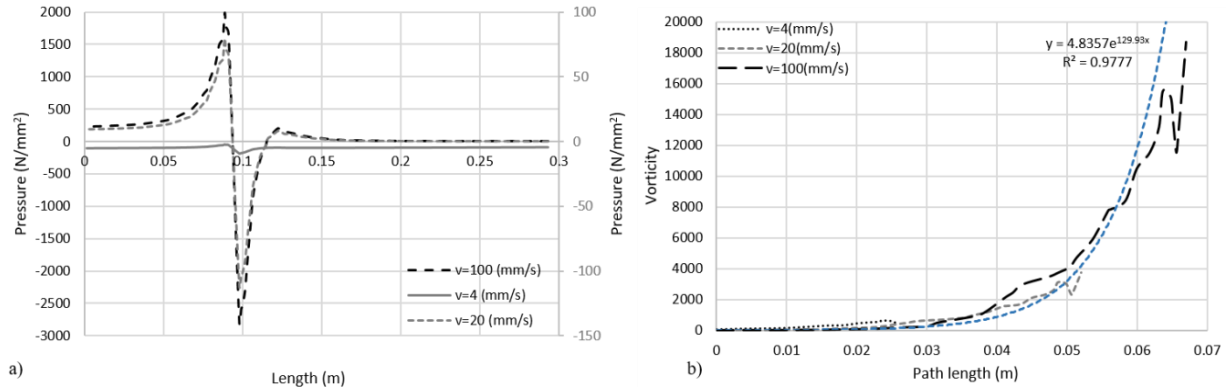
Figure 3-4: Variation of pressure and vorticity as a function of the flow speed. Mesh size is the fine mesh (presented in Figure 3-3)

As shown in Figure 3-4, two parameters, including the pressure and vorticity are analyzed along two different path lengths in the longitudinal fiber direction around a knot. It is shown in this figure that by increasing the flow speed, both parameters are increasing considerably. This increase has an exponential behavior for the vorticity.

CFD results are presented in two different forms (Figure 3-5). First, the velocity vectors, representing the magnitude of the velocities at each nodal point. Second, the streamlines, representing the flow path of the fibers through each board.

Information about the pointwise magnitude of velocities in each board helps to understand the coordinate rotations in more details and to define non-homogeneous fields for representing the orthotropic directions in boards via vector transformation.
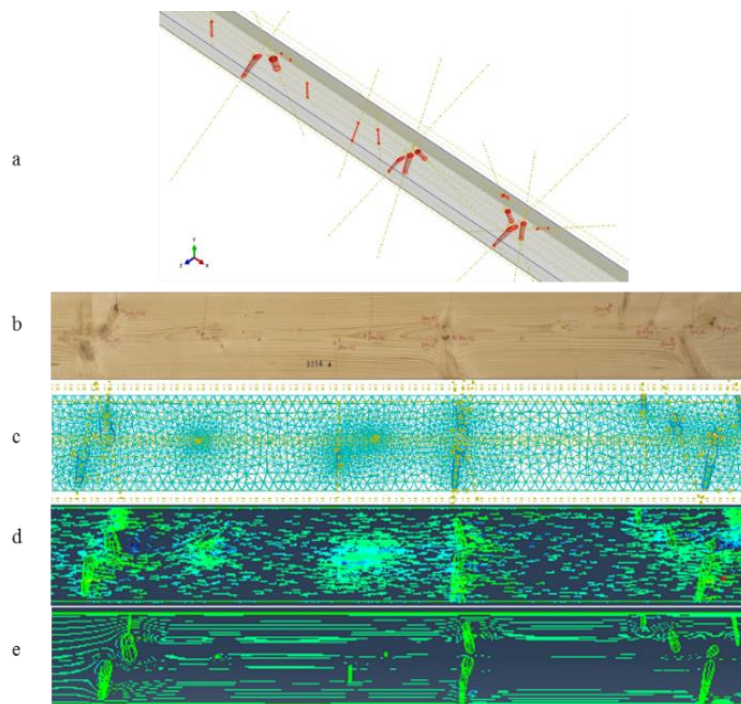
Figure 3-5: An example spruce board. a) Geometrical model with knot locations, b) real board, c) mesh around knots, d) vector plot, e) stream lines.

3.3.3 Upward and downward flow analysis

Influence of upward or downward flow on the prediction of fiber pattern in boards is checked to analyze the sensitivity of the model for fiber prediction. This analysis includes similar boundary conditions for both cases with the difference in the direction of inlet and outlet. In the downward flow, the inlet is on located on the opposite side of what has been explained before. A relatively small difference is found between the flow path of the fibers in both cases due to:

1) the geometrical rotations of the material imperfections
2) stagnation point
3) the flow hit to the obstacles
4) the chaotic flow development after passing the obstacle in the simulations

Comparing absolute values of the velocities in all nodal points of the model in both directions, deviations of 0.045% and 0.5% are found in flow paths of both directions in transverse y- and z-directions, respectively. This value is on an average 5.65% for x-direction. Percentage of the variation is increasing to 13.2% for samples with knot clusters. Therefore, downward flow model may present the wood fiber distribution slightly better. Due to the layer-wise growth of the tree, components in y- and z-directions are relatively small in real wood (with x≈2y and x≈4z). Similar behavior can be seen in the simulation results (appendix Figure A1.1).

3.4 Results

3.4.1 Description of wood fiber flow in a 3D space

Before validating the model with CT-scan images, results of the global fiber predictions are compared to the results that are obtained from ultrasonic images (Figure 3-6) (Kovryga et al. 2019). It is shown in Figure 3-6 that a reliable relation exists between the results of these both cases. Therefore, the numerical method is capable of predicting the global fiber profile of the boards. It is also shown in this figure that fiber pattern of softwoods has a more uniform structure compared to the profile of hardwoods, although more knots can be found in softwoods compared to hardwoods. Knots rarely influence fiber profile in hardwoods.
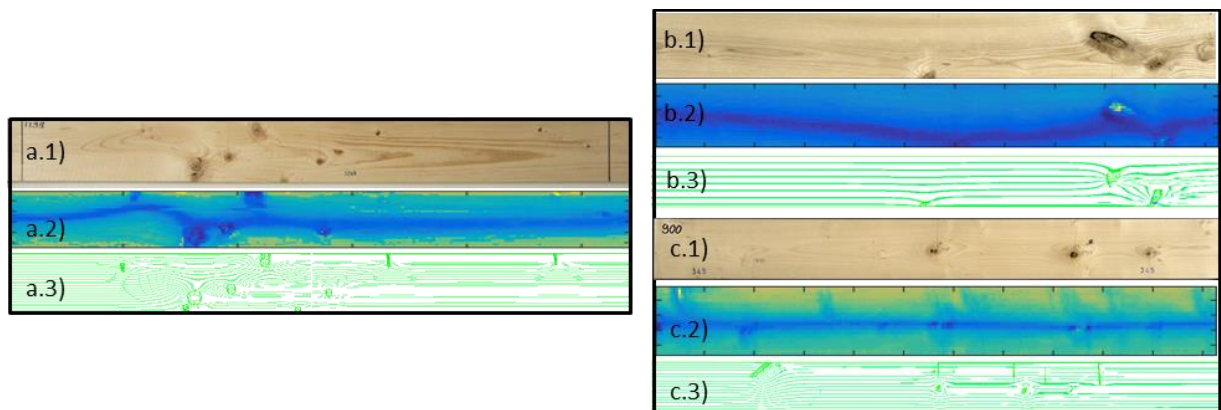
Figure 3-6: Softwood sample 2246 in reality (a.1), Ultrasound (a.2), fiber profiles (a.3). Ash sample (b) and Maple sample (c) with ultrasonic images and simulation results.

Estimation of the fiber pattern is an important step before predicting the local stiffness variation in boards. Therefore, validation of the simulation results at each local material point is done by using the slice-by-slice segmentations from CT-scan images. As an example, three surface-cuts are made in example boards (shown in Figure 3-7 and appendix Figures A1.2-6), on the upper and lower surfaces, as well as the mid-surface in the depth direction. The results of upward and downward flow directions

are compared in each case. These examples include cases with knot clusters as well as cases with well-spaced knots.
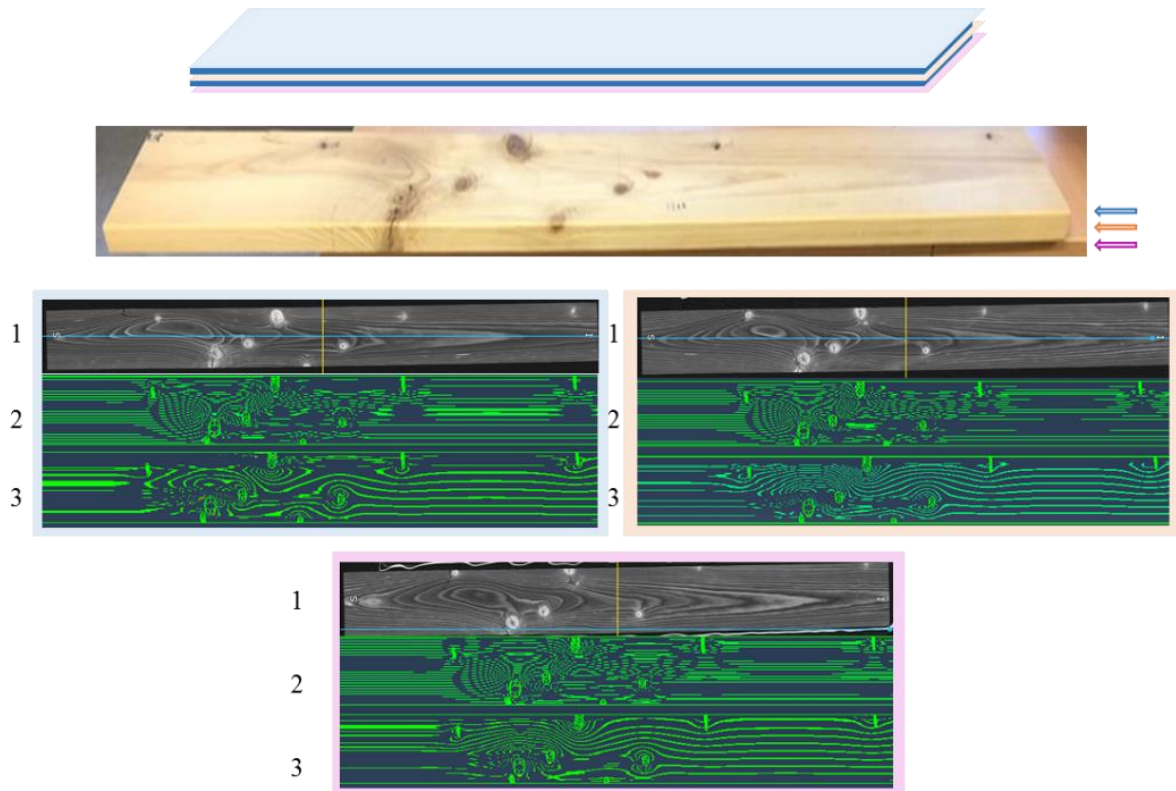
Figure 3-7: Representative spruce sample for validation of the CFD model with CT-scan images. A colour map is used in this figure to show the location of different surface cuts in a board. 1 in each case is the CT-scan image with the surface cut on top of the board (blue arrow), the internal middle cut (orange arrow), and the surface cut on lower side of the board (purple arrow), respectively. 2 and 3 are the numerical upward and downward flow conditions on each surface respectively.

Difference between the results of upward and downward flow directions for boards with well-spaced knots is minimal on all surfaces. However, downward flow is representing the fiber deviation for cases with knot clusters slightly better (Figure A1.2-4).

To validate optimum flow time, stream lines of laminar and turbulent flow are compared to the CT-scan images (Figure 3-8). As shown in Figure 3-8, the CT-scan images and the flow methods are compared to each other based on the angle of attack and angle of separation that are developing around each natural feature. Statistical comparison of these results show a higher relation between these parameters of the turbulent flow and the real fiber pattern.

Although laminar flow (Figure 3-8a) may be enough for prediction of the fiber pattern between two well-spaced knots, but it is not enough for describing the more complicated fiber deviation that is existing between the knot clusters. A thick layer with extreme vortices is also not being developed for wood. Therefore, turbulent flow model (Figure 3-8a.4) is also not a realistic model for description of the fiber deviation in wood. The flow field, presented in Figure 3-8a.3 is the best-fit representation for the fiber pattern in wood.

To validate the numerical model and in order to show the influence of turbulent component on improvement of the prediction quality for fiber pattern in wood, different aspects are analyzed and compared (Figure 3-8). Parameters such as flow rate, angle of attack of the flow, angle of rotation of the coordinate system of an obstacle and the length between the highest deviated fiber point after stagnation till the position where fibers are becoming straight are checked for laminar (Figure 3-8a.2.1) and semi-turbulent flow conditions (Figure 3-8a.3.1). Comparing the CT-scan images in such cases with both

fluid models, it is shown that length is well estimated by the turbulent model (shown with red arrow in Figure 3-8a.3.1), whereas this parameter is underestimated with the laminar model (Figure 3-8a.2.1). Angle of attack (blue arrow) is presented well with both models. Finally, the yellow arrow is well estimated with the turbulent model (Figure 3-8a.3.1). This arrow shows a sharp angle to the global coordinate system in the laminar flow model, which causes fibers to return to their straight configuration as soon as they cross the obstacle. This is due to neglecting the flow separation, when using the laminar model.
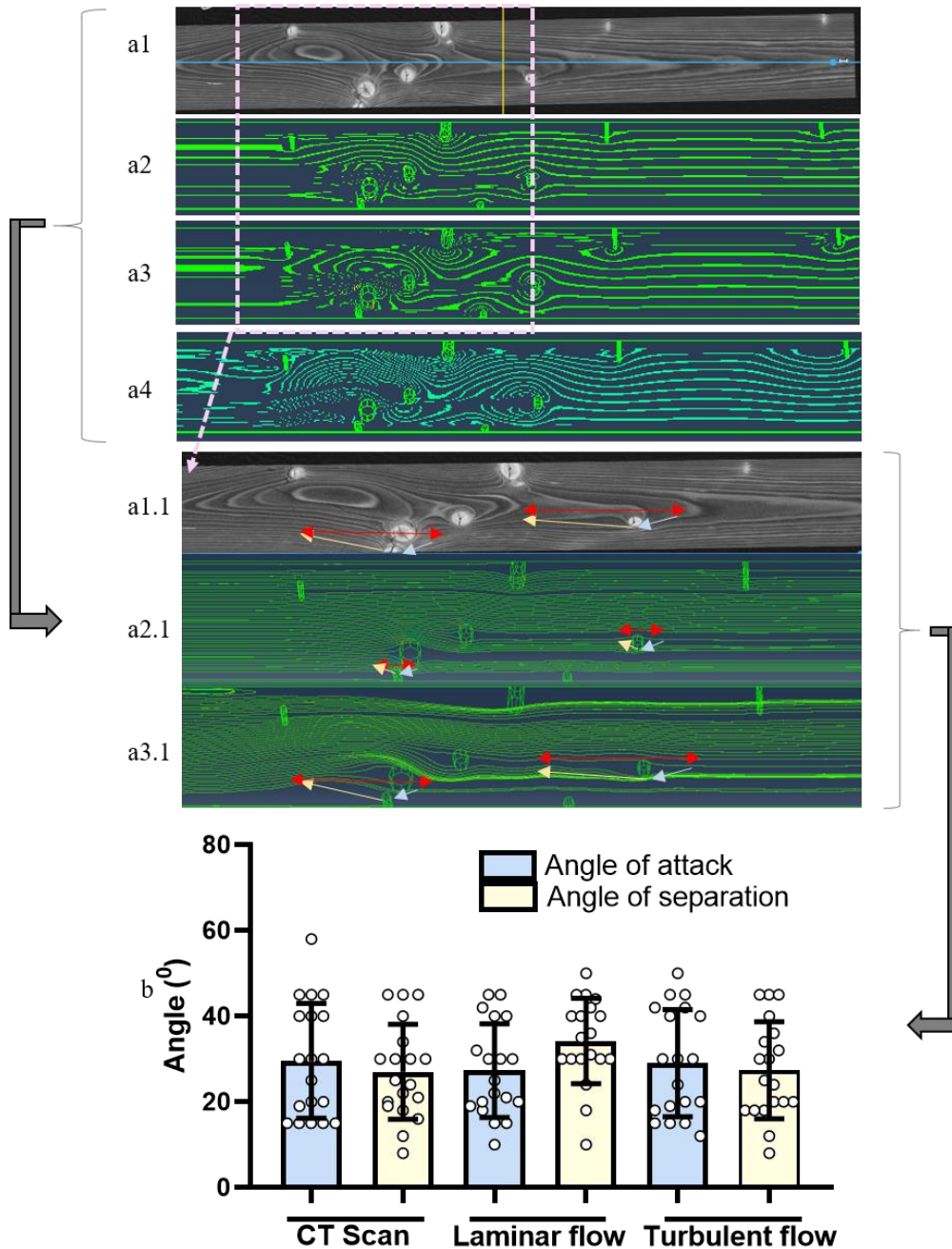
Figure 3-8: Example spruce board for flow selection (a), comparing the CT-scan image (a1) to laminar flow (a2), semi-turbulent flow (based on Eq.(3-7)) (a3), and turbulent flow (a4). The second pallet is the 2x zoom to a1 and a2, comparing the fiber pattern with the data from the CT-scan. Red arrow in this figure is the total length of the fiber disturbance around the obstacle, showing the board length around the knots where the fibers are affected by the obstacle. Blue arrow is the angle of attack, showing the angle of the fiber while hitting the obstacle. The yellow arrow is the angle of separation, showing the length to reach straight fibers again after passing the obstacle. Statistical comparison of both flow methods with the CT scan images regarding the angle of attack and angle of separation of the fibers (b).

In addition, by comparing magnitude of the transverse vectors in x-z and x-y planes, it is found that the previously used laminar flow and the recently developed semi-turbulent methods are both reasonably well for predicting the fiber pattern in x-z plane. However, this condition is valid for cases where only perfectly cylindrical knot shapes are visible in boards, whereas it is not valid for most of the cases where knot clusters and strong inclinations are present. In such conditions, fibers are not layer-wise uniform, but are slightly dislocating in different growth layers. Therefore, comparing both flow types in such conditions, it is shown that laminar flow is not capable of showing this effect in the third direction. This condition is not representative for a 3D heterogeneous case like wood. However, the semi-turbulent flow is allowing for flow separation around the obstacles, making the slight dislocation of the fibers possible. Another comparison is made for hardwoods in Figure 3-9.
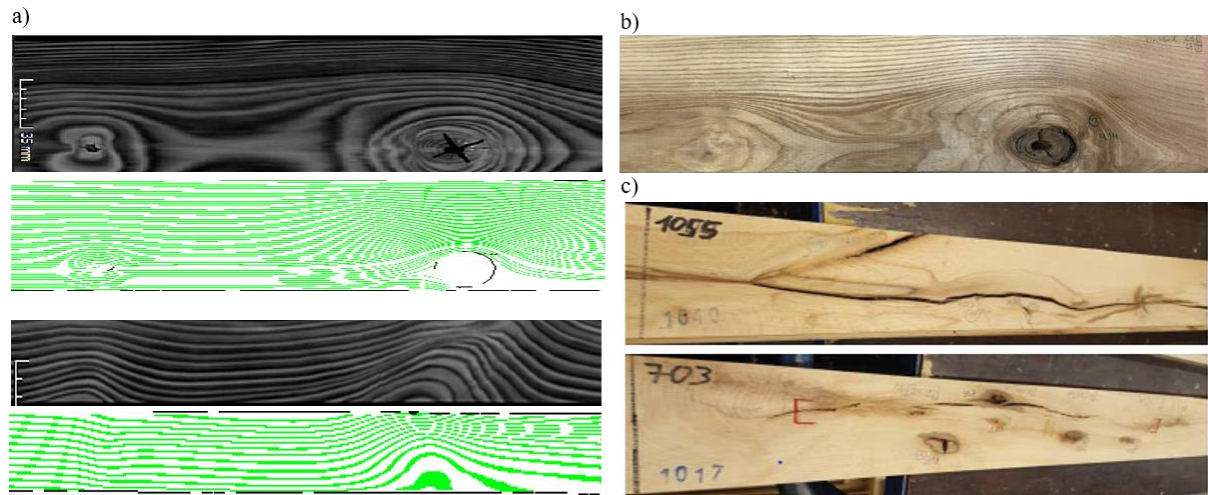
Figure 3-9: Fiber pattern in simulation of an ash board (a), ash board (b), low quality beech boards with extreme fiber deviation (c).

It is shown in Figure 3-9 that even for samples of hardwood species with fewer knots (such as the beech boards, modeled in this thesis (Figure 3-9.c)), a more complex fiber pattern can be expected. Such complex configurations with few knots could only be captured numerically by using turbulent methods for simulation. It is shown in this figure that the prediction of fiber profile can be done reasonably well for hardwoods as well. To show the longitudinal stream functions around knots, two paths are defined in this thesis in different locations over the width of the boards (Figure 3-10).

Knots have generally different shapes and sizes, they are not geometrically constant (i.e. they are rotated and deviated from their uniform cylindrical shapes), and they are fully immersed in the fluid domain. Therefore, the stream function varies considerably in each material location. For this reason, two paths are selected in boards to analyze velocity variation in the mainstream direction of boards, where no-slip conditions are applied to the walls and over the surfaces of the knots (Figure 3-10.b). These two paths cross three and four knots (aligned in their pathways) respectively. Time averaged velocity variation along these both paths shows that the average velocity remains constant in the clear wood, where no knots and defects exist. Around knots, the magnitude of velocity varies, reaching to zero on the knot and board boundaries (Figure 3-10.c). Starting from one side of the board, a linear increase in the velocity can be observed, reaching to the maximum applied velocity for the simulations. This is a common behavior of turbulent flow, where the region very close to the wall shows a linear velocity profile, which is dominated by viscosity effects. Velocity is constant in the clear part of the board with no knots. Again, a linear velocity reduction can be seen in locations close to knots, which is approaching zero on the knot boundaries. The velocity is increasing linearly again after passing the knot area, reaching to a constant value for the clear part and reducing to zero close to the wall boundary of the board. Therefore, the resulted velocity map may be a good estimator for prediction of the size and shape of knots.
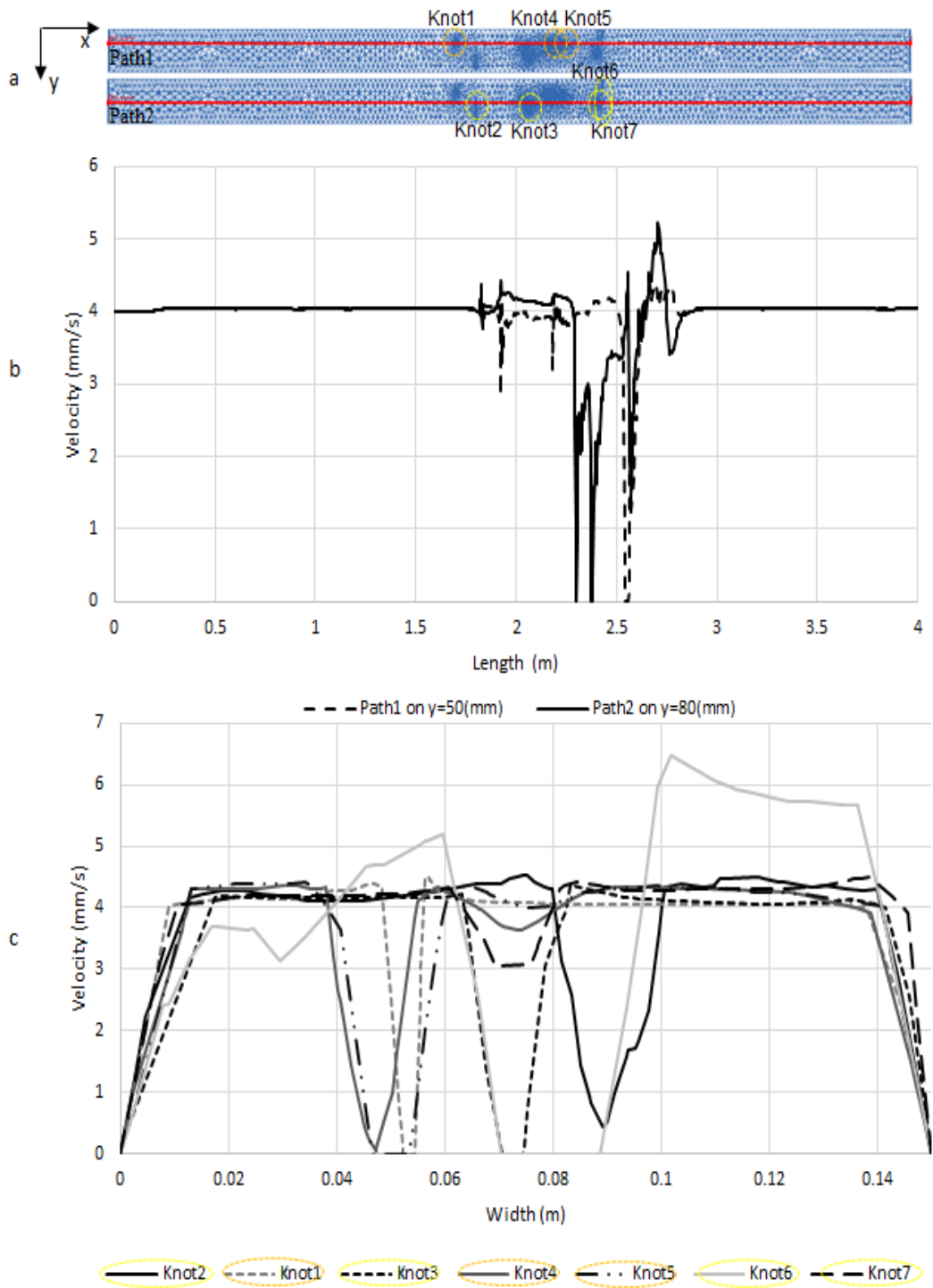
Figure 3-10: Fiber patterns over two longitudinal paths of an example spruce board. (a) Path location on width=50 (mm) and width=80 (mm). (b) Time averaged velocity magnitude along the two defined paths, (c) time averaged velocity variation along vertical paths over the width of the spruce board.

Iso-surfaces of velocity variation (Figure 3-11.a) and the variation of turbulent component $\tilde{v}$ (Figure 3-11) provide more information about the local and global fiber pattern. Turbulence concentration in the region after passing the imperfections may affect velocity measurements in these locations (Chen et al. 2016). Small concentration of this component in the region of imperfections results in a small turbulence in flow after passing the knot area, which allows for representation of the fiber deviation around knot clusters.
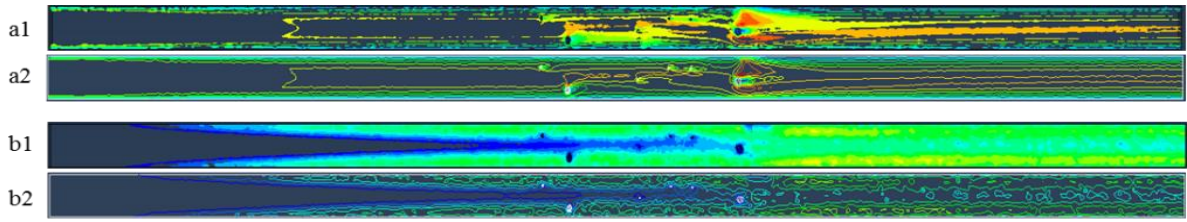
Figure 3-11: Velocity and ṽ map of an example spruce board. a) The mainstream velocity plot, b) the ṽ plot, 1) iso-surface representation, 2) line representation of the variations.

Analyzing the drag pressure along the two longitudinal paths (as described in Figure 3-10) shows a pressure increase by hitting knot volumes and a decrease after passing these obstacles (Figure 3-12).
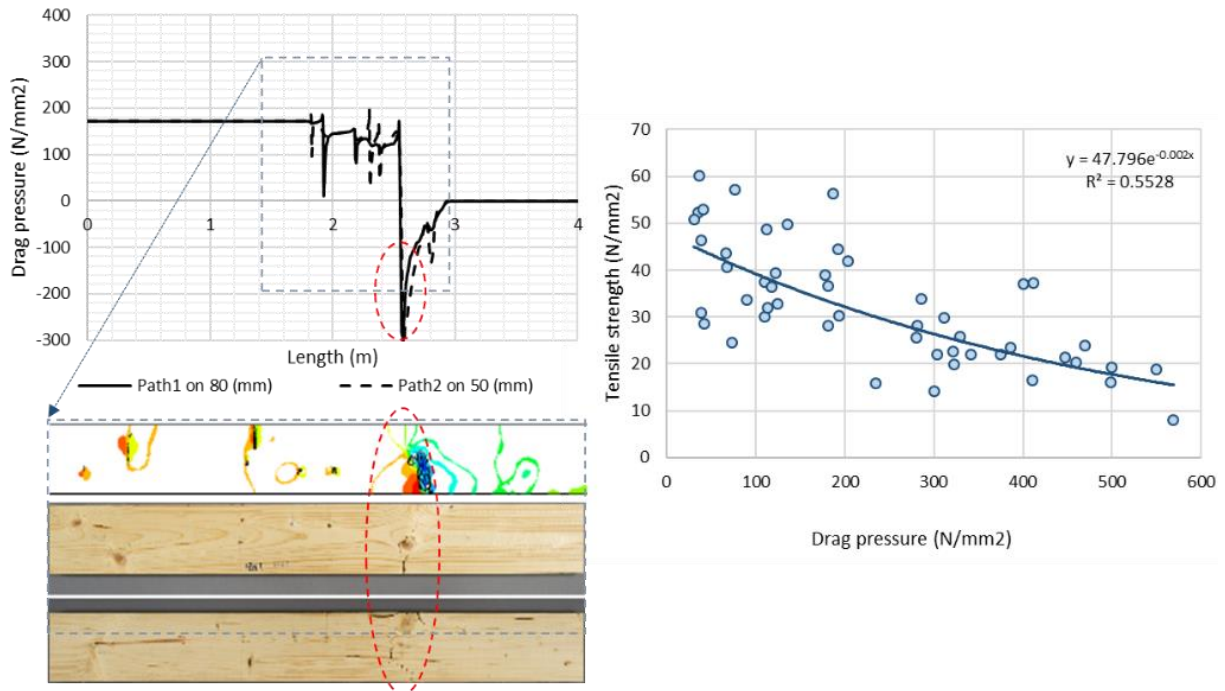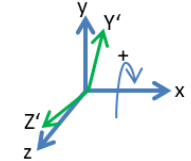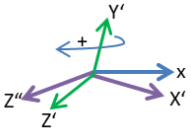
Figure 3-12: Pressure at locations where the flow is hitting knots in 50 representative boards of spruce, Douglas fir, beech, ash and maple (10 samples each). In each figure, pressure variation along two longitudinal paths (on the width of 50 and 80mm) is analyzed. By having a closer look to the knot region in the test length, iso-surface of pressure is compared to the pictures from the upper and lower surfaces of the boards. The location of material failure is marked in this region. Red ellipses in each figure show the location of the highest developed pressure, which corresponds well with the location of failure in boards. The drag pressure parameter shows a remarkable correlation with tensile strength.
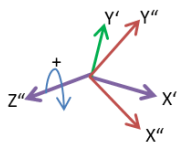
Although the pressure increase around knots is generally not considerable, a strong pressure increase is observed at locations, where knots are located relatively close to each other (Figure 3-12). This condition is valid for the last knot in Figure 3-12, which is located along each path in the longitudinal direction. It is shown in this figure that the geometrical configuration of the rotated edge-knot, located in the surrounding of a straight knot causes a strong variation in pressure amount, which may also help to predict the failure location in material. Failure may occur at a location, where the maximum pressure is reached in the simulations (Figure 3-12). In total, 50 boards are selected randomly for analyzing the relation between the developed drag pressure (especially around knot clusters) and the tensile strength, which is available from tensile tests. By using the drag pressure values of the samples in a regression analysis with the tensile strength, a negative relation is found between these both parameters (Figure 3-12). This relation may confirm a parameter that may be used as a predictor for tensile strength in macro-scale solely based on fiber pattern. Some more comparisons between the actual failure paths of the boards with the prediction of the failure based on the increasing of the drag pressure are presented in Figure A1.7-10.

3.4.2 Defining the orthotropic directions of the material

Stiffness properties of wood are varying at each material point and in each coordinate direction. Due to the heterogeneous structure of this material and the influence of different natural defects, scatter of these variations is high for wood, which is causing more difficulties in predictions. Total fiber pattern and its local deviation around knots is predicted by performing CFD analysis and by calculating the local velocities at each nodal point in the model. Based on the predicted fiber pattern, local orthotropic material directions are implemented numerically. In order to apply the coordinate directions, rotational angles around each coordinate axis are calculated based on the magnitude of velocities at each nodal point. Rotations are considered positive in the clockwise direction and negative in the other. Velocity values are integrated over each element and the rotated coordinate is assigned on the center of each element (Equations (3-15) to (3-17)). Surfaces are assumed to be linear in this case and integration is done here, as the location for mean value of the vectors is not necessarily found in the center of gravity of the elements.

$$\alpha = \lim_{1 \to n} \arctan\left(\frac{\int_1^i v_y}{\int_1^i v_x}\right) \tag{3-15}$$

$$\beta = \lim_{1 \to n} \arctan\left(\frac{\int_1^i v_y}{\int_1^i v_z}\right) \tag{3-16}$$

$$\gamma = \lim_{1 \to n} \arctan\left(\frac{\int_1^i v_z}{\int_1^i v_x}\right) \tag{3-17}$$

In Equations (3-15) to (3-17), i represents the number of the nodes per element and n is the total number of the elements in the model.

By knowing the ratio of these variations for each element, a discrete field is defined for each board, including all elements and orthotropic directions of the material at each local point in boards. Therefore, material orientation can be defined locally in solid analysis showing the stiffness distribution along the board.

An example board is shown in Figure 3-13, where a process of the full set of analyses, from CT-scanning of a board to the geometrical reconstruction, prediction of the fiber profile and prediction of the stress distribution in boards is provided. It is shown in this figure that higher stresses are developed especially around edge knots. These stresses are then developing through the path of smaller knots toward the other side of the board, causing global failure of the material. Path of the stress development is corresponding well with the failure path, shown in the same figure. Additionally, an ultrasound image of this board is shown in Figure 3-13.g. This figure shows an actual global fiber pattern of the board, which can be used for validation of the predicted global fiber pattern.
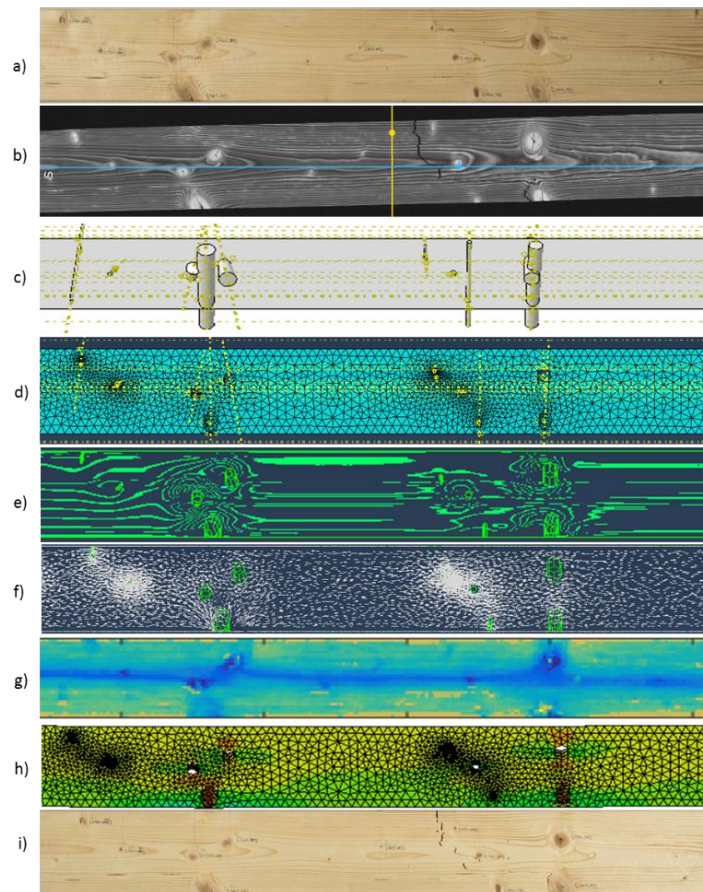
Figure 3-13: Complete procedure of the numerical analysis. Part (a) of this figure represents an example of a spruce board with the knots. Part (b) is the CT-scan image of the same board. (c) Represents the geometrical reconstruction of the board, with an exaggerated view of the knots. Part (d) is the tetrahedral mesh, used for the numerical analysis, with a finer mesh around the knots. Parts (e) and (f) are the numerical prediction of the fiber pattern from CFD analysis in the stream form (e) and the magnitude vector form (f). (g) is the ultrasonic image of the board, representing the total fiber profile of the board. (h) is the analysis of the board under a uniform tension and development of higher stresses especially around edge knots. The last picture (i) represents actual failure of the board.

3.5 Prediction of fiber pattern based on the stresses along the fibers

A study in 2013 (Lang and Kaliske 2013), concentrated on comparing the numerical models for prediction of fiber pattern based on flow-grain analogy and principal stresses. The results of this study have shown that the fiber orientation around a round knot is similar for both models. This is mainly valid for case of a single circular-shaped knot, or in cases where the geometrical features are well-spaced from each other. However, conclusions may be slightly different in cases of knot clusters or in cases where knots with different geometrical configurations are located relatively close to each other. Therefore, some stress paths are defined and analyzed around two randomly selected knots along a board to confirm the requirement for usage of turbulent model instead of the laminar one for prediction of the fiber flow in wood. As an example, a spruce sample is selected for this analysis. The board contains seven knots in total. The first selected knot has a circular shape and the second one has an elliptical shape over the surface of board. Knots are not creating clusters in this case, but they are located relatively close to each other. The geometrical configuration of knots and their location in this board influence the global fiber profile of this board. Therefore, the local fiber pattern around each knot is influenced by the other knots that are located in the vicinity. Situations may get slightly more complicated if knots are making clusters (similar to the Douglas fir boards, discussed later in this thesis), or in cases where they are creating extreme long geometrical configurations with complex spatial rotations (shown later). In

general, nine paths are defined around each of the selected two knots. One path is passing through the center of the knot, two paths crossing the knot boundaries, and three separate paths, symmetrically defined on the sides of knots with distances of 5mm, 20mm and 40mm from the boundaries. Longitudinal stresses are analyzed along each path, representing the stresses along fiber direction. It is shown in Figure 3-14 that although the paths are defined completely symmetrically around knots, but the developed stresses are not uniform along these symmetrically located paths. Small deviations are observed between the stresses of both similarly distanced paths from the knot boundaries. As the board is under uniform tension, higher stresses are developing in each case around the knot boundaries over the path that is passing through the center of knot. Stress plot along this central path is relatively symmetric for the circular knot, whereas similar stress pattern tends to follow the rotational direction of knot in the elliptical case. Analyzing stresses that are developing along the other paths show continuity of this tendency for creating non-symmetric stress distribution pattern. This deviation, in addition to the non-symmetric stress pattern along paths with similar distance to the knot boundaries confirms the fact that the stress development around each knot is affected by the stresses that are developing around the other knots. Thus, existence of multiple knots in a board distracts the uniform stress distribution through the board. Due to this reason, a laminar flow, which considers complete symmetry around the imperfection, is not enough for describing the complicated orthotropic directions in wood.
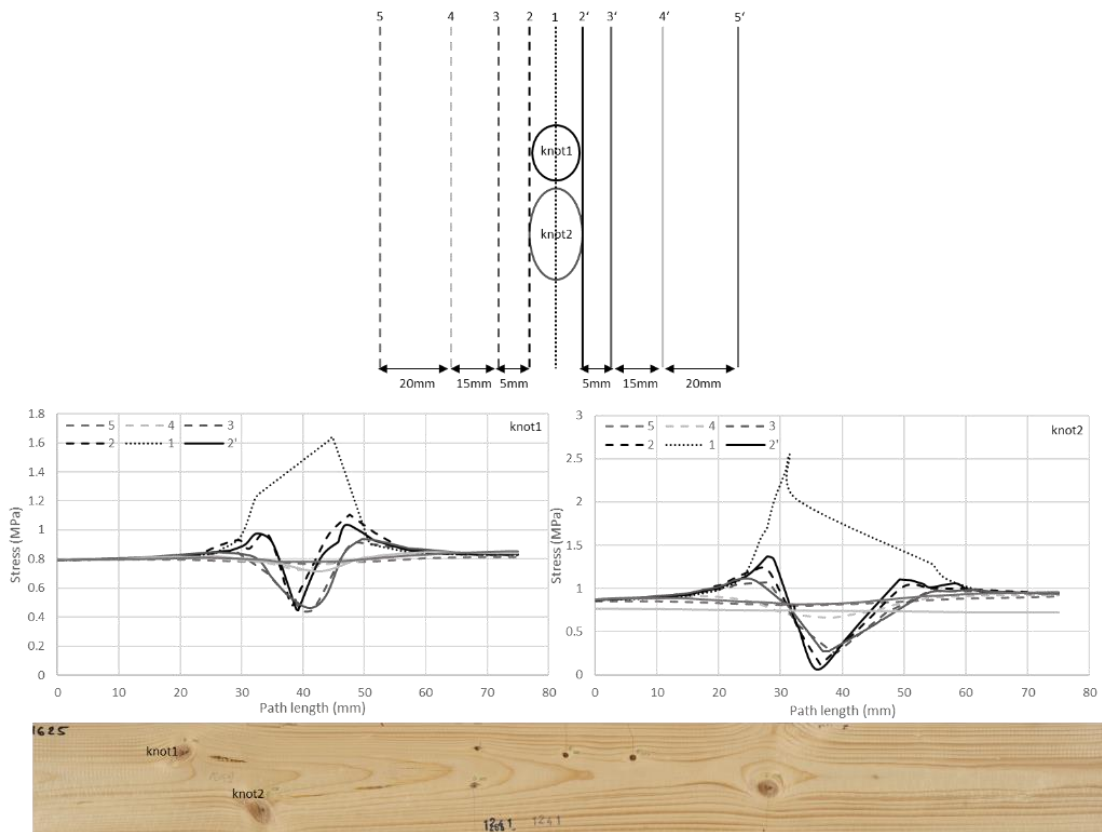
Figure 3-14: Non-symmetric variation of the stresses around two random knots.

3.6 Discussion about fiber pattern in wood

In contrast to a wooden tissue with a simple 2D structure, the 3D structure of wood has more non-uniform geometrical pattern with complicated heterogeneities that cannot be modeled with simpler models. Therefore, previously developed flow-grain analogy (Goodman and Bodig 1980, Baño et al. 2010) may fail to describe the layer-wise fiber pattern in wood. Newly developed material models (Jenkel and Kaliske 2013, Baño et al. 2010, Foley 2001, Lukacevic and Füssl 2014) consider the 3D

wood pattern by implementing streamlines of the fluid flow or developing the 2D layer-wise mesh structure (Jenkel 2016) to predict the fiber pattern and correspondingly the anisotropic material directions for wood. A more detailed study is performed in this thesis to analyze the influence of geometrical complexities due to knot accumulations in softwoods and hardwoods on fiber pattern. It is shown that streamlines of the laminar flow may be enough for prediction of the fiber pattern in cases with well-spaced and uniformly shaped knots (Goodman and Bodig 1980, Foley 2001). However, the models need to be improved to include 3D vector components of the non-linear flow for representation of the complex geometrical configurations. Scatter of fiber pattern in wood for different species makes it more complicated to model fiber deviations using laminar models and to apply the discussed simplifications. In such conditions, small turbulence can be seen in fiber pattern, which is not layer-wise uniform. This turbulence is slightly sliding in the coordinates of the transverse directions. Such conditions require semi-turbulent models to allow flow separation around knot clusters.

CT-scan images are used for validation of the numerical results and for validation of the predicted 3D fiber pattern. Extreme fiber deviation, for instance caused by top rupture or compression failure, can be a severe strength-reducing characteristic of timber (Kuisch et al. 2012, Hunger and Van de Kuilen 2018), which is difficult to be captured numerically. By looking at the longitudinal direction, the fiber angle is checked around knots in CT-scan images, as well as in both fluid models. It is shown that laminar flow similar to the turbulent flow can capture the angle of fiber deviation before the obstacle (knot). However, laminar flow causes an immediate reordering of fibers after crossing the obstacles. Sharp reordering of fibers into the straight direction overestimates the fiber angle after crossing the knot. Turbulent flow solves this problem by allowing the flow separation and letting the fibers to reorder in a longer period of time.

By assuming existence of a fluid flow around growing cells (Maquer et al. 2014, Ruffoni and van Lenthe 2017, Pistoia et al. 2002, Kowalczyk 2010), stream-lines of the laminar flow (Goodman and Bodig 1980, Jenkel and Kaliske 2013) represent the fiber pattern in timber. It is shown that this hypothesis is valid in cases of a perfect board with well-spaced knots in uniform cylindrical shapes. As soon as clustering effects appear in wood, the mentioned hypothesis starts to overestimate the fiber angle. Therefore, prediction of fiber behavior after crossing the obstacle may not be accurate when using the laminar flow. Additionally, fiber dislocations and rotations are observed in different cuts, showing the validity of the applied semi-turbulent model even on the boundary of a single knot.

By developing the 3D structural model of wood based on the flow-grain analogy (Cramer and Goodman 1982), different studies concentrated on the structural modeling of wood and predicting the strength reduction and failure, resulting from structural non-uniformities (Cramer and Goodman 1986, Goodman and Bodig 1978, Zandbergs and Smith 1987, Foley 2001, Hackspiel et al. 2014, Lukacevic and Füssl 2014, Guindos and Guaita 2013). In this part of the thesis, only flow parameters are used as parameters for strength predictions. However, in the next chapters of this thesis, different numerical parameters are presented that can be good strength predictors for wood. For this reason, the drag pressure is visualized around knots and the maximum pressure as well as its developed path is compared to the failure location of the boards from physical experiments. It is shown that a relatively good relation exists between the predicted parameter and the tensile strength of the boards, which may reduce the computational costs for implementation of damage models for prediction of failure paths.

Comparing fiber orientation based on both methods, including the flow-grain analogy and principal stresses (Foley 2001), confirmed similarity of both methods in presenting this parameter around a round knot. Analyzing the developed maximum drag pressure around knots in this study confirms this condition as well. However, this discussion is not valid anymore in cases of more complex geometrical conditions, for instance cases with knot clusters.

Chapter 4 Virtual strength prediction process

4.1 Introduction

Due to complex structural and mechanical behavior of wood, the material needs to be strength graded before it can be used for structural applications. Different methods are available for strength grading of wood. One possible method is the visual grading method, which is done by measuring visible parameters that are appearing over the surfaces of the boards (Stapel and Van de Kuilen 2013, Stapel and Van de Kuilen 2014a,b). The second approach is the machine grading method, which is done by measuring the eigenfrequency and density to calculate dynamic modulus of elasticity (Stapel and Van de Kuilen 2013). Each of the above-mentioned methods may face some measurement errors, which may reduce the prediction accuracy. Therefore, aim of this chapter of the thesis is to provide a more technologically advanced computer-based method for prediction of the tensile strength of timber.

After reconstruction of the geometrical model of boards and prediction of the fiber pattern around the material heterogeneities, four numerical parameters are extracted to be used for tensile strength predictions. These parameters include the Stress Concentration Factors (Khaloian Sarnaghi and Van de Kuilen 2019a, c) and the dynamic MoE (Khaloian Sarnaghi and Van de Kuilen 2019b, c), described in the following sub-chapters. Extracted numerical parameters are used in a non-linear multiple regression analysis and a mathematical equation is provided for the prediction of tensile strength.

4.2 Stress Concentration Factors (SCFs)

As mentioned previously, knots are the main tensile strength governing parameters. Due to a strong fiber deviation around these natural features, higher stress peaks are developing around knots, which may cause failure of the material. Developed stress peaks are visible around single knots as well as the knot clusters. It is very difficult to make a clear judgement whether peaks are always in the region of knot clusters or the biggest knot. Additionally, many different parameters, such as the natural fiber pattern or the geometrical rotation (non-uniformity) of knots, may be the factors that are affecting development of these stress peaks.

In contrast to a uniform 2D case, calculation of the stress peaks in 3D anisotropic and heterogeneous material may be more difficult. Therefore, in this thesis three mathematical equations are provided for calculation of the Stress Concentration Factors (SCFs), by considering average and maximum stresses that are developing around single knots and knot clusters over the actual cross-section of the knots or their projected cross-sections (Khaloian Sarnaghi and Van de Kuilen 2019a). The equations are briefly discussed here and are presented in details in Paper 1 (Khaloian Sarnaghi and Van de Kuilen 2019a). All samples are tested under uniform tension in fiber direction.

$$SCF_1 = \max(\sigma_{sim}.\frac{A_{knot}}{A_{total}})$$

$$SCF_2 = \sigma_{avg}.(\frac{A_{total}}{A_{total} - A_{knot}})$$
(4-1)

$$SCF_3 = \sigma_{avg}.(\frac{A_{total}}{\left|A_{total} - A_{projected}\right|})$$

Parameter σ_{sim} in these set of equations represents the maximum tensile stress parallel to the fibers in board under an applied nominal stress. Here, σ_{avg} is the average normal stress in the clear wood part, A_{knot} is the actual cross-sectional area of the knot and A_{total} is the cross-section of the board (Khaloian Sarnaghi and Van de Kuilen 2019a).

Linear relations between the tensile strength in fiber direction and each of the single SCFs are presented in Figure 4-1. Linear relations are analyzed here to be able to compare the results to the available linear relations from current standards in grading. Non-linear relations are presented in Khaloian Sarnaghi and Van de Kuilen 2019a. Non-linear relations are shown to describe the relation of the SCFs and the tensile strength better (as presented in Figure 2-12 regarding the non-linear behavior of the interacting stresses).
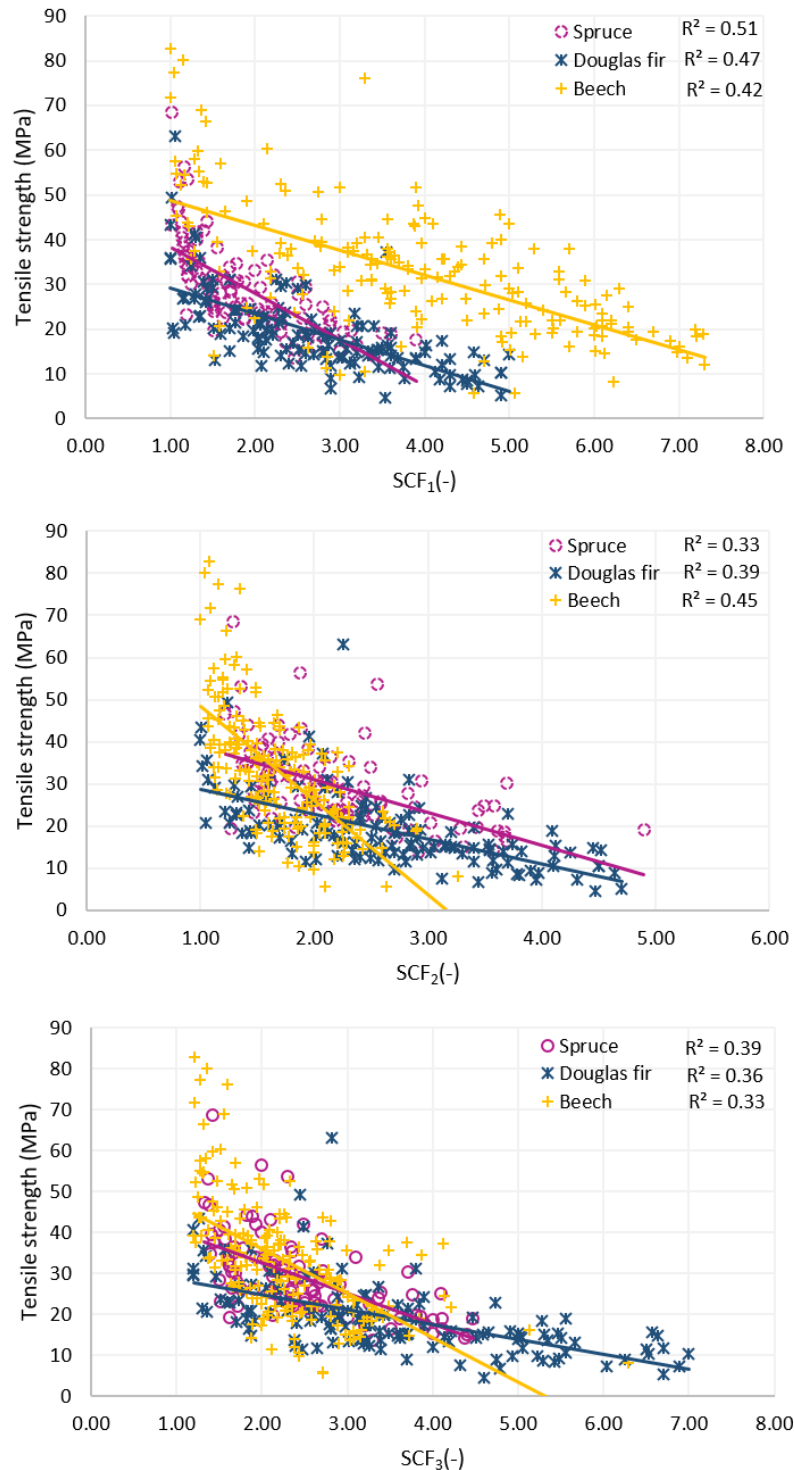
Figure 4-1: Linear correlation between the tensile strength and single SCFs.

Coefficient of determination is higher, when using the numerical SCF parameters together with the tensile strength of the boards in a regression analysis, compared to when the visual grading knot parameters (TKAR, DEB and DAB) are used in a similar analysis (Table 5-1-Table 5-3 and Khaloian Sarnaghi and Van de Kuilen 2019a). Therefore, prediction accuracy and quality are improving by implementing the numerical approach in this case.

A comparison between linear multiple regression analysis among the virtual and visual knot parameters with tensile strength is shown in Figure 4-2. Improvement of the prediction quality is shown in this figure, when using the numerical approach. Lower quality of predictions based on the visual knot parameters may be caused due to possible measurement/human errors that may occur during visual grading. Such problems are being solved by using computerized calculation methods when using the numerical approach. Coefficients of the linear set of equations of Figure 4-2 are presented in Table 4-1.
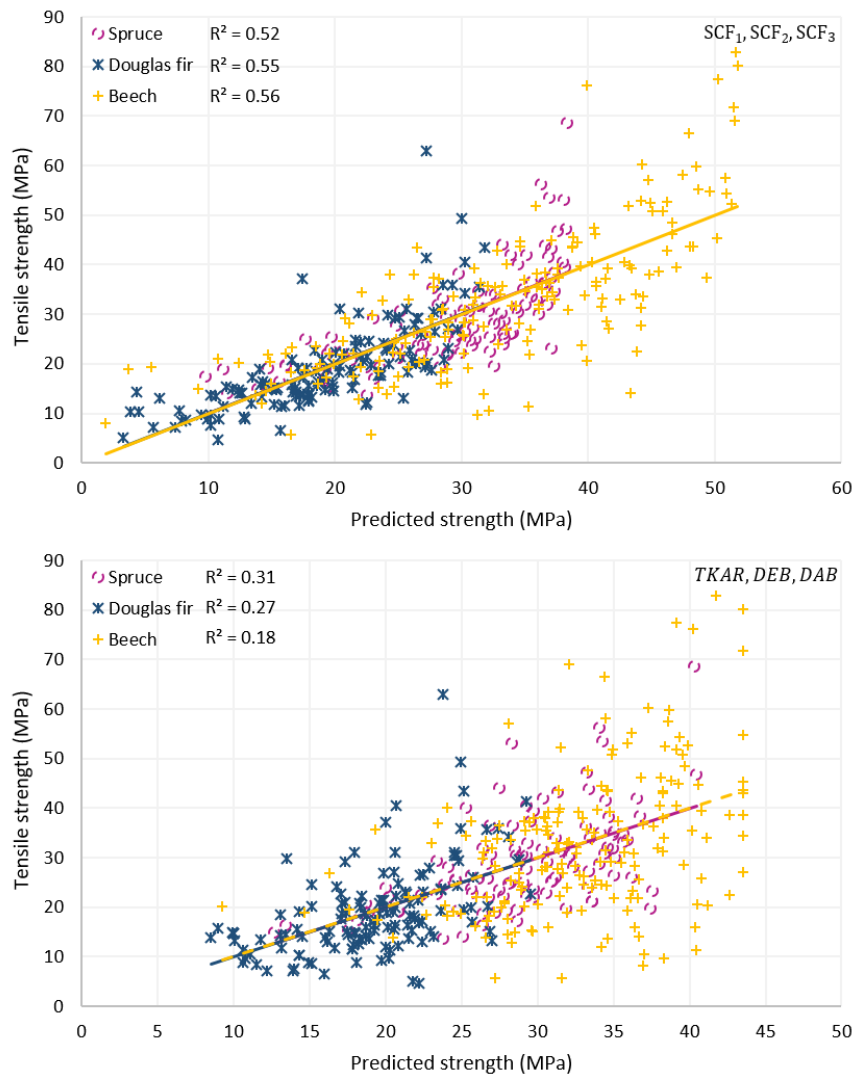
Figure 4-2: Multiple regression analysis by considering the virtual (SCF_i) and actual (TKAR, DEB, DAB) knot parameters correspondingly.

Table 4-1: Coefficients for multiple regression analysis of knot parameters

Strength	y=a.SCF_1+b.SCF_2+c.SCF_3+Constant				y=d.TKAR+e.DEB+g.DAB+Constant			
	a	b	c	Constant	d	e	g	Constant
f_{spruce}	-8.75	3.47	-4.88	49.6	-34.41	-32.84	-4.97	48.89
$f_{Douglas-fir}$	-4.08	-2.35	-0.63	38.6	-22.51	-36.11	-10.69	39.97
f_{beech}	-3.34	-14.96	0.08	71.0	-	-43.79	-11.25	43.50

4.3 Stress wave analysis and virtual dynamic MoE

4.3.1 Calculation of dynamic MoE

Calculation of the dynamic MoE in practice through an impact stress-wave propagation provides a reasonable parameter for tensile strength prediction. Therefore, a similar approach can be implemented virtually, which calculates dynamic MoE by outputting the stress wave velocity after a one-round travel of the wave in a board.

Longitudinal impact on a deformable body causes small deformation in material, which puts the material particles under compression and tension when propagating through the board (Gorwade et al. 2012; Tasdemirci and Hall 2005, Khaloian Sarnaghi and Van de Kuilen 2019b). Heterogeneities in wood and correspondingly, strong variations in density and material properties of knots are creating complex conditions for wave propagation. The heterogeneities cause a reduction in velocity of the stress wave after a complete round of wave forth and back in the board.

There are different parameters to describe the wave and its propagation in a structure. Three main properties, describing a wave are the domain of the wave, period, and the frequency. The period is the required time for one complete vibrational cycle. Frequency is inverse of the period, and is the number of the repetitions of a wave in a specific timeframe. Domain of the wave describes the maximum displacement of the wave compared to its static situation.

Wave propagations can happen in various forms under specific conditions. Some movements may have simple sinusoidal shapes, whereas the others may be combination of two or three wave cases. Instead of simple sinusoidal conditions, combined wave modes can be observed for stress wave propagation in wood, which is due to existence of strong heterogeneities in this material. Additionally, due to a very small cross-section to length ratio in boards, shear waves are neglected for wood and by limiting the transversal vibrations, total vibrations are restricted to only longitudinal vibrations for wood. In this case, loading is being applied to a control volume of the sample, which is causing a small displacement in the applied load point.

According to Hooke's law, and as the normal force (P) is not constant in longitudinal direction from one point to the other, the constitutive equation can be written as Equation (4-2) (Bodig and Jayne 1993).

$$\frac{\partial P}{\partial x} = E.A \frac{\partial^2 u}{\partial x^2} \tag{4-2}$$

where u denotes the x-displacement within the element, and is a function of space and time, E is the elastic moduli (with the average value for each set of species), and A is the cross-section.

According to Newton's equation of motion and based on Equation (4-2), the following equation can be derived:

$$\frac{\partial^2 u}{\partial t^2} = \frac{E}{\rho} \frac{\partial^2 u}{\partial x^2} \tag{4-3}$$

In Equation (4-3), ρ is the density of the sample, and E is the modulus of elasticity. According to the study of Ravenshorst (Ravenshorst 2015), the ratio of the $\frac{E}{\rho}$ is assumed to be constant for each wooden species. This ratio is square of the simplified wave velocity of an elastic material. Therefore, average density and average modulus of elasticity in parallel to fibers direction for each set of tested species can be used as input parameters for numerical analysis. Solution of the above-mentioned differential equation is in form of Equation (4-4):

$$u(t) = u_0 . \sin(\omega t - k.x) \tag{4-4}$$

where ω is the natural frequency. By solving this equation, the wave speed can be written as Equation (4-5):

$$\omega = C = \sqrt{\frac{E}{\rho}} \tag{4-5}$$

where C is the stress wave speed in the material. Therefore, if considering the plane wave propagation and approximating the constrained modulus to be the Young's modulus (Dowding 1996), velocity of the longitudinal wave can be represented by Equation (4-5).

Over the first vibration mode, the wave-length equals twice the length of the specimen (l), which leads to Equation (4-6):

$$\lambda = \frac{2l}{n} \tag{4-6}$$

where λ is the wave length, l is length of the specimen, and n is number of the mode. By relating wave-length to the wave speed and frequency (f):

$$\lambda = \frac{C}{f} = \frac{1}{f}\sqrt{\frac{E}{\rho}} \tag{4-7}$$

Therefore:

$$f = \frac{n}{2l}\sqrt{\frac{E}{\rho}} \tag{4-8}$$

For n=1, the first eigenfrequency is obtained. Therefore, dynamic modulus of elasticity is obtained by using Equation (4-9) (Görlacher 1990; Liang and Fu 2007), which is applicable for slender elements (l >> b.h).

$$E_{dyn} = 4l^2 f^2 \rho \tag{4-9}$$

Focus of this part of the thesis is to develop a numerical approach based on the stress wave propagation to predict tensile strength of wood. However, as wood is relatively heterogeneous, not all possible numerical methods are applicable for this material. One possible method to predict dynamic modulus of elasticity of the boards is to perform a modal analysis. Natural eigenfrequencies of the boards can be extracted by this method in their first eigenmode. Additional velocity or acceleration boundary conditions can also be applied to implement an impact load on the boards (Nilsson 2009). Based on this method, linear perturbation steps of frequency analysis can be performed and the natural frequencies of the material can be extracted. This method is computationally cheap and its application is not difficult. Therefore, it can be used for clear boards and it can give accurate results for the cases with simplified geometries. Due to geometrical complications of some of the samples of this thesis, explicit dynamic analysis (ABAQUS 6.14a) is used for extracting the frequencies of the system under an impact loading. Damping is neglected here and the mass matrix can be directly paired with the stiffness matrix in the equation of motion (Nilsson 2009, Clough and Penzien 2003, Cai 2016). Mass density, which is used for the numerical analysis in this thesis is the approximated average density for each wood species.

Complete modeling procedure is explained in (Khaloian Sarnaghi and Van de Kuilen 2019b,c). Dynamic stress wave is simulated by applying an impulse of 1e-5s to the specimen and by measuring the velocity of the longitudinal wave after one complete round forward and backward in a board (Khaloian Sarnaghi and Van de Kuilen 2019b). Sign of the velocities changes after the wave is passing the particle and in

its return way after reflection. Figure 4-3 shows nodal velocities of 24 individual 10-node elements that are connected to an example knot.
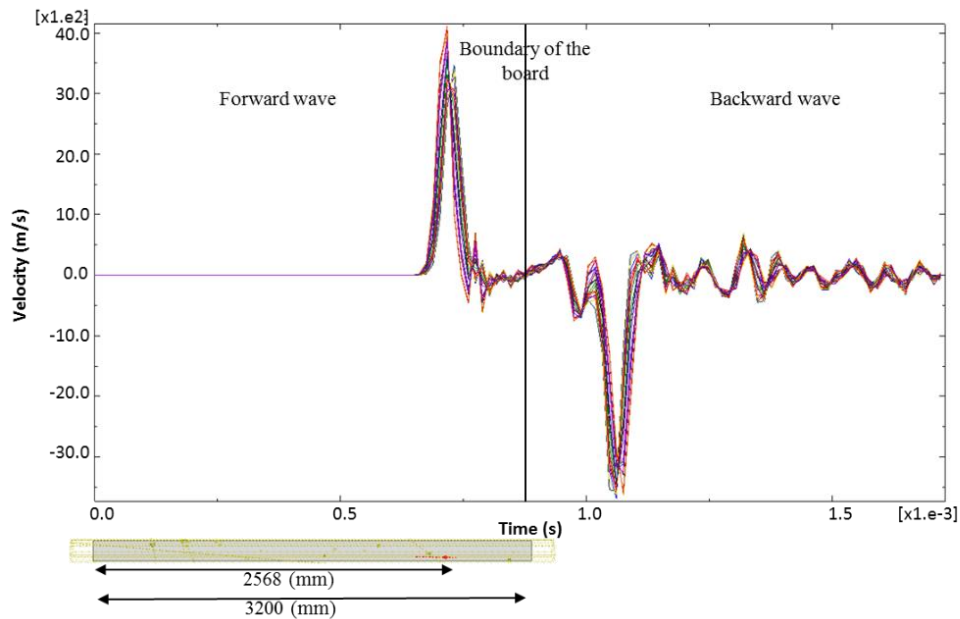
Figure 4-3: Wave velocity in an example board around the 24 elements located on the edge of the knot, which is located at x=2568 (mm) position of the board.

As knots are modeled as holes (Figure 2-11) for numerical analysis, velocity of the stress wave is being reduced after passing the knot. This is due to reflection of the wave and its transmission to the bulk material after the knot region. As shown in Figure 4-3, wave velocity does not remain the same in its return way. Small reduction is seen in the magnitude of velocity, when the wave is reaching the knot region for the second time in its return. Reflected wave from the end boundaries of the board has an inverse function of the forth wave.

4.3.2 Results of the dynamic analysis

After calculating the velocity and correspondingly the dynamic MoE of spruce, Douglas fir and beech boards, numerical parameters as well as the experimental ones are used in a single regression analysis to find their correlations with the tensile strength. Although average density of each species is always used for calculation of the velocity in numerical analysis, but the dynamic MoE is calculated by using both average and actual densities in Equation (4-9). Therefore, both dynamic MoEs are available to be used in regression analysis. In contrast to the numerical approach, the actual velocity and the dynamic MoE in measurement procedure are always measured by taking into account the actual density of each board (Khaloian Sarnaghi and Van de Kuilen 2019b, c). Therefore, the quality of predicted MoE$_{dyn}$ based on the numerical approach (by using the average density) is slightly lower or on the same level as the experimental MoE$_{dyn}$ of each set. The results are presented in Figure 4-4 and the coefficients of determinations are: $R^2=0.53$ compared to $R^2=0.50$, $R^2=0.50$ compared to $R^2=0.58$, $R^2=0.40$ compared to $R^2=0.50$ for spruce, Douglas fir and beech respectively (Khaloian Sarnaghi and Van de Kuilen 2019c). The accuracy of predictions is slightly better for higher quality spruce boards, whereas it reduces for the cases of lower quality Douglas fir and beech boards. In such cases, amount of knots and their geometrical non-uniformities, together with the strong natural fiber deviations in the locations away from knots are affecting the quality of predictions. Therefore, it is important to consider the influence of multiple parameters (including the knot parameters) for performing tensile strength predictions in such cases. These effects are discussed in details in Paper 3 (Khaloian Sarnaghi and Van de Kuilen 2019c).
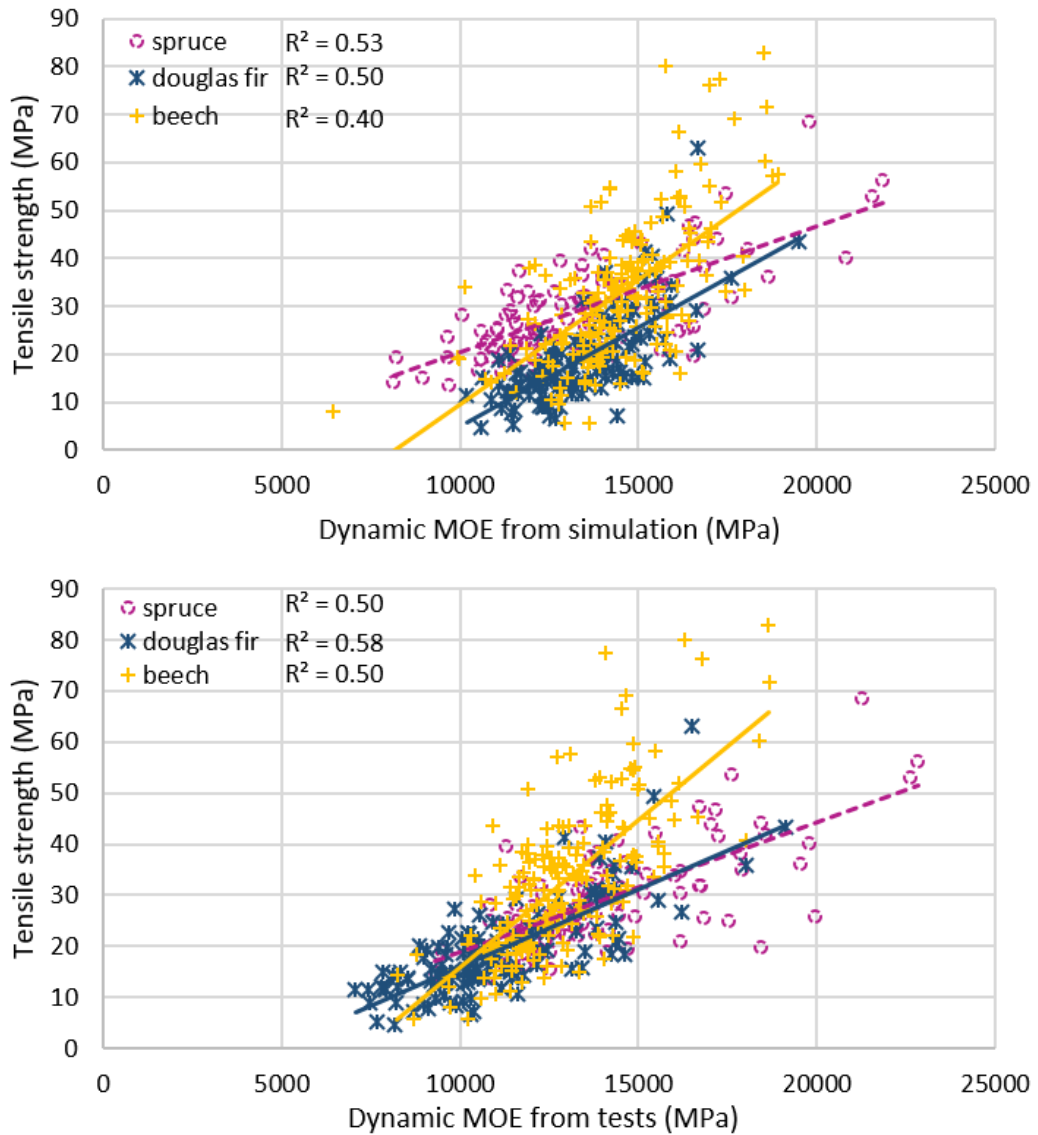
Figure 4-4: Relationship between simulated and measured dynamic MoE with tensile strength.

Linear multiple regression analysis is performed by using the dynamic MoE together with the knot parameters in combination for this analysis. The results are shown in Figure 4-5 and are compared for both numerical and experimental cases. It is shown in this figure that by using average densities for simulations and for calculation of the dynamic MoE, the prediction accuracy is on the same level as the predictions based on the actual measured parameters. However, it is shown that updating the dynamic MoE with the actual density of each board in numerical analysis improves the quality of the predictions to a level higher than the ones, based on the actual measurement methods. Results of the non-linear multiple regression analysis are presented and are discussed in details in Paper 3 (Khaloian Sarnaghi and Van de Kuilen 2019c). It is shown that due to the non-linear behavior of the stress concentration factors, non-linear function can better describe the relation of these parameters to the tensile strength.
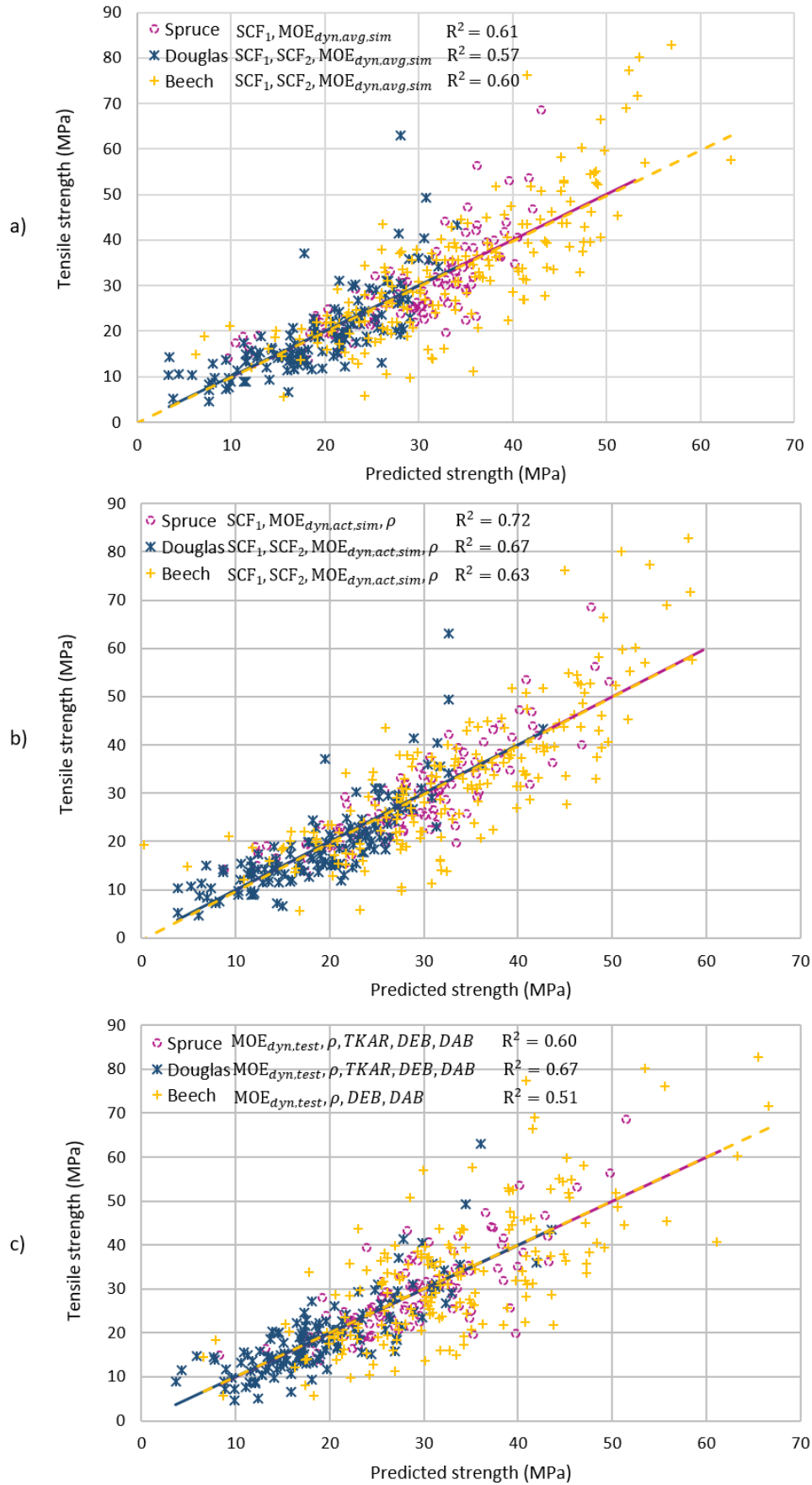
Figure 4-5: Linear multiple regression analysis for spruce, Douglas fir and beech sample by considering the average (a) and actual (b) densities in the simulations measurements (c).

Two non-linear mathematical equations (Equations (4-10) and (4-11)) are provided, which show the relation of the numerical parameters for prediction of tensile strength.

$$f_1 = \sum_{i=1}^{n} a_i . e^{b_i . SCF_i} + c.MoE_{dyn} + d \tag{4-10}$$

$$f_2 = \sum_{i=1}^{n} (a_i . SCF_i^{b_i} + c_i . SCF_i) + d.MoE_{dyn} + e \tag{4-11}$$

Parameter n in above-mentioned equations is the number of SCFs that are required for strength predictions ($n=1$ for spruce boards, and $n=2$ for Douglas fir and beech boards). SCF_i are the stress concentration factors, presented in sub-chapter 4.2. Parameter f is the tensile strength, MoE_{dyn} is the dynamic modulus of elasticity and a,b,c,d,e are the model constants, provided in Paper 3 (Khaloian Sarnaghi and Van de Kuilen 2019c).

Knots have mainly uniform shapes for higher quality spruce boards that are analyzed in this thesis. Additionally, amount of knots are not very high for these cases. Therefore, only one knot parameter (SCF_1) is enough for representing knot configurations and the stress distributions for such cases. However, for lower quality Douglas fir and beech boards, more than one SCF is required to represent the more complex geometrical configuration of knots and the heterogeneous domain of these samples. Detailed discussion of these effects can be found in Paper 3 (Khaloian Sarnaghi and Van de Kuilen 2019c).

4.4 Numerical modeling of growth defects in small groups of medium dense European hardwoods

4.4.1 Short introduction on hardwoods

Structural wood-based materials such as glulam are widely used in larger spans for construction purposes. Generally made of spruce, there are other species in use such as beech, ash, oak as well as a number of more exotic hardwoods such as iroko. As already shown in previous chapters, anisotropy and heterogeneity of each board may cause significant variation in mechanical properties of that board. In order to predict mechanical properties of lamellas for glulam, numerical models need to be further-developed to cover the natural scatter of this material (described in details in the next chapter).

In timber engineering, main research has been performed on softwoods as a basic component for glued laminated timber. Therefore, there is a large experimental database available for these species, covering mechanical (strength, stiffness, density) and geometrical properties (cross-sections, knot sizes and locations) of the material.

Due to lack of data for hardwoods compared to softwoods, numerical studies are rarely performed for hardwoods. Recently, new studies are being done for better prediction of the strength properties of these species including a classification system for tensile lamellas (Kovryga et al. 2016).

As already have shown in the previous chapters, structural differences between hardwoods and softwoods require the generalization of the model in order to be able to cover the natural scatter. Similar methods, as presented in the previous chapters, are used in this part of the thesis, for prediction of the stress concentrations factors, the virtual MoE_{dyn} and for prediction of the tensile strength.

The main species that are used in this part of the thesis for generalization of the method are higher quality ash (with an average strength of 70 MPa) and maple (with average strength of 38 MPa) boards. Small groups of these samples are selected for this analysis, as these samples are used for only generalization and validation of the model. The properties of these species have been already presented in Table 1 of Paper 3 (Khaloian Sarnaghi and Van de Kuilen 2019c).

4.4.2 Correlation of single numerical and measurement parameters with the tensile strength

The three SCFs and the virtual dynamic modulus of elasticity of these samples are used in a linear multiple regression analysis with the tensile strength of these samples. The results are shown in Figure A2.1 (appendix) and are compared to the parameters of the measurements (including the knot parameters: TKAR, DEB, DAB and the measured dynamic MoE) in Figure A2.2.

Similar to the previous cases, stress concentration factors have relatively high correlation with the tensile strength (with R^2 values higher than 0.65). As these parameters have nonlinear features, the R^2 value is increasing, when performing the non-linear analysis (Spearman) (R^2: SCF_1=0.90, SCF_2=77, SCF_3=0.76). Comparing these numerical knot parameters to the ones from the measurements (TKAR, DEB, DAB with R^2 values higher than 0.54), the quality of strength predictions improves considerably, when using the numerical knot parameters.

By comparing the dynamic MoE of the tests and the simulations, a lower correlation is found, when using the virtual method (R^2=0.32 compared to R^2=0.37 for the simulations and the measurements, respectively). Similar to the beech boards (described in Paper 3), virtual dynamic MoE gives a slight underestimation of the tensile strength due to the natural fiber deviation of these hardwood species. Therefore, consideration of the influence of multiple parameters, including the knot parameters in a multiple regression analysis helps for better strength predictions for these samples.

As shown in Figure A2.2, density has a very low correlation with the tensile strength of these species (R^2=0.02). Therefore, it is expected that usage of this parameter in multiple regression analysis will not improve the quality of the strength predictions considerably.

As small groups of these samples are considered in this thesis, very high correlations are observed between the SCFs and the tensile strength in this case. However, similar to the previous species that are analysed for this thesis, it is expected that the correlations will decrease, when increasing the number of the samples in these groups as well.

4.4.3 Multiple regression analysis

Similar to the previous samples, the parameters are used in a linear multiple regression analysis to check possible improvements in the quality of predictions. Initially, all knot parameters from simulations (SCFs) and measurements (TKAR, DEB, DAB) are used in a multiple regression analysis with tensile strength separately, and the results are compared to each other. The comparisons can be found in Figure A2.3. Similar to the previous cases, it is shown that the quality of predictions improves considerably, when using the numerical SCFs for predictions compared to the knot parameters from visual grading method (R^2=0.89 compared to R^2=0.62 for the simulation and measured parameters, respectively).

By using all measured parameters (including the dynamic MoE, density, TKAR, DEB, DAB) in a linear multiple regression analysis with tensile strength, an improvement in the quality of predictions can be observed (R^2=0.73 in Figure 4-6). Addition of the virtual dynamic MoE of these samples in the numerical case to the multiple regression analysis does not considerably improve the quality of predictions (R^2=0.90).
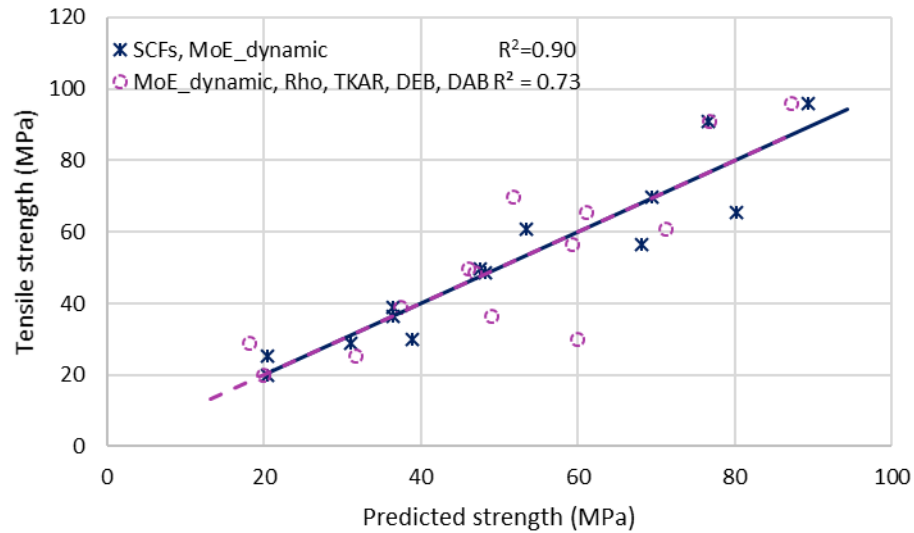
Figure 4-6: Linear multiple regression analysis for all measured parameters.

Linear Equations (4-12) and (4-13) represent the relations between the numerical and measurement parameters and the tensile strengths of these sets of hardwood species, respectively.

$$f_{1,hardwood} = -150.8 SCF_1 - 23 SCF_2 + 44 SCF_3 - 0.0012 MoE_{dyn,sim} + 238 \tag{4-12}$$

$$f_{2,hardwood} = 0.0006 MoE_{dyn,test} - 0.018\rho - 140.3 TKAR + 148.8 DEB - 122 DAB - 9.15 \tag{4-13}$$

However, as mentioned before, equations that are provided in this part of the thesis for tensile strength prediction of these two groups of hardwood species are for small groups of these species. Correlations and the quality of predictions are expected to decrease by increasing the number of samples within these groups.

4.5 Failure analysis

After discovering the required information for representation of the boards in the previous chapters and validating the developed numerical method for strength prediction of more than 450 lamellas, focus of this small chapter of the thesis is to perform failure analysis for single lamellas to predict failure development and its path based on the predicted fiber pattern. As explained in Chapter 2.4 and in Equations (2-6)-(2-10) (Sandhaas 2011), eight failure criteria are defined for wood to represent brittle and ductile failure of wood under different loading conditions. Results are compared to the information of the stress concentration factors about prediction of the failure path. Figure 4-7 shows a comparative case for an example spruce board.
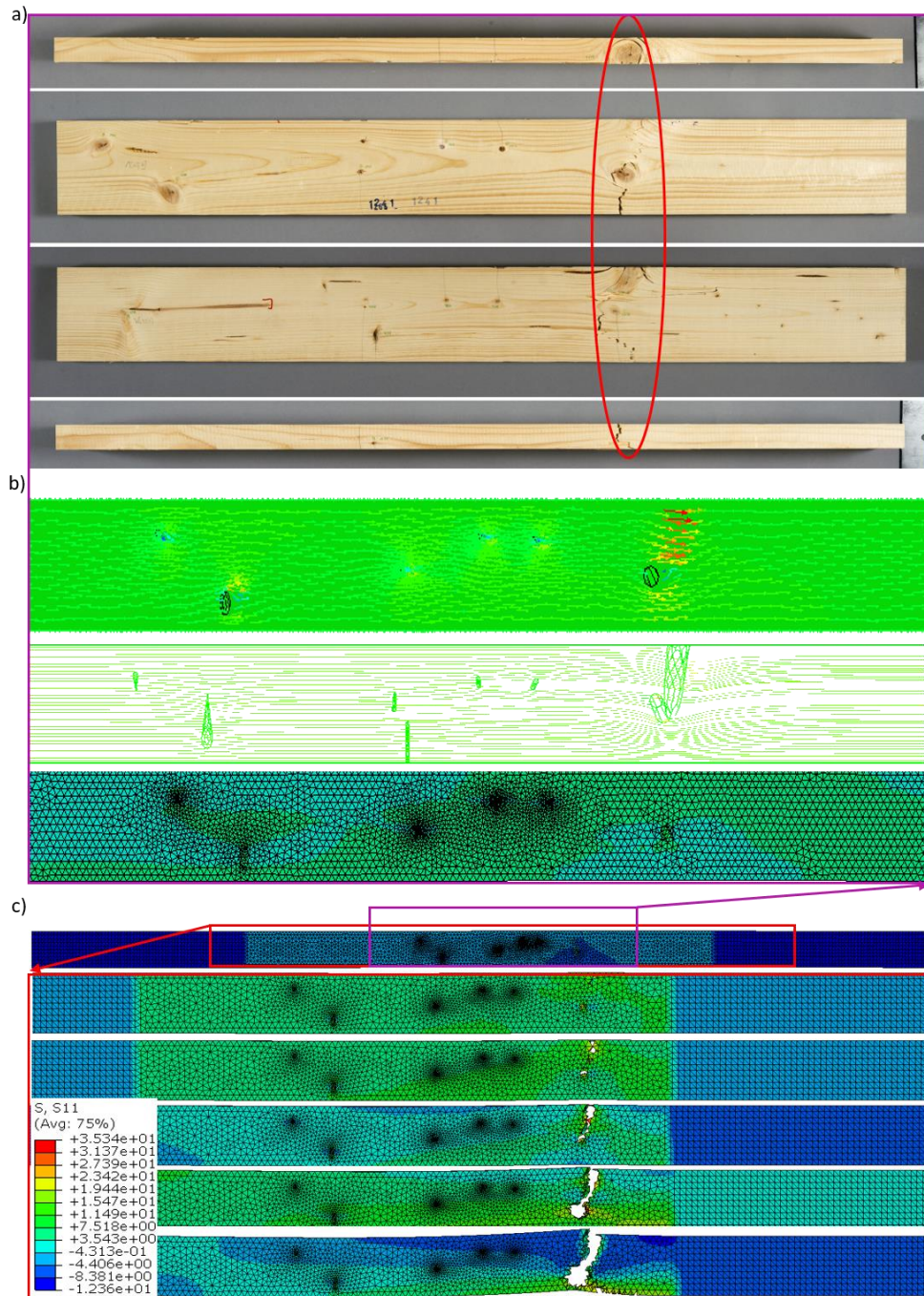
Figure 4-7: Modeling of failure propagation in an example of spruce board, the real failure (a), fiber pattern with higher deviation around edge knot (b), stress development in board and failure analysis by propagation of failure through the elements and element deletion (c). S11 (MPa) is the stress in the principal direction of the board. (Simulation with scale factor of 100).

In this set of analysis, instead of applying uniform tension and scaling the load in one time period to reach the stress concentration, actual strength values of each species under tension, compression (in both parallel and perpendicular direction to the fibers) and shear are implemented as input parameters to calculate failure in wood. As soon as stresses are reached to a value to satisfy one of the limit criteria for failure of wood, the element deletion is being activated which shows the track of failure in wood.

As shown in Figure 4-7, predictions correspond well with the actual failure in wood. Due to existence of an edge knot and development of knot cluster on the right side of the board (as shown with red ellipse in Figure 4-7.a) critical conditions are provided for failure of wood. Figure 4-7.b shows the velocity vectors in longitudinal (mainstream) direction of board. Higher velocities are developed around the knot, where failure has been occurred during actual physical tests in this case (shown in Figure 4-7.a). By having a closer look at the fiber pattern in this board, it is shown that the fiber pattern is relatively uniform in the board and around knots, with strong deviations in the location of failure. Similar behavior can be seen in the predictions. Correspondingly, by development of higher velocities at this location, stronger fiber deviation is implemented for solid analysis with rotation of the orthotropic directions, which causes development of higher stresses at the region. Therefore, higher stress concentration factors may be obtained at the same location under uniform tension, which may represent failure location of the material. Similar effect is shown when applying full failure analysis for predictions (Figure 4-7.c). Failure starts at the knot with strongest fiber deviation and propagates in the direction of the fibers toward the second knot. Failure initiation location and its path of propagation corresponds well with the actual case (shown in Figure 4-7.a). Definition of the status parameter in this case helps in visualization of the deletion of the elements during the quasi-static tensile analysis, by reaching the failure criteria.

Chapter 5 Summary, conclusion and outlook

5.1 Summary

This thesis concentrated on the three following main steps for modeling of wood and its composite structures:

1. Geometrical reconstruction
2. Fiber prediction
3. Strength prediction

Geometrical reconstruction has been performed solely based on the surface information of knots (as geometrical imperfections in wood). Detailed information about knots, their location and their geometrical configurations provided the possibility to consider fiber deviation and correspondingly the rotation of the orthotropic directions around the defects in details. Therefore, the structural model of wood has been created by considering a more realistic fiber flow in wood, using one-equation Spalart Allmaras turbulent method, which allowed for flow separation after passing the obstacle.

Strength prediction has been performed by considering four numerical Identifying Parameters (IPs) including three Stress Concentration Factors (SCFs) and the dynamic MoE. SCFs have been calculated by taking the effects of the maximum stresses and average stresses that are developing around the geometrical features under uniform tension, as well as their actual and projected areas into account. Dynamic MoE has been analyzed by considering the velocity of the stress wave after its one complete round propagation in the board. Analysis has been performed by considering both lower quality as well as higher quality softwood and hardwood species. Therefore, numerical analysis has been generalized to cover the quality range and the natural scatter of wood.

Single correlation of each of the numerical parameters has been checked with the actual tensile strength of the boards. These results have been compared to the correlation results of knot parameters from visual grading and the measured dynamic MoE with the tensile strength. Correlation matrices of spruce, Douglas fir and beech samples are presented in Table 5-1 - Table 5-3 respectively. Single relations between actual and numerical parameters can be found in these tables. As expected and shown in these tables, negative correlation exists between the visual and virtual knot parameters with the tensile strength. This confirms the reduction of the material strength by increasing the concentration of stresses around geometrical imperfections.

Virtual IPs of each of the species are then used in a multiple regression analysis, and the predicted strength is validated with the one from the IPs of the recently available visual and machine grading methods. Comparisons can be found in Paper 3 (Khaloian Sarnaghi and Van de Kuilen 2019c).

Table 5-1: Linear correlation matrix for Spruce (n=103 boards)

Spruce	Strength	SCF$_1$	SCF$_2$	SCF$_3$	MoE$_{dyn,sim,act}$	MoE$_{dyn,sim,avg}$	MoE$_{dyn,test}$	Density	TKAR	DEB	DAB	MoE$_{static}$	Freq.$_{sim}$	Freq.$_{test}$
Strength	1													
SCF$_1$	-0.71	1												
SCF$_2$	-0.57	0.76	1											
SCF$_3$	-0.63	0.79	0.95	1										
MoE$_{dyn,sim,act}$	0.73	-0.46	-0.33	-0.36	1									
MoE$_{dyn,sim,avg}$	0.63	-0.50	-0.34	-0.43	0.73	1								
MoE$_{dyn,test}$	0.71	-0.41	-0.30	-0.32	0.95	0.64	1							
Density	0.50	-0.23	-0.16	-0.14	0.81	0.20	0.82	1						
TKAR	-0.47	0.47	0.45	0.43	-0.30	-0.30	-0.33	-0.16	1					
DEB	-0.41	0.42	0.41	0.49	-0.23	-0.42	-0.24	0.02	0.28	1				
DAB	-0.48	0.46	0.52	0.48	-0.31	-0.29	-0.32	-0.19	0.69	0.62	1			
MoE$_{static}$	0.76	-0.50	-0.36	-0.40	0.89	0.60	0.94	0.77	-0.41	-0.32	-0.41	1		
Frequency$_{sim}$	0.63	-0.50	-0.35	-0.44	0.73	0.99	0.64	0.20	-0.31	-0.42	-0.30	0.60	1	
Frequency$_{test}$	0.59	-0.42	-0.30	-0.40	0.63	0.86	0.70	0.17	-0.37	-0.44	-0.32	0.65	0.86	1

Table 5-2: Linear correlation matrix for Douglas fir (n=151 boards*)

Douglas fir	Strength	SCF$_1$	SCF$_2$	SCF$_3$	MoE$_{dyn,sim,act}$	MoE$_{dyn,sim,avg}$	MoE$_{dyn,test}$	Density	TKAR	DEB	DAB	MoE$_{static}$	Freq.$_{sim}$	Freq.$_{test}$
Strength	1													
SCF$_1$	-0.68	1												
SCF$_2$	-0.62	0.58	1											
SCF$_3$	-0.60	0.56	0.91	1										
MoE$_{dyn,sim,act}$	0.71	-0.53	-0.49	-0.47	1									
MoE$_{dyn,sim,avg}$	0.53	-0.49	-0.48	-0.50	0.66	1								
MoE$_{dyn,test}$	0.76	-0.52	-0.47	-0.43	0.79	0.34	1							
Density	0.33	-0.16	-0.12	-0.07	0.57	-0.24	0.65	1						
TKAR	-0.44	0.41	0.37	0.34	-0.36	-0.37	-0.35	-0.06	1					
DEB	-0.36	0.38	0.39	0.43	-0.20	-0.42	-0.18	0.20	0.20	1				
DAB	-0.47	0.48	0.35	0.31	-0.40	-0.37	-0.44	-0.10	0.80	0.43	1			
MoE$_{static}$	0.87	-0.64	-0.58	-0.55	0.78	0.46	0.90	0.50	-0.48	-0.31	-0.52	1		
Frequency$_{sim}$	0.52	-0.48	-0.48	-0.49	0.65	0.99	0.33	-0.25	-0.36	-0.42	-0.37	0.45	1	
Frequency$_{test}$	0.76	-0.56	-0.52	-0.50	0.68	0.58	0.88	0.24	-0.42	-0.34	-0.51	0.85	0.57	1

*From in total 151 samples the analysis was performed for 137 samples

Table 5-3: Linear correlation matrix for Beech (n=200 boards)

Beech	Strength	SCF$_1$	SCF$_2$	SCF$_3$	MoE$_{dyn,sim,act}$	MoE$_{dyn,sim,avg}$	MoE$_{dyn,test}$	Density	DEB	DAB	MoE$_{static}$	Freq.$_{test}$	Freq.$_{sim}$
Strength	1												
SCF$_1$	-0.65	1											
SCF$_2$	-0.67	0.58	1										
SCF$_3$	-0.58	0.55	0.81	1									
MoE$_{dyn,sim,act}$	0.63	-0.45	-0.50	-0.46	1								
MoE$_{dyn,sim,avg}$	0.59	-0.43	-0.51	-0.48	0.90	1							
MoE$_{dyn,test}$	0.71	-0.43	-0.52	-0.46	0.53	0.41	1						
Density	0.22	-0.14	-0.07	-0.06	0.44	-0.01	0.33	1					
DEB	-0.42	0.45	0.40	0.37	-0.17	-0.19	-0.44	0.01	1				
DAB	-0.40	0.39	0.36	0.32	-0.16	-0.20	-0.43	0.06	0.91	1			
MoE$_{static}$	0.69	-0.41	-0.50	-0.44	0.41	0.32	0.82	0.26	-0.52	-0.48	1		
Frequency$_{test}$	0.65	-0.40	-0.52	-0.46	0.41	0.44	0.93	0.01	-0.47	-0.48	0.76	1	
Frequency$_{sim}$	0.57	-0.41	-0.51	-0.49	0.89	0.99	0.41	-0.01	-0.18	-0.19	0.32	0.44	1

5.2 Check on the combination of the IPs of visual, machine and virtual methods

In the end, after developing and validating the virtual method for strength prediction of wood, all IPs of the visual, virtual and machine grading methods for each species are used in combination with each other in a multiple regression analysis to predict tensile strength and to check possible improvements in the quality of predictions. Figure 5-1 and Table 5-4 are showing the results of this set of analysis respectively.
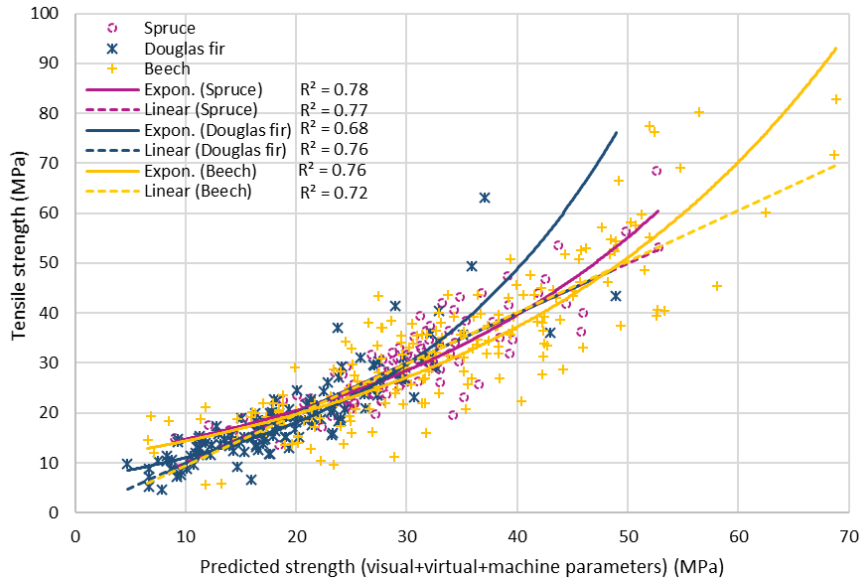
Figure 5-1: Linear and non-linear multiple regression analysis for strength prediction of spruce, Douglas fir and beech based on the IPs of the tests and simulations (MoE_{dyn}, TKAR, DEB, DAB, density, SCFs, $MoE_{dyn,sim}$).

Table 5-4: Comparison of the predictions, when using different IPs

R^2	Spruce	Douglas-fir	Beech
Simulation parameters*	0.75	0.72	0.61
Test parameters*	0.60	0.64	0.48
Test and simulation parameters*	0.77	0.76	0.72
*Simulation parameters: SCFs, $MoE_{dyn,sim}$			
Test parameters: MoE_{dyn}, TKAR, DEB, DAB, density			
Test and simulation parameters: MoE_{dyn}, TKAR, DEB, DAB, density, SCFs, $MoE_{dyn,sim}$			

As shown in Table 5-4, the quality of predictions improves by using all the test and simulation parameters together as IPs for tensile strength predictions. Improvement of the quality is more significant for the case of lower quality Douglas fir ($R^2_{combined}$=0.76 compared to R^2_{test}=0.64 and $R^2_{simulation}$=0.72) and beech boards ($R^2_{combined}$=0.72 compared to R^2_{test}=0.48 and $R^2_{simulation}$=0.61).

For the case of higher quality spruce boards, the results are improving considerably, when using the numerical parameters compared to the predictions based on the test parameters. Using all IP's in a regression analysis only slightly improves the quality of predictions compared to the predictions based on the simulation parameters. Therefore, information about the geometrical features of the knots are providing enough information for strength prediction of higher quality boards. Additional information about the density of boards does not improve the quality of predictions significantly. Fiber deviations are strong in cases of lower quality boards (especially the case for hardwoods). As the developed numerical model in this thesis can capture the fiber pattern based on possible imperfections in the material, the strong local fiber deviations may be underestimated in knot free boards. Therefore,

additional information, such as information about the single density of each board improves the quality of predictions of such samples ($R^2_{combined}$=0.72 compared to $R^2_{simulation}$=0.61).

In addition, by using IPs (test and simulation) of all samples (spruce, Douglas fir, beech, ash and maple) together in a regression analysis, without considering the species and their material variation, the relationship between each of the single parameters with the actual tensile strength of the boards is found (Figure 5-2 to Figure 5-4). As already have been mentioned in previous chapters, samples that are studied in this thesis are mainly the ones with knots or extreme fiber deviations. Influence of these non-homogeneities can especially be seen on the relationship of the SCFs with the tensile strength. In this case SCF=1 represents a clear wood with no knots and natural features. There are very few samples with SCF=1 in this thesis. Most of the samples have at least one knot or a natural imperfection that is influencing the SCFs. Natural scatter of wood makes the analysis more complicated. The scatter and variation of the properties can especially be seen for density distribution. A large scatter of strength may be observed for specific density values in this case. It is shown that density has a very low correlation with the tensile strength. From these figures it can be seen that tensile strength has the highest correlation with the dynamic MoE, independent of the wood type. Similarly, SCF parameters (especially SCF_2 and SCF_3) have high correlation with tensile strength, when considering one general group for wood, independent of the wood species.
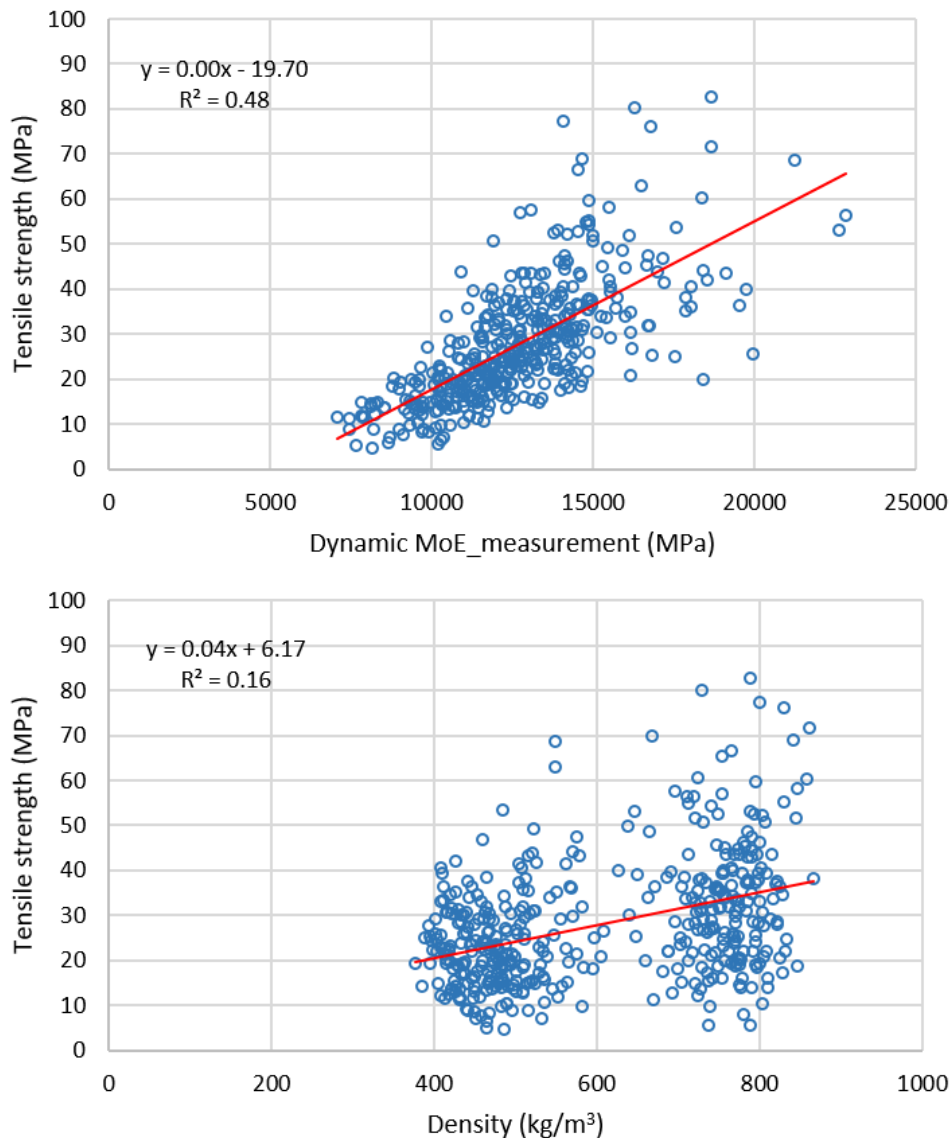
Figure 5-2: Relationship between measured dynamic MoE and density with actual tensile strength.
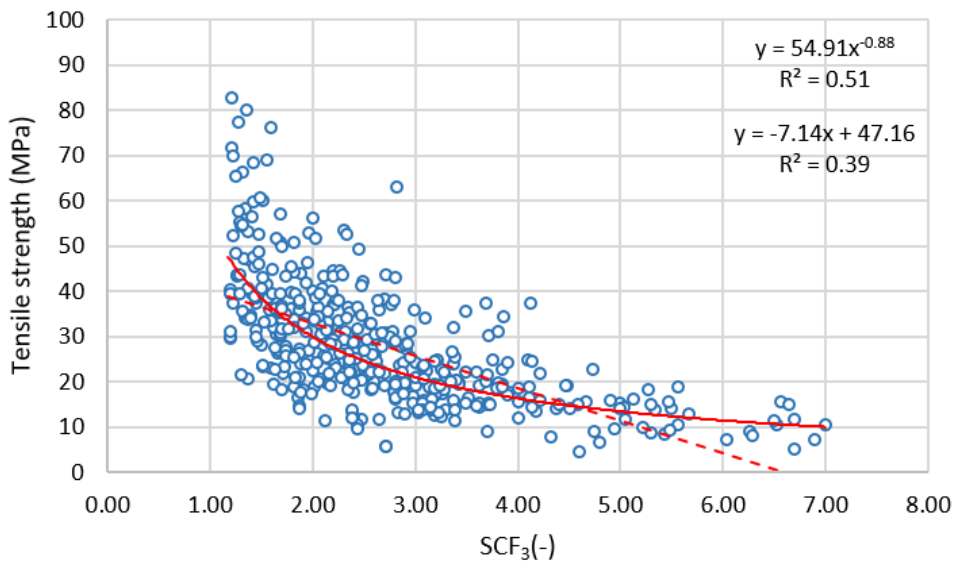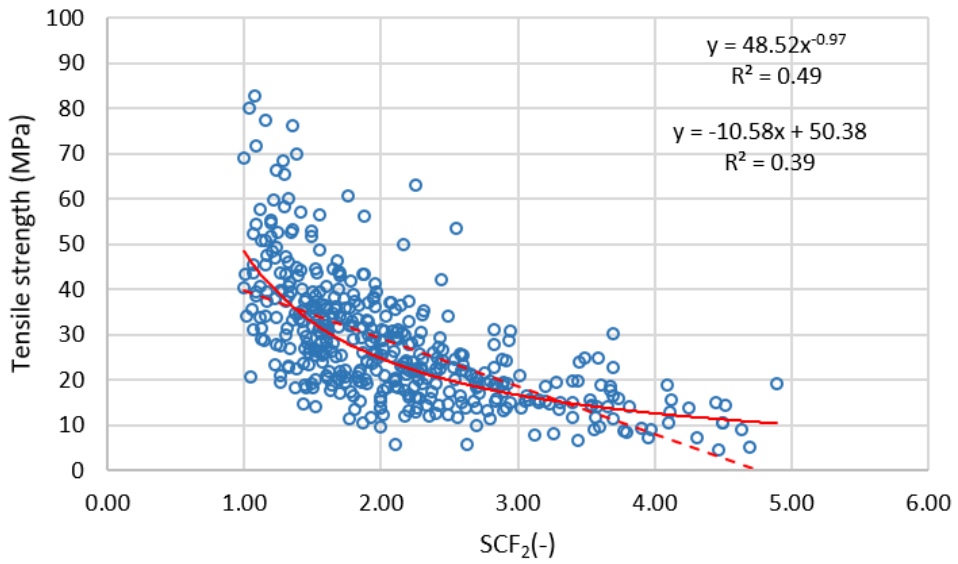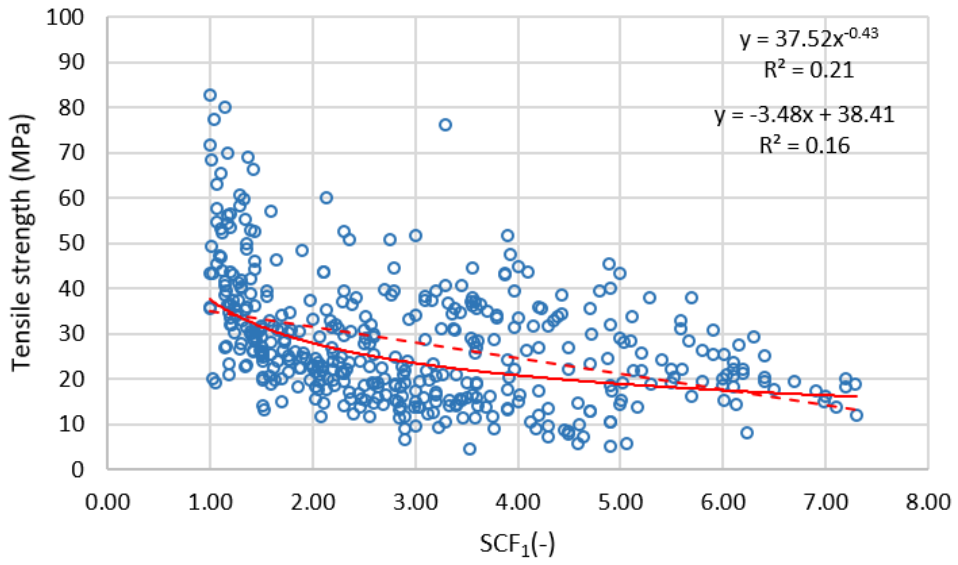
Figure 5-3: Relationship between stress concentration factors and actual tensile strength.
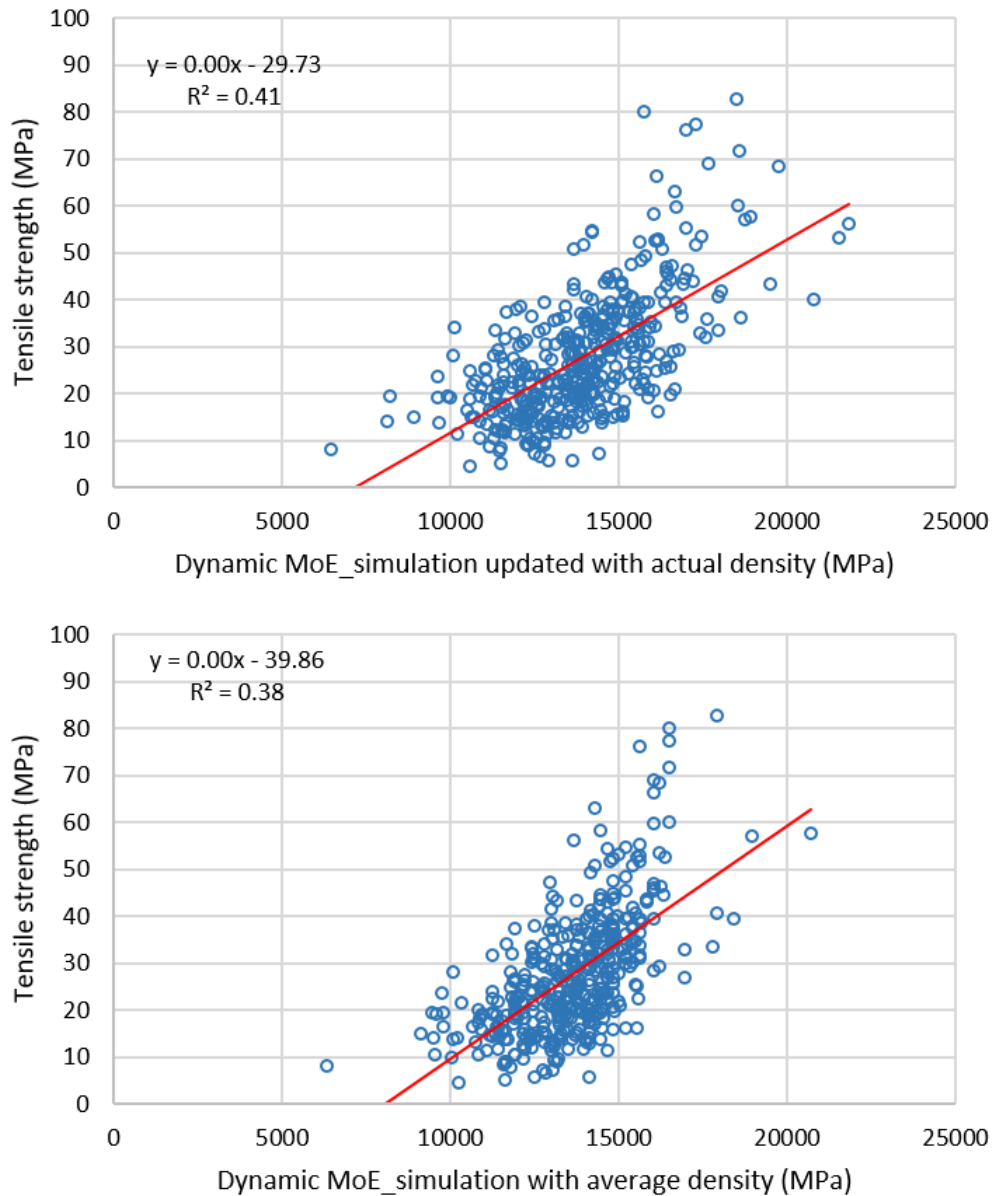
Figure 5-4: Relationship between simulated dynamic MoE by usage of average (upper) and actual density (lower) with actual tensile strength.

Although SCF_1 has a high correlation with tensile strength for single species, but the relationship between this parameter and the tensile strength is decreased when considering the general wood group by neglecting the wood species. The reason for the decreased R^2 in this case may be due to the local influence of the SCF_1 parameter. Initially, all knots are analyzed separately for this parameter and maximum of the obtained stress concentrations is selected as the value for this parameter for each sample in the end. For low quality beech boards that are studied for this thesis, extreme fiber deviations are influencing the tensile strength beside the knot parameters. In the next step, SCF parameters are analyzed separately for softwoods and hardwoods. High correlations are found between these parameters with the tensile strength for these groups (Figure 5-5).

By using the parameters of visual, numerical and machine grading methods in a multiple regression analysis for the general group of wood (independent of species), a linear equation is provided for strength prediction of timber (Equation (5-1)). Figure 5-6 shows the results of this set of analysis. As shown in this figure, high correlation is found between predicted tensile strength and the actual tensile strength (R^2=0.74), when using all IPs of visual, numerical and machine grading methods in a multiple

regression analysis with tensile strength for wood. Therefore, the provided mathematical model covers the quality scatter of this material in this thesis.
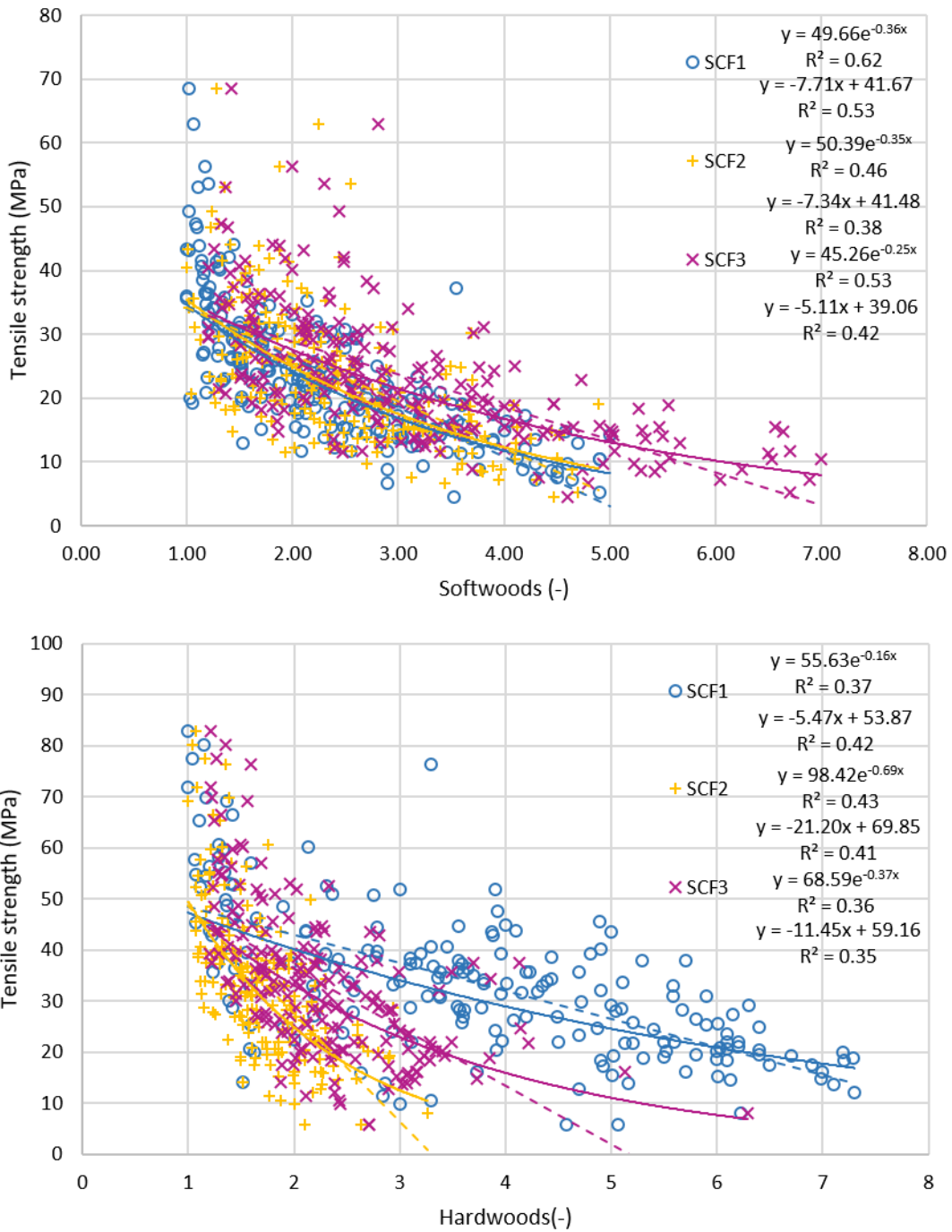
Figure 5-5: Relationship between the tensile strength and SCFs for softwoods (upper) and hardwoods(lower).

$$f_{S,DF,B,A,M} = -3.01SCF_1 - 1.85SCF_2 - 0.67SCF_3 + 0.0001MoE_{dyn,avg,sim}$$

$$+ 0.002MoE_{dyn,tes\ t} + 0.03\rho - 12.7DEB - 4.5DAB - 7.73$$

(5-1)

Parameter $f_{S,DF,B,A,M}$ in Equation (5-1) represents the strength of all samples (spruce, Douglas fir, beech, ash and maple), regardless of the species.
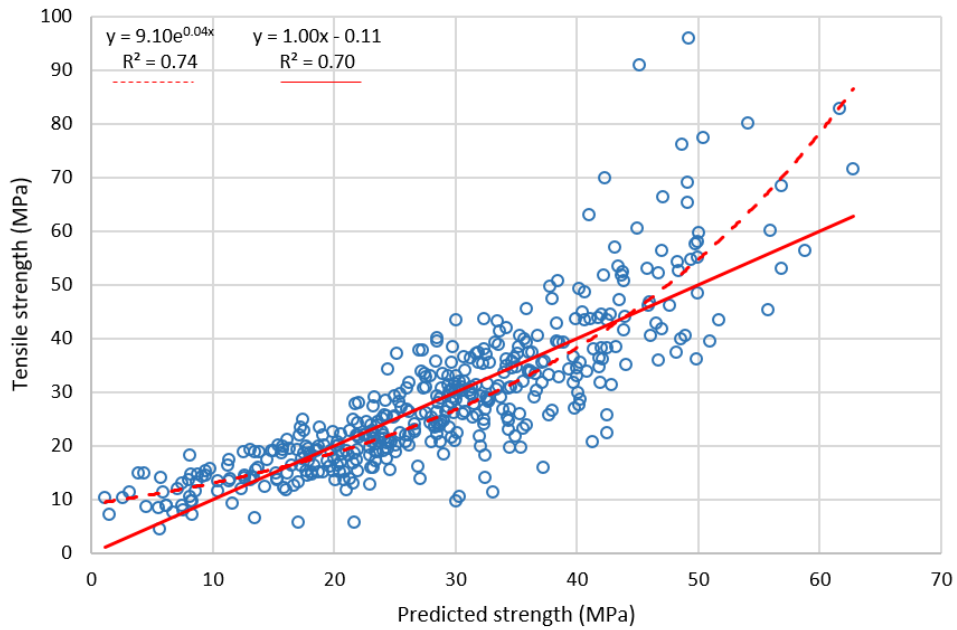
Figure 5-6: Relationship between the virtual and actual tensile strengths without considering the wood species. Virtual strength predictions are based on the IPs of the visual, machine and numerical strength prediction methods (MoE$_{dyn}$, TKAR, DEB, DAB, density, SCFs, MoE$_{dyn,sim}$).

5.3 Discussion

Parameters that are obtained from numerical simulations, including the SCFs and the MoE$_{dyn}$ are used for tensile strength predictions. The results are compared in this case to the cases, where the parameters from experiments and measurements are used for the same purpose. Coefficients of determinations are in ranges of 0.6 to 0.75, when checking the relation between simulation parameters with the tensile strength (Table 5-4). Prediction quality in this case is slightly higher than the quality of predictions based on the test/measurement parameters. By comparing the results to the previous studies, most of the previous studies have focused on bending strength prediction, which is less relevant for glued laminated timber. Therefore, studies on tensile strength predictions are quite limited (Baño et al. 2010, Lukacevic and Füssl 2014, Oscarsson 2014, Hu et al. 2017). By predicting the bending strength for a dataset of 105 boards, R^2 value of 0.71 is provided in the study of Oscarsson (2014). Lukacevic and Füssl (2014) provided a R^2 value of 0.79 in their study for 12 spruce boards that are modelled in tension out of in total 93 boards that are tested in tension and in bending. Similarly, a very high relation could be found between the predicted and actual tensile strengths (R^2=0.9) for two small groups of medium dense European hardwoods (n=14) in this thesis (provided in Chapter 4). However, as already have been discussed in Chapter 4, accuracy of the predictions is expected to decrease by increasing the amount of the samples to 200, which was the case for the beech boards in this thesis. Therefore, natural scatter of wood may strongly influence the results of the predictions. A large natural variation/scatter of the material is considered in this thesis by generalization of the method to develop a species independent model for tensile strength prediction of timber. The numerical approach requires solely the surface information of the knots and a-priori known ratio between modulus of elasticity and density. Therefore, a high precision surface scanner with knot identification is sufficient to extract the necessary data and perform an accurate strength prediction (Khaloian Sarnaghi and Van de Kuilen 2019a). The developed method seems to be robust to be used for strength prediction of wood, considering a large scatter for the quality of this material.

5.4 Conclusions

The primary goal of this thesis was to develop a more accurate method for strength prediction of the structural softwood timber based on the surface information of knots. The focus was on numerical approaches, to be able to reduce the class assignment that may appear during the visual grading and to go beyond the parameters that cannot currently be measured by visual or machine grading methods.

The thesis is structured around the following points:

- Automatic geometrical reconstruction of timber, by detailed consideration of the material imperfections and defects, especially knots.
- Development of a method for prediction of the wood fiber pattern around knots and their interactions, considering the scatter of wood.
- Validation of the predicted fiber profile with CT-scan images of the boards.
- Providing mathematical methods for calculation of the stress concentration factors in a 3D anisotropic and heterogeneous space. This is done, by considering the single and the group effects of the knots, their real or projected areas, and finally the average or maximum stresses that are developing around the knots or in the clear part of the wood under uniform tensile analysis.
- Development and validation of FEM based stress wave analysis.
- Calculation of the dynamic modulus of elasticity by using the average or actual density of each board.
- Linear and non-linear single and multiple regression analysis by using parameters of the visual, machine and virtual measurements for predictions.
- Development of a mathematical model for prediction of the tensile strength of structural timber.
- Validation of the results by actual experimentally obtained tensile strength and stiffness values.
- Analyzing improvement of the quality of the strength predictions by using multiple IPs of all mentioned methods in a regression analysis.
- Generalization of the developed method to a species independent model.

The most important conclusions of this thesis can be summarized as follows:

- In higher quality boards, virtual dynamic MoE is a good single strength predictor.
- In lower quality boards, influence of the knots need to be taken into account for accurate strength predictions, which is at the level of the best performing strength grading machines.
- Stress concentration factors alone are better strength predictors compared to the knot parameters of the visual grading methods for tensile strength prediction of wood.
- By analyzing the influence of multiple virtual parameters for tensile strength predictions, it is shown that a single stress concentration factor in combination with the dynamic MoE is enough for providing a high quality strength prediction for timber. For lower quality boards, at least two stress concentration factors in combination with the dynamic MoE may be considered in order to get better quality of predictions.
- Quality of the strength prediction is much higher for higher quality boards, when it is based on the parameters of the virtual method, compared to when it is based on the parameters of the visual and machine grading methods.
- Quality of the strength prediction is at the same level for lower quality boards, when it is based on the parameters of the virtual method, compared to when it is based on the parameters of the visual and machine grading methods.
-

- Using the IPs of all mentioned methods together in a multiple regression analysis, as predictors for tensile strength, slightly improves the quality of the predictions for lower quality boards. The same predictors cause a considerable improvements in the quality of the predictions for higher quality boards
- Strength prediction of small groups of timber by usingthe mathematical equation for all samples showed a high correlation with the real values.
- If the information about the single lamellas is available, the glulam model (without finger joints) can be reconstructed and analyzed.

5.5 Outlook

The method that is developed during this thesis improves the quality of the strength prediction of timber and may be integrated in the prediction process of sawmills to increase accuracy and yield. Different scanners are being integrated in sawmills, such as the Logeye or the Goldeneye from Microtec. These machineries facilitate scanning of the logs and boards, respectively. Therefore, automatic reconstruction of the boards may be possible by taking into account the knottiness effects and the fiber pattern. Yield of the logs is being predicted by considering the knottiness parameters in such cases. Therefore, yield may be estimated by considering the quality of the boards, which is estimated solely based on the knottiness parameters rather than their quantity.

In the next step, by performing the non-destructive measurement methods, grading of the boards is performed before the application and after the drying process is completed. Having a direct impression about the strength of the lamellas is more important than knowing the knottiness values in most of the engineering applications. This information may especially help in case of the glulam production, where the boards need to be classified and categorized before the production process. Therefore, scanners could be optimized in a way to provide the yield based on the strength of the boards, beside the knottiness. Based on the developed model in this thesis, a computer can be integrated directly to the scanners in the sawmills, which makes it possible to perform FE-analysis directly after board reconstructions. By this integration, the scanners could be upgraded to a level considering both knot effects as well as the dynamic MoE to predict the tensile strength.

Although the model is working well for strength prediction of wood as an anisotropic and heterogeneous material, the following points can be further developed to complete the model:

1) In this thesis, a simple model has been developed for tensile strength prediction of timber based on the surface information of knots. The model is kept relatively simple to facilitate generalization process of the method, in order to cover the natural structural variation of wood. The developed model can be extended for strength predictions under different loading conditions such as edgewise or flatwise bending. Therefore, a larger scatter in strength values can be covered, which is necessary for structural applications with primarily bending loading.

2) Prediction of fiber pattern for estimation of anisotropic directions and assignment of the stiffness properties is done based on the flow analysis and calculation of the flow deviation around knots and material heterogeneities. Therefore, reasonable results can be obtained when knots and geometrical non-uniformities are involved in the model. However, from some wooden species such as tropical hardwoods mainly knot free boards can be obtained, where only the natural scatter of fibers are influencing strength of the boards. Additionally, in many engineering applications, only knot-free boards are required, which reduce the risk for concentration of the stresses around these natural features. The developed model in this thesis is not able to capture the scatter solely based on the natural fiber deviation and without consideration of the knots. Therefore, more investigations need to be done and the model needs to be further developed to

include the cases with only natural fiber deviations and no visible defects. In such cases, information about the MoE of the boards may provide a valuable information about the natural scatter in boards. As shown previously, this parameter varies strongly when comparing different knot-free boards and has a strong correlation with strength. Thus, defining a stochastic field based on the information of the MoE my help for estimating the anisotropic material direction in such cases. Another possible approach would be direct mapping of the density to the stiffness after reconstruction of the boards from CT-scan images. However, it needs to be considered that this approach may be more costly, both from application as well as computational point of view, when being integrated in a fully automatized process. In addition, it needs to be considered that the density map is strongly varying not only for knots, but also for the annual rings in wood, which may cause more complications during the reconstruction and stiffness mapping procedures.

Based on the results of this thesis, the reconstruction method for single boards can be used for reconstruction of more complicated engineered products such as glulam, by consideration of the imperfections in single lamellas. Additionally, a selection process can be performed and a mixture of high and low quality boards can be selected and can be positioned in different setups to develop the required quality of the glulam. The developed model can be used for prediction of the SCFs and the dynamic MoE in a bigger scale for glulam by expecting the SCFs to reduce due to the bonding effects. However, there are two main points that need to be considered in the modeling process of glulam:

- Influence of the adhesive
- Influence of the finger joints

As the thickness of adhesive layer is relatively small compared to the layer of wood in wood composites, further studies need to be performed to analyze importance of consideration of these additional layers on transfer of stresses and on total strength of glulam. Additionally, variation of the material properties in the porous region on the boundaries of wood and adhesive layer need to be checked. For composition of the bond-lines, Marra (1992) presented a model with a chain of nine layers showing the pure adhesive layer, penetration layer, and the wood layer. If the adhesive layer plays a considerable role with respect to the load carrying capacity of the glulam, this bond-line composition needs to be taken in to account for numerical analyses. In such cases, development of the stresses in the interface region needs to be analyzed as well. In addition, different adhesive types (Stoeckel et al. 2013) need to be considered to be able to generalize the model by considering the scatter.

Summary of Papers

Paper 1

Strength prediction of timber boards using 3D FE-Analysis

A. Khaloian Sarnaghi[1*], J.G.W. van de Kuilen [1,2,3]

[1] Department of Wood Technology, Technical University of Munich, 80797 Munich, Germany
[2] Faculty of Civil Engineering and Geosciences, Delft University of Technology, Delft, Netherlands
[3] Guest researcher, CNR-Ivalsa, Florence, Italy

Timber boards are numerically reconstructed in the full 3D space based on knot information on the wood surface. The 3D model is then transformed into a full 3D-FEM model and successively used for tensile strength prediction. By knowing the exact locations of the knots, as the main strength governing parameters in timber boards, simulations are run for a large quality range of wood laminations. This includes low-medium quality Douglas fir and medium-high quality spruce boards. ABAQUS and PYTHON are used for the numerical simulations. An automatic link is programmed to extract data of the database and to create the 3D geometrical model. From the numerical simulations, three mathematical methods are presented to calculate the stress concentration factors (SCFs) around the 3D heterogeneous defects in anisotropic wooden boards. Additionally, the explicit dynamic analysis are run to obtain the dynamic modulus of elasticity (MoE_{dyn}). To reduce the dependency of the numerical predictions on the real density of the boards, the average density of each sample is used for the simulations. Each board is tested in tension physically and is used for the validation of the model. The FEM results are used in a regression analysis to analyze the correlation with the visual measurements and to predict the tensile strength. Based on the results of a multiple regression analysis, two SCFs and MoE_{dyn} are sufficient to accurately predict the strength of spruce and Douglas fir boards. The results of the current study show that an improvement in the strength prediction of wood is possible in comparison with current machine grading systems based on dynamic MoE and knot parameters.

In this paper, the authors tried to develop a mathematical method for representation of the stress concentration factors (SCFs) in a 3D anisotropic and heterogeneous space under the influence of fiber deviations. The method is developed after the geometrical reconstruction of the timber boards based on the surface information of knots. SCFs are represented by three mathematical equations in this paper.

Paper 2

Tensile strength prediction of softwood glulam lamellas using virtual vibration technique

A. Khaloian Sarnaghi[1*], J.W.G. van de Kuilen [2,3,4]

[1] *Ph.D. Department of Wood Technology, Technical University of Munich, 80797 Munich, Germany, +498921806716, sarnaghi@hfm.tum.de*

[2] *Professor, Department of Wood Technology, Technical University of Munich, 80797 Munich, Germany, +498921806462, vandekuilen@hfm.tum.de*

[3] *Professor, Faculty of Civil Engineering and Geosciences, Delft University of Technology, Delft, Netherlands, +3115 2782322, J.W.G.vandeKuilen@tudelft.nl*

[4] *Guest researcher, CNR-Ivalsa, Florence, Italy*

Strength of wooden boards is related to its natural defects and the ability of the stress wave to propagate around them. Anisotropy, heterogeneity and strong moisture dependency of wood are making it difficult to predict its strength. Covering the ordinary quality range of wood, a numerical simulation model is developed for strength prediction of timber and 250 boards are numerically simulated. In this study, by virtually reconstructing the three dimensional (3D) geometrical model of each case based on the surface information of the knots, and by predicting the fiber patterns, the material properties of wood are virtually predicted. Thus, the strength predictions are done solely based on the surface information of the knots. Strength variation in a knot-free board is only dependent on the variation of the actual density of the board. As the actual-density of wood may not be available under different environmental conditions for measuring the dynamic modulus of elasticity (MoE$_{dyn}$), average-density of each set is used as one of the only input parameters for simulations. The resonance kind stress wave propagation and its return is calculated in the reconstructed boards. Numerical results of the finite element (FE) stress wave analysis are used in a linear regression analysis for prediction of the tensile strength based on the information of the calculated time of the stress wave. The predicted results are benchmarked against the measured values in laboratory. Performing a multiple regression analysis, the virtual results provide much higher strength predictions than the geometrical parameters available from scanners. However, strong knot interactions in lower-quality boards also affect the strength predictions. This study provides a comprehensive system (starting from the geometrical reconstruction of the boards to the virtual analysis for calculation of the virtual MoE$_{dyn}$) for the strength prediction of wood, which is based solely on the surface images. The developed model gives the possibility to predict the tensile strength of timber with relatively high accuracy, which is approximately in the same level as current grading machines.

Dynamic MoE is a parameter that has generally a high correlation with tensile strength of wood. Therefore, focus of the authors in this paper is on virtual estimation of the stress wave propagation in boards for calculation of the virtual dynamic MoE. Measurement of this parameter in the beginning of

the grading step is not possible, as the density of wet wood is different from the one in dried condition. Therefore, focus of the authors here is to develop an equation, independent of the actual density of the boards to predict tensile strength by covering the natural scatter of wood.

Paper 3

An advanced virtual grading method for wood based on surface information of knots

A. Khaloian Sarnaghi[1*], J.W.G. van de Kuilen [1,2,3]

[1] Department of Wood Technology, Technical University of Munich, 80797 Munich, Germany

[2] Faculty of Civil Engineering and Geosciences, Delft University of Technology, Delft, Netherlands

[3] Guest researcher, CNR-Ivalsa, Florence, Italy

Strength grading of timber boards is an important step before boards can be used as lamellas in glued laminated timber. Grading is generally done visually or by machine, whereby machine grading is the faster and more accurate process. Machine grading gives the best strength prediction when dynamic modulus of elasticity (MoE_{dyn}) is measured and some kind of knot assessment algorithm is included as well. As access to the actual density for the measurement of MoE_{dyn} may be impossible in some conditions, this grading method may face some problems in strength prediction. As the strength of a board is related to its natural defects and the ability of the stress waves to propagate around these defects, a virtual method for more accurate strength predictions is developed based on the knot information on the surface. Full 3D reconstruction of the boards, based on knot information on the surfaces of these boards is an important step in this study. Simulations were run for 450 boards of spruce, Douglas fir, beech, ash and maple, covering a large quality range. ABAQUS and PYTHON were used for the numerical simulations. From the numerical simulations, three different stress concentration factors (SCFs) were calculated in the vicinity of the defects. Additionally, a virtual longitudinal stress wave propagation was modeled for the determination of the dynamic modulus of elasticity. The FEM results were used to predict the tensile strength. By means of a regression analysis, the correlation with actual visual and machine readings was validated. An improvement in the strength prediction was observed based on the virtual method, when compared to currently available grading machines. It shows the potential of numerical methods for strength prediction of wood based on visual knot information.

In this paper, focus of the authors is on generalization of the model and development of a mathematical model to predict tensile strength by considering the non-linear influence of the parameters that obtained in the previous papers. Generalization is an important step in this process due to a high natural scatter of wood. In the end, the method is used for strength prediction of two additional small sets of samples from different wooden species and the results are compared to the results from the recently available grading methods. The results confirm the quality of the virtual method for tensile strength prediction of timber.

List of additional papers

Khaloian A., Gard W.F., van de Kuilen J.W.G. (2017) *3D FE-numerical modeling of growth defects in medium dense European hardwoods.* Proceedings of the sixth international scientific conference on hardwood processing ISCHP, Lahti, Finland, pp. 60-67.

Khaloian A., van de Kuilen J.W.G. (2018) *Development of an advanced FE-Numerical method for virtual grading of timber.* Proceedings of the 18th World Conference on Timber Engineering. Seoul, Republic of Korea.

Kovryga A., Khaloian Sarnaghi A., van de Kuilen J.W.G. (2019) *Strength grading of hardwoods using transversal ultrasound.* Proceedings of the seventh international scientific conference on hardwood processing ISCHP, Delft, The Netherlands, pp. 220-229.

Khaloian A., Rais A., Kovryga A., Gard W.F., van de Kuilen J.W.G. (2020) *Yield optimization and surface image-based strength prediction of beech.* European Journal of Wood and Wood Products. https://doi.org/10.1007/s00107-020-01571-4.

Sandhaas C., Khaloian A., van de Kuilen J.W.G. (2019) *Testing and modeling of hardwood joints using beech and azobé.* Proceedings of the seventh international scientific conference on hardwood processing ISCHP, Delft, The Netherlands, pp. 85-92.

Sandhaas C., Khaloian A., van de Kuilen J.W.G. (2020) *Numerical modeling of timber and timber joints: Computational aspects.* Wood Sci. Technol. 54:31–61. https://doi.org/10.1007/s00226-019-01142-8.

References

ABAQUS 6.14 Documentation-a. *Abaqus Analysis Users Guide, 6.3.3 Explicit dynamic analysis*.

ABAQUS 6.14 Documentation-b. *Abaqus Analysis Users Guide, 28.2.2 Fluid element library.*

ABAQUS 6.14 Documentation-c. *Abaqus Analysis Users Guide, 6.6.2 Incompressible fluid analysis.*

Bodig J., Jayne B.A. (1993) *Mechanics of wood and wood composites*. Second edition. Krieger Publishing Company, New York, USA. ISBN13: 9780894647772.

Aupoix B., Spalart P.R. (2003) *Extensions of the Spalart-Allmaras turbulence model to account for wall roughness*. International Journal of Heat and Fluid Flow, Elsevier. 24(4), 454-462.

Spalart P.R., Allmaras S.R. (1994) *A one-equation turbulence model for aerodynamic flows*. La Recherche Aerospatiale 1, 5–21.

Baño V., Arriaga F., Soilán A., Guaita M. (2010) *F.E.M. analysis of the strength loss in timber due to the presence of knots.* World Conference on Timber Engineering, Riva del Garda, Italy. ISBN: 978-88-901660—3-7.

Bao Y., Zhou D., Huang C. (2010) *Numerical simulation of flow over three circular cylinders in equilateral arrangements at low Reynolds number by a second order characteristic-based split finite element method*. Computers & Fluids 39, 882–899.

Bent J. (2003) *Neutron-Mapping Polymer Flow: Scattering, Flow Visualization, and Molecular Theory*. Science 301, 1691–1695.

Buksnowitz C., Hackspiel C., Hofstetter K., Müller U., Gindl W., Teischinger A., Konnerth J. (2010) *Knots in trees: strain distribution in a naturally optimized structure*. Wood Science and Technology 44: 389-398

Burgert I., Eckstein D. (2001) *The tensile strength of isolated wood rays of beech (Fagus sylvatica L.) and its significance for the biomechanics of living trees.* Trees-Structure and Function 15:168–170.

Burgert I., Keckes J., Frühmann K., Fratzl P., Tschegg S.E. (2002) *A comparison of two techniques for wood fibre isolation evaluation by tensile tests on single fibres with different microfibril angle*. Plant Biology 4:9–12.

Burghardt W. R., Brown E. F., Auad M. L., Kornfield J. A. (2005) *Molecular orientation of a commercial thermotropic liquid crystalline polymer in simple shear and complex flow*. Rheol. Acta 44, 446–456.

Cai L.W. (2016) *Fundamentals of mechanical vibrations. Wiley, ISBN: 9781119050124*

Chatterjee D., Biswas G., Amiroudine S. (2010) *Numerical simulation of flow past row of square cylinders for various separation ratios*. Computers & Fluids 39, 49–59.

Chen H.Y., Peelukhana S.V., Berwick Z.C., Kratzberg J., Krieger J.F., Roeder B., Chambers S., Kassab G.S. (2016) *Editor's Choice-Fluid-Structure Interaction Simulations of Aortic Dissection with Bench Validation*. Eur. J. Vasc. Endovasc. Surg. 52, 589-595.

Clough R.W., Penzien J. (2003) *Dynamics of structures. Third edition,* Computers and Structures.

Cofer W.F., Du Y., Hermanson J.C. (1999) *Development of a simple three dimensional constitutive model for the analysis of wood*. American Society of Mechanical Engineers, Applied Mechanics Division (AMD), Mechanics of Cellulosic Materials, Volume 231, pp. 107-124.

Contro R., Vena P., Gastaldi D., Franzoso G. (2004) *Biomechanical behavior of a new SMA spinal implant through a computational approach*. Proceedings of the sixth world congress on computational mechanics in conjunction with the second Asian-Pacific congress on computational mechanics, Beijing China.

Corona P.T., Ruocco N., Weigandt K.M., Leal L.G., Helgeson M.E. (2018) *Probing flow-induced nanostructure of complex fluids in arbitrary 2D flows using a fluidic four-roll mill (FFoRM).* Nature Scientific Reports 8, 15559

Cramer S.M., Goodman J.R. (1982) *Model for stress analysis and strength prediction of lumber*. Wood and Fiber Science. 15(4): 338-349

Cramer S.M., Goodman J.R. (1986) *Failure modeling: A basis for strength prediction of lumber*. Wood and Fiber Science. 18: 446-459

Dowding Charles H. (1996) *Construction vibrations.* Prentice-Hall, Upper Saddle River, New Jersey.

De Backer J.W., Vos W.G., Vinchurkar S.C., Claes R., Drollmann A., Wulfrank D., Parizel P.M., Germonpré P., De Backer W. (2010) *Validation of Computational Fluid Dynamics in CT-based Airway Models with SPECT/CT*. Journal of Radiology 257(3), 854-62.

Dias A.M.P.G., Van de Kuilen J.W.G., Cruz H.M.P., Lopes S.M.R. (2010) *Numerical modeling of the load-deformation behavior of doweled softwood and hardwood joints.* Wood and Fiber Science 42(4):480-489.

DIN EN 338. (2016) *Structural timber—strength classes*.

DIN 4074. (2012) *Strength grading of wood – Part 1: Coniferous sawn timber.*

Dinwoodie J.M. (1981) *Timber: Its nature and behaviour*. Van Nostrand Reinhold, New York.

Durelli A.J., Lake R.L., Phillips E. (1952) *Stress concentrations produced by multiple semi-circular notches in infinite plates under uniaxial states of stress.* Proceedings of the Society of Experimental Stress Analysis.Vol. 10, No. 1

Eberhardsteiner J. (2002) *Mechanische Verhalten von Fichtenholz*. Springer, Wien.

EN 14081-1. (2016). *Timber structures - Strength graded structural timber with rectangular cross section - Part 1: General requirements*.

EN 408. (2010) *Timber structures—structural timber and glued laminated timber—determination of some physical and mechanical properties*. CEN, Brussels, Belgium.

EN 338. (2010) *Structural timber – Strength classes*. European Committee for Standardizations, CEN, Brussels, Belgium.

Ferziger J.H., Peric M. (2002) *Computational methods for fluid dynamics*. 3rd Edition. Springer Verlag. 2-540-42074-6.

Fink G., Köhler J., Frangi A. (2012a) *Experimental analysis of the deformation and failure behaviour of significant knot clusters*. World Conference on Timber Engineering WCTE, University of Auckland, New Zealand. 270-279.

Fink G., Köhler J. (2012b) *Zerstörungsfreie Versuche zur Ermittlung des Elastizitätsmodules von Holzbrettern.* IBK-Bericht 339, Institut für Baustatik und Konstruktion, ETH Zürich.

Fink G., Köhler J. (2014) *Influence of varying material properties on the load-bearingcapacity of glued laminated timber.* PhD thesis, Institute für Baustatik und Konstruktion, ETH Zürich.

Foley C. (2001) *A three-dimensional paradigm of fibre orientation in timber.* Wood Sci. and Tech., 35: 453–65.

Foslie M. (1971) *Norsk granvirkes styrkeegenskaper. Del 3 – Styrkeegenskaper for små, feilfrie prøver (Strength properties of Norwegian spruce (Picea abies karst). Part 3 – Strength properties of small, clear specimens).* Report No. 42. The Norwegian Institute of Wood Working and Wood Technology (in Norwegian).

Franco W., Sen M., Yang K. T. (2006) *Flows in large, self-similar tree networks and their control.* Proc. R. Soc. 462, 2907-2926.

Frese M. (2016) *Computergestützte Verfahren zur pragmatischen Beurteilung der Tragwiderstände von Brettschichtholz: Zusammenfassung exemplarischer Simulationsstudien.* Karlsruher Berichte zum Ingenieurholzbau 31, Universität Karlsruhe.

Görlacher R. (1990) *Klassifizierung von Brettschichtholzlamellen durch Messung von Longitudinalschwingungen.* Universität Fridericiana in Karlsruhe, Germany. Doctoral thesis.

Goodman J.R., Bodig J. (1978) *Mathematical model of the tension behavior of wood with knots and cross grain.* Proc. First Int. Conf. On Wood Fracture, Banff. Alberta, pp. 53-61.

Goodman J.R., Bodig J. (1980) *Tension behavior of wood − an anisotropic, inhomogeneous material.* Structural research report No. 32. Colorado State University, Fort Collins.

Gorwade C.V., Ashcroft I.A., Silberschmidt V.V., Hughes F.T.R., Swallowe G.M. (2012) *Experimental and numerical analysis of stress wave propagation in polymers and the role of interfaces in armour systems.* Cent. Eur. J. Eng., 10.2478/s13531-012-0034-0.

Guindos P., Guaita M. (2013) *A three-dimensional wood material model to simulate the behavior of wood with any type of knot at the macro-scale.* Wood Sci. and Tech., 47: 585–599.

Hackspiel C. (2010) *A numerical simulation tool for wood grading.* PhD thesis, Vienna University of Technology.

Hackspiel C., de Borst K., Lukacevic M. (2014) *A numerical simulation tool for wood grading model development.* Wood Sci. Technol. 48(3), 633-649. doi 10.1007/s00226-014-0629-0.

Hambli R. (2013) *A quasi-brittle continuum damage finite element model of the human proximal femur based on element deletion.* Medical and Biological Engineering and Computing 51(1-2), 219-231. doi:10.1007/s11517-012-0986-5.

Hankinson, R.L. (1921) *Investigation of crushing strength of spruce at varying angles of grain.* Air Service Information Circular, 3(259), Material Section Report No 130, US Air Service, USA.

Hashin Z (1980) *Failure criteria for unidirectional fiber composites.* Journal of Applied Mechanics, Transactions ASME 47(2):329-334. doi:10.1115/1.3153664.

Hofstetter K., Eberhardsteiner J., Stürzenbecher R., Hackspiel C. (2009) *Wood and wood products-linking multiscale analysis and structural numerical simulations.* 7th European LS-DYNA Conference, Salzburg. A-I-02.

Hunger F., van de Kuilen J.W.G. (2018) *Slope of grain measurement - a tool to improve machine strength grading by detecting top ruptures.* Wood Sci. and Tech. 52, 821–838.

Hu M., Briggert A., Olsson A., Johansson M., Oscarsson J., Säll J. (2017) *Growth layer and fiber orientation around knots in Norway spruce: a laboratory investigation.* Wood Sci. and Tech. 52(1), 7-27. doi 10.1007/s00226-017-0952-3.

Inthavong K., Wen J., Tu J., Tian Z. (2014) *From CT Scans to CFD Modeling – Fluid and Heat Transfer in a Realistic Human Nasal Cavity.* Journal of Engineering Applications of Computational Fluid Mechanics 3(3), 321-335. doi: 10.1080/19942060.2009.11015274.

Jenkel C., Kaliske M. (2013) *Analyse von Holzbauteilen unter Berücksichtigung struktureller Inhomogenitäten.* Bauingenieur 88, 494-507.

Jenkel C. (2016) *Structural and material inhomogenities in timber, Modeling by means of the finite element method.* PhD thesis, Technische Universität Dresden.

Khaloian A., Gard W.F., van de Kuilen J.W.G. (2017) *3D FE-numerical modeling of growth defects in medium dense European hardwoods.* Proceedings of the sixth international scientific conference on hardwood processing ISCHP, Lahti, Finland, pp.60-67.

Khaloian Sarnaghi A., van de Kuilen J.W.G (2019a) *Strength prediction of timber boards using 3D FE-analysis.* Construction and Building Materials 202: 563-573, doi: 10.1016/j.conbuildmat.2019.01.032.

Khaloian Sarnaghi A., van de Kuilen J.W.G (2019b) *An advanced virtual grading method for wood based on surface information of knots.* Wood Sci. Technol. 53 (3): 535–557, doi: 10.1007/s00226-019-01089-w

Khaloian Sarnaghi A., van de Kuilen J.W.G (2019c) *Tensile strength prediction of softwood glulam lamellas using virtual vibration technique.* ASCE, Journal of Materials in Civil Engineering.

Khelifa M., Khennane A., El Ganaoui M., Celzard A. (2016) *Numerical damage prediction in dowel connections of wooden structures.* Materials and Structures 49:1829-1840. doi:10.1617/s11527-015-0615-5.

Khennane A., Khelifa M., Bleron L., Viguier J. (2014) *Numerical modeling of ductile damage evolution in tensile and bending tests of timber structures.* Mechanics of Materials 68:228-236. doi:10.1016/j.mechmat.2013.09.004.

Kollmann F.F.P., Cote W.A. (1984) *Principles of wood science and technology.* Springer-Verlag, Berlin.

Kovryga A., Stapel P., van de Kuilen J.W.G. (2016) *Tensile strength classes for hardwoods.* INTER-3rd Meeting, Graz, Austria. 49 - 10 – 1, pp. 97-113.

Kovryga A., Khaloian Sarnaghi A., van de Kuilen J.W.G. (2019) *Strength grading of hardwoods using transversal ultrasound.* Proceedings of the seventh international scientific conference on hardwood processing ISCHP, Delft, The Netherlands, pp. 220-229.

Kowalczyk P. (2010) *Simulation of orthotropic microstructure remodeling of cancellous bone.* Journal of Biomechanics 43, 563–569.

Kretschmann D.E. (2010) *Mechanical properties of wood.* ROSS, R.J. (ed.): Wood Handbook- Wood as an Engineering Material. U.S. Department of Agriculture. Chapter 5, 5/1-5.

Kuisch H., Gard W., Botter E., van de Kuilen J.W.G (2012) *Brittleheart as a critical feature for visual strength grading of tropical hardwood-approach of detection.* World Conference on Timber Engineering WCTE, University of Auckland, New Zealand. Pp. 20-29.

Lang R., Kaliske M. (2013) *Description of inhomogeneities in wooden structures: modeling of branches.* Wood Sci. and Tech., 47:1051−1070.

Lee H. (2015) *Damage modeling for composite structures.* PhD thesis, University of Manchester.

Li M., Füssl J., Lukacevic M., Eberhardsteiner J., Martin C.M. (2018) *Strength predictions of clear wood at multiple scales using numerical limit analysis approaches*. Computers and Structures 196:200-216. doi:10.1016/j.compstruc.2017.11.005.

Liang S.Q., Fu F. (2007) *Comparative study on three dynamic modulus of elasticity and static modulus of elasticity for Lodgepole pine lumber,* Journal of Forestry Research, 18(4): 309-312.

Ling C.B. (1968) *On Stress Concentration Factor in a Notched Strip*. Trans. ASME, Applied Mechanics Section. 90:833.

Lopes C.S. (2009) *Damage and failure of non-conventional composite laminates*. PhD thesis, Delft University of Technology.

Lukacevic M., Füssl J. (2014) *Numerical simulation tool for wooden boards with a physically based approach to identify structural failure.* Eur J Wood Prod, 72:497−508.

Lukacevic, M., Füssl, J., Eberhardsteiner, J. (2015) *Discussion of common and new indicating properties for the strength grading of wooden boards*. Wood Sci Technol., 49:551–576. doi 10.1007/s00226-015-0712-1

Maimí P. (2006) *Modelización constitutiva y computacional del daño y la fractura de materiales compuestos*. PhD thesis, Universitat de Girona, Spain.

Maimí P., Mayugo J.A., Camanho P.P. (2008) *A three-dimensional damage model for transversely isotropic composite laminates*. Journal of Composite Materials 42(25):2717-2745. doi:10.1177/0021998308094965.

Maquer G., Schwiedrzik L., Zysset P.K. (2014) *Embedding of human vertebral bodies leads to higher ultimate load and altered damage localisation under axial compression*. Computer Methods in Biomechanics and Biomedical Engineering 17 (12), 1311-1322. doi: 10.1080/10255842.2012.744400.

Marra A.A. (1992) *Technology in wood bonding. Principles in practice*. Van Nostrand Reinhold, New York. ISBN: 0-442-00797-3.

Mattheck C. (1997) *Design in der Natur*, 3rd edn. Rombach Verlag, Freiburg

Matzenmiller A., Lubliner J., Taylor R.L. (1995) *A constitutive model for anisotropic damage in fiber-composites*. Mechanics of Materials 20(2):125-152. doi:10.1016/0167-6636(94)00053-0.

Mindlin, R.D. (1948) *Stress distribution around a hole near the edge of a plane in tension*. Proc. SESA, 5: 56-68

Nilsson C. (2009) *Modeling of dynamically loaded shotcrete*, Royal Institute of Technology, Stockholm. Master's thesis. ISSN: 1103-4297

Oscarsson, J. (2014) *Strength grading of structural timber and EWP laminations of Norway spruce-development potentials and industrial applications*. Linnaeus University, Sweden. Doctoral thesis.

Ouro P., Wilson C.A.M.E., Evans P., Angeloudis A. (2017) *Large-eddy simulation of shallow turbulent wakes behind a conical island.* American Institute of Physics, Physics of Fluids 29(12). doi 10.1063/1.5004028

Pettersson P., Lundström T.S., Wikström T. (2006) *A method to measure the permeability of dry fiber mats.* Wood and Fiber Science 38(3), 417-426.

Phillips G.E., Bodig J., Goodman J.R. (1981) *Flow-grain Analogy*. Wood Science 14: 55-65

Pilkey W.D., Pilkey D.F. (2008) *Peterson's Stress Concentration Factors*. 3rd Edition, John Wiley & Sons.

Pistoia W., van Rietbergen B., Lochmüller E-M., Lill C.A., Eckstein E., Rüegsegger P. (2002) *Estimation of distal radius failure load with micro-finite element analysis models based on three-dimensional peripheral quantitative computed tomography images*. Bone 30(6),842-848. doi:10.1016/S8756-3282(02)00736-6.

Rabbani H., Joekar-Niasar V., Shokri N. (2016) *Effects of intermediate wettability on entry capillary pressure in angular pores*. Journal of Colloid and Interface Science 473, 34–43.

Rabbani H.S., Zhao B., Juanes R., Shokri N. (2018) *Pore geometry control of apparent wetting in porous media.* Nature Scientific Reports 8, 15729.

Rais A., Poschenrieder W., Pretzsch H., van de Kuilen J.W.G. (2014a) *Influence of initial plant density on sawn timber properties for Douglas-fir (Pseudotsuga menziesii (Mirb.) Franco).* Annals of Forest Science. 71:617-626.

Rais A., van de Kuilen J.W.G., Pretzsch H. (2014b) *Growth reaction patterns of tree height, diameter, and volume of Douglas-fir (Pseudotsuga menziesii [Mirb.] Franco) under acute drought stress in Southern Germany.* Eur J Forest Res. 133(6):1043-1056. DOI 10.1007/s10342-014-0821-7.

Ravenshorst G.J.P. (2015). *Species independent strength grading of structural timber*. PhD Thesis, Delft University of Technology, the Netherlands.

Ruffoni D., van Lenthe G.H. (2017) *3.10 – Finite element analysis in bone research: A computational method relating structure to mechanical function*. In: Ducheyne P (ed) Comprehensive Biomaterials II, Volume 3. Elsevier, Oxford, pp. 169-196.

Sandhaas C. (2011) *3D material model for wood, based on continuum damage mechanics.* Stevinrapport 6-11-4, Stevin II Laboratory, Delft University of Technology, The Netherlands.

Sandhaas C. (2012) *Mechanical Behaviour of Timber Joints with Slotted-in Steel Plates*. PhD thesis, Delft University of Technology.

Staab G.H. (1999) *Laminar Composites*. Elsevier. Butterworth-Heinemann, ISBN: 9780080523927

Stapel P., van de Kuilen J.W.G. (2013) *Effects of grading procedures on the scatter of characteristic values of European grown sawn timber.* Mater Struct 46:1587-1598. Doi:10.1617/s11527-012-9999-7.

Stapel P., van de Kuilen J.W.G. (2014a) *Influence of cross-section and knot assessment on the strength of visually graded Norway spruce.* Eur. J. Wood Prod. 72(2):213-227. doi: 10.1007/s00107-013-0771-7.

Stapel P., van de Kuilen J.W.G. (2014b*) Efficiency of visual strength grading of timber with respect to origin, species, cross section, and grading rules: a critical evaluation of the common standards.* Holzforschung 68(2):203-216. doi 10.1515/hf-2013-0042.

Stoeckel F., Konnerth J., Gindl-Altmutter W. (2013) *Mechanical properties of adhesives for bonding wood-A review.* International Journal of Adhesion & Adhesives 45:32–41

Stübi T. (2011) *Gütesortierung von Schweizer Holz durch Kombination von mehreren Erkennungsmethoden.* Diplomarbeit, Schweizerische Hochschule für die Holzwirtschaft, SH-Holz, Biel.

Tasdemirci A., Hall I. W. (2005) *Experimental and Modeling Studies of Stress Wave Propagation in Multilayer Composite Materials: Low Modulus Interlayer Effects.* Journal of Composite Materials. Doi: 10.1177/0021998305048736.

Valipour H., Khorsandnia N., Crews K., Foster S. (2014) *A simple strategy for constitutive modeling of timber*. Construction and Building Materials 53:138-148. doi:10.1016/j .conbuildmat .2013 .11.100.

Van der Linden M.R.L., Van de Kuilen J.W.G., Blaß H.J. (1994) *Application of the Hoffman yield criterion for load sharing in timber sheet pile walls*. Pacific Timber Engineering Conference, Gold Coast, Australia 412-417.

Wang Y.T., Yan Z.M., Wang H.M. (2013) *Numerical simulation of low Reynolds number flows past two tandem cylinders of different diameters.* Water Science and Engineering 6(4), 433-445.

Westermayr M., Stapel P., van de Kuilen J.W.G. (2018) *Tensile and Compression Strength of Small Cross Section Beech (Fagus s.) Glulam Members*. Proceeding of INTER International Network on Timber Engineering Research, Tallinn, Estonia. 51-12-2

Whitley D.W. (2013) *Interacting stress concentration factors and their effect on fatigue of metallic aerostructures*. Missouri University of Science and Technology, PhD thesis.

Wong K.K.L., Wang D., Ko J.K.L., Mazumdar J. , Le T.T., Ghista D. (2017) *Computational medical imaging and hemodynamics framework for functional analysis and assessment of cardiovascular structures.* Biomed engineering online 16(1), 35. doi: 10.1186/s12938-017-0326-y.

Xu B.H., Taazount M., Bouchaïr A., Racher P. (2009) *Numerical 3D finite element modeling and experimental tests for dowel-type timber joints*. Construction and Building Materials 23 (9):3043-3052. doi:10.1016/j.conbuildmat.2009.04.006.

Zandbergs J.G., Smith F.W. (1987) *Finite Elements fracture prediction for wood with knots and cross grain*. Wood and Fiber Science. 20: 97-106.

Zdravkovich M.M. (1987) *The effects of interference between circular cylinders in cross flow.* Journal of Fluids and Structures 1, 239-261.

Appendix 1: Fiber pattern
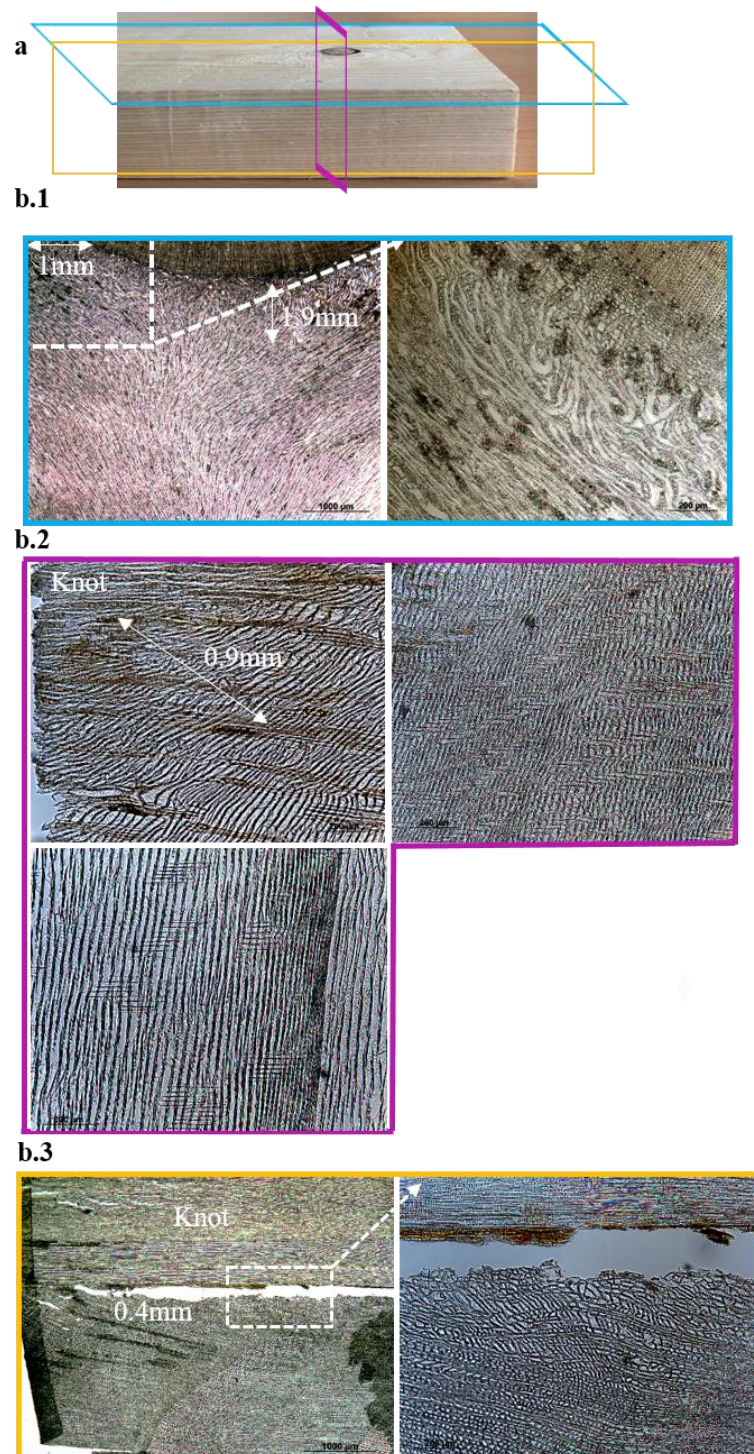
Figure A1.1: Detailed look to the knot area in three coordinate directions and in different surface cuts (a). Different cuts of 20 мм are made from the x (b.1), z (b.2) and y (b.3) directions of the board and images are made with a magnification of x25 and x100 from the areas close to the knot to show the rotational behavior of the fibers in the vicinity. Thickness of the complex-vortex layer around the knot is measured and is compared in both physical and numerical samples. Thickness of this layer in front of the knot is the largest with 1.9 mm (b.1). Thickness of this layer is reduced to about 1 mm on the side of the knot in z-direction (b.1 and b.2). However, a very small vortex layer is observed in y-direction with 0.4 mm (b.3).
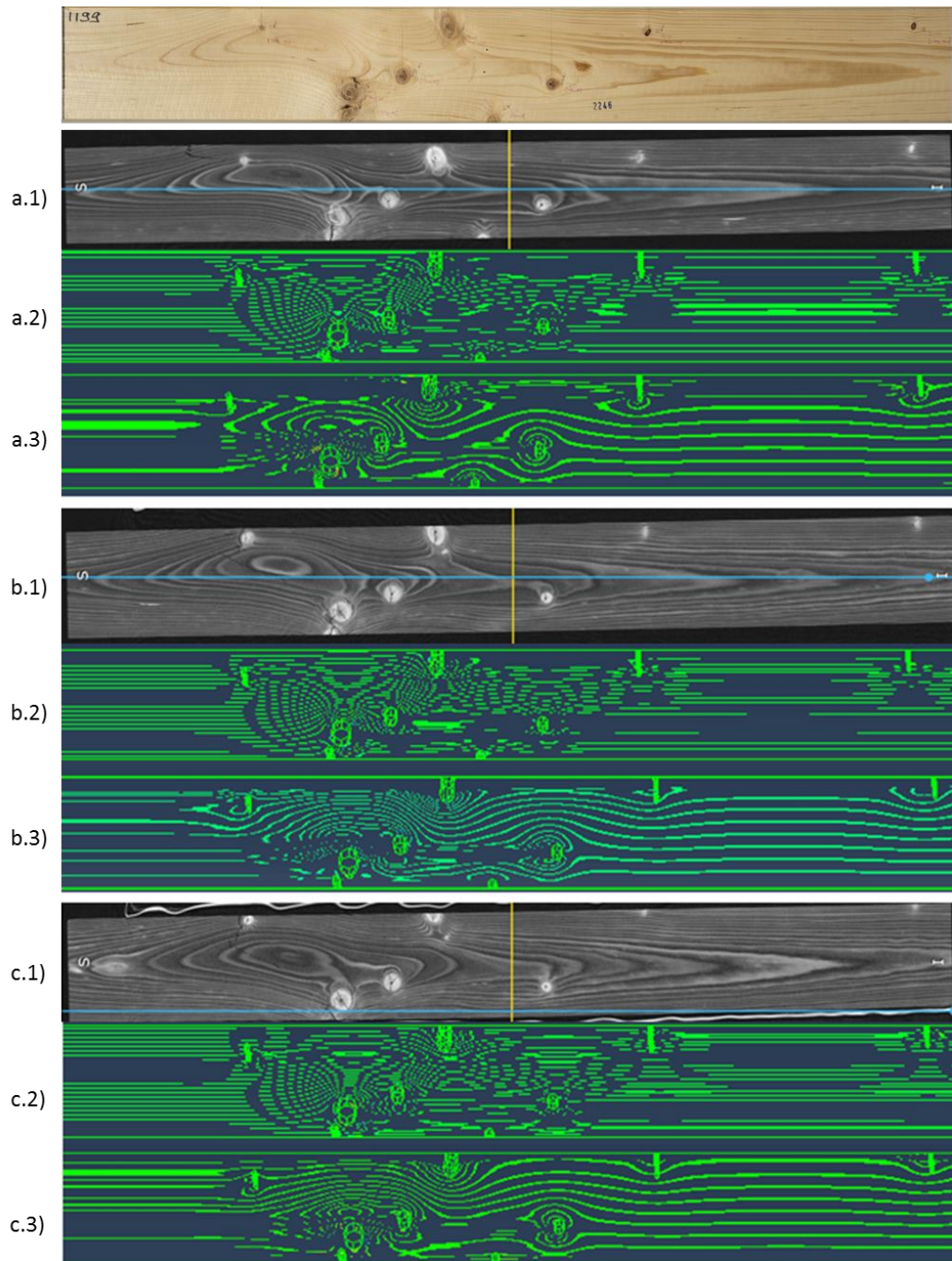
Figure A1.2: Spruce sample 2246 with upper, middle and lower surface cuts respectively and the analysis of upward and downward flow in each case.
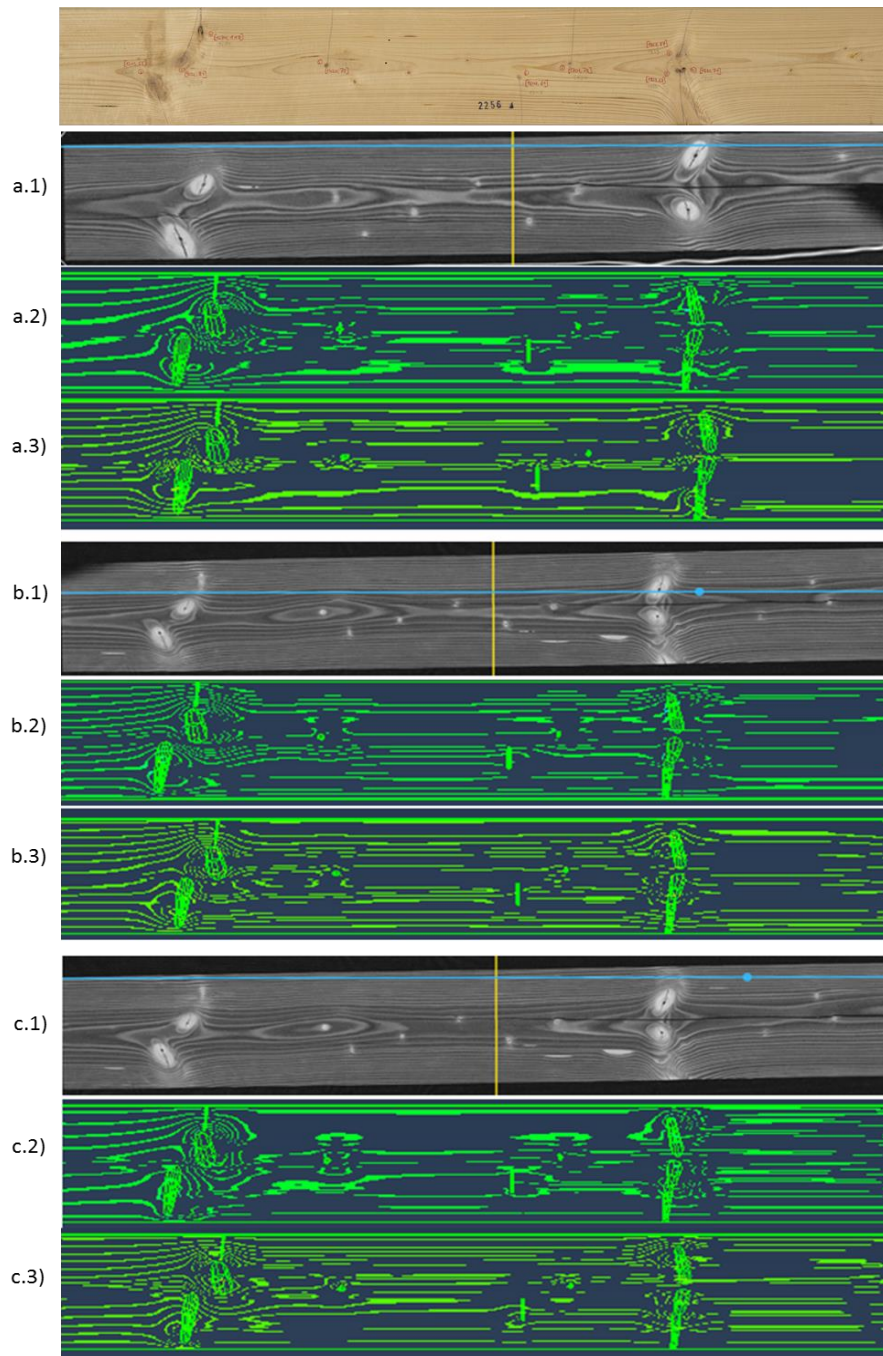
Figure A1.3: Spruce sample 2256 with upper, middle and lower surface cuts respectively and the analysis of upward and downward flow in each case.
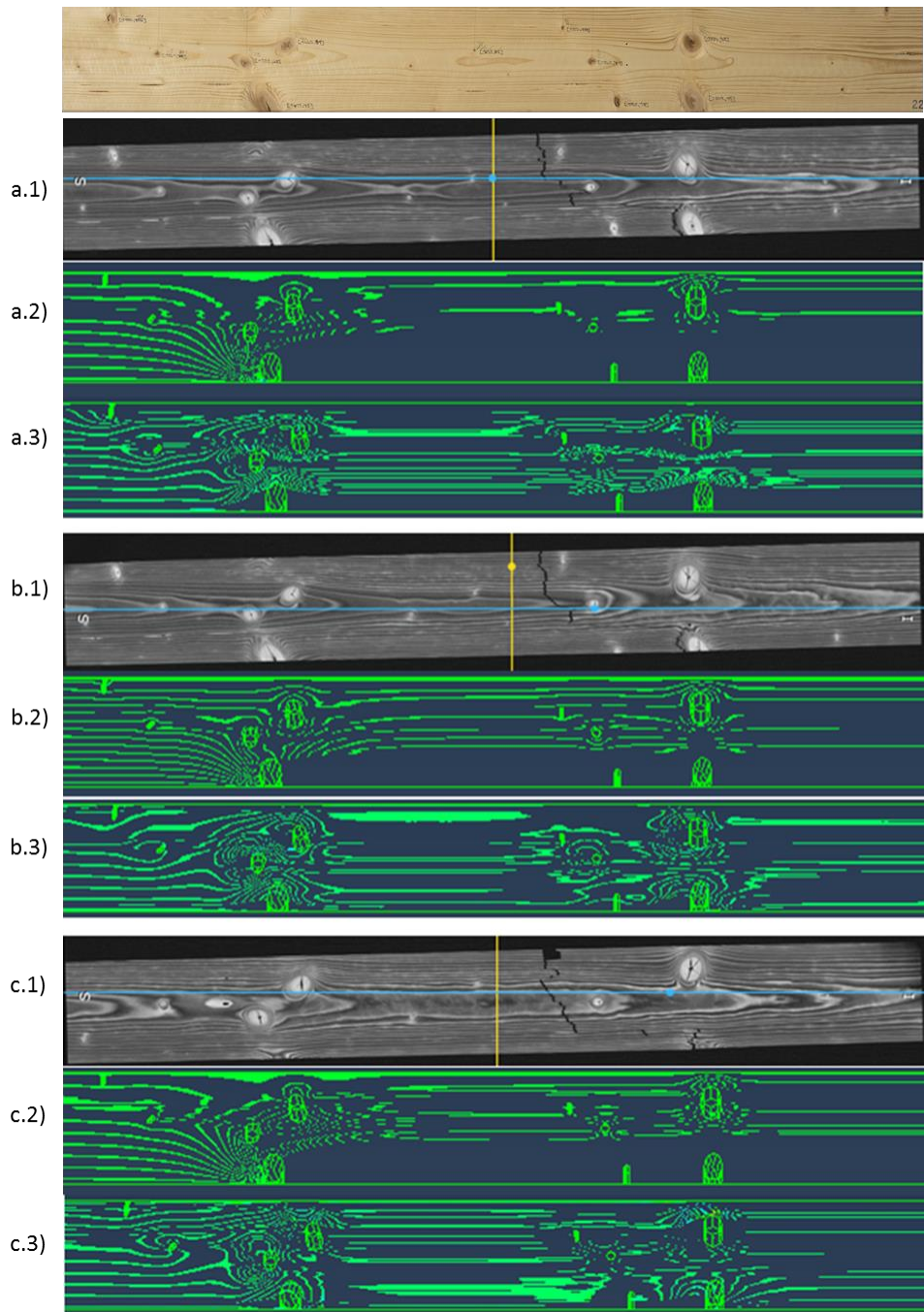
Figure A1.4: Spruce sample 2248 with upper, middle and lower surface cuts respectively and the analysis of upward and downward flow in each case.
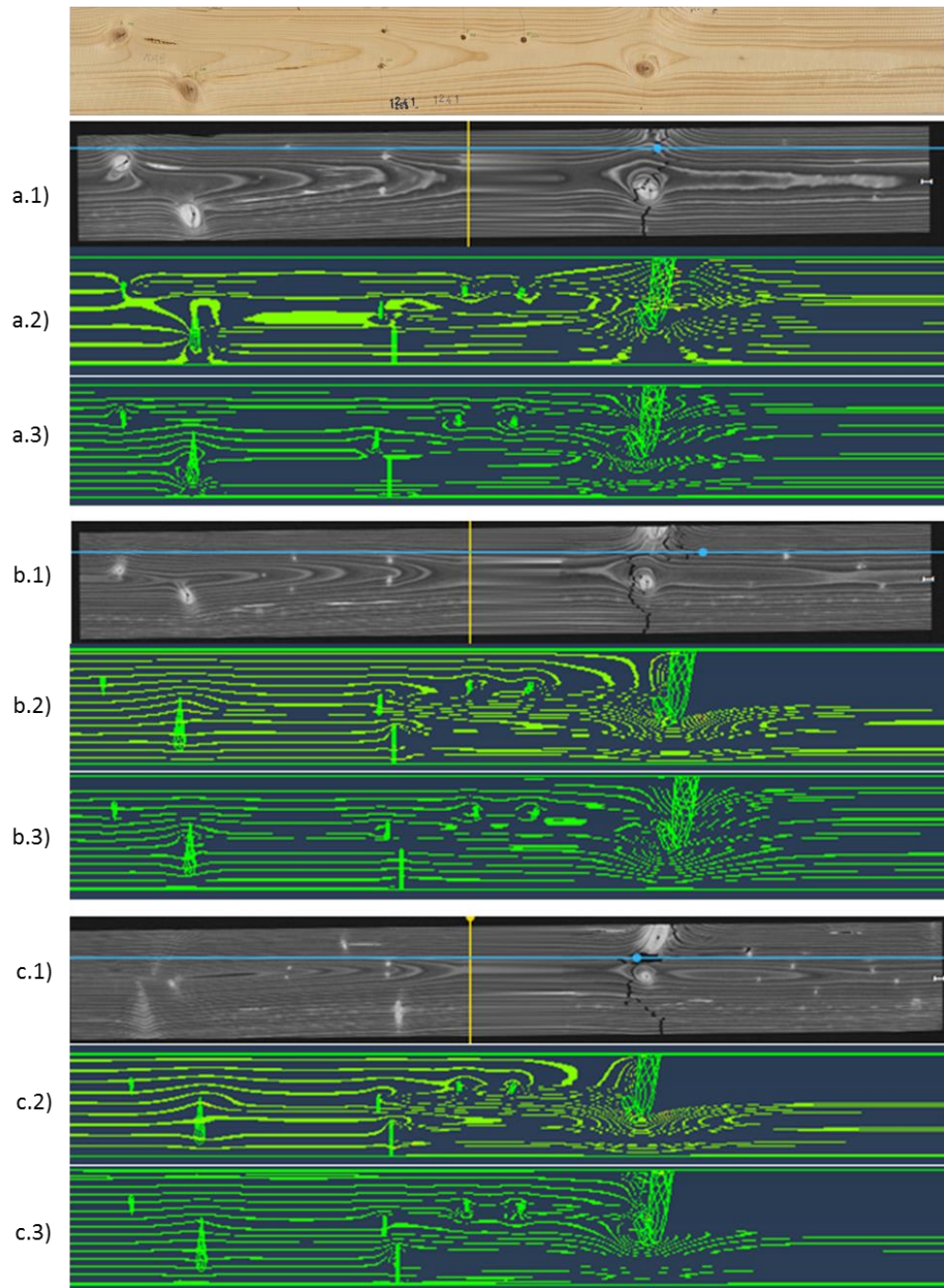
Figure A1.5: Spruce sample 1241 with upper, middle and lower surface cuts respectively and the analysis of upward and downward flow in each case.
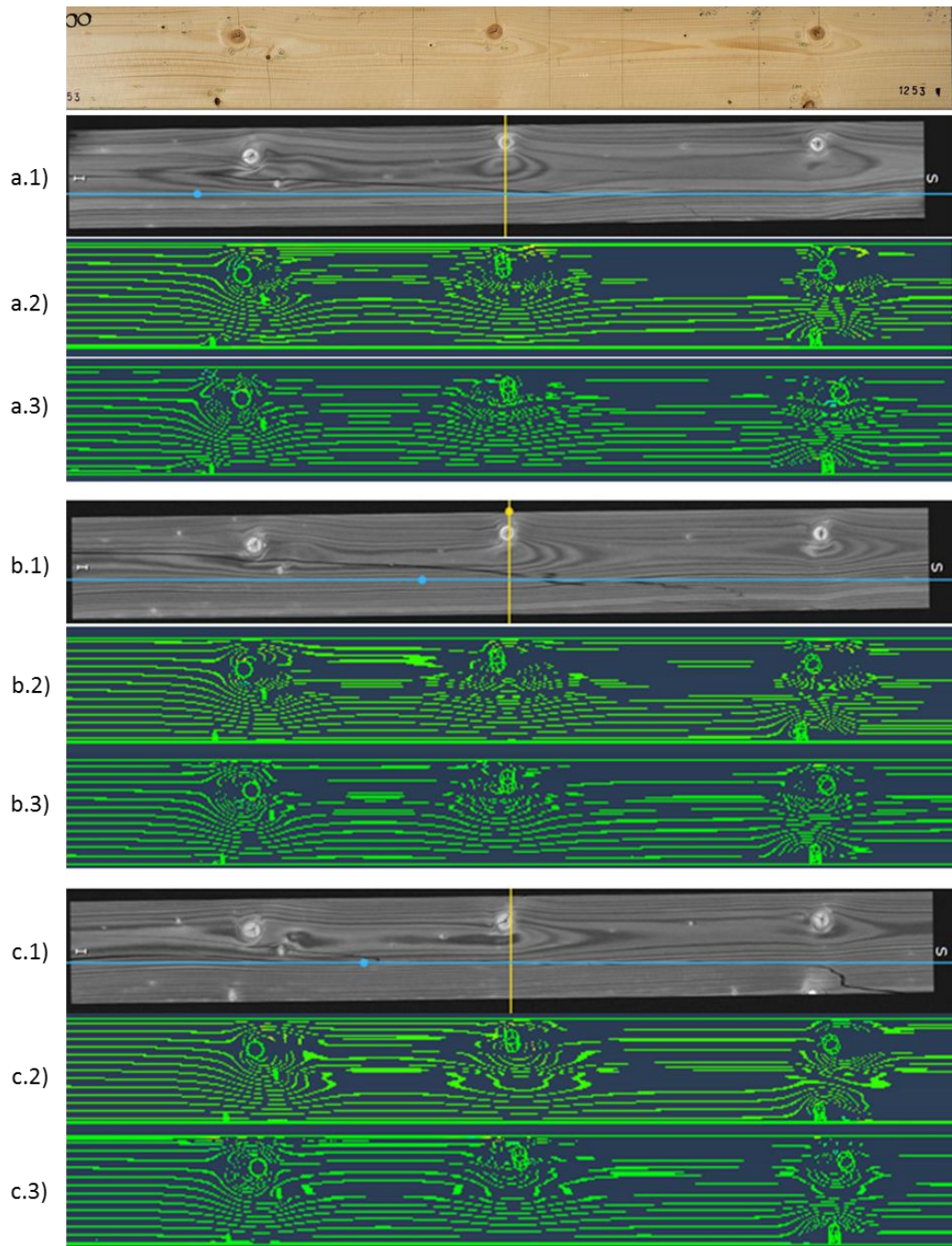
Figure A1.6: Spruce sample 1253 with upper, middle and lower surface cuts respectively and the analysis of upward and downward flow in each case.
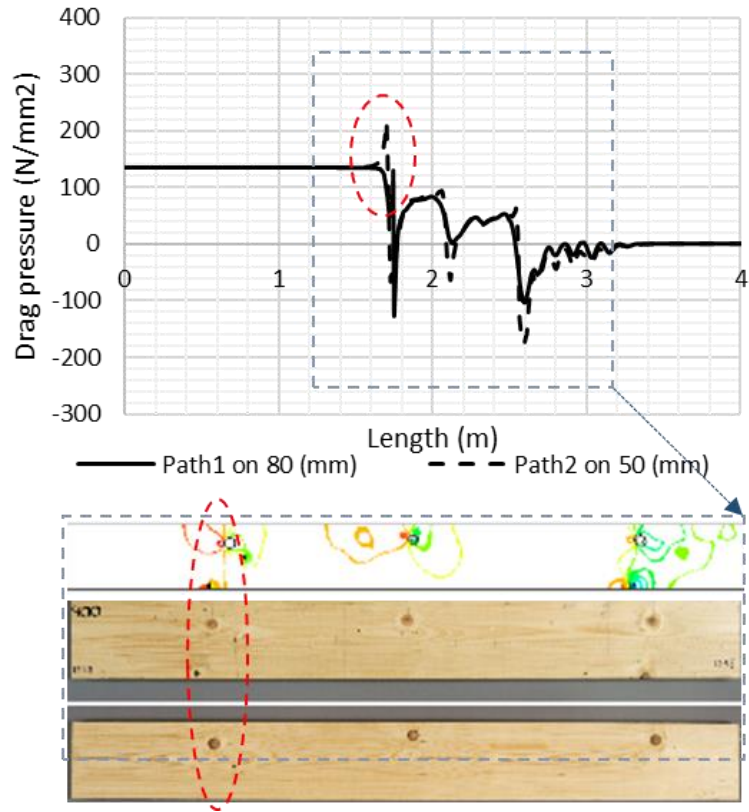
Figure A1.7: Prediction of the failure in sample 1253 and comparison to its actual failure pattern.
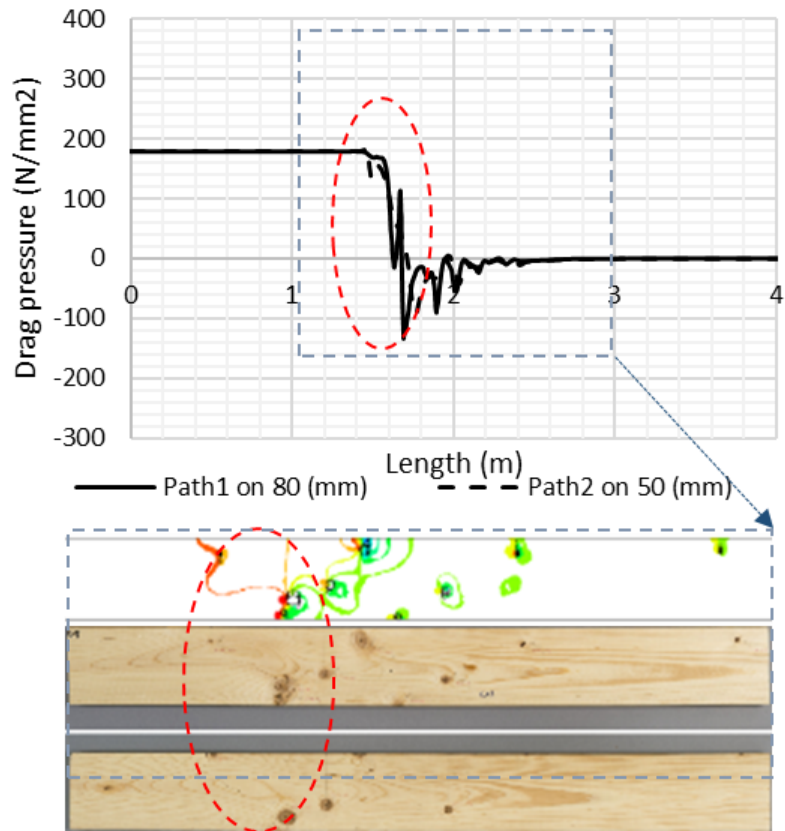
Figure A1.8: Prediction of the failure in sample 2246 and comparison to its actual failure pattern.
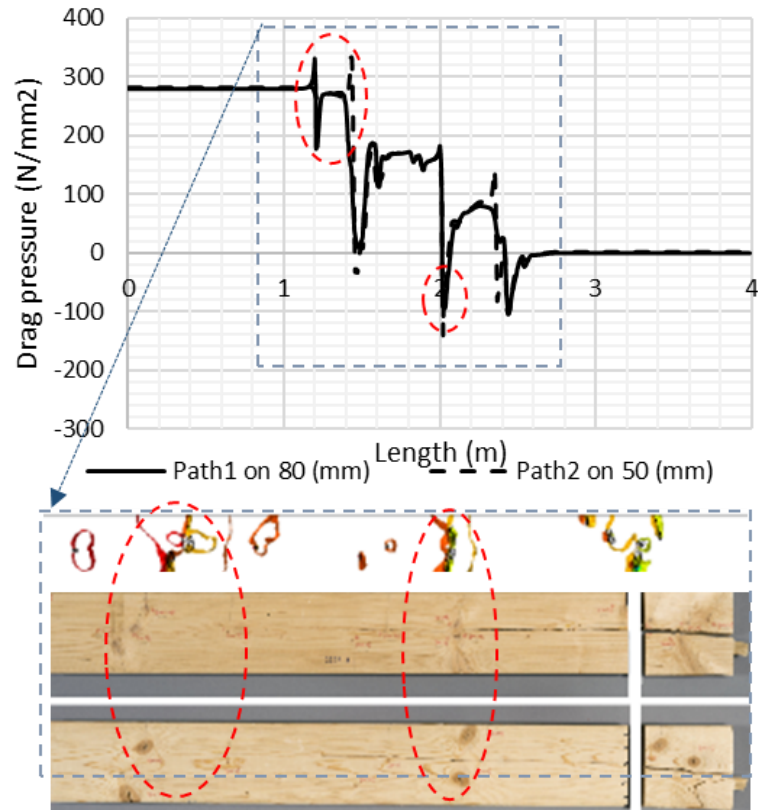
Figure A1.9: Prediction of the failure in sample 2256 and comparison to its actual failure pattern.
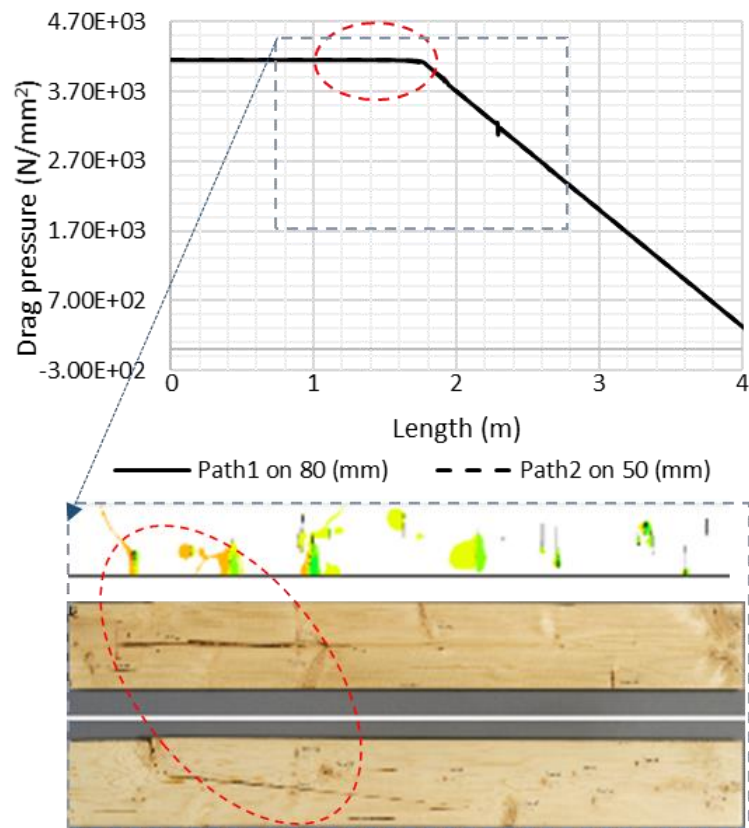
Figure A1.10: Prediction of the failure in sample 2239 and comparison to its actual failure pattern.

Appendix 2: Hardwood ash and maple
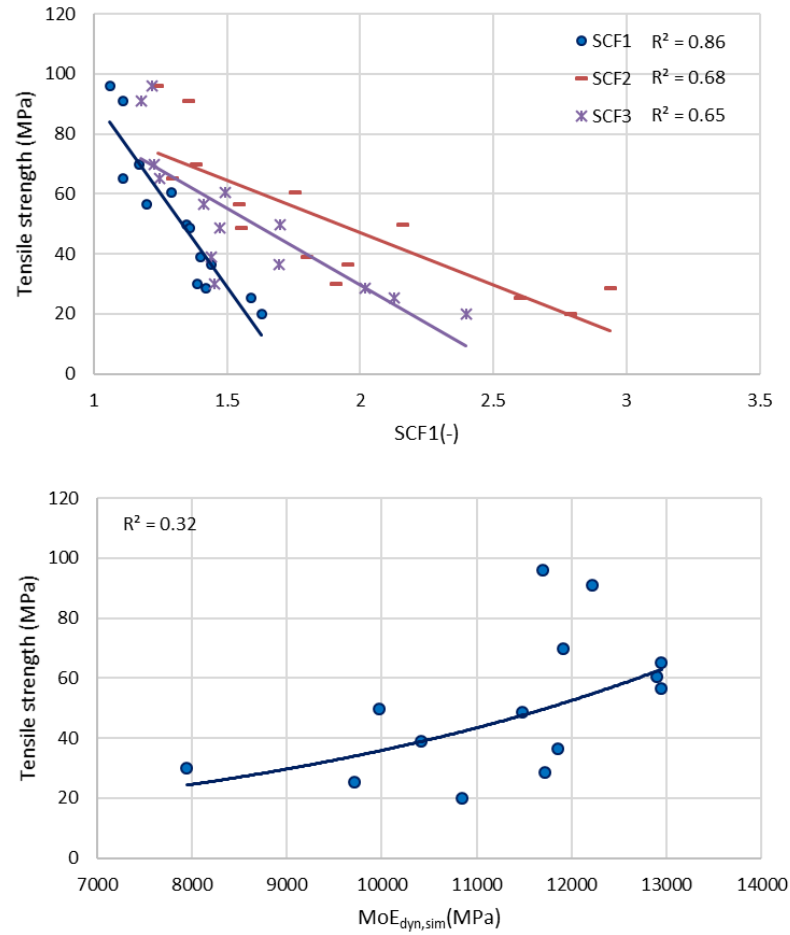
Figure A2.1: R*elation between the SCFs and virtual dynamic MoE with the tensile strength of the boards.*
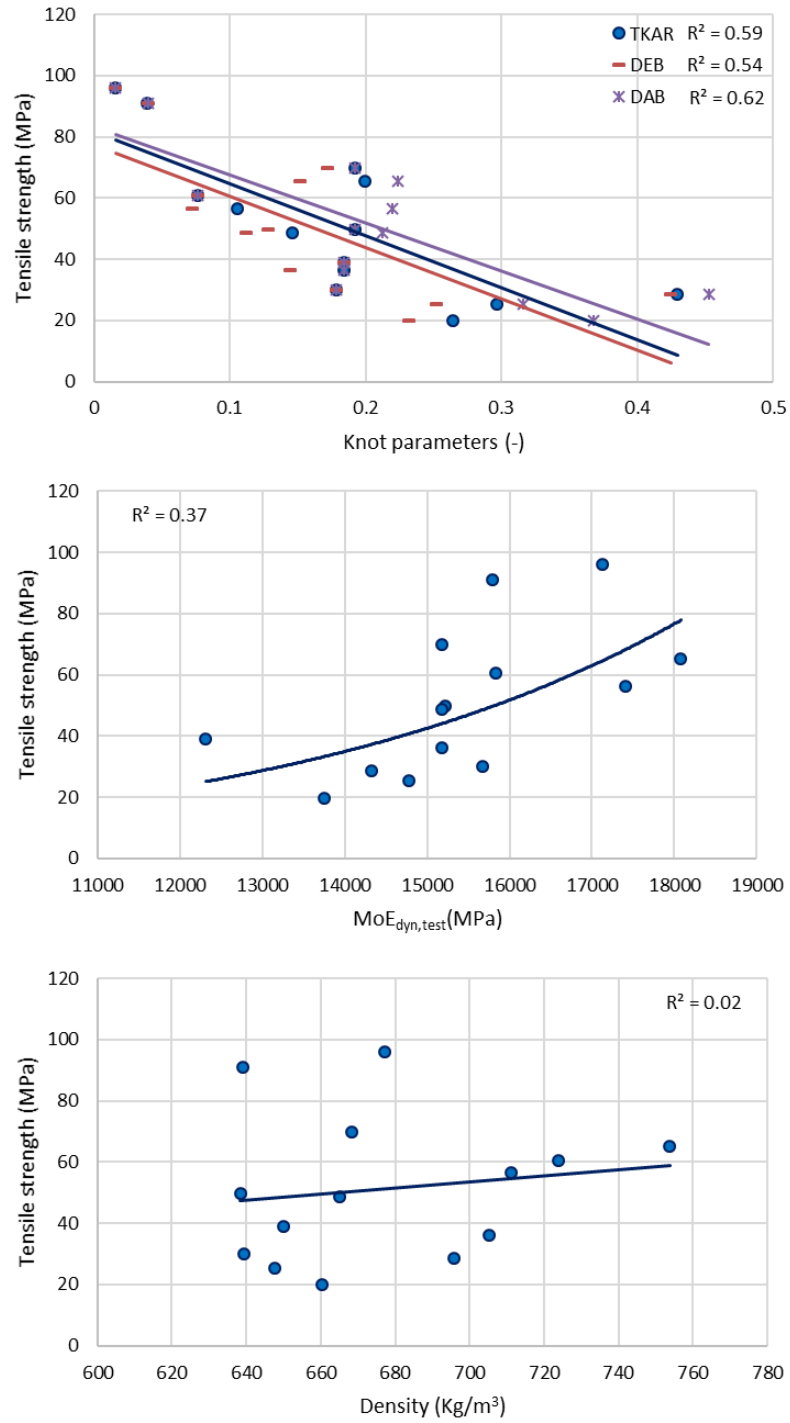
Figure A2.2: Relation between the measured parameters (TKAR, DEB, DAB, dynamic MoE and density) with the tensile strength of the boards.
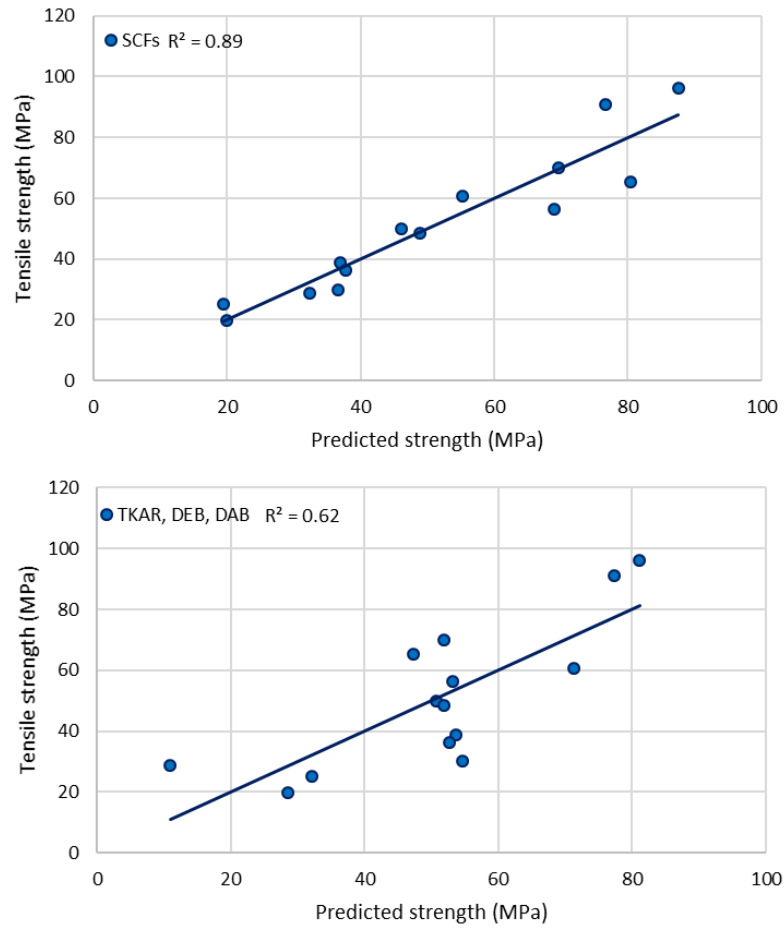
Figure A2.3: Linear multiple regression analysis between the numerical and measured knot parameters.

Appendix 3: Papers for complete virtual strength prediction process

Paper 1: Strength prediction of timber boards using 3D FE-analysis
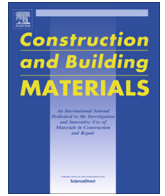
Strength prediction of timber boards using 3D FE-analysis

A. Khaloian Sarnaghi [a,*], J.W.G. van de Kuilen [a,b,c]

[a] *Department of Wood Technology, Technical University of Munich, 80797 Munich, Germany*
[b] *Faculty of Civil Engineering and Geosciences, Delft University of Technology, Delft, Netherlands*
[c] *CNR-Ivalsa, Florence, Italy*

HIGHLIGHTS

- Full 3D anisotropic model is based on the visible knot geometries on the surfaces.
- Stress concentration factors represent the stress effects of multiple knots.
- Virtual dynamic modulus of elasticity is determined for a range of wood qualities.
- Wood surface image and average density are sufficient as input parameters.
- The 3D FE-model is a better strength predictor than current grading methods.

ARTICLE INFO

ABSTRACT

Timber boards are numerically reconstructed in the full 3D space based on knot information on the wood surface. The 3D model is then transformed into a full 3D-FEM model and successively used for tensile strength prediction. By knowing the exact locations of the knots, as the main strength governing parameters in timber boards, simulations are run for a large quality range of wood laminations. This includes low-medium quality Douglas fir and medium-high quality spruce boards. ABAQUS and PYTHON are used for the numerical simulations. An automatic link is programmed to extract data of the database and to create the 3D geometrical model. From the numerical simulations, three mathematical methods are presented to calculate the stress concentration factors (SCFs) around the 3D heterogeneous defects in anisotropic wooden boards. Additionally, the explicit dynamic analysis are run to obtain the dynamic modulus of elasticity (MoE_{dyn}). To reduce the dependency of the numerical predictions on the real density of the boards, the average density of each sample is used for the simulations. Each board is tested in tension physically and is used for the validation of the model. The FEM results are used in a regression analysis to analyze the correlation with the visual measurements and to predict the tensile strength. Based on the results of a multiple regression analysis, two SCFs and MoE_{dyn} are sufficient to accurately predict the strength of spruce and Douglas fir boards. The results of the current study show that an improvement in the strength prediction of wood is possible in comparison with current machine grading systems based on dynamic MoE and knot parameters.

© 2019 Elsevier Ltd. All rights reserved.

1. Introduction

Wood is a strongly anisotropic and non-homogeneous material. For use in engineered structures, the material needs to be graded, a process that estimates the mechanical properties in order to optimize its use. In softwood, the main strength governing parameters are knots. These natural defects are causing weak spots and local fiber deviations that cause locally reduced strength properties, especially when loaded in tension or bending. Knots can be

assigned to different subgroups, depending on the location of the center of the tree in timber. These geometrical features can have different shapes and can be visible on multiple surfaces. Fiber deviations around knots and natural defects are some aspects making wood a unique but complex material for structural applications. The tensile strength properties of boards are strongly correlated with these heterogeneities. Having more accurate information about these geometrical features and their consequences for the strength may lead to more accurate strength predictions and thus more economic use of the material. Different studies are concentrated on the structural modelling of wood and predicting the strength reduction and failure, resulting from structural

---

non-uniformities [1–13]. Generally, these studies tried to predict localized bending strength reductions [14] as well as the static modulus of elasticity of beams with various degrees of success [14,15].

Geometrical non-uniformities in wooden boards generally lead to high-localized stresses, and thus premature failure with low strength values. This is a general condition, valid for different isotropic and anisotropic thin materials, where the stress development around the imperfections get three times higher than the stresses developed in the clear part of the material [16]. These stress concentration effects are slightly more complicated for the 3D anisotropic and heterogeneous wood compared to other materials such as metals and fiber reinforced plastics [17–19]. The main difference is, however, that in these materials the defects are located at a-priori known locations, and with well-known geometries. In wood, both location and geometry are much less well-defined, not only leading to more complex stress-strain fields, but also the interaction between the defects is more complicated [20–26]. Couple of studies [16,17,23] have been considering the effects of multiple features under specific loading conditions and the interacting stresses as a consequence, especially in aerostructural applications. Variation of the stiffness map along the wooden boards due to the deviation of the fibers around these locations is another factor affecting the distribution of the stresses in this material. Consequently, the scatter in strength values can be quite large and CoV values up to 0.4 are not uncommon [27].

Due to the geometrical non-symmetry of the knots in wooden boards and due to the close proximity of other knots, the stresses that are developing around multiple knots are not the same as the stresses that would develop in a board with a single knot. In locations with multiple knots, the total maximum stress is affected by stresses of other knots in the vicinity. As a consequence, the stress development in boards is analyzed along different paths and compared to a perfect board without any knots.

Currently, wood needs to be strength graded before it is used in structural engineering products such as glulam. This process can be done either visually or by machine or in combination [28]. Visual grading is done based mainly on visible aspects such as knot geometry, size and location and growth ring width. Based on known relationships and declared boundary values, strength, stiffness and density values are assigned or the material is assigned to a certain strength class, such as those specified in EN 338 [27,29,30].

Machine grading uses non-destructive measurements to predict the mechanical properties. The non-destructive measurements generally comprise density and dynamic modulus of elasticity, sometimes combined with a knot recognition system [27]. The strength prediction is then based on a multiple regression analysis as will also be applied in this work.

In this paper, a model is provided for the strength prediction of spruce and Douglas-fir boards, solely based on the visual appearance of the knots on the wood surface and the ratio of modulus of elasticity over density [31]. The model is used for the calculation of stress concentration factors that are correlated to the strength. In addition, the knots and geometrical imperfections in the boards cause variations in the distribution and transfer of the stress waves, which influence the dynamic modulus of elasticity. Considering different numerical methods for the propagation of microwaves [32] and waves [33,34] in materials, as concrete and steel [35–38], layered elastic materials [39], and wood [40–44], the virtual dynamic modulus of elasticity of the boards is estimated, which is then used as an additional parameter for strength predictions.

Each of the boards used for the numerical simulations are tested in tension [45,46] in the laboratory after being visually graded. Therefore, the stiffness and strength results of the boards are available for each case, which makes it possible to validate the results.

Finally, the simulation results are used in regression analyses and each parameter is compared to the experimental tensile strength values. This is done to validate the prediction capabilities based on both visual and numerical methods. By performing a multiple regression analysis for each species, it will be shown that reliable correlation exist between the derived stress concentration factors and dynamic modulus of elasticity on the one side and the tensile strength on the other.

2. Materials

2.1. Spruce and Douglas fir samples

Both spruce and Douglas fir samples are analysed as these species are commonly used for glulam tensile boards. In general, 102 medium to high quality spruce boards and 150 low to medium quality Douglas fir boards are used for this study. Spruce boards have dimensions of (4200*40*150) whereas the dimensions of the Douglas fir boards are (4500*46*146). In contrast to the spruce boards, the Douglas fir boards contained up to 89 knots. The geometrical configuration of the knots and their orientations in the spatial coordinate are causing reductions in the strength of the Douglas fir boards. The full sample analysis is given in [47] and [48]. The basic data, which also forms the basis for the numerical model, is given in form of the primary grading parameters as knottiness, MoE$_{static}$, MoE$_{dyn}$, density in Table 1. As shown in this table, the scatter is quite large and a CoV value higher than 0.4 is found in the case of Douglas fir. The boards are visually graded and the knot structure in each board is registered, but the way of registration is different for the two samples.

Visual grading is done based on the visible parameters of the knot geometries and growth ring width, where the strength, stiffness and density values can be estimated by known relationships [28,29]. The experimental data includes the density measurements of the boards, the measurements of the dynamic [27] and static modulus of elasticity, the strength values of the tensile tests, and finally, the knot measurement and visualization parameters of DEB, DAB, and TKAR [27,29].

DEB is measured based on the sum of the length of all the edges of the surfaces, where knot is appearing [49]. DAB is measured by considering a window of 150 mm over the board and summing up the edges of the projected areas of the knots, existing in the window after minimizing the overlapping edges of the knots [49]. TKAR is measured similar to DAB but instead considering the entire cross sectional areas in a window of 150 mm, mathematically presented by Eq. (1).

$$DEB = \max\left[\frac{\sum a_i}{2.b}\right] \quad DAB = \max\left[\frac{\sum a_i}{2.b}\right] \quad TKAR = \max\left[\frac{\sum A_i}{d.b}\right] \quad (1)$$

Generally, the best possible strength prediction is obtained by combining the data of MoE$_{dyn}$ and knots in a multiple regression analysis.

2.2. Surface knot data registration of the boards of Table 1

The knot data of the medium-high quality spruce boards are measured with high accuracy allowing for a full 3D reconstruction, whereas the knot data of the low-medium quality Douglas-fir is less precise, and some assumptions need to be made for the full 3D board reconstruction. Before preforming the tests, each board is visually graded, through which the knot dimensions are evaluated. Therefore, the database contains the detailed data regarding the geometrical representation of the knots with their spatial locations in the 3D coordinate space on each surface, the diameters and the angle of rotations. Fig. 1 shows schematically an example of a

Table 1
Basic data of the spruce (S) and Douglas fir (DF) boards.

	Sample	E_{static} (N/mm^2)	$E_{dynamic}$ (N/mm^2)	Density (Kg/m^3)	Knottiness			Tensile Strength (N/mm^2)
					TKAR(−)	DEB(−)	DAB(−)	
AVG	S	11,900	12,300	462	0.30	0.22	0.40	29.19
	DF	10,200	12,010	489	0.35	0.23	0.44	19.31
CoV	S	0.20	0.11	0.13	0.32	0.36	0.38	0.34
	DF	0.25	0.14	0.09	0.31	0.26	0.30	0.47
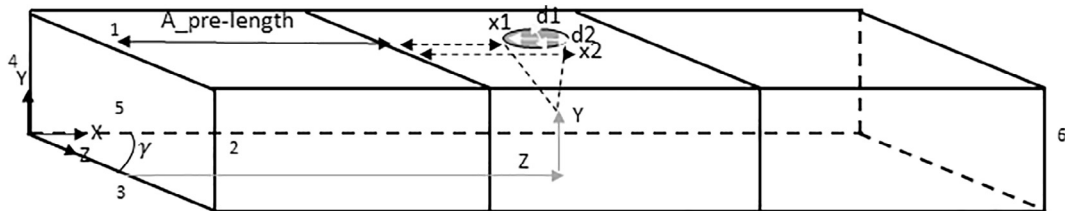
Fig. 1. The position of the global coordinate system and numbering of the surfaces for visual and numerical knot position registrations. Dotted black arrow shows the x-coordinate based on the local measurements in the test length, and black arrow shows the transformation to the global coordinate system. Light grey arrows show the maximum and minimum diameters of the knot. Dark grey arrows show the coordinates of the internal point.

board with one knot, which is visible only on surface number 1. Due to the representation of the x-coordinate of the knot as the center of the gravity of the knot volume for the Douglas fir boards, not enough information can be found about the exact coordinates of the beginning and ending points of the knot areas in the x-direction.

Based on the registered data regarding the maximum and minimum diameter of the knot an approximation has been made to predict these coordinates for creation of the geometrical model. This condition is shown in Fig. 2.

Dynamic Modulus of Elasticity (MoE$_{dyn}$) and density of each board are additional parameters that are measured in laboratory. Finally, by performing the physical tests (tension or bending) the strength parameters are determined. Thus, all the required parameters that are necessary for complete representation of the material are available.

3. Methods

3.1. Three dimensional board generation

As mentioned before, knots may have different shapes and geometrical configurations. Depending on the location of the center (pith) of the tree, some knots create only a point on one surface or internally in the board. In contrast to these knot types, if the center is located outside of board, knots create circular or elliptical areas on each of the covered surfaces, where the beginning and
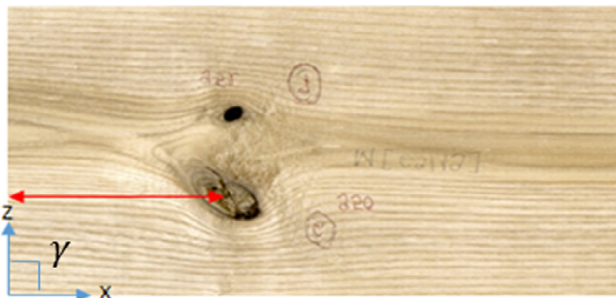
Fig. 2. Registration of the center of the gravity of the knot volume as x-coordinate (red arrow). (For interpretation of the references to color in this figure legend, the reader is referred to the web version of this article.)

ending position of the knot area on each surface need to be considered.

The 3D representation of the boards is generated through the following steps:

1) Knot data extraction from the database
2) Definition of separate plane and axis of rotation for each knot showing its center. Based on this consideration, the knot directions and angles are assigned to each knot separately, according to the data of visual measurements. The construction axis represents the central axis and rotation axis of the knot. Based on the location of the pith in the boards, knots are modelled with different conical or cylindrical shapes.
3) The location, orientation and shape of the knot, and evaluating the visibility of the knots on each surface.

An example of a geometrical model of a spruce board with knots, which are measured and presented in the test length of the board, is represented in Fig. 3. All knots with their complete geometrical configuration are represented.

To be able to reduce the effects of the dependency of the model to the extreme accuracy of the presented coordinate system of the knots, an error term of ±5 mm is added randomly, to be able to change slightly the geometry of the knots. This is done by using the uncertainties package with the ufloat () function in Python which takes the real dimension of the knot and generates numbers with uncertainties in the reconstruction process. The error term is added to all boards during the reconstruction process, based on which the coordinates of the knots are changed randomly in each direction by taking random values between zero and five.

4) After having created the 3D knot structure, the wood fiber structure of the board is generated using the flow-grain analogy around knots [1,50,51], as shown in Fig. 4.

By considering fluid flow around the knot, the stream function around the defect can be represented as Eq. (2).

$$\psi = V(a + b)\sinh(\zeta - \zeta_0)\sin(\eta - \alpha) \tag{2}$$

where, ψ is the stream function (showing the fiber direction in wood). a and b are the bigger and smaller radius of the elliptical knots, respectively. V is a constant, taking the flow rate. ζ and η
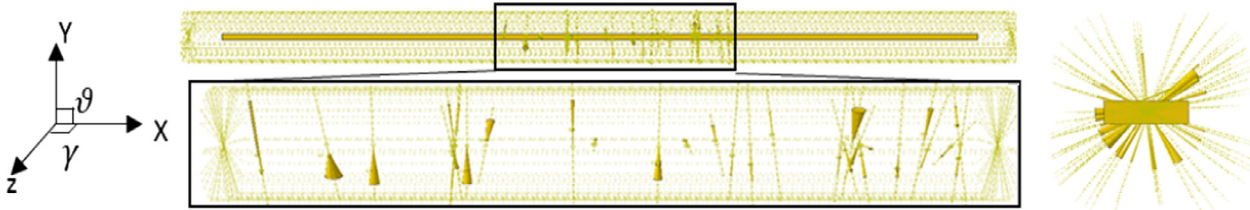
Fig. 3. Geometrical reconstruction of a spruce board with 39 knots in the test length with different planes and construction axis for each individual knot.
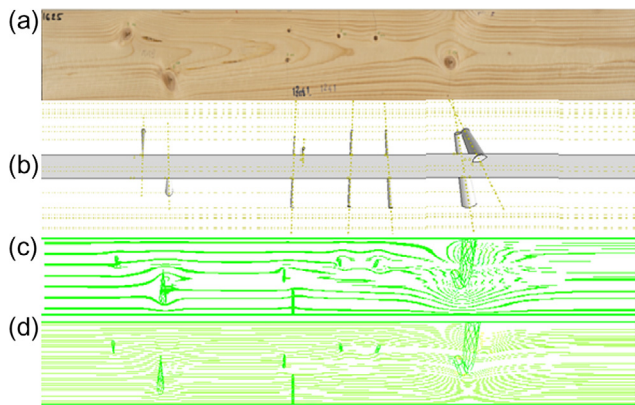
Fig. 4. a) Presentation of the real spruce board, b) geometrical reconstruction of the knots, c) structural model of fibers on the upper surface of the board, d) structural model of fibers on the lower surface of the board.

are the elliptical coordinates (representing the knot). α is the angle of the flow direction, before reaching the stagnation point, with respect to the bigger diameter of the knot. Finally, ζ_0 is a constant, presented in Eq. (3):

$$\zeta_0 = \frac{1}{2}\ln\left(\frac{a+b}{a-b}\right) \tag{3}$$

By extracting the data of the fiber deviations from the structural model, the orthotropic directions are defined for the mechanical model.

3.2. Numerical modelling

Python (2.7.3) and ABAQUS/Standard (Simulia, 6.14-2) are used in this study for creation of the automatic link to the database and for the numerical simulations respectively. The model is created in the following steps:

1. Read measurement data as input data for board reconstruction
2. Geometrical 3D reconstruction of the boards (Python script) and mesh generation
3. Application of flow grain analogy to derive the (3D) fiber pattern over the full board length
4. Assignment of orthotropic material properties based on the fiber pattern
5. Calculation of the stress distribution under a unit tensile load
6. Numerical stress wave analysis and modulus of elasticity prediction
7. Extraction of maximum stresses around each knot and stress concentration factor calculation.

In this process, Python is used as a tool to create the connection to the measured data and link it to ABAQUS. ABAQUS is used as a graphic user interface to reconstruct the knots, by defining separate central axis and plane for each case. Therefore, ABAQUS is used

as a CAD based software to create the geometrical view of the boards and as a CAE tool to run the numerical analysis. The mechanical behavior of wood is estimated under uniform tension [45,46]. Similar to the measurements, two reconstruction methods are followed in the modelling process (in the first case, knowing the exact geometrical coordinated of the knots on the surfaces of the board and in the second case knowing the center of the gravity of the knot volume as the x-axis). Based on the registered data, 3D geometry of each board is reconstructed in ABAQUS by automatically analyzing the location, orientation and shape of the knot, and evaluating the visibility of the knots on each surfaces.

C3D10 tetrahedral quadratic elements are used for the mesh. The mesh is generated from the knot boundaries outwards to the board boundaries. Therefore, a finer mesh is generated around the knots, which allows the detailed observation of the stress transfer. The mesh is kept relatively coarse in the clear wood part to save computational cost. A close-up of a typical mesh is shown in Fig. 5. Simulations are run considering the orthotropic properties of wood [52], applying the basic data of spruce and Douglas fir as presented in Table 1. The compliance matrix (S_{ijkl}) of this material is presented in Eq. (4).

$$\varepsilon_{ij} = S_{ijkl}.\sigma_{kl} \tag{4}$$

The boards are tested and simulated with a 1 MPa unit tensile stress. The boundary conditions of this study is schematically presented in Fig. 5. Two reference points are coupled to the board volume on the sides, which take the load and the boundary conditions and apply it to the board. The analyses are run in the linear elastic range, as the development of the elastic stresses around the knots are the point of interest here.

The knots are modeled as holes with different geometrical shapes and configurations. The difference in shapes and geometrical configurations follow from the knot measurements as shown in Figs. 1 and 2. The actual test length is equal to 9 times the width of the boards [36,37].

Although there are 150 Douglas fir boards in the sample, due to numerical instabilities and geometrical complications of some of them, 13 boards could not be accurately reconstructed in the 3D space. To consider the 3D interacting stress concentration factors in the vicinity of the knot clusters, three different methods are represented in the current study for calculation of the stress concentration factors of each board, which can be used for comparisons and predictions. The output parameters of the numerical procedure for the calculation of the stress concentration factors and the MoE$_{dyn}$ are presented in details in Section 3.3. The algorithm, which is developed in this study showing the complete numerical procedure, is schematically shown in Fig. 6.

3.3. Model output parameters

3.3.1. The stress concentration factors (SCFs)

The stress peaks are considered as the strength governing parameters and the possible locations where failure would initiate during the physical tests. Due to the complicated geometry, the
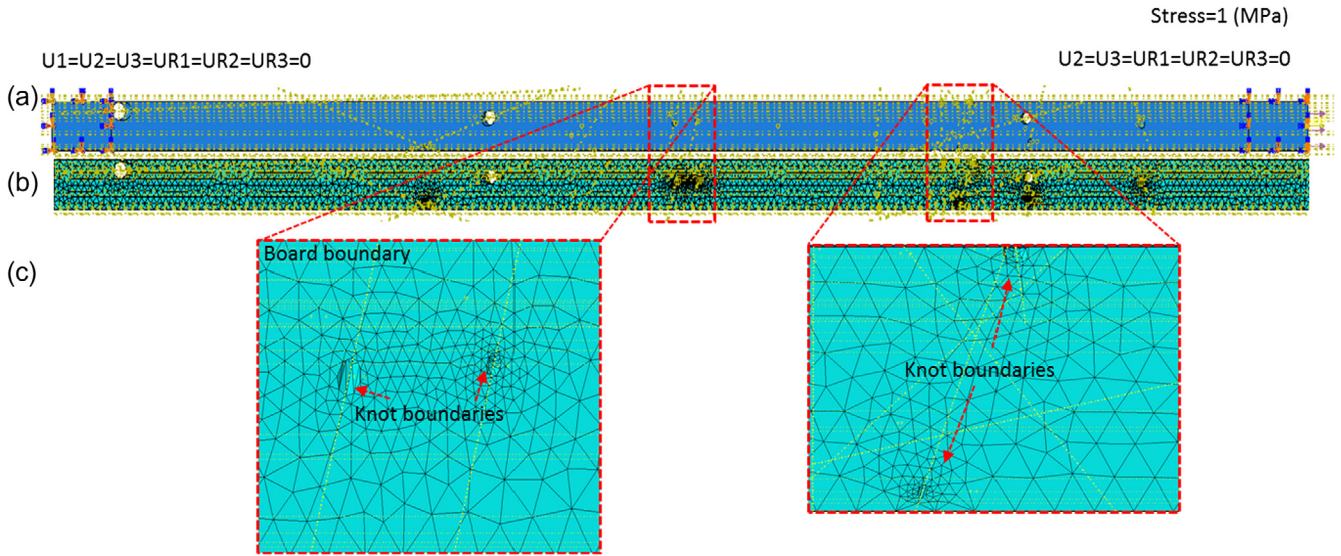
Fig. 5. The mechanical model. a) Applied boundary conditions in this study, b) mesh generation around knots, c) zoom in to the location of the knots.
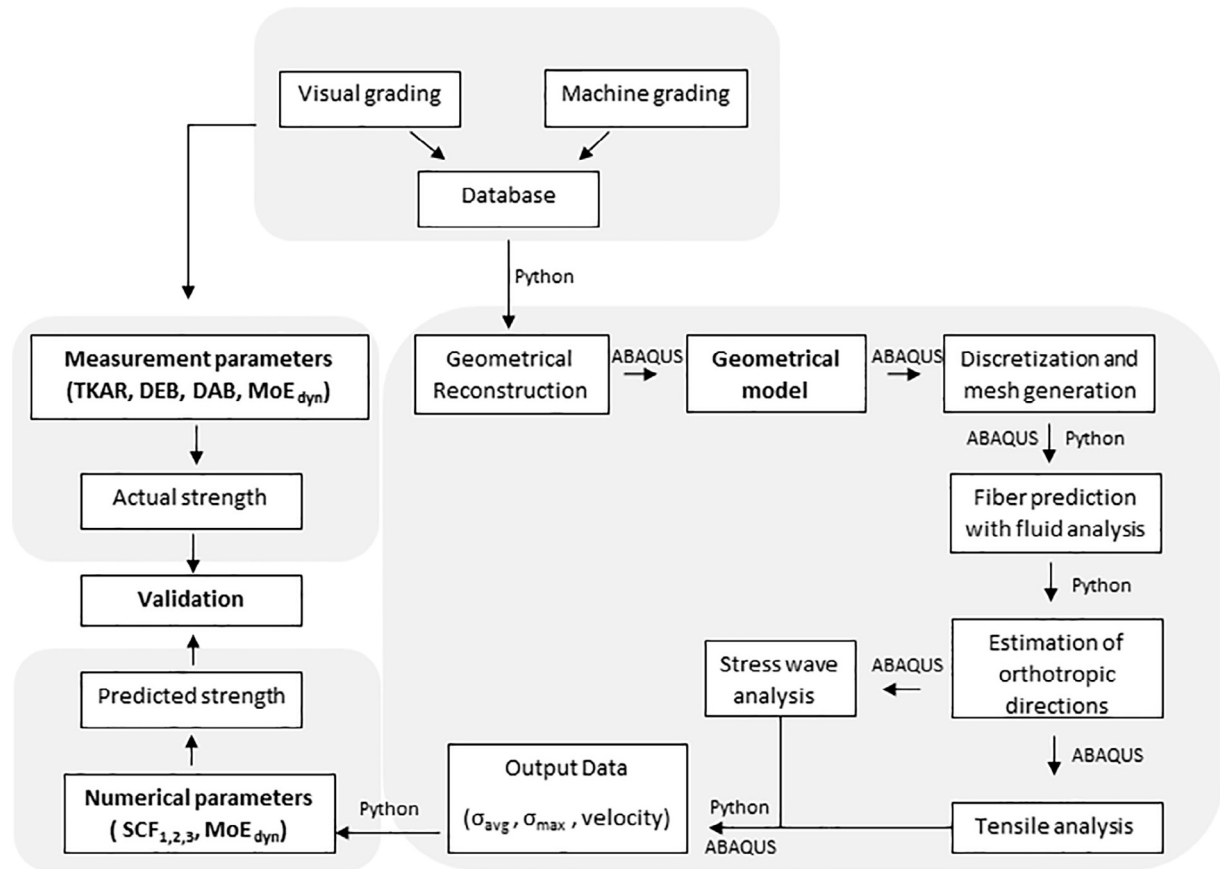
Fig. 6. The algorithm for the complete numerical process. The upper box shows the measurement process, the right-side box shows the numerical process and the left-side boxes show the validation procedure.

highest stress is not necessarily the location of the biggest knot. It can be due to the effects of the multiple knots, eccentricities and knot geometries. In contrast to the perfect board without any knots and defects, which is able to transfer the applied stress through the whole board uniformly, the board with knots develops these high stresses around the knots, which is due to the abrupt geometrical and boundary variations in the model. This condition is shown in the results part in Fig. 9.

In this study, three methods for the calculation of the SCFs in wooden boards are presented. The three SCFs are calculated based on the cross sections of the knots and the maximum and average stresses, obtained from the numerical analysis.

SCF$_1$ is calculated using mathematical Eq. (5).

$$SCF_1 = \max\left(\sigma_{sim} \cdot \frac{A_{knot}}{A_{total}}\right) \tag{5}$$

where σ_{sim} is the maximum stress around each knot. This stress is maximum σ_{11} of the elements, in a window from the beginning to the end of each knot separately. The nominal stress (σ_{nom}) of 1 MPa is applied on each board. A_{knot} is the biggest total cross sectional area of each knot on its central axis. A_{total} is the cross section of the board, as shown in Fig. 7.

The second SCF is calculated using the Eq. (6).

$$SCF_2 = \sigma_{avg} \cdot \left(\frac{A_{total}}{A_{total} - A_{knot}}\right) \tag{6}$$

where σ_{avg} is the average stress σ_{11} in the remaining clear part of the wood along path1 and path2 (shown in Fig. 8) for the knot with the maximum stress in the total board. A_{knot} is the area of the knot at that location.

The third SCF is calculated based on the Eq. (7).

$$SCF_3 = \sigma_{avg} \cdot \left(\frac{A_{total}}{|A_{total} - A_{projected}|}\right) \tag{7}$$

For calculation of the SCF$_3$ the board is divided into windows of 150 mm length, and the projected surfaces of the knots are summed up. $A_{projected}$ in Eq. (7) is the biggest projected knots surface in the window on the cross section.

3.3.2. Dynamic modulus of elasticity

For this set of analysis, the stress impact of 0.1 MPa is applied for a short time of 1e−5s and is set to zero for the rest of the analysis.

By extracting the velocity of the longitudinal stress wave, and by knowing the length of the boards, the eigen frequencies are calculated for each case using Eq. (8), representing the wave, which is traveling forth and back.

$$f = \frac{v}{2l} \tag{8}$$

where v is the velocity and l is the length of the board.

After calculating the frequencies, the dynamic modulus of elasticity is calculated, using Eq. (9).

$$E_{dyn} = 4l^2 f^2 \rho \tag{9}$$

where l is the length of the specimen and f is the first eigen-frequency.

Based on the analytical calculations, and according to the average material parameters of the wooden boards, an approximate velocity and time of flight for the stress wave propagation in the wooden boards are calculated. The approximated mean velocities are obtained as 4950 and 4750 (m/s) for the spruce and Douglas fir boards, respectively. By knowing the approximated velocities and the length of the boards, the total time of flight is estimated to be 1.7e−3 and 2e−3s for spruce and Douglas fir boards, respectively.
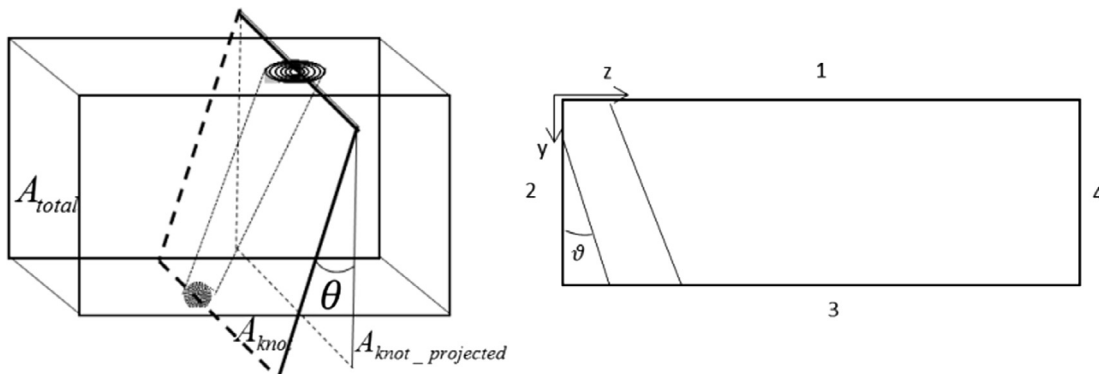
Fig. 7. Knot projection for calculation of SCF$_1$ and SCF$_3$.
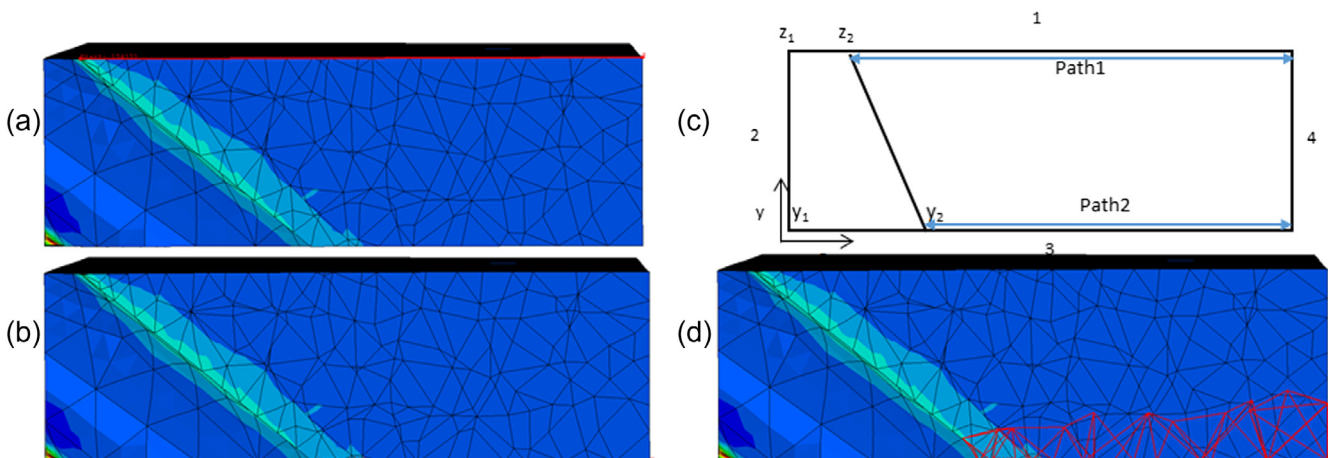
Fig. 8. Selection of the knot with maximum stress in the board. a) path1 on the upper edge of the cross-cut surface (from the end coordinate of the knot till the end of the board), b) path2 on the lower edge of the cross-cut surface, c) schematic representation, d) inclusion of the intersection point for calculation of the average stress along the path.

To reduce the dependency of the predictions on the density of the boards, the average density and average modulus of elasticity of each specimen set is used as an input parameter for the numerical simulations, as the individual board values are still unknown at the moment of the predictions. According to Ravenshorst [31] a linear correlation is existing between the density and the modulus of elasticity, and the ratio of these parameters remain constant for the total cluster of wood species.

4. Results

A typical example of the stress variation over the length of a board is shown in Fig. 9. The board is characterized by two big edge knots and multiple scattered small knots. The marked region contains the biggest edge knots and couple of smaller ones in the vicinity. Higher stresses are found in this area, which is also the area where failure occurred in the experimental test.

In Fig. 10 a board with many knots and knot clusters over the length is presented, indicating the knots in the 3D space. The

development of maximum stresses σ_{11} along the x-axis is shown through three different paths, located on the center of the board and on the center of the front and back edges. σ_{11} in Fig. 10 is the maximum stress that is developing around each individual knot. These stresses are then transformed to σ_{sim} and SCF_1 in accordance with Eq. (5).

Due to the complicated geometries and the existence of the knots with different central axis and rotations, the stresses are not uniformly distributed in the boards anymore. Instead, some locations with high stresses are found in the model.

As shown in Figs. 9 and 10, the most critical knots are the edge knots, which are located on the sides of the boards, showing the highest stresses in the boards. Additionally, the interacting stresses around the knot clusters are visible from Fig. 10. Development of the peak stresses can be seen especially for the first knot cluster in the board. This may be due to the existence of a combination of edge and middle knots at this location, which are located relatively close to each other. It is also shown in Fig. 10 that the stresses (σ_{11}) in a perfect board without any knots remain constant.
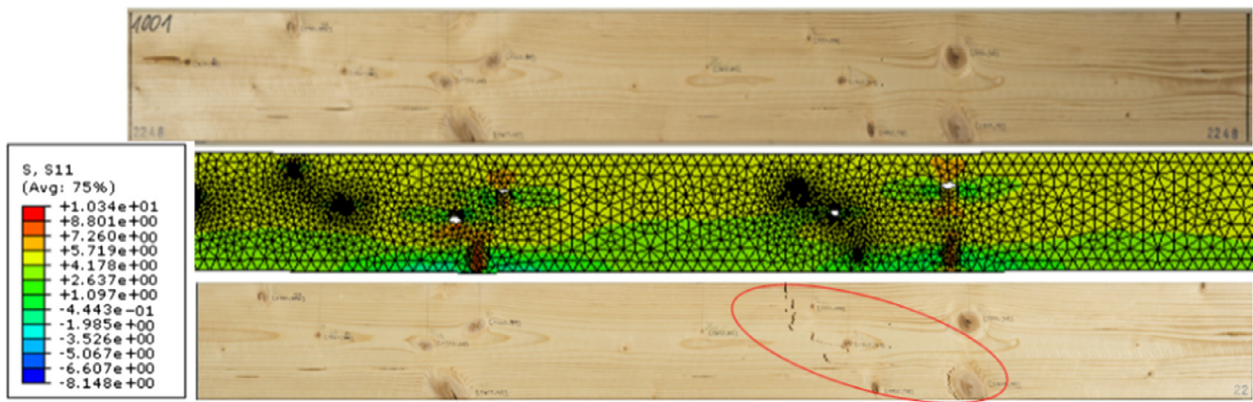
Fig. 9. Physical and numerical representation of the board, and the development of the maximum stresses around the knots.
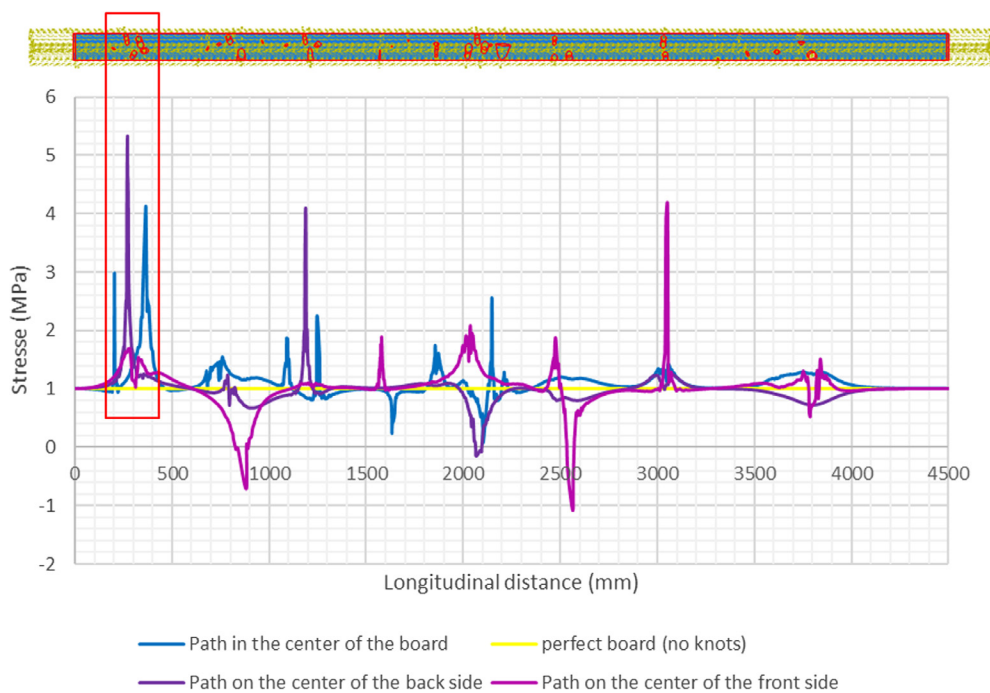
Fig. 10. Development of the longitudinal stresses (σ_{11}) along the board. Marked area in red is the location of the first knot cluster.

Therefore, the applied 1 MPa stress does not have any variation in the board along the path.

Therefore, each knot in each board is analyzed for the three stress concentration factors (SCF_1, SCF_2 and SCF_3) and for each board the maximum value of the SCFs are registered.

The correlation of the SCFs and the numerical value of MoE_{dyn} with the experimental tensile strength in each case are shown in Fig. 11. For the SCFs both a linear and a power regression function are shown, as the SCFs have non-linear characters. The MoE_{dyn} has a linear correlation to the experimental tensile strength.

Fig. 11 shows the inverse correlation between the three stress concentration factors of the boards with the experimental tensile strength. This confirms the strength reduction by an increase in the stress concentration factors due to the existence of the critical defects (specifically edge knots or knot clusters). As shown in this figure, among the stress concentration factors, the SCF_1 has the highest correlation to the experimental tensile strength values, which can affect the quality of the virtual predictions.

The quality of these predictions are benchmarked to the quality of the predictions based on TKAR, DEB and DAB, which are the visual knot assessment methods (shown in Fig. 12). As shown in this figure, the correlation between these parameters and the tested tensile strength of the boards are relatively low, showing the weakness of the visual parameters to be used as good strength predictors. Among the experimental measurements, the MoE_{dyn} has the highest correlation with the tensile strength, confirming its importance for grading. The coefficient of determination is comparable to that of the simulations.

From the predictions, it is shown that the SCFs have higher correlation with the strength compared to the visual grading parameters (TKAR, DAB, DEB) for both samples.

With respect to the dynamic MoE it can be seen that the prediction for spruce is slightly better than the experimental values

$(R^2 = 0.53$ compared to 0.50), whereas for Douglas fir the prediction is slightly worse ($R^2 = 0.50$ compared to 0.58). The differences may be due to the geometrical complexities of the Douglas fir boards as compared to the spruce.

For the visual measurements, a non-linear correlation does not give higher coefficients of determination, whereas this is the case for the stress concentration factors.

Additionally, multiple regression analysis is done, considering the effects of the knots and MoE_{dyn} together for the best possible strength predictions. The linear and non-linear combinations of the parameters are considered in the equations 10–13. The prediction results are validated with the linear multiple regression analysis of the measured values (TKAR, DAB, DEB and MoE_{dyn}, presented in Eq. (13)). The constants of these equations together with the R^2 values are presented in Table 2 for each case. As shown, using only the three stress concentration factors (Eq. (10)), which have non-linear character, in a multiple regression analysis provides an equally good strength prediction as the visual knot parameters plus MoE_{dyn} (f_4). Adding MoE_{dyn} to the analysis improves the quality of the predictions in both linear (f_3) and non-linear cases (f_2). In case of f_1 and f_3 all three stress concentration factors are used for the strength prediction, whereas in case of f_2 only the first two stress concentration factors are used in combination with MoE_{dyn}. Adding SCF_3 in this case does not improve the strength prediction any further. The linear combination of the numerical parameters (f_3) is about 10% better than the linear combination of the measurements (f_4), (R^2 values).

$$f_1 = \sum_{i=1}^{n} a_i . e^{b_i . SCF_i} + c \qquad (10)$$

$$f_2 = \sum_{i=1}^{n} a_i . e^{b_i . SCF_i} + c.MOE_{dyn} + d \qquad (11)$$
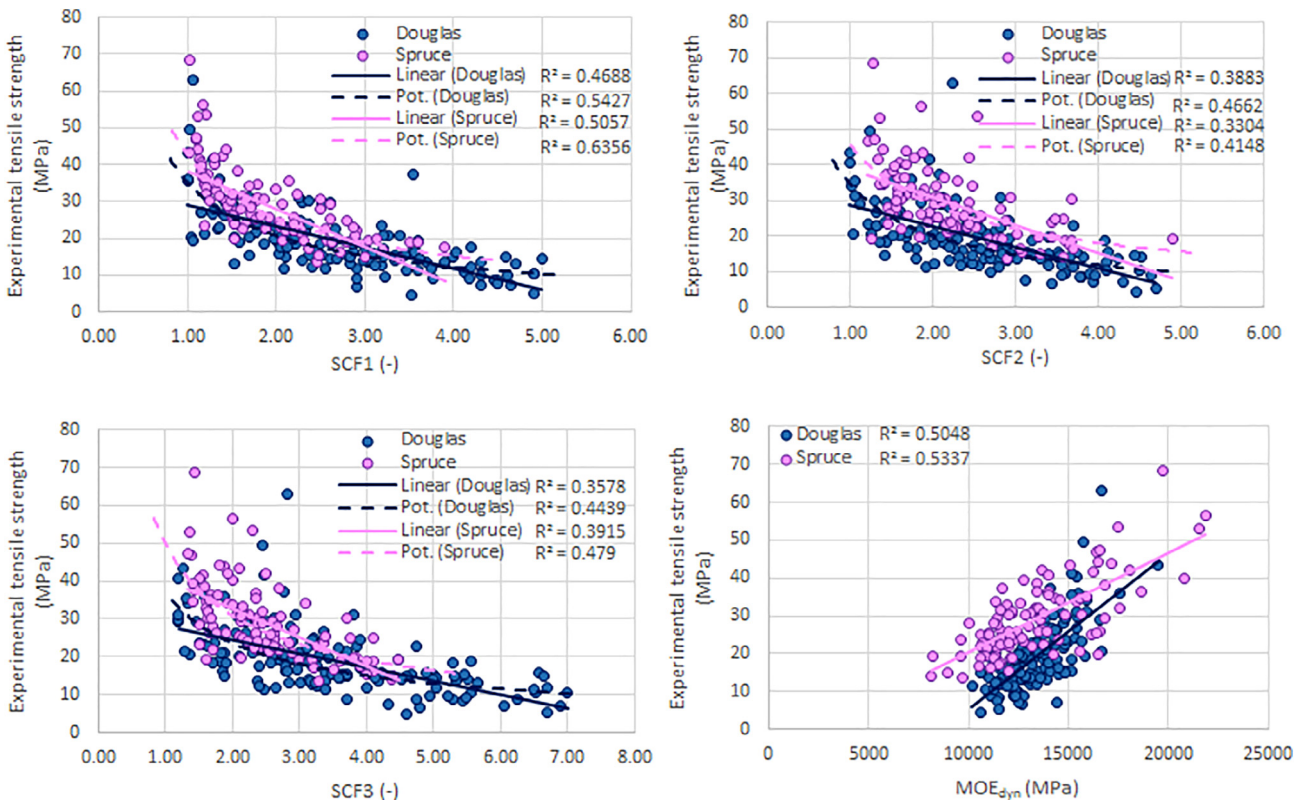
Fig. 11. Relation between numerical parameters with experimental tensile strength for both samples.
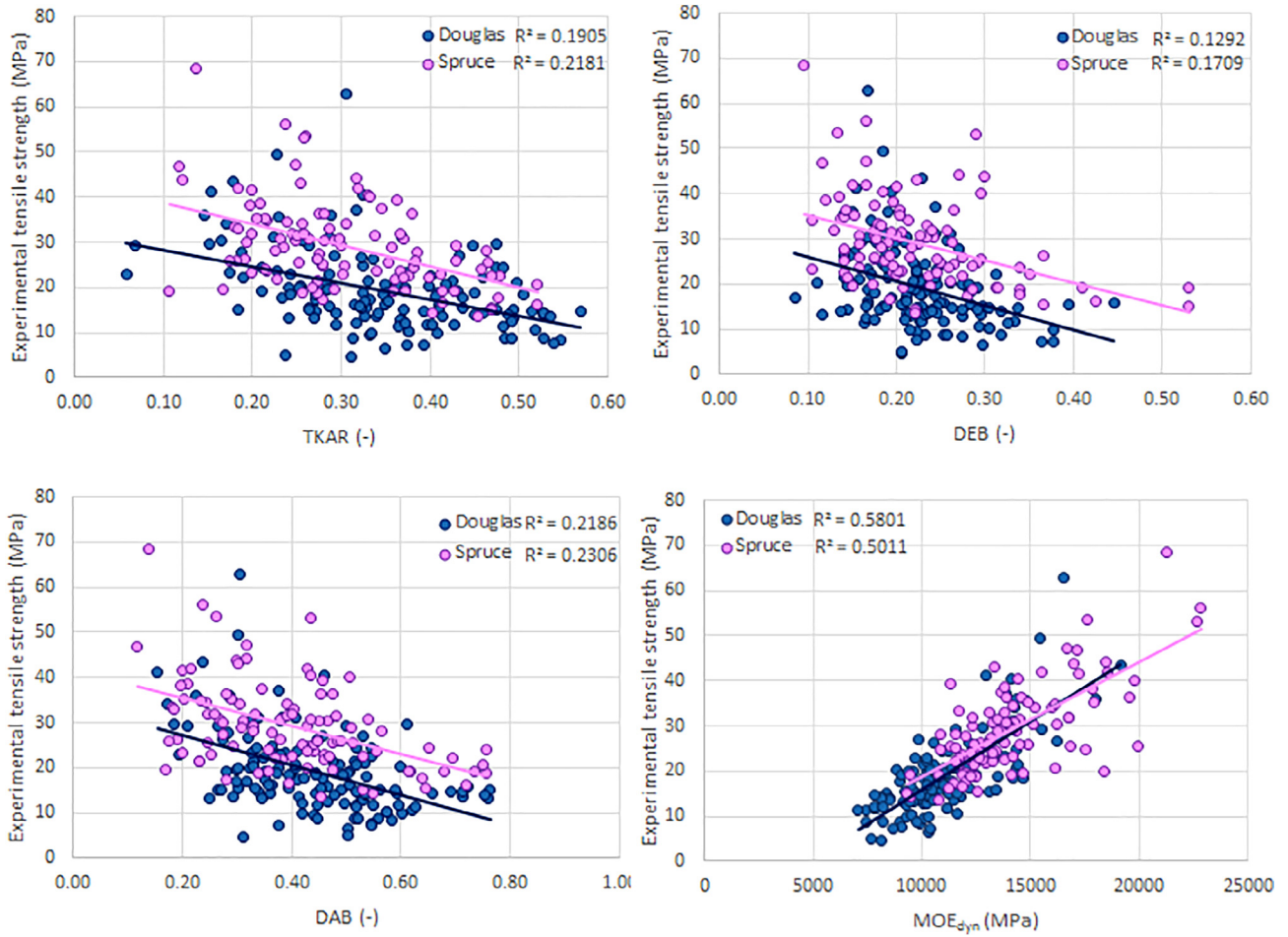
Fig. 12. Correlation plots of the measured parameters with tensile strength for both samples.

Table 2
Coefficients of the Eqs. (10) and (13) (Spruce S, Douglas fir DF).

		a_1	a_2	a_3	b_1	b_2	b_3	c	R^2_{linear}	R^2_{exp}
f_1	S	249.00	29.73	178.32	−2.19	−4.37	−3.34	20.59	–	0.62
	DF	42.25	7.42	18.83	−0.84	−1.01	−0.65	8.40	–	0.65

		a_1	a_2	b_1	b_2	c	d			
f_2	S	−135.13	−17.68	0.04	0.06	0.0019	−170.17		–	0.75
	DF	−5.93	−6.62	0.22	0.17	0.0030	1.88		–	0.72

		a	b	c	d	e				
f_3	S	−4.98	2.20	−3.95	0.0018	18.79			0.73	–
	DF	−2.79	−1.47	−0.45	−0.0024	−0.93			0.67	–
f_4	S	−19.81	−24.18	−2.06	0.0021	11.69			0.66	–
	DF	−22.38	−37.33	10.66	0.0027	0.13			0.60	–

$$f_3 = a.SCF1 + b.SCF2 + c.SCF3 + d.MOE_{dyn} + e \tag{12}$$

$$f_4 = a.TKAR + b.DEB + c.DAB + d.MOE_{dyn} + e \tag{13}$$

where f_i is the tensile strength, $SCFs$ are the stress concentration factors, MoE_{dyn} is the dynamic modulus of elasticity and a,b,c,d,e are the constants, provided in Table 2.

The correlation between the predicted strength based on the numerical parameters and the experimental tensile strength is shown in Fig. 13 in a linear and non-linear form. It is shown in this figure that due to the effects of the stress concentration factors in the multiple regression analysis, the non-linear correlation is much higher compared to the linear one. Additionally, the R^2 values comparing the numerical predictions and the physical measurements are presented in Table 2.

5. Discussion

A direct comparison of the predictive quality of only visual grading approach (TKAR, DEB and DAB) and the FEM approach (SCF$_1$, SCF$_2$ and SCF$_3$) shows that the strength prediction is better using the 3D FEM model. R^2 values are 0.62 compared to 0.35 for spruce based on the numerical and visual grading methods respectively. Similarly, a high improvement of the prediction with R^2 values of 0.65 compared to 0.27 is visible for Douglas fir boards. It needs to be mentioned that the knots in the boards were all mea-
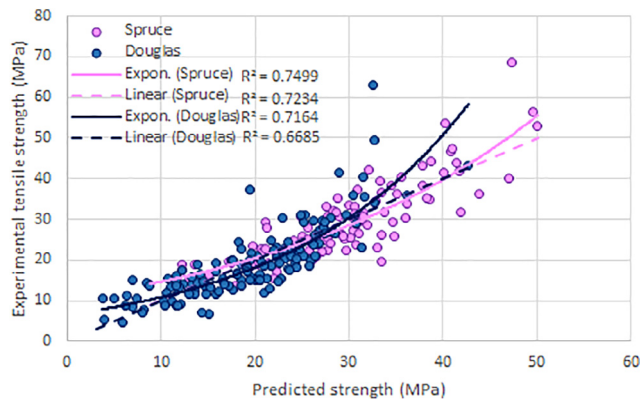
Fig. 13. Multiple correlation analysis of the SCF_1, SCF_2 and MoE_{dyn} with the experimental tensile strength for both samples.

sured under ideal circumstances in the laboratory, whereas in a factory this method is subjected to human or scanning errors, thus giving less accurate grading results. Although due to the lower accuracy of the knot data for Douglas-fir boards, the 3D model of them differs (more) from the actual ones than in the case of spruce, the quality of the prediction, only based on the calculated stress concentration factors is still good, with a R^2 value in the same range for spruce and Douglas fir ($R^2 = 0.62$ compared to $R^2 = 0.65$ respectively). This shows both the validity as well as the robustness of the approach. Even if the knot data is insufficient for a full 3D representation, the calculated factors still allow for an accurate strength prediction.

Using the three SCFs in a non-linear multiple regression equation gives a similarly good strength predictions as the visual plus MoE_{dyn} method ($R^2 = 0.62$ compared to 0.66 for spruce as well as the $R^2 = 0.65$ compared to 0.60 for Douglas fir).

By correlating linearly all simulation results of the spruce boards to their experimental tensile strength and comparing them to the multiple correlation of the visual plus machine grading methods and tensile strength, similar results are obtained for both cases ($R^2 = 0.73$ compared to $R^2 = 0.66$). Similar condition is also valid for Douglas fir ($R^2 = 0.67$ compared to $R^2 = 0.60$).

Considering the non-linear multiple regression analysis, considering only the effects of the first two stress concentration factors and the MoE_{dyn} is improving the quality of the predictions.

The results of the simulations show R^2-values between 0.6 and 0.7 when based on an SCFs, and higher than 0.7 when considering the effect of the MoE_{dyn} in the regression equations for the strength predictions. Other studies on tensile strength predictions are very limited as most have focused on bending strength prediction, which is less relevant for glued laminated timber [2,10,13,14]. In [14] the bending strength is analyzed for a dataset of 105 boards with an R^2 value of 0.71, whereas an R^2 value of 0.79 for a mixture of tensile and bending results is presented in [10], modelling 12 boards in tension out of a total of 93 spruce boards. A similar amount (n = 14) of medium dense beech tensile boards was analyzed in [53] and an R^2 value of 0.9 was obtained using the approach presented in this paper. It is assumed that increasing the number of the samples will result in the reduction of the accuracy of numerical predictions as the natural scatter in bending and tension is very large [27]. The quality of the model predictions as presented here seems to be robust, considering the large natural variation. In addition, the model is applied on two different softwood species with low to high quality material, the Douglas fir sometimes showing more than 80 knots per board. The main differences with the mentioned studies is however that the presented procedure here is based solely on knot data that can be extracted directly from the board surfaces and an a-priori known ratio

between modulus of elasticity and density. Consequently, a high precision surface scanner with knot identification is sufficient to extract the necessary data and perform an accurate strength prediction.

6. Conclusion

A comprehensive 3D FE model of softwood boards has been created based on a representation of strength governing knots as visible on the surfaces of the boards. The modelled boards cover a large quality range of laminations for glued laminated timber and varies from low-medium quality Douglas fir to medium-high quality spruce boards. The model allows for an accurate prediction of the tensile strength of the boards. The numerical parameters include:

- Three types of stress concentration factors around knots, covering the interaction of the stress developments around multiple features. These factors are related to the geometrical configuration of the knots as well as the stress flow around them.
- The dynamic modulus based on a stress-wave analysis of longitudinal vibration.

To cover the total quality range of the boards, two stress concentration factors (SCF_1, SCF_2) with MoE_{dyn} is shown to be sufficient for a good strength prediction. Adding SCF_3 does not improve the prediction quality.

The highest possible coefficient of determination is obtained as $R^2 = 0.75$ and $R^2 = 0.72$ for spruce and Douglas fir respectively, compared to $R^2 = 0.66$ and $R^2 = 0.60$ when using the visual approach (TKAR, DEB, DAB and MoE_{dyn}) for the same samples respectively.

Even in the case of Douglas fir where the knot data was not sufficient for a complete 3D reconstruction of the board (missing exact x-coordinate and knot angle in 3D space), the calculated stress concentration factors still allowed for an accurate strength prediction.

With the created model it has been shown that, two stress concentration factors plus MoE_{dyn} are sufficient for a strength prediction that is equal or better than current strength predictions based on machine grading measurements such as X-ray and MoE_{dyn} from a stress wave machine. The model is also performing better when comparing to the best possible visual strength grading predictions that includes MoE_{dyn} as additional parameter.

Conflict of interest

None.

References

[1] C. Foley, A three-dimensional paradigm of fibre orientation in timber, Wood Sci. Tech. 35 (2001) 453–465.
[2] V. Baño, F. Arriaga, A. Soilán, M. Guaita, F.E.M. Analysis of the Strength Loss in Timber due to the Presence of Knots, World Conference on Timber Engineering, Riva del Garda, Italy, 2010. ISBN: 978-88-901660-3-7.
[3] S.M. Cramer, J.R. Goodman, Failure modeling: a basis for strength prediction of lumber, Wood Fiber Sci. 18 (1986) 446–459.
[4] J.R. Goodman, J. Bodig, Tension Behavior of Wood – An Anisotropic, Inhomogeneous Material Structural research report No. 32, Colorado State University, Fort Collins, 1980.

[5] P. Guindos, M. Guaita, A three-dimensional wood material model to simulate the behavior of wood with any type of knot at the macro-scale, Wood Sci. Tech. 47 (2013) 585–599.

[6] C. Hackspiel, K. de Borst, M. Lukacevic, A numerical simulation tool for wood grading model developement, Wood Sci. Technol. (2014), https://doi.org/10.1007/s00226-014-0629-0.

[7] C. Jenkel, Structural and material inhomogenities in timber, modelling by means of the finite element method, Dissertation, Technische Universttät Dresden (2016).

[8] C. Jenkel, M. Kaliske, Anlayse von Holzbauteilen unter Berücksichtigungstruktureller Inhomogenitäten, Bauingenieur 88 (2013) 494–507.

[9] R. Lang, M. Kaliske, Description of inhomogeneities in wooden structures: modelling of branches, Wood Sci. Tech. 47 (2013) 1051–1070.

[10] M. Lukacevic, J. Füssl, Numerical simulation tool for wooden boards with a physically based approach to identify structural failure, Eur. J. Wood Prod. 72 (2014) 497–508.

[11] G.E. Phillips, J. Bodig, J.R. Goodman, Flow-grain Analogy, Wood Sci. 14 (1981) 55–65.

[12] J.G. Zandbergs, F.W. Smith, Finite elements fracture prediction for wood with knots and cross grain, Wood Fiber Sci. 20 (1987) 97–106.

[13] M. Hu, A. Briggert, A. Olsson, M. Johansson, J. Oscarsson, J. Säll, Growth layer and fiber orientation arount knots in Norway spruce: a laboratory investigation, Wood Sci. Tech. (2017), https://doi.org/10.1007/s00226-017-0952-3.

[14] J. Oscarsson, Strength grading of structural timber and EWP laminations of Norway spruce-development potentials and industrial applications, Linnaeus University, Sweden, 2014.

[15] A. Olsson, A. Oscarsson, E. Serrano, B. Källsner, M. Johansson, B. Enquist, Prediction of timber bending strength and in-member cross-sectional stiffness variation on the basis of local wood fiber orientation, Eur. J. Wood Prod. 71 (2013) 319–333.

[16] W.D. Pilkey, Peterson's Stress Concentration Factors, 2nd Edition., John Wiley & Sons, 1997.

[17] D.W. Whitley, Interacting stress concentration factors and their effect on fatigue of metallic aerostructures Doctoral thesis, Missouri University of Science and Technology, 2013.

[18] R.D. Mindlin, Stress distribution around a hole near the edge of a plane in tension, Proc. SESA 5 (1948) 56–68.

[19] A.J. Durelli, R.L. Lake, E. Phillips, Stress concentrations produced by multiple semi-circular notches in infinite plates under uniaxial states of stress, Proc. Soc. Exp. Stress Anal. 10 (1) (1952).

[20] A.J. Durelli, R.L. Lake, E. Phillips, Stress distribution in plates under a uniaxial state of stress with multiple semi-circular and flat-bottom notches, Proc. First Natl. Congress Appl. Mech. (1952).

[21] R.H. Graham, M. Raines, K.G. Swift, L. Gill, Prediction of stress concentrations associated with interacting stress-raisers within aircraft design: methodology development and application, Proc. Inst. Mech. Eng., Part G: J. Aerospace Eng. (2005).

[22] R.A.W. Haddon, Stresses in an Infinite Plate with Two Unequal Circular Holes, Quarter. J. Mech. Appl. Math. 20 (1967) 277–291.

[23] C.B. Ling, On the stresses in a plate containing two circular holes, J. Appl. Phys. 19 (1948).

[24] NASA, Astronautic Structures Manual, Volume 1, George C. Marshall Space Flight Center, Marshall Space Flight Center, Alabama, 1975.

[25] W.D. Pilkey, D.F. Pilkey, Peterson's Stress Concentration Factors, 3rd Edition., John Wiley & Sons, 2008.

[26] C.B. Ling, On stress concentration factor in a notched Strip. Trans. ASME, Appl. Mech. Section 90 (1968) 833.

[27] P. Stapel, J.W.G. van de Kuilen, Influence of cross-section and knot assessment on the strength of visually graded Norway spruce, Eur. J. Wood Prod. (2013), https://doi.org/10.1007/s00107-013-0771-7.

[28] P. Stapel, J.W.G. van de Kuilen, Effects of grading procedures on the scatter of characteristic values of European grown sawn timber, Mater. Struct. (2013), https://doi.org/10.1617/s11527-012-9999-7.

[29] P. Stapel, J.W.G. van de Kuilen, Efficiency of visual strength grading of timber with respect to origin, species, cross section, and grading rules: a critical evaluation of the common standards, Holzforschung (2013), https://doi.org/10.1515/hf-2013-0042.

[30] EN 338, Structural timber-Strength classes. CEN, Brussels, Belgium, 2016.

[31] G. Ravenshorst, Species Independent Strength Grading of Structural Timber PhD Thesis, Delft University of Technology, 2015.

[32] L. Hansson, N. Lundgren, A.L. Antti, Finite element modeling (FEM) simulation of interactions between wood and microwaves, J. Wood Sci. 52 (2006) 406–410.

[33] J.H. Kim, G. Anandakumar, Stress Wave Propagation in Functionally Graded Solids under Impact Loading, Proceedings of the IMPLAST 2010 Conference, Island, USA, 2010.

[34] A.S.J. Suiker, A.V. Metrikine, R. de Borst, Comparison of wave propagation characteristics of the Cosserat continuum model and corresponding discrete lattice models, International Journal of Solids and Structures, Rourkela, India, 2001, pp. 1563–1583. Master's thesis, 2013.

[35] S. Nath, Stress Wave Propagation in split Hopkinson Pressure Bar, National Institute of Technology, 2015.

[36] C. Nilsson, Modelling of dynamically loaded shotcrete, Royal Institute of Technology, Stockholm. Master's thesis, 2009. ISSN: 1103-4297.

[37] M. Shantharaja, G.M. Sandeep, Experimental and numerical analysis of propagation of stress wave in sheet metal, Int. J. Sci. Technol. Res. 3 (10) (2014). ISSN: 2277-8616.

[38] E.A. Verner, E.B. Becket, Finite element stress formulation for wave propagation, Internat. J. Numer. Methods Engin. 7 (1973) 441–459.

[39] C.J. Costantino, Finite element approach to stress wave problems, J. Eng. Mech. Div. ASCE 93 (EM2) (1967) 153–176.

[40] R. Görlacher, Klassifizierung von Brettschichtholzlamellen durch Messung von Longitudinalschwingungen Doctoral thesis, Universität Fridericiana in Karlsruhe, Germany, 1990.

[41] W.M. Bulleit, H. Mich, R.H. Falk, P. Wash, Modeling stress wave passage times in wood utility poles, Wood Sci. Technol. 19 (1985) 183–191.

[42] R.J. Ross, M.O. Hunt, Stress wave timing nondestructive evaluation tools for inspecting historic structures: a guide for use and interpretation. Gen. Tech. Rep. FPL GTR 119. Madison, WI: U.S. Department of Agriculture, Forest Service, Forest Products Lab. (2000).

[43] N. Yaitskova, J.W. van de Kuilen, Time-of-flight modeling of transversal ultrasonic scan of wood, J. Acoust. Soc. Am. 135 (6) (2014) 3409–3415.

[44] F. Tallavo, G. Cascante, M.D. Pandey, Experimental verification of an orthotropic finite element model for numerical simulations of ultrasonic testing of wood poles, Eur. J. Wood Prod. (2017).

[45] EN 384, Structural timber-determination of characteristic values of mechanical properties and density. CEN, Brussels, Belgium, 2010.

[46] EN 408, Timber structures-structural timber and glued laminated timber-determination of some physical and mechanical properties. CEN, Brussels, Belgium, 2010.

[47] A. Rais, W. Poschenrieder, H. Pretzsch, J.W.G. van de Kuilen, Influence of initial plant density on sawn timber properties for Douglas-fir (Pseudotsuga menziesii (Mirb.) Franco), Ann. Forest Sci. 71 (2014) 617–626.

[48] A. Rais, J.W.G. van de Kuilen, H. Pretzsch, Growth reaction patterns of tree height, diameter, and volume of Douglas-fir (Pseudotsuga menziesii [Mirb.] Franco) under acute drought stress in Southern Germany, Eur. J. Forest Res. (2014), https://doi.org/10.1007/s10342-014-0821-7.

[49] DIN 4074, Strength grading of wood – Part 1: coniferous sawn, Timber (2012).

[50] S.M. Cramer, J.R. Goodman, Model for stress analysis and strength prediction of lumber, Wood Fiber Sci. 15 (4) (1982) 338–349.

[51] J.R. Goodman, J. Bodig, Mathematical model of the tension behavior of wood with knots and cross grain, Proc. First Int. Conf. Wood Fracture, Banff. Alberta (1978).

[52] J. Bodig, B.A. Jayne, Mechanics of wood and wood composites, Second edition., Krieger Publishing Company, 1993.

[53] A. Khaloian, W.F. Gard, J.W. van de Kuilen, 3D FE-numerical modelling of growth defects in medium dense European hardwoods. ISCHP2017 proceedings, 2017.

Paper 2: Tensile strength prediction of softwood glulam lamellas using virtual vibration technique
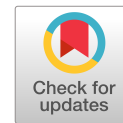
Tensile Strength Prediction of Softwood Glulam Lamellas Using Virtual Vibration Technique

A. Khaloian Sarnaghi[1] and J. W. G. van de Kuilen[2]

Abstract: The strength of wooden boards is related to its natural defects and the ability of a stress wave to propagate around them. Anisotropy, heterogeneity, and the strong moisture dependency of wood make it difficult to predict its strength. Covering the ordinary quality range of wood, a numerical simulation model was developed for strength prediction of timber, and 250 boards were numerically simulated. In this study, by virtually reconstructing a three-dimensional (3D) geometrical model of each case based on the surface information of the knots, and by predicting the fiber patterns, the material properties of wood were virtually predicted. Thus, the strength predictions were done solely based on the surface information of the knots. Strength variation in a knot-free board is only dependent on the variation of the actual density of the board. As the actual density of wood may not be available under different environmental conditions for measuring the dynamic modulus of elasticity (MoE_{dyn}), the average density of each set was used as one of the only input parameters for simulations. The resonance kind stress wave propagation and its return were calculated in the reconstructed boards. Numerical results of the finite-element (FE) stress wave analysis were used in a linear regression analysis for prediction of the tensile strength based on the information of the calculated time of the stress wave. The predicted results were benchmarked against the measured values in the laboratory. Performing a multiple regression analysis, the virtual results provided much higher strength predictions than the geometrical parameters available from scanners. However, strong knot interactions in lower-quality boards also affect the strength predictions. This study provides a comprehensive system (starting from the geometrical reconstruction of the boards to the virtual analysis for calculation of the virtual MoE_{dyn}) for the strength prediction of wood that is based solely on the surface images. The developed model makes it possible to predict the tensile strength of timber with relatively high accuracy, which is approximately at the same level as current grading machines. **DOI:** 10.1061/(ASCE)MT.1943-5533.0002936. © *2019 American Society of Civil Engineers.*

Author keywords: Finite-element (FE)-analysis; Virtual dynamic modulus of elasticity (MoE); Knots; Stress wave; Quality; Strength prediction.

Introduction

Wood is a natural composite with the fibers oriented primarily in the longitudinal axis of boards. Heterogeneities in the structure make it difficult to predict the strength of this material, which is essential for the use of wood in engineered structures. As a consequence, the material needs to be strength graded before it can be applied. This process can be done either visually or by machine (Stapel and Van de Kuilen 2013). Visual grading is done based mainly on the visible parameters of the knot geometries and growth ring width, where the strength, stiffness, and density values can be estimated by known relationships (Stapel and Van de Kuilen 2014a, b). This method can be performed based on a surface scanning system such as WoodEye or an X-ray system [Microtec (Bressanone, Italy), LuxScan (Foetz, Luxembourg)]. Machine grading uses nondestructive measurements in order to predict the mechanical properties

generally based on the measurement of eigenfrequency and density to predict dynamic modulus of elasticity (MoE_{dyn}) in combination with knot parameters (Stapel and Van de Kuilen 2013). This method can also be performed by measurement of the fiber angle using RemaSawco and WoodEye strength graders. From previous studies, it is known that for high-quality strength prediction, an accurate estimate of the modulus of elasticity (MoE) is of prime importance because the correlation with strength is generally high (Stapel and Van de Kuilen 2013, 2014a, b), but including data on the knot structure improves strength prediction even further (Khaloian et al. 2017). Knots are basically the main strength-governing parameters that affect the strength by causing local fiber deviations and changing the structure of the material. Starting in 1978, different studies focused on the prediction of strength, using two-dimensional (2D) and three-dimensional (3D) structural models of wood, applying different numerical methods (Cramer and Goodman 1983, 1986; Foley 2001; Goodman and Bodig 1978, 1980; Guindos and Guaita 2013; Hackspiel et al. 2014; Hu et al. 2018a; Jenkel 2016; Jenkel and Kaliske 2013; Lang and Kaliske 2013; Lukacevic and Füssl 2014; Phillips et al. 1981; Zandbergs and Smith 1987). Some focused on the prediction of material failure based on the predicted structural model of wood (Baño et al. 2010; Cramer and Goodman 1983; Pellicane and Franco 1994) and the prediction of material properties based on knots and fiber deviations (Briggert et al. 2018; Hu et al. 2018b). Because of the significant influence of fiber deviations in the vicinity of knots and material imperfections on the strength, these structural models play an important role for estimating strength and stiffness values.

In practice, strength prediction is based on nondestructive longitudinal vibration to determine the eigenfrequency, sometimes

[1]Ph.D. Canditate, Dept. of Wood Technology, Technical Univ. of Munich, Munich 80797, Germany (corresponding author). Email: sarnaghi@hfm.tum.de

[2]Professor, Dept. of Wood Technology, Technical Univ. of Munich, Munich 80797, Germany; Professor, Faculty of Civil Engineering and Geosciences, Delft Univ. of Technology, Stevinweg 1, CN Delft 2628, Netherlands; Guest Researcher, Consiglio Nazionale delle Ricerche-Ivalsa, Via Biasi 75, San Michele all'Adige, 38010, Italy. Email: J.W.G.vandeKuilen@tudelft.nl; vandekuilen@hfm.tum.de

© ASCE   04019309-1   J. Mater. Civ. Eng.

J. Mater. Civ. Eng., 2019, 31(12): 04019309

extended with X-ray scanning for knot detection. Therefore, having a predictive model of strength and stiffness is useful.

Impact-generated stress and sound waves can be used as non-destructive evaluation methods for the determination of mechanical properties and are widely used in different materials for quality control and defect characterization (Graff 1975; Miklowitz 1984; Rayleigh 1888; Sansalone and Street 1997).

There have been few numerical studies focused on the calculation of the dynamic modulus of elasticity, based on the extraction of the natural eigenfrequencies of the material (Görlacher 1990). Longitudinal stress wave propagation has been analyzed numerically for different applications in different studies (Kim and Anandakumar 2010; Suiker et al. 2001). Concrete and steel (Kim and Anandakumar 2010; Shantharaja and Sandeep 2014; Suiker et al. 2001; Verner and Becket 1973), layered elastic materials (Costantino 1967), and wood (Bulleit and Falk 1985) are some of the materials that have been numerically analyzed for wave propagation. Few studies have also considered transverse ultrasonic wave propagation in wood (Ross and Hunt 2000; Tallavo et al. 2017; Yaitskova and Van de Kuilen 2014). The scattering of microwaves has also been modeled in few studies; see, for instance, Hansson et al. (2006).

Longitudinal impact on the deformable body results in small deformations in the material, which propagate from the impact zone at a specific speed (Gorwade et al. 2012; Tasdemirci and Hall 2005). When the material particles come closer to each other, compressive stresses are caused in the material. Tensile stresses may also occur by wave propagation and diverge the particles from each other. Depending on the boundary conditions, the wave can turn from compression to tension after hitting a boundary. The resulting linear deformation in the solid body due to the applied transient force can be measured as the propagation of the stress wave. Any nonuniformity and heterogeneity in the material results in the reflection and transmission of the wave in the interfaces, which causes a disturbance in the uniform propagation.

Heterogeneities in material and variation in the densities and material properties of knots create a complex surface for wave propagation regarding its reflection and transmission. Similar to all other materials, for perfect wood without any imperfections, simple sinusoidal behavior of the wave can be expected in most cases. In contrast to clear wood, most of the wood species, such as spruce or Douglas fir, which are the cases for the current study, contain significant material imperfections, which disturb wave propagation from simple sinusoidal movements. Therefore, group wave effects can be observed for stress wave propagation in these samples instead of a simple sinusoidal condition. In this study, the longitudinal vibration is considered, which is one of the simplest cases, containing much smaller cross-sectional sizes as compared to the length. Such conditions limit transversal vibrations, restricting the total vibrations to longitudinal ones only, and simplify the wave equation.

The focus of this study was to provide an alternative method for the estimation of the strength of wood. This study concentrated on

calculation of the dynamic modulus of elasticity for wooden lamellas with complicated internal structure. Especially the fiber flow around knots and geometrical aspects of knots are of concern because these are considered the main strength-determining properties for structural wood use, such as laminated timber. Based on the location of the knots that are visible on the surface of the boards, a full 3D geometrical representation of boards is possible for numerical studies. The prime analysis that is performed with the model is the determination of the virtual dynamic modulus of elasticity based on a virtual dynamic stress wave analysis. In the following, a method was developed to describe the boards in 3D space, and numerical procedures were chosen in order to derive the dynamic modulus of elasticity of the individual boards. Finally, the numerical results were compared to experimentally determined values. The practicality of this method is its independence from the actual density in the initial steps. Numerical loading of the boards under tension, analysis of the stress distributions in the boards, and calculation of the stress concentration factors is another method to predict the tensile strength of sawed timber (Khaloian et al. 2017), which is not part of this study. The aim of this study was to only analyze the potential of the virtual dynamic modulus of elasticity for prediction of the tensile strength.

Materials and Methods

Numerical Modeling

For this study, two sets of softwood species were selected, covering the ordinary range of the quality. These samples include 103 medium-quality to high-quality spruce boards and 150 low-quality to medium-quality Douglas fir boards (Rais et al. 2014a, b). In contrast to the spruce boards with relatively small and more uniformly shaped knots, in the low-to-medium-quality Douglas fir boards, the tested knots were less uniform and closely spaced, leading to more irregular fiber flow patterns. The spruce boards had dimensions of $4,200 \times 40 \times 150$ mm^3, whereas the dimensions of the Douglas fir boards were $4,500 \times 46 \times 146$ mm^3. The basic material properties of these boards are presented in Table 1 (Stapel and Van de Kuilen 2013, 2014a, b; Rais et al. 2014b).

In order to reduce the dependency of the predictions on the individual density of the boards, the average density and modulus of elasticity of each specimen set were used as input parameters for the numerical simulations. From Ravenshorst (2015), a linear correlation between the density and the modulus of elasticity can be assumed. Additionally, different correlations are known for these species for the prediction of their bending strength (Olsson et al. 2018).

Because knots are considered the primary weak points in the material when under mechanical loading conditions, they may initiate failure by stress peaks and crack formation. Different geometrical aspects of the knots can be taken into account for better

Table 1. Basic data of the spruce (S) and Douglas fir (DF) boards

Statistic	Sample	E_{static} (N/mm^2)	$E_{dynamic}$ (N/mm^2)	Density (kg/m^3)	Knottiness			Tensile strength (N/mm^2)
					TKAR	DEB	DAB	
AVG	S	11,900	12,300	462	0.30	0.22	0.40	29.19
	DF	10,200	12,000	489	0.35	0.23	0.44	19.31
CoV	S	0.20	0.11	0.13	0.32	0.36	0.38	0.34
	DF	0.25	0.14	0.09	0.31	0.26	0.30	0.47

Note: TKAR = total knot area ratio; DEB = single knot or DIN Einzelast Brett; and DAB = knot cluster or DIN Abstandsammlung Brett.

© ASCE   04019309-2   J. Mater. Civ. Eng.

J. Mater. Civ. Eng., 2019, 31(12): 04019309
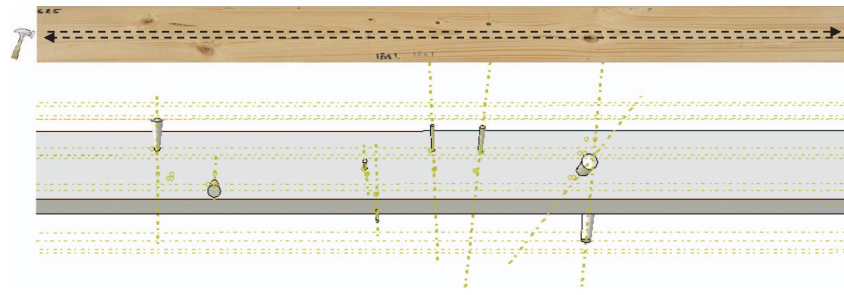
Fig. 1. (Color) Geometrical reconstruction of a spruce board and the path of the stress wave.

predictions, as will be shown on the basis of visual grading knot parameters calculated based on DIN 4074 knot definitions. The knots are tested in the test length of the board, typically nine times the board width [EN 384 (CEN 2016a); EN 408 (CEN 2012)].

Python (2.7.3) and ABAQUS/Standard (Simulia version 6.14-2) were used as tools for reconstruction and numerical analysis.

During the reconstruction process, 15 different surface configurations were checked to analyze the possibility of each surface being part of the knot. This was done after analyzing the geometrical configuration, orientation, and shape of each knot separately. Each knot had a separate volume and axis of rotation, where its material properties can be assigned. Knots were modeled as holes in this study to reduce the computational costs. Because the wave follows the path of the fibers in both cases, this simplification does not affect the numerical results in this case. Because the reconstruction and assignment of orthotropic directions were not performed based on the information of the density map of the material in this study, the total average density of each species was enough for dynamic analysis. This makes the difference for this study, where only an average density and static modulus of elasticity are enough to represent the material properties of the boards.

To be able to reduce the effects of the dependency of the model to the extreme accuracy of the presented coordinate system of the knots, an uncertainty of ± 5 mm was implemented in the code, using the ufloat() function in Python, to be able to change slightly the geometry of the knots and verify the sensibility of the model predictions for possible measurement errors. The error term was added to all boards during the reconstruction process, based on which the coordinates of the knots were changed randomly in each direction by taking random values between zero and five.

A typical example of a reconstructed geometrical model of a spruce board and its stress wave path is presented in Fig. 1.

The automated geometrical reconstruction of some knots and therefore the discretization of the model for the numerical analysis failed sometimes for the Douglas fir case (Rais et al. 2014a) due to the complex geometrical aspects, such as extremely long knots with steep angles. Although the selected set of Douglas fir originally had 150 boards, 137 boards of this sample were modeled at the end because of the numerical instabilities and geometrical complications of 13 boards.

Wood Orthotropic Representation

Although wood is an anisotropic material, orthotropic properties can represent wood reasonably well in different applications (Baño et al. 2010; Guindos and Guaita 2013). The compliance matrix of this material is presented in Eq. (1)

$$
\begin{bmatrix} \varepsilon_{LL} \\ \varepsilon_{RR} \\ \varepsilon_{TT} \\ \gamma_{LR} \\ \gamma_{LT} \\ \gamma_{RT} \end{bmatrix} = \begin{bmatrix} \dfrac{1}{E_L} & \dfrac{-\nu_{RL}}{E_R} & \dfrac{-\nu_{TL}}{E_T} & 0 & 0 & 0 \\ \dfrac{-\nu_{LR}}{E_L} & \dfrac{1}{E_R} & \dfrac{-\nu_{TR}}{E_T} & 0 & 0 & 0 \\ \dfrac{-\nu_{LT}}{E_L} & \dfrac{-\nu_{RT}}{E_R} & \dfrac{1}{E_T} & 0 & 0 & 0 \\ 0 & 0 & 0 & \dfrac{1}{G_{LR}} & 0 & 0 \\ 0 & 0 & 0 & 0 & \dfrac{1}{G_{LT}} & 0 \\ 0 & 0 & 0 & 0 & 0 & \dfrac{1}{G_{RT}} \end{bmatrix} \cdot \begin{bmatrix} \sigma_{LL} \\ \sigma_{RR} \\ \sigma_{TT} \\ \sigma_{LR} \\ \sigma_{LT} \\ \sigma_{RT} \end{bmatrix}
$$

(1)

where R, T, and L represent the radial, tangential, and longitudinal directions, respectively; E_{ij} = moduli of elasticity; G_{ij} = shear moduli; and v_{ij} = Poisson's ratio.

The compliance matrix should be symmetric, which results in Eq. (2)

$$
\nu_{RL} = \nu_{LR} \frac{E_R}{E_L} \qquad \nu_{TL} = \nu_{LT} \frac{E_T}{E_L} \qquad \nu_{TR} = \nu_{RT} \frac{E_T}{E_R} \qquad (2)
$$

The elastic and shear modulus, used for each case for the numerical analysis, are presented in Table 2. The E_{11} is the average stiffness value, obtained from the tensile tests for each of the sets (spruce and Douglas fir). The rest are estimated based on the available correlations.

The focus of the numerical method in the current study is on calculation of the dynamic modulus of elasticity for prediction of the strength of the material. Without having information on the individual board density at the moment of virtual grading, a strength prediction can be done based on the stress wave analysis using the average density of the species. It will be shown that the actual density will improve the derived values, but also that without the density, a good prediction of the strength is still possible. In fact, in the practice of grading in sawmills, both options exist because there are machines that measure the eigenfrequency of a board and from that derive the dynamic modulus of elasticity using either a mean density value or a measured one.

Table 2. Modulus of elasticity and shear modulus (N/mm²) for spruce and Douglas fir boards

Samples	E_{11}	$E_{22} = E_{33}$	$G_{12} = G_{13}$	G_{23}
Spruce	11,900	370	690	50
Douglas fir	10,200	330	630	46

© ASCE

04019309-3

J. Mater. Civ. Eng.

The fiber deviations in this study were numerically simulated based on previously developed numerical methods (Goodman and Bodig 1978, 1980; Foley 2001), which in turn are based on the predicted orthotropic coordinate directions of the material.

The results of the numerical calculations were benchmarked against the measured dynamic modulus of elasticity and eigenfrequencies of the boards based on the stress wave method as used by strength grading machines.

In order to cover the difficulties of the complicated geometries in extracting the frequencies of the system under an impact loading, explicit dynamic analysis was used for the numerical simulations (Chang and Randall 1988; Ham and Bathe 2012).

Because the velocity of any given point in the material is zero before the wave has passed the point, the velocity of the point after passing the wave is equal to the particle velocity U_p. Therefore, the impulse (I) of the system can be presented as in Eq. (3)

$$I = mU_p \tag{3}$$

where m = mass and equals $m = \rho V = \rho A dx$ (where:= ρ is the density, V is the volume, and A is the cross-section). By using Navier's equation and rewriting the mass, Eq. (3) can be stated as

$$\sigma A dt = \rho A dx U_p \tag{4}$$

By solving Eq. (4) for the stresses (σ), it can be seen that the stresses are not related to the cross-sectional area of the specimen, but they are related to the density and velocity of the wave and particles.

According to Newton's equation of motion and Hooke's law (Bodig and Jayne 1993; Leppänen 2002), the following equation can be derived for longitudinal stress waves:

$$\frac{\partial^2 u}{\partial t^2} = \frac{E_{II}}{\rho} \frac{\partial^2 u}{\partial x^2} \tag{5}$$

where ρ = density of the sample; and $E_{//}$ = modulus of elasticity parallel to the fibers. As mentioned previously, the ratio of E/ρ is known for almost all wooden species (Ravenshorst 2015). In the simulations, the average density and stiffness values were used as input parameters. For these sets of analysis, an average density of 451 and 485 kg/m^3 was used for spruce and Douglas fir boards, respectively. Knowledge about the ratio of E/ρ may be helpful for the case of the knot-free boards with structural nonuniformities, to provide a stiffness map for the numerical analysis.

Considering the plane wave propagation and approximating the constrained modulus to be the Young's modulus, the velocity of the longitudinal wave can be represented by Eq. (6)

$$c = \sqrt{\frac{E_{//}}{\rho}} \tag{6}$$

where c = speed of the wave in the material.

Over the first vibration mode, the wave length (λ) equals twice the length of the specimen, and the dynamic modulus of elasticity can be calculated using the following equation (Görlacher 1990; Liang and Fu 2007):

$$E_{\text{dyn}} = 4l^2 f^2 \rho = v^2 \rho \tag{7}$$

where l = length of the specimen; f = first eigenfrequency; and v = velocity.

Due to the geometrical complications and low quality of the boards in the current study, application of the linear modal analysis may fail in predicting the modulus of elasticity because the small

element deformations due to the impact load were neglected. This is a condition that cannot be neglected for timber (especially Douglas fir) in the area of knots and knot clusters, where geometrical imperfections exist.

In this study, the stress impact was applied for a short time of 1×10^{-5} s and was set to zero for the rest of the analysis. The dynamic stress wave was simulated by applying an impact stress of 0.1 MPa to the specimen and measuring the velocity of the longitudinal wave after one complete round forward and backward in the board.

By extracting the velocity of the stress wave, and by knowing the length of the boards, the frequencies were calculated for each case. Therefore, the frequencies contained information about the average density of the boards.

The dynamic modulus of elasticity was calculated using Eq. (8), based on the average density of the boards. In practice, if the density of an individual board is measured, the simulation results of the dynamic modulus of elasticity can be updated with the new measured density values, which will increase the accuracy.

In this study, 3D quadratic tetrahedral elements (C3D10) were used for numerical analysis.

Based on the analytical calculations, and according to the average material parameters of the boards, an approximate velocity and time of flight for the stress wave propagation in the boards were calculated. The approximated mean velocities were obtained as 4,950 and 4,750 m/s for the spruce and Douglas fir boards, respectively. By knowing the approximated velocities and the length of the boards, the total time of flight was estimated to be 1.7×10^{-3} s and 2×10^{-3} s for spruce and Douglas fir boards, respectively.

Results and Discussion

Stress Wave Propagation and Frequency Determination

As an example, the stress wave propagation in a board with local knot areas is plotted over the impact path of the board in Fig. 2. The wave is disturbed after reaching the knot cluster in the board. This figure shows half of the stress wave propagation until the end of the board. The return wave is not plotted for reasons of clarity. However, the return wave will also be disturbed when coming to the area of the knots again, all located in the standardized test length of EN 408 (CEN 2012). Fig. 2(b) represents the wave propagation through the board and its disturbance by reaching the knot area (red rectangles in the model) at Stage 7 [shown in Fig. 2(c)]. This part of the figure, with six horizontal bars, shows the stepwise propagation of the wave and the output of the stress wave at the time interval of 8.5×10^{-5} s. Therefore, the wave output can be seen in 10 time steps in each wave direction [Fig. 2(c)]. In Fig. 2(b), this output is shown for six time steps, to show the wave disturbance when the wave is getting closer to the knot and leaving the knot area. The blue color shows the location of the wave in each step, when the wave reaches the knot area. Additionally, the development of the compressive stresses can be seen in Fig. 2(b) (in blue) when the material particles come closer together after being hit by the wave. These stresses are turned to tension in the same particles after the wave passes and the particles are back to their initial location in the elastic wave propagation. The complete wave deformation occurs after the wave passes the first knot cluster. The wave in such a location needs to pass through the knots, which are defined as holes in this model. Therefore, the stress wave is deformed to pass through the knot cluster in the solid area of wood. Additionally, part of the wave is reflected on the knot boundaries, which causes a

© ASCE 04019309-4 J. Mater. Civ. Eng.

J. Mater. Civ. Eng., 2019, 31(12): 04019309
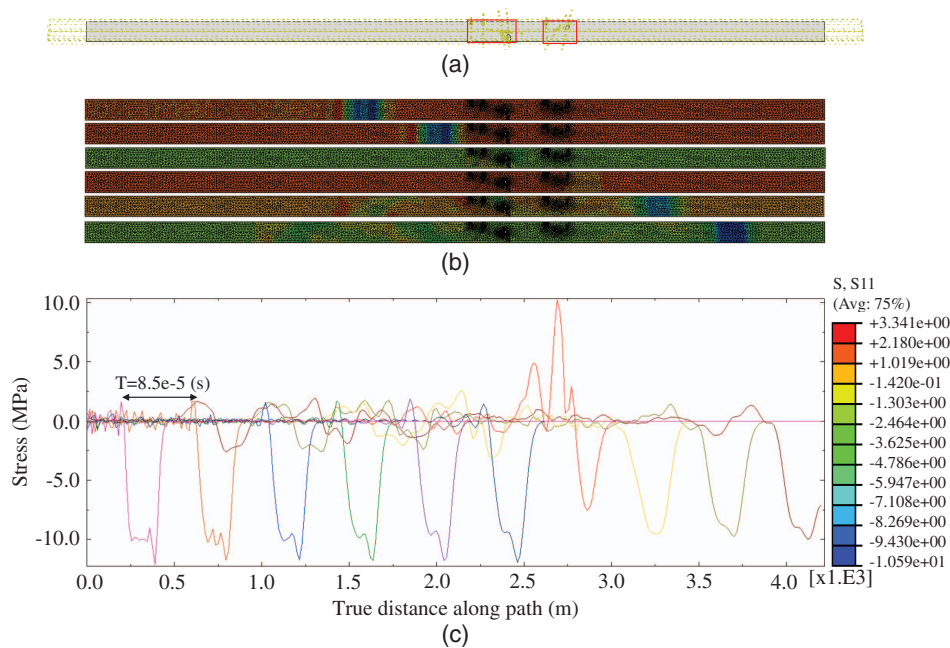
Fig. 2. (Color) Stress wave analysis. One stress wave, propagating with the time interval of 8.5×10^{-5} s: (a) geometry of the real board; (b) stress wave passage through the knots; and (c) half stress wave propagation in wooden boards.

reduction in the magnitude of the stresses compared to the wave propagated in the initial steps. The propagation becomes uniform on the rest of its way through the clear wood to the end of the board, after which it will return.

Because the knots were modeled as holes in this study, the velocity of the wave is being reduced after passing through the knot. This is due to the reflection of the wave and the transmission to the bulk material after the knot region. The reflected wave from the end boundaries of the board has the inverse function of the forth wave.

Due to the simulated impact force, an elastic stress wave was created that propagates through the material. Because the impact was low, no permanent deformation occurred in the material. The velocity of the wave at the end depends on the material parameters (including the elastic and shear modulus) and the heterogeneities in the material. Additionally, the magnitude of the strains was checked on the forward and backward waves to check the elastic deformations in the model due to the small impact.

The magnitude of the strains increased after the wave reached the knots. This is due to the definition of the knots as holes in the numerical simulations and free movement of the particles on the boundaries of the knots. The magnitude of the strains on the backward wave was about 13% less compared to the forward one. This could be due to the reduction of the velocity of the wave on its return after passing the heterogeneities in the material.

Density is another important parameter, affecting wave propagation. Each sample in this study was assigned an average density based on more than 100 boards. Therefore, the calculated velocities and virtual frequencies were always extracted based on this density value because the individual board density was not yet known at the time of the strength prediction. However, for the real measurements in the laboratory, the actual density of the boards at the time of measurements were considered. Therefore, in contrast to the virtual methods, the frequencies in the laboratory measurements were always based on the actual densities of the boards. The coefficient of determination (R^2) between the virtual and actual frequencies

showed $R^2 = 0.74$ and $R^2 = 0.32$ for spruce and Douglas fir samples, respectively (Fig. 3).

Thus, the correlation between the measured and estimated frequencies of the high-quality spruce boards were relatively high, although different density values were used for both cases. The correlation decreased for the case of the low-quality Douglas fir boards. This is mainly due to the geometrical complications in these boards. A high amount of natural defects in Douglas fir boards and their interactions formed more knot clusters in these boards, which caused a variation in the wave speed and resulted in higher inaccuracies in the model compared to the high-quality spruce boards.

Determination of Dynamic Modulus of Elasticity

For calculation of the dynamic modulus of elasticity [Eq. (7)], the density can be applied as an average or actual density of the boards. Initially, the average density value is used. Later, by measuring the actual density of the material, the density parameter in Eq. (7) was updated to see the possible improvement in the quality of the prediction of the dynamic modulus of elasticity. In a similar way, the measured dynamic modulus of elasticity was modified with the average density in order to be able to make a comparison between both approaches. This was done by multiplying the measured dynamic MoE with the ratio of the average to actual density. Due to the high correlation between the static and dynamic moduli of elasticity, this case was analyzed for both samples. The correlation between the measured and simulated MoE_{dyn} and the correlation of each MoE case with its tensile strength are shown in Table 3.

As shown in Table 3, the correlation reduced considerably in both cases when applying the average densities of each set ($R^2 = 0.60$ compared to $R^2 = 0.21$ and $R^2 = 0.79$ compared to $R^2 = 0.36$ for Douglas fir and spruce boards, respectively). Also, in the laboratory measurements, a reduction could be observed when modifying the measured dynamic MoE with the average density of the set, presented in Table 3. As shown already with the R^2 values, the variation between the values with average and actual

© ASCE 04019309-5 J. Mater. Civ. Eng.

J. Mater. Civ. Eng., 2019, 31(12): 04019309
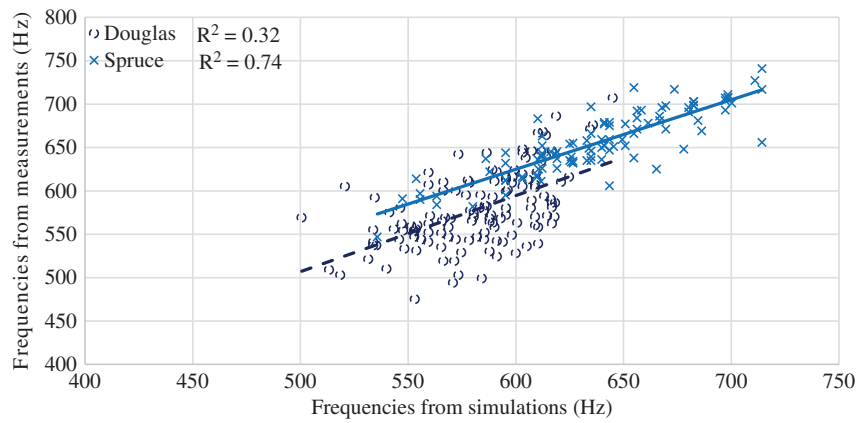
Fig. 3. (Color) Linear correlation of the frequencies from simulations and measurements for both spruce and Douglas fir samples.

Table 3. Correlation between the material parameters

R^2	Sample	Density	MoE_{static}	$MoE_{dyn,measurement}$	Tensile strength
$MoE_{dyn,simulation}$	S	ρ_{avg}	0.36	0.40	0.40
	DF	ρ_{avg}	0.21	0.11	0.27
	S	ρ_{actual}	0.79	0.63	0.53
	DF	ρ_{actual}	0.60	0.89	0.50
$MoE_{dyn,measurement}$	S	ρ_{avg}	0.43	—	0.35
	DF	ρ_{avg}	0.71	—	0.52
	S	ρ_{actual}	0.88	—	0.50
	DF	ρ_{actual}	0.81	—	0.58

densities was much higher for the case of the spruce boards compared to the case of the Douglas fir boards. This may have resulted from the difference in the geometrical configuration of the boards and the amount of the bulk material in each case.

As shown in Table 3, the quality of the strength predictions increased when calculating the dynamic modulus of elasticity based on the actual density of the boards. It can be concluded that virtual dynamic MoE is sufficient for strength prediction of high-quality spruce boards. The R^2 values of the virtual method were in the same range as the test values ($R^2 = 0.53$ compared to $R^2 = 0.50$ applying actual board densities). When applying the mean density, correlations were lower with $R^2 = 0.40$ for simulated and $R^2 = 0.35$ for tested boards. For the low-to-medium-quality Douglas fir, it seems that only a simulated MoE with actual density gave an acceptable result, whereas applying the mean density resulted in a considerable reduction of the R^2 value (R^2 dropped from 0.52 to 0.27).

As mentioned before, all laboratory measurements were done using the actual density of the boards, whereas the simulations were

performed using their average density. Using average density for the simulations enables one to make decisions in the initial stages of processing sawed wood to see if it is useful for structural applications or not. If the outcome is positive, the density value can be updated anyway after drying and further processing. If, after drying, the actual density is known, the predicted value of the dynamic MoE can be updated with the new density without having to rerun the transient analysis.

By showing the coefficients of determination (Table 3) in cases of using only the average density for calculation of MoE_{dyn}, the effect of the actual density as a separate parameter was analyzed in the next step to check possible improvement of the quality of the predictions. Because measurement of density in the initial steps may be difficult, this parameter can be measured and inserted in the calculations later.

Eq. (8) was obtained by performing a linear multiple regression analysis with all numerical parameters of the stress wave analysis and similarly for all measured values

$$f_{pred} = a \cdot MOE_{dyn,i} + b \cdot \rho + c \cdot f_i + d \tag{8}$$

where f_{pred} = predicted strength; MoE_{dyn} = dynamic modulus of elasticity; ρ = density; f_i = frequency; and a, b, c, and d = constants provided in Table 4.

The results of the multiple regression analysis were benchmarked against the laboratory measurements and are shown in Fig. 4. The quality of the predictions solely based on the parameters of the simulations was good. This quality was higher than the experimental values for the high-quality spruce boards both for average as well as actual densities ($R^2 = 0.54$ and $R^2 = 0.56$). Modification of the measurements with the average density values

Table 4. Coefficients of different linear multiple correlation analysis of the simulated parameters for spruce and Douglas fir based on Eq. (8)

Tensile strength	Case	a MoE_{dyn1}	MoE_{dyn2}	MoE_{dyn3}	b Density	c f_1	f_2	d Constant
$f_{pred,spruce}$	1	—	—	0.005	−0.102	—	−0.086	58.067
	2	0.015	—	—	0.062	−0.454	—	100.594
	3	—	0.008	—	−0.181	−0.189	—	125.878
$f_{pred,douglasfir}$	1	—	—	0.003	−0.022	—	−0.051	−28.324
	2	0.027	—	—	0.096	−0.956	—	186.361
	3	—	0.0133	—	−0.265	−0.417	—	213.466

Note: MoE_{dyn1} = simulated dynamic modulus of elasticity, using the average density in Eq. (7); MoE_{dyn2} = simulated dynamic modulus of elasticity, using the actual density in Eq. (7); MoE_{dyn3} = measured dynamic modulus of elasticity; f_1 = predicted frequencies from simulations; and f_2 = measured frequencies.
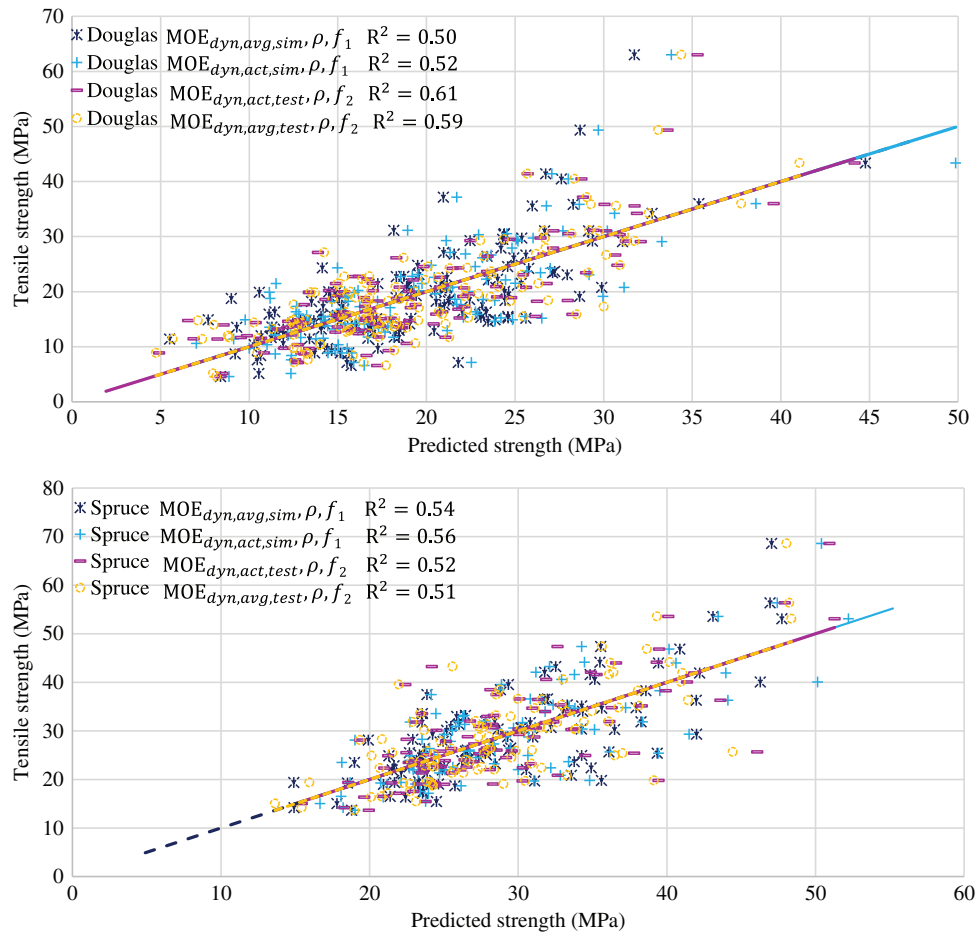
Fig. 4. (Color) Multiple regression analysis for spruce and Douglas fir boards, using the calculated and measured MoE_{dyn} based on average and actual densities, the actual density (ρ), and the frequency [average (f_1) and actual (f_2)]. The value $MoE_{dyn,avg,sim}$ is the calculated MoE_{dyn} based on average density, and $MoE_{dyn,act,test}$ is the measured MoE_{dyn} based on actual density. The value $MoE_{dyn,act,sim}$ is the calculated MoE_{dyn} based on actual density, and $MoE_{dyn,avg,test}$ is the measured MoE_{dyn} based on average density.

as simulations reduced the quality of the predictions, but the virtual methods were still slightly better in this case as well.

The quality of the predictions for the case of the low-to-medium-quality Douglas fir boards was lower for the case of the simulations than for the experiments ($R^2 = 0.52$ compared to $R^2 = 0.61$), but considering that individual boards contained up to 80 knots, the predictive capacity of the simulations is still promising.

Another comparison was done in this case by using the average density as an additional parameter for the regression analysis [in Eq. (8)] because the numerical MoE_{dyn} is calculated based on the average density as well. In this case, the correlation was reduced for both species, resulting in $R^2 = 0.31$ compared to $R^2 = 0.50$ for Douglas fir and $R^2 = 0.40$ compared to $R^2 = 0.54$ for spruce boards. However, by recalculating the numerical frequencies with the actual densities of the boards and performing the same multiple correlation analysis again considering all numerical parameters with actual density values, the correlation increased considerably for both samples ($R^2 = 0.56$ and $R^2 = 0.46$ for spruce and Douglas fir, respectively). The full analysis with average or actual densities is presented in Fig. 5.

In addition to the dynamic modulus of elasticity, knot parameters influence the quality of the strength predictions (Khaloian et al. 2017). Similar to advanced grading machines, a combination of MoE_{dyn}, density, and knot parameters can be used. Because the

shape of each knot in the cross section is already known during the reconstruction process, all knot values in accordance with DIN 4074 (DIN 2012) or EN 14081-1 (CEN 2016b) (or any other visual grading standard) can be derived as well. In order to verify whether the virtual dynamic MoE approach is a feasible alternative, the results of the virtual dynamic MoE simulations were used in the following two ways:

1. Benchmarked against the strength prediction using all available knot data in terms of total knot area ratio ($TKAR$), single knot, or DIN Einzelast Brett (DEB) and knot cluster or DIN Abstandsammlung Brett (DAB), as presented and discussed in Stapel and Van de Kuilen (2014a, b).
2. As parameters in a multiple regression analysis, adding the knot parameters as given in Eq. (9)

$$f_{pred} = a \cdot MOE_{dyn,avg} + b \cdot \text{Frequency} + c \cdot TKAR$$
$$+ d \cdot DEB + e \cdot DAB + f \qquad (9)$$

The parameter $MoE_{dyn,avg}$ is the dynamic MoE, calculated by using the average density. The constants of Eq. (9) are presented in Table 5.

Therefore, the virtual dynamic parameters were benchmarked to the visual knot parameters because these are the parameters that are related to the geometrical aspects of the knots (Fig. 6).

© ASCE   04019309-7   J. Mater. Civ. Eng.

J. Mater. Civ. Eng., 2019, 31(12): 04019309
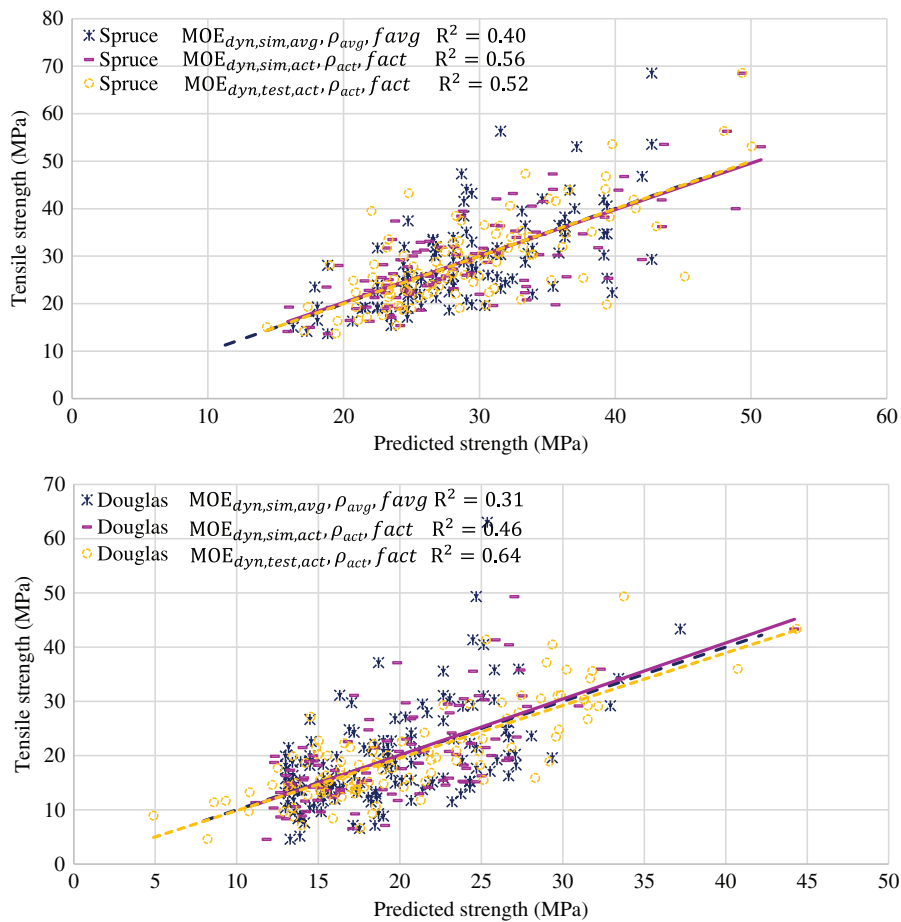
Fig. 5. (Color) Full multiple regression analysis for spruce and Douglas fir boards using the average and actual densities and frequencies (ρ_{avg} is the average density, ρ_{act} is the actual density, f_{avg} is the average frequency, and f_{act} is the actual frequency).

Table 5. Constants of different linear multiple correlation analysis of the simulated and tested parameters for spruce and Douglas fir based on Eq. (9)

		a			b			c	d	e	f
Tensile strength	Case	MoE_{dyn1}	MoE_{dyn2}	MoE_{dyn3}	f_1	f_2	f_3	TKAR	DEB	DAB	Constant
$f_{pred,S}$	1	0.019	—	—	−0.59	—	—	−21.08	−7.76	−9.98	188
	2	—	0.003	—	—	−0.03	—	−20.09	−18.87	−3.06	15
	3	—	—	0.002	—	—	0.01	−19.05	−22.82	−2.64	8
$f_{pred,DF}$	1	0.037	—	—	−1.51	—	—	−9.31	−15.88	−12.23	432
	2	—	−0.003	—	—	0.01	—	−16.05	−32.22	0.93	−17
	3	—	—	0.002	—	—	0.04	−20.53	−32.37	10.38	−17

Note: MoE_{dyn1} = simulated dynamic modulus of elasticity, using the average density in Eq. (7); MoE_{dyn2} = simulated dynamic modulus of elasticity, using the actual density in Eq. (7); MoE_{dyn3} = measured dynamic modulus of elasticity; f_1 = predicted frequencies from simulations; f_2 = updated frequencies from simulations with actual density; f_3 = measured frequencies; S = spruce; and DF = Douglas fir.

By using the average density values for both frequencies and the dynamic modulus of elasticity, and by comparing the regression values of the virtual dynamic methods for the strength prediction of the boards with visual strength prediction methods, virtual methods are considerably better predictors for the tensile strength ($R^2 = 0.54$ compared to $R^2 = 0.30$ and $R^2 = 0.50$ compared to $R^2 = 0.27$ for spruce and Douglas fir boards, respectively).

It also needs to be mentioned that the knot parameters measured in the laboratory are measured in ideal circumstances, and the R^2 values obtained for the visual methods are the optimal conditions (Stapel and Van de Kuilen 2013, 2014a, b).

Because the dynamic modulus of elasticity alone is not a good strength predictor for low-quality Douglas fir boards, the geometrical parameters need to be considered as well to provide better quality of predictions.

Considering similar knot parameters as visual methods {TKAR, DEB, and DAB [DIN 4074 (DIN 2012)]} for the virtual predictions, the quality of the predictions improved significantly ($R^2 = 0.59$ compared to $R^2 = 0.50$ and $R^2 = 0.65$ compared to $R^2 = 0.54$ for Douglas fir and spruce boards, respectively). This provides the same quality strength predictions as machine grading methods combining MoE_{dyn} and knot parameters. The correlation graphs of this case are shown in Fig. 7.

© ASCE   04019309-8   J. Mater. Civ. Eng.

J. Mater. Civ. Eng., 2019, 31(12): 04019309
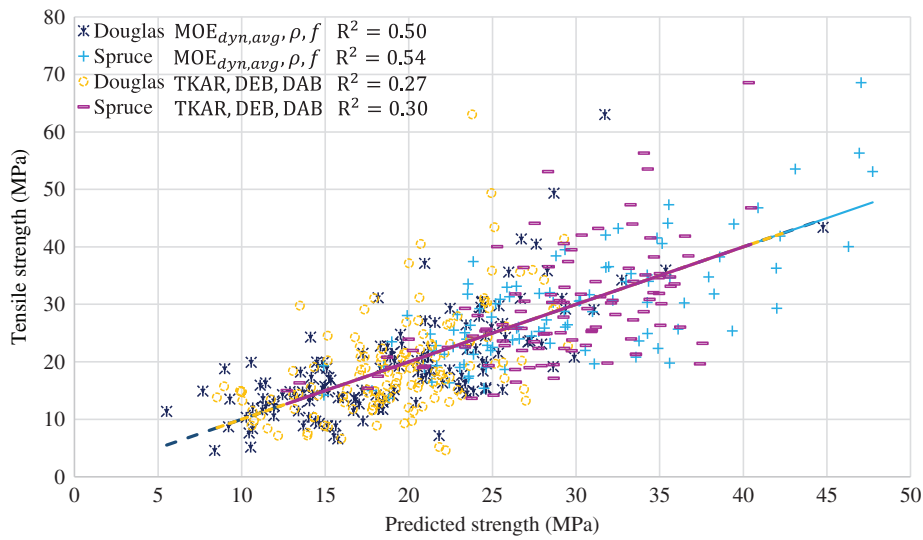
Fig. 6. (Color) Benchmarking the parameters of the virtual dynamic *MoE* method to DIN 4074 knot parameters (*TKAR*, *DEB*, and *DAB*).

Few studies have concentrated on prediction of the material strength using different identifying parameters (IPs) (Baño et al. 2010; Lukacevic et al. 2015; Olsson et al. 2012, 2013, 2018). A high correlation with $R^2 = 0.72$ and $R^2 = 0.62$ is presented between the bending strength and the IPs of machine grading methods (including the axial MoE_{dyn} and local fiber orientation) for spruce and Douglas fir samples, respectively (Olsson et al. 2018).

The method developed in the current study provides a reconstruction process that is only based on the surface information of the knots. Using the dynamic parameters of the developed numerical method for prediction of the tensile strength gives a correlation with $R^2 = 0.65$ and $R^2 = 0.59$ for spruce and Douglas fir samples, respectively, that is qualitatively in the same range as the currently available machine grading methods.
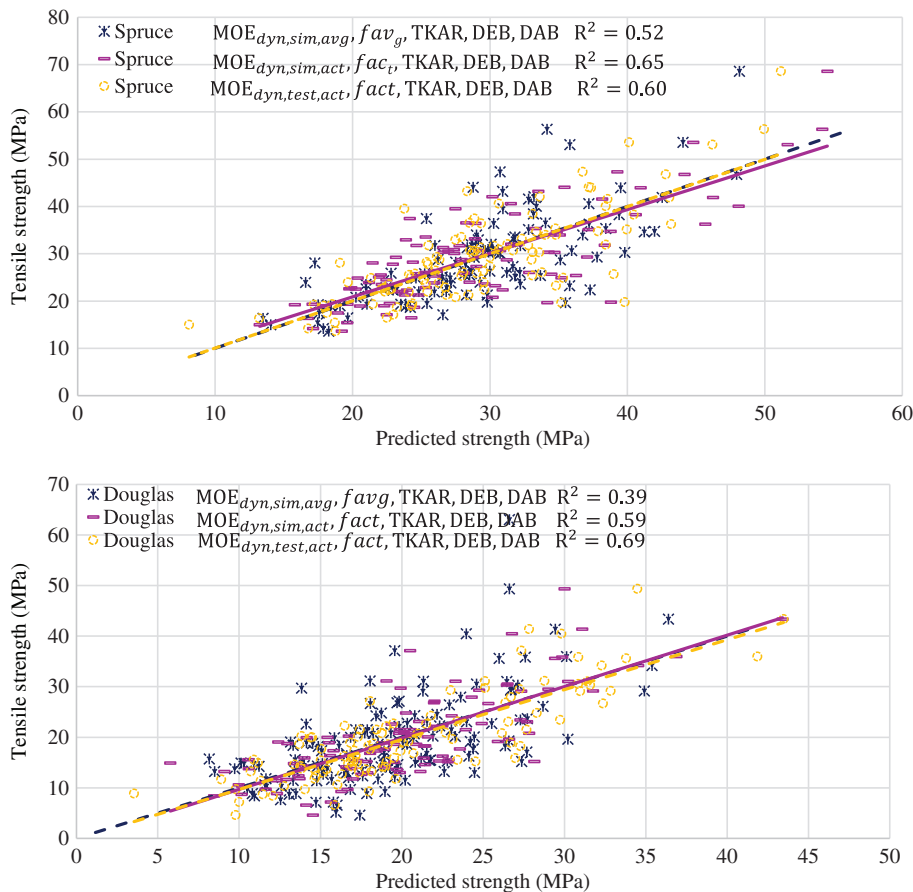
Fig. 7. (Color) Multiple correlation analysis of the virtual dynamic parameters and knot information for spruce and Douglas fir boards.

Conclusion

A comprehensive finite-element (FE) model of softwood was generated based on a visual representation of strength governing knots in boards. The modeled boards covered a large quality range of laminations for glued laminated timber and varies from low–medium quality Douglas fir to medium–high quality spruce boards. The tensile strength of the boards was predicted using parameters derived from the finite-element model. The parameters covered the dynamic modulus of elasticity of the boards, as well as the knot parameters from visual assessment methods, such as DIN 4074.

The dynamic modulus of elasticity of the boards was based on an explicit stress-wave analysis of longitudinal vibration and the extraction of the velocity of the wave. The values for MoE_{dyn} were determined using the average density, as well as the actual density of the individual boards for spruce and Douglas fir, respectively. The computer model was solely based on the description of the knots visible on the surface of the boards, transforming this into a full 3D generic FE model with knots and an average ratio of modulus of elasticity or density.

The parameters generated were used in a regression analysis for the prediction of the tensile strength, which is the governing strength parameter for boards in glued laminated timber.

It has been shown that the virtual dynamic stress wave approach is viable and that predicted values for MoE_{dyn} are comparable with experimental results in the case of medium-to-high-quality spruce. In the case of Douglas fir, the quality of the prediction is slightly less, mainly caused by the very high number of knots and knot clusters in this sample (up to 89 per board). Using the actual density of the boards for the calculation of the dynamic modulus of elasticity improves the quality of the strength predictions considerably for both species.

Adding knot parameters improves the quality of the prediction to a level that is comparable to or better than current strength predictions from grading machines that apply knot information or MoE_{dyn} measurements. The geometrical configuration of the knots in this case plays an important role for strength predictions because the knots generally govern the strength. The model also performs considerably better when compared to the best possible visual strength grading. In general, it can be concluded that on the basis of knot shapes as visible on the four surfaces of boards, a high-quality strength prediction is possible.

Data Availability Statement

Some or all data, models, or code generated or used during the study are proprietary or confidential in nature and may only be provided with restrictions (test and the measurement data, code and the model).

Acknowledgments

References

Baño, V., F. Arriaga, A. Soilán, and M. Guaita. 2010. "F.E.M. analysis of the strength loss in timber due to the presence of knots." In *Proc., World Conf. on Timber Engineering*. Matera, Italy: Centro UC de Innovación de Madera.

Bodig, J., and B. A. Jayne. 1993. *Mechanics of wood and wood composites*. 2nd ed. New York: Krieger Publishing.

Briggert, A., M. Hu, A. Olsson, and J. Oscarsson. 2018. "Tracheid effect scanning and evaluation of in-plane and out-of-plane fiber direction in Norway spruce timber." *Wood Fiber Sci.* 50 (4): 411–429. https://doi.or/10.22382/wfs-2018-053.

Bulleit, W. M., and R. H. Falk. 1985. "Modeling stress wave passage times in wood utility poles." *Wood Sci. Technol.* 19 (2): 183–191. https://doi.or/10.1007/BF00353080002E.

CEN (European Committee for Standardization). 2012. *Timber structures—Structural timber and glued laminated timber—Determination of some physical and mechanical properties*. EN 408. Brussels, Belgium: CEN.

CEN (European Committee for Standardization). 2016a. *Structural timber—Determination of characteristic values of mechanical properties and density*. EN 384. Brussels, Belgium: CEN.

CEN (European Committee for Standardization). 2016b. *Timber structures—Strength graded structural timber with rectangular cross section—Part 1: General requirements*. EN 14081-1. Brussels, Belgium: CEN.

Chang, H. W., and C. J. Randall. 1988. "Finite-difference time-domain modeling of elastic wave propagation in the cylindrical coordinate system." In *Proc., Ultrasonics Symp.*, 397–402. New York: IEEE.

Costantino, C. J. 1967. "Finite element approach to stress wave problems." *J. Eng. Mech. Div.* 93 (EM2): 153–176.

Cramer, S. M., and J. R. Goodman. 1983. "Model for stress analysis and strength prediction of lumber." *Wood Fiber Sci.* 15 (4): 338–349.

Cramer, S. M., and J. R. Goodman. 1986. "Failure modeling: A basis for strength prediction of lumber." *Wood Fiber Sci.* 18 (3): 446–459.

DIN (German Institute for Standardization). 2012. *Strength grading of wood—Part 1: Coniferous sawn timber*. DIN 4074. Berlin: DIN.

Foley, C. 2001. "A three-dimensional paradigm of fibre orientation in timber." *Wood Sci. Technol.* 35 (5): 453–465. https://doi.or/10.1007/s002260100112.

Goodman, J. R., and J. Bodig. 1978. "Mathematical model of the tension behavior of wood with knots and cross grain." In *Proc., 1st Int. Conf. on Wood Fracture*. Vancouver, BC, Canada: Forintek Canada Corp.

Goodman, J. R., and J. Bodig. 1980. *Tension behavior of wood—An anisotropic, inhomogeneous material*. Structural Research Rep. No. 32. Fort Collins, CO: Colorado State Univ.

Görlacher, R. 1990. "Klassifizierung von Brettschichtholzlamellen durch Messung von Longitudinalschwingungen." Ph.D. thesis, Versuchsanstalt für Stahl, Holz und Steine der Universität Fridericiana in Karlsruhe, Universität Fridericiana.

Gorwade, C. V., I. A. Ashcroft, V. V. Silberschmidt, F. T. R. Hughes, and G. M. Swallowe. 2012. "Experimental and numerical analysis of stress wave propagation in polymers and the role of interfaces in armour systems." *Cent. Eur. J. Eng.* 2 (4): 578–584. https://doi.org/10.2478/s13531-012-0034-0.

Graff, K. F. 1975. *Wave motion in elastic solids*. Newburyport, MA: Courier Dover Publications.

Guindos, P., and M. Guaita. 2013. "A three-dimensional wood material model to simulate the behavior of wood with any type of knot at the macro-scale." *Wood Sci. Technol.* 47 (3): 585–599. https://doi.org/10.1007/s00226-012-0517-4.

Hackspiel, C., K. de Borst, and M. Lukacevic. 2014. "A numerical simulation tool for wood grading model development." *Wood Sci. Technol.* 48 (3): 633–649. https://doi.org/10.1007/s00226-014-0629-0.

Ham, S., and K. J. Bathe. 2012. "A finite element method enriched for wave propagation problems." *Comput. Struct.* 94–95 (Mar): 1–12. https://doi.org/10.1016/j.compstruc.2012.01.001.

Hansson, L., N. Lundgren, and A. L. Antti. 2006. "Finite element modeling (FEM) simulation of interactions between wood and microwaves." *J. Wood Sci.* 52 (5): 406–410. https://doi.org/10.1007/s10086-005-0794-8.

Hu, M., A. Briggert, A. Olsson, M. Johansson, J. Oscarsson, and J. Säll. 2018a. "Growth layer and fiber orientation around knots in Norway spruce: A laboratory investigation." *Wood Sci. Technol.* 52 (1): 7–27. https://doi.org/10.1007/s00226-017-0952-3.

Hu, M., A. Olsson, M. Johansson, and J. Oscarsson. 2018b. "Modelling local bending stiffness based on fibre orientation in sawn timber."

© ASCE 04019309-10 J. Mater. Civ. Eng.

J. Mater. Civ. Eng., 2019, 31(12): 04019309

Eur. J. Wood Wood Prod. 76 (6): 1605–1621. https://doi.org/10.1007/s00107-018-1348-2.

Jenkel, C. 2016. "Structural and material inhomogenities in timber, modelling by means of the finite element method." Ph.D. dissertation, Institut für Statik und Dynamik der Tragwerke, Technische Universttät Dresden.

Jenkel, C., and M. Kaliske. 2013. "Anlayse von Holzbauteilen unter Berücksichtigungstruktureller Inhomogenitäten." [Analysis of timber components taking into account structural inhomogeneities]. *Bauingenieur* 88: 494–507.

Khaloian, A., W. F. Gard, and J. W. G. van de Kuilen. 2017. "3D FE-numerical modelling of growth defects in medium dense European hardwoods." In *Proc., 6th Int. Scientific Conf. on Hardwood Processing*, edited by V. Möttönen, and E. Heinonen, 60–67. Helsinki, Finland: Natural Resources Institute Finland.

Kim, J. H., and G. Anandakumar. 2010. "Stress wave propagation in functionally graded solids under impact loading." In *Proc., IMPLAST 2010 Conf.* Bethel, CT: Society for Experimental Mechanics.

Lang, R., and M. Kaliske. 2013. "Description of inhomogeneities in wooden structures: Modelling of branches." *Wood Sci. Technol.* 47 (5): 1051–1070. https://doi.org/10.1007/s00226-013-0557-4.

Leppänen, J. 2002. *Dynamic behaviour of concrete structures subjected to blast and fragment impacts.* Gothenburg, Sweden: Chalmers Univ. of Technology.

Liang, S. Q., and F. Fu. 2007. "Comparative study on three dynamic modulus of elasticity and static modulus of elasticity for Lodgepole pine lumber." *J. For. Res.* 18 (4): 309–312. https://doi.org/10.1007/s11676-007-0062-4.

Lukacevic, M., and J. Füssl. 2014. "Numerical simulation tool for wooden boards with a physically based approach to identify structural failure." *Eur. J. Wood Wood Prod.* 72 (4): 497–508. https://doi.org/10.1007/s00107-014-0803-y.

Lukacevic, M., J. Füssl, and J. Eberhardsteiner. 2015. "Discussion of common and new indicating properties for the strength grading of wooden boards." *Wood Sci. Technol.* 49 (3): 551–576. https://doi.org/10.1007/s00226-015-0712-1.

Miklowitz, J. 1984. Vol. 22 of *The theory of elastic waves and waveguides.* Oxford, UK: Elsevier.

Olsson, A., J. Oscarsson, M. Johansson, and B. Källsner. 2012. "Prediction of timber bending strength on basis of bending stiffness and material homogeneity assessed from dynamic excitation." *Wood Sci. Technol.* 46 (4): 667–683. https://doi.or/10.1007/s00226-011-0427-x.

Olsson, A., J. Oscarsson, E. Serrano, B. Källsner, M. Johansson, and B. Enquist. 2013. "Prediction of timber bending strength and in-member cross-sectional stiffness variation on the basis of local wood fibre orientation." *Eur. J. Wood Wood Prod.* 71 (3): 319–333. https://doi.org/10.1007/s00107-013-0684-5.

Olsson, A., G. Pot, J. Viguier, J. Faydi, and J. Oscarsson. 2018. "Performance of strength grading methods based on fibre orientation and axial resonance frequency applied to Norway spruce (*Picea abies* L.), Douglas fir (*Pseudotsuga menziesii* (Mirb.) Franco) and European oak (*Quercus petraea* (Matt.) Liebl./*Quercus robur* L.)." *Ann. For. Sci.* 75 (4): 102. https://doi.org/10.1007/s13595-018-0781-z.

Pellicane, P. J., and N. Franco. 1994. "Modeling wood pole failure, Part 2. Material and geometric considerations." *Wood Sci. Technol.* 28 (3): 261–274. https://doi.or/10.1007/BF00193330.

Phillips, G. E., J. Bodig, and J. R. Goodman. 1981. "Flow-grain analogy." *Wood Sci.* 14 (2): 55–64.

Rais, A., W. Poschenrieder, H. Pretzsch, and J. W. G. van de Kuilen. 2014a. "Influence of initial plant density on sawn timber properties for Douglas fir (*Pseudotsuga menziesii* (Mirb.) Franco)." *Ann. For. Sci.* 71 (5): 617–626. https://doi.org/10.1007/s13595-014-0362-8.

Rais, A., J. W. G. van de Kuilen, and H. Pretzsch. 2014b. "Growth reaction patterns of tree height, diameter, and volume of Douglas-fir (*Pseudotsuga menziesii* [Mirb.] Franco) under acute drought stress in Southern Germany." *Eur. J. For. Res.* 133 (6): 1043–1056. https://doi.org/10.1007/s10342-014-0821-7.

Ravenshorst, G. 2015. "Species independent strength grading of structural timber." Ph.D. thesis, Dept. of Civil Engineering and Geo-Sciences, Delft Univ. of Technology.

Rayleigh, L. 1888. "On the free vibrations of an infinite plate of homogeneous isotropic elastic matter." *Proc. London Math. Soc.* 1 (1): 225–237. https://doi.org/10.1112/plms/s1-20.1.225.

Ross, R. J., and M. O. Hunt. 2000. *Stress wave timing nondestructive evaluation tools for inspecting historic structures: A guide for use and interpretation.* General Technical Rep. No. FPL GTR 119. Madison, WI: US Dept. of Agriculture, Forest Service, Forest Products Laboratory.

Sansalone, M., and W. Street. 1997. *Impact-echo: Nondestructive evaluation of concrete and masonry.* Ithaca, NY: Bullbrier Press.

Shantharaja, M., and G. M. Sandeep. 2014. "Experimental and numerical analysis of propagation of stress wave in sheet metal." *Int. J. Sci. Technol. Res.* 3 (10): 40–42. https://doi.org/10.2478/s13531-012-0034-0.

Stapel, P., and J. W. G. van de Kuilen. 2013. "Effects of grading procedures on the scatter of characteristic values of European grown sawn timber." *Mater. Struct.* 46 (9): 1587–1598. https://doi.org/10.1617/s11527-012-9999-7.

Stapel, P., and J. W. G. van de Kuilen. 2014a. "Efficiency of visual strength grading of timber with respect to origin, species, cross section, and grading rules: A critical evaluation of the common standards." *Holzforschung* 68 (2): 203–216. https://doi.org/10.1515/hf-2013-0042.

Stapel, P., and J. W. G. van de Kuilen. 2014b. "Influence of cross-section and knot assessment on the strength of visually graded Norway spruce." *Eur. J. Wood Prod.* 72 (2): 213–227. https://doi.org/10.1007/s00107-013-0771-7.

Suiker, A. S. J., A. V. Metrikine, and R. de Borst. 2001. "Comparison of wave propagation characteristics of the Cosserat continuum model and corresponding discrete lattice models." *Int. J. Solids Struct.* 38 (9): 1563–1583. https://doi.org/10.1016/S0020-7683(00)00104-9.

Tallavo, F., G. Cascante, and M. D. Pandey. 2017. "Experimental verification of an orthotropic finite element model for numerical simulations of ultrasonic testing of wood poles." *Eur. J. Wood Wood Prod.* 75 (4): 543–551. https://doi.org/10.1007/s00107-016-1065-7.

Tasdemirci, A., and I. W. Hall. 2005. "Experimental and modeling studies of stress wave propagation in multilayer composite materials: Low modulus interlayer effects." *J. Compos. Mater.* 39 (11): 981–1005. https://oi.org/10.1177/0021998305048736.

Verner, E. A., and E. B. Becket. 1973. "Finite element stress formulation for wave propagation." *Int. J. Numer. Methods Eng.* 7 (4): 441–459. https://doi.org/10.1002/nme.1620070404.

Yaitskova, N., and J. W. van de Kuilen. 2014. "Time-of-flight modeling of transversal ultrasonic scan of wood." *J. Acoust. Soc. Am.* 135 (6): 3409–3415. https://doi.or/10.1121/1.4873519.

Zandbergs, J. G., and F. W. Smith. 1987. "Finite elements fracture prediction for wood with knots and cross grain." *Wood Fiber Sci.* 20 (1): 97–106.

© ASCE   04019309-11   J. Mater. Civ. Eng.

J. Mater. Civ. Eng., 2019, 31(12): 04019309

Paper 3: An advanced virtual grading method for wood based on surface information of knots

An advanced virtual grading method for wood based on surface information of knots

A. Khaloian Sarnaghi[1] · J. W. G. van de Kuilen[1,2,3]

Abstract

Strength grading of timber boards is an important step before boards can be used as lamellas in glued laminated timber. Grading is generally done visually or by machine, whereby machine grading is the faster and more accurate process. Machine grading gives the best strength prediction when dynamic modulus of elasticity (MoE_{dyn}) is measured and some kind of knot assessment algorithm is included as well. As access to the actual density for the measurement of MoE_{dyn} may be impossible in some conditions, this grading method may face some problems in strength prediction. As the strength of a board is related to its natural defects and the ability of the stress waves to propagate around these defects, a virtual method for more accurate strength predictions is developed based on the knot information on the surface. Full 3D reconstruction of the boards, based on knot information on the surfaces of these boards, is an important step in this study. Simulations were run for 450 boards of spruce, Douglas fir, beech, ash and maple, covering a large quality range. Abaqus and Python were used for the numerical simulations. From the numerical simulations, three different stress concentration factors were calculated in the vicinity of the defects. Additionally, a virtual longitudinal stress wave propagation was modeled for the determination of the dynamic modulus of elasticity. The FEM results were used to predict the tensile strength. By means of a regression analysis, the correlation with actual visual and machine readings was validated. An improvement in the strength prediction was observed based on the virtual method, when compared to currently available grading machines. It shows the potential of numerical methods for strength prediction of wood based on visual knot information.

✉ A. Khaloian Sarnaghi
   sarnaghi@hfm.tum.de

Extended author information available on the last page of the article

🌀 Springer

Introduction

Wood is a naturally grown material with strong heterogeneities. Natural defects in this material cause local fiber deviations and therefore affect the mechanical properties of wood. Knots in timber may have different geometrical shapes and configurations, which may affect the localization of the stresses and may initiate failure in the material. Thus, the strength scatter of this material is significant, which is also partly affected by the knots. Therefore, before using wood for structural engineering products, such as glulam, the material needs to be strength graded. Predicting the strength of wood for engineering products is generally based on the determination of the modulus of elasticity based on longitudinal vibration measurement, in some cases extended with a knot assessment system. The latter can be a surface scanning system, such as WoodEye or an X-ray system (Microtec, LuxScan). As visual grading is done solely based on the visible geometrical knot parameters, it is not the best method for the strength prediction of wood (Stapel and van de Kuilen 2013, 2014a, b). With the introduction of CT scanning, a new and powerful scanning technology has become available. The technology is primarily used for round wood scanning at the sawmill entrance. With regard to strength grading of boards, CT scanning is not optimal, as no (dynamic) modulus of elasticity can be determined from the scans, neither the derived 'knottiness' of virtually sawn boards. A separate vibration analysis of the trunks to determine the (dynamic) modulus of elasticity of the trunks is not a viable alternative either, as the dynamic modulus of elasticity of the trunk does not correlate well with the modulus of elasticity of the boards sawn from it. The decrease in predictive capacity along the value chain has been analyzed in Rais et al. (2014b).

Thus, numerical methods with more accurate geometrical reconstruction of the knots may be an alternative method to improve the strength prediction of the material. Due to the complex geometrical aspects of the biological materials, different studies on numerical modeling of biomaterials concentrated on the 3D reconstruction of the geometrical models based on the grayscale information of the CT scans (Tabor and Rokita 2007; Baudoin et al. 2008; Kowalczyk 2010; Hazrati Marangalou et al. 2013). To optimize yield in wood, commercial CT scanning has recently become available through Microtec (Giudeiceandrea et al. 2018), who developed a CT scanner for the wood industry. Yield is expected to increase when applied in sawmills. However, as CT scanning is giving information on the wood quality, it does not measure the modulus of elasticity of the material. In order to overcome this problem, a new procedure to grade the material for strength has been developed. This method only needs information on knots as visual on the surface of a board. Any additional information about fiber flow around knots is not necessary as this is implemented in the model. This means that a virtual board from a CT scan or any other type of wood surface scanner, able to detect knots, is sufficient for this study. The geometrical reconstruction in this study is done solely based on the surface information of the knots from the visual grading. A database is created after visual measurements, which contains the spatial coordinates of the knots that are visible on each surface, the diameters and the angle of rotation in each case.

The fiber patterns and the orthotropic properties do not have a uniform distribution in wood, but they strongly vary among the boards and in each board separately. Different studies focused on the structural modeling of wood and predicting the strength reduction and failure resulting from structural non-uniformities (Goodman and Bodig 1980; Phillips et al. 1981; Cramer and Goodman 1986; Zandbergs and Smith 1987; Bodig and Jayne 1993; Foley 2001; Baño et al. 2010; Guindos and Guaita 2013; Jenkel and Kaliske 2013; Lang and Kaliske 2013; Hackspiel et al. 2014; Lukacevic and Füssl 2014; Jenkel 2016). The basis of most of these models is a 2D flow-grain analogy (Goodman and Bodig 1978; Cramer and Goodman 1982; Foley 2001), which is extended for the 3D case here to consider the vector component in the third direction (Khaloian et al. 2017).

As knots, by localizing the fiber deviations and the stresses, are the main strength governing parameters, mathematical methods were developed in this study for calculation of the stress concentration factors around multiple knots in a 3D anisotropic and heterogeneous space. Development of grooves and holes in materials disturbs the uniformity of the stress distribution patterns. The concentration of the stresses around the defects may lead to the collapse of the material or structure. Different studies focused on analyzing the multiple notch effects in different engineering fields (such as aero structural applications) (Ling 1948; Durelli et al. 1952; Haddon 1967; NASA 1975; Pilkey 1997; Graham et al. 2005; Pilkey and Pilkey 2008; Whitley 2013).

Stress wave propagation is another parameter checked in this study to predict the strength of wood. Any heterogeneities in the material attenuate the magnitude of the signal wave and cause scattering and reflection around the non-uniform defects in the material. Stress wave propagation is also numerically used in studies for different materials and applications, including concrete, steel and wood (Verner and Becket 1973; Suiker et al. 2001; Nilsson 2009; Kim and Anandakumar 2010; Nath 2013; Shantharaja and Sandeep 2014; Bulleit and Falk 1985).

Considering the natural scatter in the structure and mechanical performance of wood as a biomaterial, limitation and simplification of the numerical model to specific species may result in an over-/underestimation of its global behavior and prevent the adaption of the model to other species. Due to the lack of information regarding the consideration of the natural scatter of this material in the numerical analysis, the aim of this study was to develop a method that adapts to the natural scatter of both softwoods and hardwoods. Therefore, the objective of this study is to provide a virtual method for the strength prediction of timber, solely based on the surface information of the knots.

By covering the total quality range of timber in this study, numerical simulations were mainly run for spruce, Douglas fir and beech, as the mainly used species for glulam lamellas. Additionally, simulations were run for small sets of ash and maple boards for the validation.

The simulation results were used in a multiple regression analysis for the tensile strength predictions. The statistical analysis showed the strength of the virtual methods compared to any available visual or machine methods for the strength prediction of low- and high-quality softwood and hardwood species.

Materials and methods

Material properties and board reconstruction

The method of the reconstruction in this study was applied to 468 different boards, including softwood and hardwood samples, and was shown to be a successful approach for numerical analysis. Recently available approaches for the grading of timber are the visual and machine grading methods, based on the knot information, dynamic modulus of elasticity and the density of the boards. Therefore, a similar approach was taken into account in the numerical simulations for the strength prediction of the wooden boards.

Initially, the analyses were run for spruce and Douglas fir softwood species, as the commonly used species for the glulam production. Covering the total quality range of the boards, the analysis was done for 103 medium–high-quality spruce (Stapel and van de Kuilen 2013) and 151 low–medium-quality Douglas fir (Rais et al. 2014a, b) boards, based on which a dataset was created registering the geometrical aspects of the knots (coordinates, diameters, surfaces and angles). By developing the virtual method for the strength prediction of softwood species, the model was further developed for the representation of the hardwood species, including beech, ash and maple. The analysis was done for 200 low-quality beech boards with two different cross-sectional dimensions and 14 high-quality ash and maple boards. The information on the boards is presented in Table 1. The quality of the boards was categorized based on their strength values, previously obtained from the tensile tests (Table 1). The samples contained different dimensions, and the samples of each specific specimen were separated based on their cross-sectional areas. Due to the small groups of ash and maple boards in this study, high CoV values for these samples in Table 1 are not uncommon. These sets with only few boards are statistically not relevant for comparisons. Therefore, these sets were used as reference samples for the validation and generalization of the developed model.

To provide a general view of the heterogeneities in different samples and species, comparisons were made among the knot numbers and knot clusters in the samples considered in this study. Among the softwood species in this study, spruce boards contain 1–41 knots, whereas the Douglas fir may contain up to 89 knots. Among the hardwood species, beech boards have maximum 22 knots, whereas the ash and maple boards have maximum of 12 and 11 knots, respectively. Knots in hardwood species have generally more uniform shapes and are well distanced from each other.

The geometrically complicated structure of the Douglas fir boards with the formation of the big knot clusters along the board, and existence of the pith and defects, causing extreme fiber deviations in beech boards, are some conditions that are affecting the quality of these boards compared to the others.

Comparing the geometrical structure of spruce and beech boards together in Fig. 1, it was shown that the hardwood boards have more complicated fiber deviations and structural patterns compared to the softwoods, which have many complicated knot shapes and natural defects.

Table 1 Material and mechanical properties of the boards used for the simulations

Species	Spruce	Douglas fir	Beech		Ash		Maple	
			Beech$_1$	Beech$_2$	Ash$_1$	Ash$_2$	Maple$_1$	Maple$_2$
Number	103	151	100	100	3	3	5	3
Length (mm)								
Avg.	4101	4467	3102	3102	3143	3130	3135	3121
CoV	0.008	0.02	0.003	0.002	0.004	0.005	0.001	0.006
Thickness (mm)								
Avg.	40	46	24	24	31	35	30	35
CoV	0.014	0.01	0.01	0.01	0.05	0.0003	0.09	0.005
Width (mm)								
Avg.	150	146	151	100	125	125	125	125
CoV	0.002	0.002	0.003	0.002	0.001	0.002	0.003	0.001
Strength (MPa)								
Avg.	29.19	19.31	31.11	34.56	67.41	72.31	34.30	41.99
CoV	0.34	0.47	0.43	0.44	0.37	0.23	0.28	0.61
Density (kg/m^3)								
Avg.	462	490	758	773	676	706	659	678
CoV	0.13	0.09	0.05	0.05	0.05	0.08	0.03	0.04
MoE$_{static}$ (MPa)								
Avg.	12,000	10,200	11,100	11,300	16,500	19,000	13,800	14,100
CoV	0.20	0.25	0.18	0.24	0.08	0.15	0.15	0.16
TKAR (–)								
Avg.	0.3	0.35	–	–	0.10	0.10	0.25	0.21
CoV	0.32	0.31	–	–	0.84	0.80	0.47	0.20
DEB (–)								
Avg.	0.22	0.23	0.18	0.21	0.072	0.09	0.23	0.18
CoV	0.36	0.26	0.55	0.55	0.77	0.64	0.51	0.24
DAB (–)								
Avg.	0.40	0.44	0.20	0.24	0.14	0.11	0.26	0.25
CoV	0.38	0.29	0.61	0.59	0.77	0.86	0.43	0.41

Fig. 1 Fiber deviations in softwoods and hardwoods. **a** Spruce board, **b** beech board

In this study, all boards were tested in tension (EN 408 2010). Tensile strength values (presented as average in Table 1) were used for the validation of the model developed in this study. Additionally, based on the information on the strength of

single boards, the model can be extended to adapt to any required hardwood or softwood specimen. Each board was also visually graded prior to the tensile tests. Therefore, all information about the location of the pith, knots and the geometrical configurations of the knots over the surfaces of the boards was recorded (TKAR, DEB, DAB in Table 1).

DEB was calculated by summing up the length of all the edges of the surfaces, where a knot appears (DIN 4074-1 2012). DAB was calculated by summing up the edges of the projected areas of the knots, after minimizing the overlapping edges in a moving window of 150 mm over the board (DIN 4074-1 2012). TKAR was calculated similar to DAB. However, the entire cross-sectional areas in a window of 150 mm were considered in this case (Eq. 1) (Stapel and van de Kuilen 2013, 2014a).

$$\mathrm{DEB} = \max\left[\frac{\sum a_i}{2 \cdot b}\right] \quad \mathrm{DAB} = \max\left[\frac{\sum a_i}{2 \cdot b}\right] \quad \mathrm{TKAR} = \max\left[\frac{\sum A_i}{d \cdot b}\right] \quad (1)$$

Based on this information, the exact geometrical reconstruction of the boards was possible and thereby the prediction of the fiber deviations.

In addition to the geometrical representation of the boards in Table 1, the average values of each material parameter and the corresponding CoV values are also provided in Table 1, giving the opportunity for comparison of the quality between the samples. By considering each set separately, the scatter among the boards of each set is quite big, with CoV values higher than 0.4 for the strength of Douglas fir, beech and maple samples. This condition makes it difficult to develop a general model for wood to consider the heterogeneities in different species. Additionally, the scatter between the samples is also quite high, and the strength values between 19 and 72 and densities between 460 and 770 (as shown in Table 1) were considered in this study.

Although the groups of the ash and maple samples in this study are too small to be statistically analyzed and compared, these species were used as reference samples for the validation of the model and as example boards for the strength predictions based on the regression equations derived from the other samples.

By covering the total scatter in the quality of the boards, a model was developed for the prediction of the tensile strength based on the FE-numerical parameters.

Numerical analysis

A different approach to the CT scan and grayscale-based approach (Tabor and Rokita 2007; Baudoin et al. 2008; Kowalczyk 2010; Hazrati Marangalou et al. 2013) was used in this study regarding the geometrical reconstruction of the wooden boards. This process was done solely based on the information about the knots on the surfaces of the boards from the visual grading, and the 3D geometrical model was predicted for each case. In contrast to the grayscale-based geometrical reconstruction, this approach is relatively cheap and based on assumptions of the coordinate directions and advanced modeling techniques. Additionally, it can be applied to many different species and boards.

Abaqus (Simulia 6.14-2) and Python 2.7.3 were the tools used for the numerical modeling. The geometrical reconstruction of the boards based on the surface information of the knots was done by programming a Python script to extract this information directly from the measurements and reconstruct the boards. Further numerical analysis was performed in Abaqus CAE.

The geometrical data of the knots on the surfaces of the boards, including the coordinates and rotation directions of each knot, as well as the diameters of each case were extracted directly from the database by creating an automatic link to the visual knot parameters. A comprehensive geometrical model of the boards was reconstructed in Abaqus based on this surface information, after analyzing typical knot orientations (DIN 4074 2012) that are summarized in 15 different surface possibilities (Figure 1s). As exact representation of the board may not always be possible, and some errors could happen during the visual knot registration process, an additional error term of ± 5 (mm) was added to the program for the extraction of the coordinate direction and the calculation of the angle of rotation of the knot. This was done by using the uncertainties package with ufloat () function in Python, which takes the real dimension of the knot and generates numbers with uncertainties in the reconstruction process.

Additionally, a separate central axis and plane were defined for each knot, which represents the axis of the rotation of the knot. This makes it possible to assign different material properties in different locations of the model, as the program can find the axis of rotation of the knots and correspondingly the knot volumes easily and assign the required material properties. Knots are geometrically reconstructed as cones or cylinders, depending on the location of the pith in the board. A complete representation of the conical knot reconstruction was presented in the work by Kandler et al. (2016). In this study, the conical reconstruction was done by considering the minimum x-coordinate of the knot in the longitudinal direction (on both board faces) and the diameters of the ellipses. Therefore, the opening angle of the knot may be slightly under- or overestimated. The same will happen when applying a random error to the knot diameter through the random error analysis for knot reconstruction. Although the geometry of the knot is slightly deviated in such cases, the effect on the results of the final predictions is negligible. The visual information about the dimensions of the knots on upper and lower surfaces of the boards gives us an estimation about the location of the pith. Figure 2 shows the geometrical reconstruction of the spruce, Douglas fir and beech boards.

Due to the extreme interactions between knots, their rotations/bad geometrical configurations, the geometrical reconstruction and performance of the numerical analysis have failed in some cases. Such condition could occur due to the extremely long knots or knots with extremely steep angles (shown in Fig. 3) as well. This was mainly a problem for 13 out of 151 Douglas fir and 6 out of 200 beech boards. Therefore, simulations were run for a total of 448 boards. The mentioned problem in the reconstruction process may be due to the implemented uncertainty during the reconstruction process.

In this study, knots were modeled as holes after a preliminary study had been performed on the validity of this approach. It was found that the ratio of the stress peaks along the board is independent of the chosen modeling approach. Additionally, the
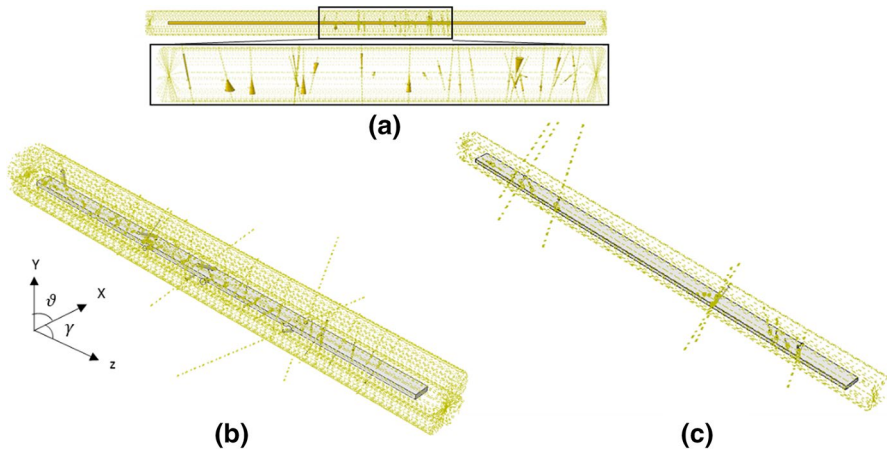
Fig. 2 Virtual geometrical reconstruction of the boards. Example of **a** spruce board, **b** Douglas fir board, **c** a beech board
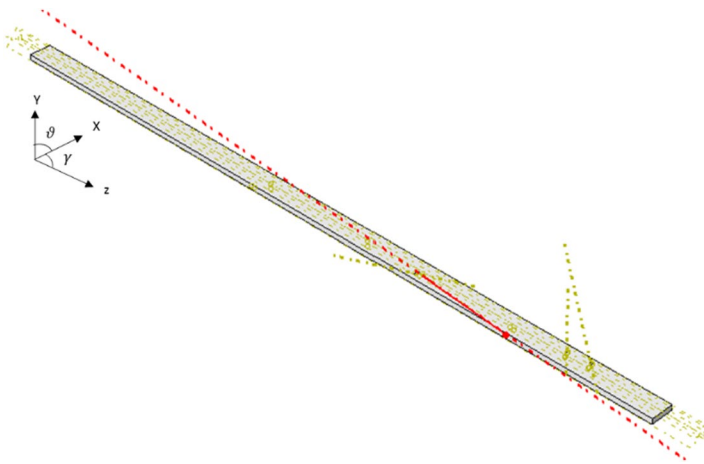
Fig. 3 Example of a board with extremely long and steep knot

ratio of the stress variation between both approaches remains the same in different samples and species. Although the exact location of the maximum stress around a knot is slightly varying for each method, the maximum stress always occurs at the same knot. By merging the knots and the bulk wood as one part in the model, all knots are being considered as live knots that have a fixed contact with their bulk material in contrast to the holes that represent the dead knots with no contact to their bulk material. Taking these aspects into account and by considering the increasing computational complexity when modeling knots as solid volumes, increasing contact nonlinearities and number of the elements, it was decided to model the knots as holes.

As wood is a natural material with non-homogeneous structure, knots and the resultant fiber deviations are affecting its strength. Due to the strong anisotropy of wood, the spatial coordinate directions are not constant along the boards. Therefore, the stiffness properties of this material are varying according to the fiber directions. Since the main fluid transport occurs in the growing cells, an actual fluid flow exists around knots when the cells are growing (Goodman and Bodig 1980; Hu et al. 2018). For this reason, the concepts of the flow-grain analogy were used for the numerical simulations and the prediction of the fiber patterns in wood (Goodman and Bodig 1980; Foley 2001; Khaloian et al. 2017). This concept considers the stream behavior of the laminar flows for the deviation of the fibers in wood around the knots. The integrated velocity information over the nodes of each local element was then used in a transformation to predict the coordinate rotations for the discrete field of the wooden boards, showing the orthotropic directions of the material. The obtained local coordinate system was assigned to the center of each local element. Using the static and dynamic solvers, the knot effects on the stress distribution patterns and the dynamic modulus of elasticity of the boards were predicted in this study. Interaction of the knots in an anisotropic 3D space causes localized high stresses in the boards, which affect the strength properties. This is due to the abrupt geometrical changes in the numerical model. Therefore, three mathematical equations are provided in Eqs. 2–4 for the extraction of these local and global stress concentration factors in each wooden board. The boards in this case were analyzed under uniform tension in the linear elastic range (EN 408 2010), through which the development of the stresses in the boards and the maximum stresses around the knots were analyzed. The results of these analyses were benchmarked to the visual knot grading parameters of the TKAR, DEB and DAB (DIN 4074-1 2012). The stress concentration factors (SCFs) are calculated as:

$$SCF_1 = \max\left(\sigma_{sim} \cdot \frac{A_{knot}}{A_{total}}\right) \tag{2}$$

$$SCF_2 = \sigma_{avg} \cdot \left(\frac{A_{total}}{A_{total} - A_{knot,max}}\right) \tag{3}$$

$$SCF_3 = \sigma_{avg} \cdot \left(\frac{A_{total}}{\left|A_{total} - A_{projected}\right|}\right) \tag{4}$$

σ_{sim} for SCF_1 is the maximum tensile stress parallel to the fibers around each knot, which is extracted for each knot separately.

The nominal stress (σ_{nom}) of 1 (MPa) was applied to each board. A_{knot} is the biggest total cross-sectional area of each knot on its central axis. A_{total} is the end cross section of the board, where the load is applied.

σ_{avg} for SCF_2 is the average stress parallel to the fibers in the clear part of the wood around the knot with the maximum stress in the total board (along the two

paths shown in Fig. 4). $A_{\text{knot,max}}$ is the area of the knot with the maximum stress in the total board. This area is selected based on the maximum stress, instead of the biggest knot volume. Finally, $A_{\text{projected}}$ in Eq. 4 is the biggest projected knot cluster surface in the window of 150 (mm).

Different SCFs were calculated by considering the single or average effects of the stresses perpendicular to the fiber directions. However, as these components are relatively small compared to the longitudinal component and the extracted parameters did not improve the quality of the tensile strength predictions, the effects of these components were neglected in this study.

By analyzing the longitudinal vibration based on the explicit dynamic stress wave analysis, the dynamic modulus of elasticity of each board was calculated. The average density and stiffness properties of each set of sample (as presented in Table 1) were used as input parameters for the numerical simulations. The average density in the numerical analysis was used to reduce the dependency of the numerical predictions on the actual density of the samples. Knowing the velocity of the stress wave after its reflection and transmission by reaching the knot locations, the frequencies and correspondingly the dynamic modulus of elasticity are calculated for each board, using Eq. 5.

$$E_{\text{dyn}} = 4l^2 f^2 \rho \tag{5}$$

where l is the length of the specimen and f is the first eigenfrequency.

Later, by measuring the actual density values of each board, the density parameter in Eq. 5 can be replaced with the actual density of each board to have more accurate predictions of the dynamic modulus of elasticity.

Therefore, finally four numerical parameters (including SCF_1, SCF_2, SCF_3 and MoE_{dyn}) were extracted from the simulations, which were later used in a regression analysis with the tensile strength obtained from the tests to provide a model for the prediction of the strength of the boards. Each case was validated with the same parameters extracted from the measurements or visual grading.

Statistical analysis was mainly done for the three samples of spruce, Douglas fir and beech. Later in this study, all boards of these three samples were used together in the multiple regression analysis to predict the regression equation for the complete range, independent of the type of the wood. The strength of the ash and maple boards was then predicted based on the virtual parameters of each board from the simulation and the regression equation. Additionally, the ash and maple samples

Fig. 4 Representation of the σ_{avg} around the knot with maximum stress
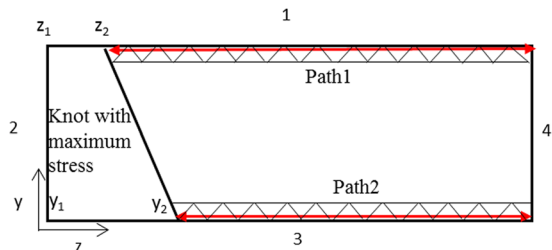
were used in combination with the three other samples in a multiple regression analysis, and the second regression equation is provided for the whole range of the samples, independent of the type of the wood. The results in each case were validated with the results of their experimental values.

Results and discussion

General results

For tensile strength predictions, each of the single numerical parameters was correlated to the experimental tensile strength. By performing similar correlations for the parameters of the visual and machine grading methods (including the TKAR, DEB, DAB, density, and MoE_{dyn}), the model was validated with the currently available grading methods. Later, the multiple effects of these parameters were checked in a regression analysis, and the results were compared and validated with the same ones from measurements.

From the single regression analysis of each of the stress concentration factors and the experimental tensile strength, an inverse correlation was found between these numerical parameters and the strength. This condition shows the fact that increasing the stress concentration around the geometrical non-uniformities in the boards causes reduction in the strength of the material. The estimated linear equation for each of these cases and for each set is presented in Eq. 6. The R^2 values are presented in Tables 1s–3s in Electronic Supplementary Material.

$$
\begin{aligned}
f_{\text{beech}} &= -5.6\text{SCF}_1 + 54 & f_{\text{spruce}} &= -10.4\text{SCF}_1 + 49 & f_{\text{Douglasfir}} &= -5.8\text{SCF}_1 + 35 \\
f_{\text{beech}} &= -22.3\text{SCF}_2 + 71 & f_{\text{spruce}} &= -7.8\text{SCF}_2 + 47 & f_{\text{Douglasfir}} &= -5.9\text{SCF}_2 + 35 \\
f_{\text{beech}} &= -10.8\text{SCF}_3 + 58 & f_{\text{spruce}} &= -7.5\text{SCF}_3 + 48 & f_{\text{Douglasfir}} &= -3.6\text{SCF}_3 + 32
\end{aligned}
$$

$$(6)$$

The strength prediction based on the dynamic modulus of elasticity was once performed by considering the average density values in Eq. 5 and later by recalculating this parameter by replacing the actual density values in the same equation. The correlation between the calculated dynamic modulus of elasticity and the tensile strength of three wooden species is presented in Fig. 5.

The regression values of all single parameters with the experimental tensile strength are presented in Tables 1s–3s in Electronic Supplementary Material for the spruce, Douglas fir and beech boards, respectively. As shown in Fig. 5, the current study covers the typical quality range of the softwood and hardwood boards, including low–medium-quality Douglas fir, medium–high-quality spruce boards and low-quality beech boards (according to Table 1).

As expected and shown in Fig. 5 and Tables 1s–3s, the quality of the predictions increases in the case of the calculation of the dynamic modulus of elasticity based on the actual density of the boards. The increase is more significant for the case of Douglas fir boards ($R^2 = 0.27$ compared to $R^2 = 0.50$ in the case of the calculation of the MoE_{dyn} with average and actual densities, respectively).

Fig. 5 Correlation of the MoE_{dyn} with tensile strength
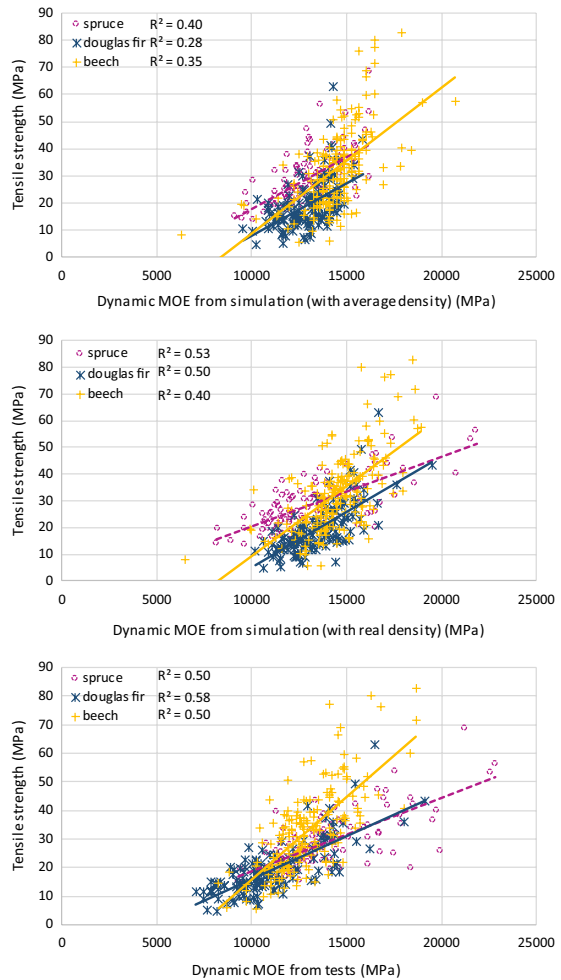
This difference is smaller for spruce and beech boards with $R^2 = 0.40$ compared to $R^2 = 0.53$ and $R^2 = 0.34$ compared to $R^2 = 0.40$, respectively. The strong variation here between different species may result from the strong non-uniformity and existence of many natural defects in Douglas fir boards.

To check the multiple effects of the different parameters on the strength prediction, linear multiple correlation analyses were performed considering linear combinations of different parameters, including the stress concentration factors, the simulated MoE_{dyn} and the density for the numerically extracted parameters. This linear combination is shown in Eq. 7. The same behavior was analyzed for the measured knot parameters, including the TKAR, DEB, DAB, tested MoE_{dyn} and density. The linear combination for this set of parameters is shown in Eq. 8. The coefficients of the linear correlations and correspondingly the R^2 values of

Table 2 Coefficient of different linear multiple correlation analyses of the simulated parameters for spruce, Douglas fir and beech based on Eq. 7

Case	SCF$_1$	SCF$_2$	SCF$_3$	MoE$_{dyn,avg}$	MoE$_{dyn,act}$	ρ	Constant	R^2
	a	b	c	d		e	g	
$f_{pred,spruce}$								
1	−6.2294	−0.0288	−1.5554	0.0022	–	–	16	0.62
2	−7.6943	–	–	0.0023	–	–	14	0.61
3	−6.7208	–	–	–	0.0021	−0.0135	20	0.71
$f_{pred,douglasfir}$								
1	−3.6528	−2.3046	−0.3038	0.0013	–	–	20	0.57
2	−3.6614	−2.7106	–	0.0013	–	–	19	0.57
3	−2.8324	−2.1081	–	–	0.0024	0.0033	−1.6	0.67
$f_{pred,beech}$								
1	−2.9349	−12.2828	0.8054	0.0024	–	–	27	0.62
2	−2.8944	−11.2678	–	0.0024	–	–	28	0.62
3	−2.6526	−11.0531	–	–	0.0026	0.0063	19	0.64

MoE$_{dyn,avg}$ is the simulated dynamic modulus of elasticity, using the average density in Eq. 5

MoE$_{dyn,act}$ is the simulated dynamic modulus of elasticity, using the actual density in Eq. 5

Table 3 Coefficient of different linear multiple correlation analyses of the measured parameters for spruce, Douglas fir and beech based on Eq. 8

Case	TKAR	DEB	DAB	MoE$_{dyn,test}$	ρ	Constant	R^2
	a	b	c	d	e	g	
$f_{pred,spruce}$							
1	−18.4359	−21.7498	−3.0950	0.0023	−0.0095	13	0.60
2	−34.4056	−32.8446	−4.9715	–	–	49	0.52
$f_{pred,douglasfir}$							
1	−20.0228	−29.5413	10.0295	0.0032	−0.0325	8.5	0.67
2	−22.5075	−36.1036	−10.6911	–	–	40	0.55
$f_{pred,beech}$							
1	–	−18.2578	−0.6857	0.0052	0.0049	−35	0.52
2	–	−43.7953	−11.2540	–	–	44	0.56

MoE$_{dyn,test}$ is the measured dynamic modulus of elasticity from the tests

each case can be found in Tables 2 and 3 (and in Tables 4s and 5s in Electronic Supplementary Material) for spruce, Douglas fir and beech boards.

$$f_{pred} = a \cdot SCF_1 + b \cdot SCF_2 + c \cdot SCF_3 + d \cdot MoE_{dynamic} + e \cdot \rho + g \qquad (7)$$

$$f_{pred} = a \cdot TKAR + b \cdot DEB + c \cdot DAB + d \cdot MoE_{dynamic} + e \cdot \rho + g \qquad (8)$$

For the case of the lower-quality Douglas fir and beech boards, it is shown that applying two or three SCF parameters in combination with the MoE$_{dyn}$ gives the

same coefficients of determination. This is also valid for the spruce boards, and the results are shown in Table 1s in Electronic Supplementary Material. Applying actual density in Eq. 5 and updating the regression Eq. 7 improve the quality of the predictions for spruce and Douglas fir considerably ($R^2=0.71$, $R^2=0.67$, respectively), while for beech it increases slightly from $R^2=0.62$ to $R^2=0.64$.

All results of the simulations, including the knot parameters and the virtual MoE_{dyn}, were used in a multiple regression analysis to predict the tensile strength of the material. Considering different combinations of these parameters (shown in Tables 1s–3s in Electronic Supplementary Material) for each case, the optimum combinations were selected for the strength prediction of each set of samples.

As the SCFs are of nonlinear nature, nonlinear multiple regression analyses were also performed to analyze the improvements.

The results show that only SCF_1 and MoE_{dyn} based on the average density are enough for the virtual tensile strength predictions of the spruce boards. Addition of the SCF_2 and SCF_3 does not improve the quality of the predictions anymore ($R^2=0.69$ compared to 0.70 and 0.71 in the nonlinear analysis).

Douglas fir and beech boards are slightly different. Due to the geometrically complex conditions of the Douglas fir boards and due to the knot superpositions and structural complications of, in particular, beech hardwoods, the quality of the strength predictions strongly depends on the knots and the geometrical parameters. Therefore, in addition to the SCF_1 and the MOE_{dyn}, the SCF_2 parameter also improves the quality of the predictions ($R^2=0.58$ compared to 0.67 and $R^2=0.51$ compared to 0.60 for the Douglas fir and beech boards, respectively). The addition of the SCF_3 has no effect on the quality of the predictions in these cases ($R^2=0.67$ compared to 0.67 and $R^2=0.60$ compared to 0.60 for the Douglas fir and beech boards, respectively).

Comparing only the simulated knot parameters (SCF_1, SCF_2 and SCF_3) to the measured ones (TKAR, DEB, DAB), significant improvements are seen in the quality of the predictions based on the numerical parameters for all three cases ($R^2=0.62$ compared to 0.35, $R^2=0.65$ compared to 0.27 and $R^2=0.54$ compared to 0.15 for the spruce, Douglas fir and beech boards, respectively). This confirms the quality of the virtual methods compared to the visual ones for the tensile strength predictions.

The mathematical Eqs. 9 and 10 show the nonlinear regression equations of the strength with each of the numerical parameters of the simulations.

$$f_1 = \sum_{i=1}^{n} a_i \cdot e^{b_i \cdot \mathrm{SCF}_i} + c \cdot \mathrm{MoE_{dyn}} + d \tag{9}$$

$$f_2 = \sum_{i=1}^{n} \left(a_i \cdot \mathrm{SCF}_i^{b_i} + c_i \cdot \mathrm{SCF}_i \right) + d \cdot \mathrm{MoE_{dyn}} + e \tag{10}$$

where n is the number of the SCFs required for the strength predictions, SCF_i are the stress concentration factors, presented above, f is the tensile strength, MoE_{dyn} is the

Table 4 Coefficients of Eq. 9 for cases of MoE_{dyn} with average density and modification of the MoE_{dyn} with measured density

	a_1	a_2	b_1	b_2	c	d	R^2
f_1							
S							
ρ_{avg}	− 1411.56	0.00	0.0054	0.00	0.0023	1425.54	0.69
ρ_{act}	− 1212.53	0.00	0.0056	0.00	0.0019	1229.94	0.75
DF							
ρ_{avg}	− 3.35	− 5.12	0.32	0.21	0.0027	1.90	0.66
ρ_{act}	− 5.93	− 6.62	0.22	0.17	0.0030	1.88	0.73
B							
ρ_{avg}	− 15.89	− 35.35	0.11	0.21	0.0024	73.24	0.58
ρ_{act}	− 286.34	− 458.20	0.009	0.023	0.0027	765.71	0.61

S spruce, *DF* Douglas fir, *B* beech

Table 5 Coefficients of Eq. 10 for cases of MoE_{dyn} with average density and modification of the MoE_{dyn} with measured density

	a_1	a_2	b_1	b_2	c_1	c_2	d	e	R^2
f_2									
S									
ρ_{avg}	27.33	0.00	− 6.50	0.00	− 3.27	0.00	0.0019	7.03	0.68
ρ_{act}	22.89	0.00	− 8.60	0.00	− 4.66	0.00	0.0014	16.70	0.75
DF									
ρ_{avg}	16.34	7.99	− 1.52	− 1.21	− 0.72	− 1.12	0.0011	1.57	0.62
ρ_{act}	10.85	1.64	− 2.16	− 1.39	− 1.20	− 2.13	0.0018	1.04	0.70
B									
ρ_{avg}	16.53	21.92	− 3.63	− 2.23	− 1.61	− 2.28	0.0022	0.65	0.66
ρ_{act}	15.71	19.38	− 3.62	− 2.52	− 1.48	− 3.11	0.0024	0.37	0.69

S spruce, *DF* Douglas fir, *B* beech

dynamic modulus of elasticity, *a*, *b*, *c*, *d*, *e* are the constants, provided in Tables 4 and 5.

n is represented as: $n = 1$ for spruce boards and $n = 2$ for Douglas fir and beech boards. The value of n for spruce, Douglas fir and beech samples shows that only one SCF is enough for the strength prediction of the good-quality spruce boards, whereas an additional second SCF needs to be defined to improve the strength predictions for low–medium-quality Douglas fir and low-quality beech boards. These equations show the nonlinear correlation of the numerical parameters with the tensile strength. As mentioned above, density is not considered as a separate parameter for the multiple regression analysis, but the density parameter in the calculation of the dynamic modulus of elasticity is modified with the actual density. The results of the analysis are presented in Fig. 6.
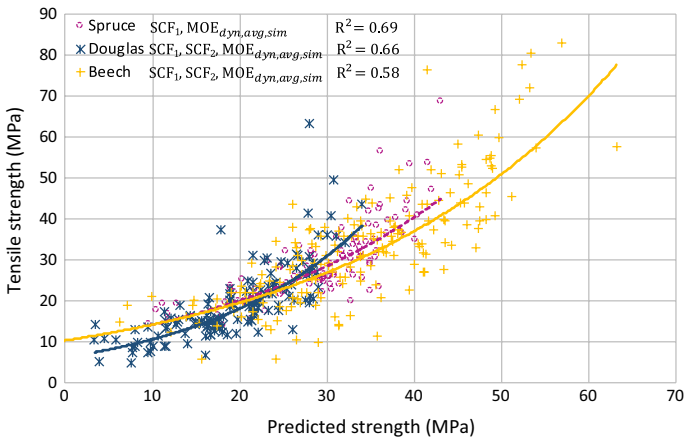
Fig. 6 Correlation diagram of numerical parameters with tensile strength for spruce, Douglas fir and beech sets. $MoE_{dyn,avg,sim}$ is the calculated MoE_{dyn} based on the average density for each set

From Tables 4 and 5, it can be seen that only one SCF is used for the prediction of the spruce behavior, whereas two SCFs improve the quality of the predictions for the low-quality Douglas fir and beech boards. As adding the second stress concentration factor to the analysis does not improve the quality of the virtual predictions for the spruce boards significantly, the a_2 and b_2 parameters in Tables 5 and 6 were set to zero for this set. These parameters are taking values for the lower-quality Douglas fir and beech boards, due to the considerable improvement of the virtual predictions, by addition of the second stress concentration factor. This condition is discussed in Eqs. 9 and 10. Considering different parameters for the tensile strength predictions in this study, those parameters were selected that improve the predictions by more than 10%. This means that if adding a parameter to the multiple regression analysis does not improve the quality of the predictions by more than 10%, this parameter is not taken as a strength predictor. The values of all single parameters are presented in Tables 1s–3s. Additionally, it is shown in Tables 4 and 5 that using the actual density of the boards for calculation of the MoE_{dyn} considerably improves the quality of the predictions.

Influence of density on the predictions

The results of the multiple regression analysis improve considerably, when the actual density is known. Known actual density can be used as an improvement of

Table 6 R^2 values of the nonlinear multiple regression analysis for three sets of parameters and for three wood species

|	Simulation parameters	Knot parameters	Tested parameters
Spruce	0.71	0.35	0.60
Douglas fir	0.66	0.27	0.64
Beech	0.59	0.18	0.51

the MoE_{dyn} in Eq. 5, or as a separate parameter or both. The results of the multiple regression analysis by adding the actual density as an additional parameter are shown in Fig. 7. In this figure, the MoE_{dyn} is also re-calculated by applying the actual density of each board instead of the average one.

As shown in Fig. 7, a nonlinear correlation exists between the predicted and the tested tensile strengths. By comparing the regression values of this analysis with the one shown in Fig. 6, considerable improvements are visible in the quality of the virtual strength predictions for both cases of spruce and Douglas fir samples ($R^2 = 0.75$ compared to 0.69 and $R^2 = 0.72$ compared to 0.66 for spruce and Douglas fir boards, respectively). These variations are reduced for the case of the beech boards ($R^2 = 0.61$ compared to 0.58), which show the strong dependency of the predictions on the knot parameters rather than the MoE_{dyn} measurements.

By comparing the regression results of the simulations, considering only the average density values (Fig. 6) with the same results of the experiments and measurements (Fig. 8), the quality of the predictions is better than any recently available machine grading methods. This, results in $R^2 = 0.69$ compared to 0.60, $R^2 = 0.66$ compared to 0.64 and $R^2 = 0.58$ compared to 0.48 for spruce, Douglas fir and beech boards, respectively. The quality of the predictions is increased by application of the actual density for the calculation of the MoE_{dyn}.

From Tables 1s–3s in Electronic Supplementary Material, it can be seen that the experimental values have higher linear correlations, whereas, due to the nonlinear effects of the stress concentration factors, the simulated results have higher nonlinear correlation. The highlighted cells in these tables are the combination of the parameters of Eqs. 9 and 10, which were used for the strength predictions of the spruce, Douglas fir and beech boards in this study.

Table 6 summarizes the results of the multiple regression analysis for all the simulation parameters (SCF_1, SCF_2, SCF_3 and MoE_{dyn}), knot parameters
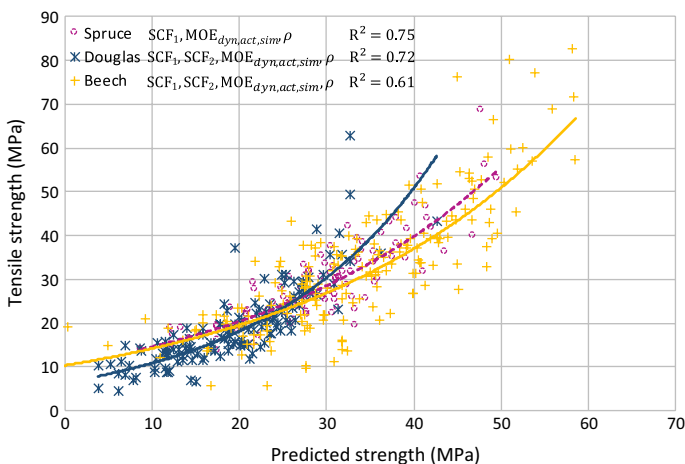
Fig. 7 Addition of the measured density of the boards as an extra parameter to the multiple correlation analysis, and modification of the MoE_{dyn} with the actual density ($MoE_{dyn,act}$)
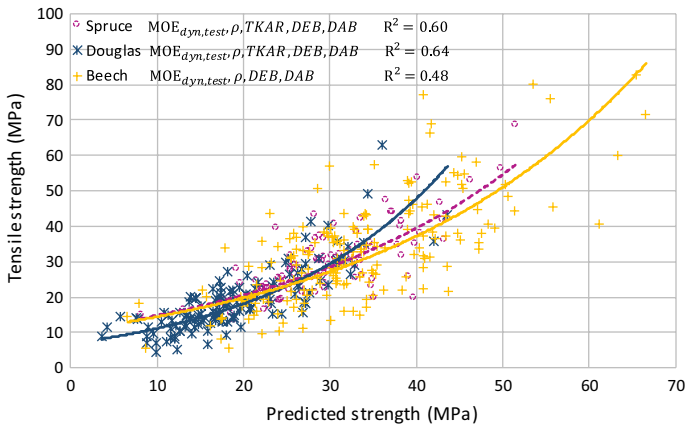
Fig. 8 Correlation of all tested and measured parameters, including MoE_{dyn}, TKAR, DEB, DAB and density, with the tensile strength

(TKAR, DEB and DAB) and tested parameters (MoE_{dyn}, density, TKAR, DEB and DAB).

As shown in Table 6, the simulation parameters for all three samples have much higher R^2 values compared to the visual knot assessment parameters (R^2 value of 0.59 for low-quality samples and R^2 value of 0.71 for high-quality ones). This shows the strength of the numerical predictions in comparison with the visual grading. The R^2 values of the numerical parameters are also higher compared to the tested parameters, which are the parameters of the visual plus machine grading methods. Therefore, the parameters of the FE model highly improve the quality of the strength predictions compared to the currently available visual plus machine grading methods.

Most other studies have focused on bending strength prediction (Baño et al. 2010; Olsson et al. 2012, 2013; Lukacevic and Füssl 2014; Oscarsson 2014; Hu et al. 2018); the studies on prediction of the tensile strength are quite limited. In Lukacevic et al. (2015), a list is provided with R^2 values of different IPs for prediction of the bending strength. The R^2 value of 0.71 is presented in Oscarsson (2014) based on a dataset of 105 boards for predictions of the bending strength. In Lukacevic and Füssl (2014), an R^2 value of 0.79 is presented for a mixture of tensile and bending results of 93 spruce boards, among which 12 boards were analyzed in tension. In Khaloian et al. (2017), an R^2 value of 0.90 is presented for tensile strength prediction of 14 hardwood boards. However, as expected and observed in this study, this value is reduced by increasing the number of the samples.

Predictive analysis of ash and maple

As the final step, the three species (spruce, Douglas fir and beech) were used together in a multiple regression analysis to predict the strength of ash and maple boards. Equation 11 shows the linear correlation of the numerical parameters.

Figure 9 shows the linear and nonlinear correlation of these samples. The results are validated with the experimental parameters (TKAR, DEB, DAB and MoE$_{dyn}$), as shown in this figure. Higher numerical R^2 value in this figure is the result of the nonlinear analysis ($R^2 = 0.62$), whereas the higher experimental R^2 value is from the linear analysis ($R^2 = 0.58$). By predicting the strength of a total of 14 ash and maple samples, described in Table 1, the predicted strength is correlated with the experimental tensile strengths in Fig. 10, which shows a strong correlation ($R^2 = 0.66$).

$$f_{S,DF,B_{sim}} = -1.785 \cdot SCF_1 - 4.93 \cdot SCF_2 - 1.32 \cdot SCF_3 + 0.0027 \cdot MoE_{dynamic} + 10.01$$

(11)

Although having small groups of ash and maple boards, and by being aware of the small influence of this number on the final results, all 448 softwood and hardwood samples, including spruce, Douglas fir, beech, ash and maple, were used together in a multiple regression analysis. It was observed that generalizing the developed model for all different samples is still giving equally good correlation compared to the experimental data ($R^2 = 0.6075$ compared to $R^2 = 0.6006$, respectively), which shows the robustness of the developed model for the tensile strength predictions.

Conclusion

Based on the surface representation of the knots, as the main strength governing parameters, a full 3D geometrical model of different softwood and hardwood species was reconstructed. Due to the geometrical configuration of the knots and, accordingly, localization of high stresses around them, three mathematical methods are provided for the calculation of the stress concentration factors in wood. The dynamic modulus of elasticity was calculated virtually using the average density and
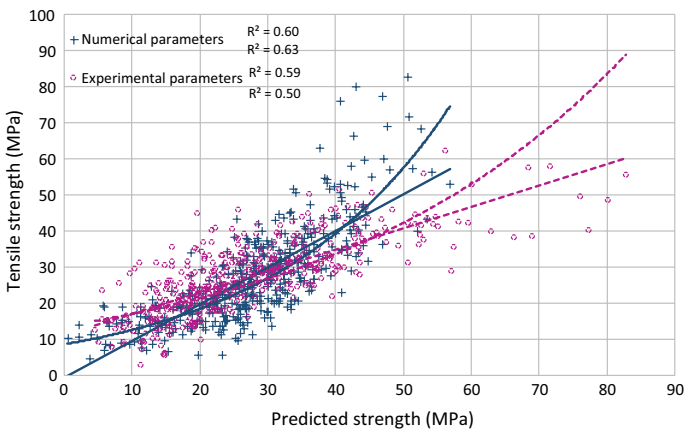
Fig. 9 Strength prediction of 434 samples independent of the species and comparison with the experimental data for both linear and nonlinear correlations
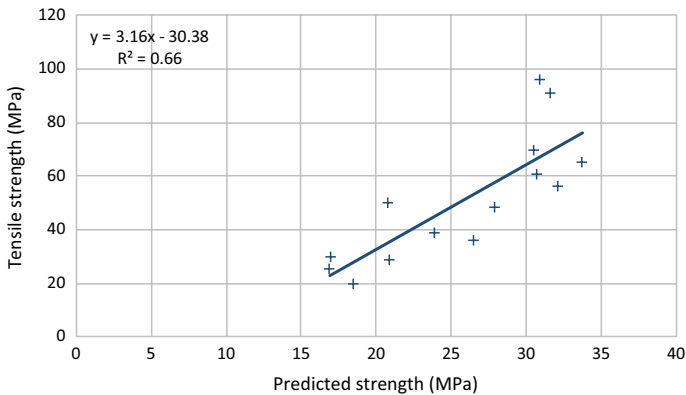
Fig. 10 Correlation of the predicted strength of ash and maple boards, calculated using Eq. 10 with the experimental tensile strength

stiffness of each set as input parameters for the simulations. The analysis was done for a total of 448 boards, covering the complete quality range of the boards used for the glulam production. The simulations were run for medium–high-quality spruce, low–medium-quality Douglas fir, low-quality beech and high-quality ash and maple boards. Initially, the numerical parameters were used in a multiple regression analysis for each set for the prediction of the tensile strength. These results were benchmarked against the visual and machine grading parameters available. Much higher regression values were obtained for the virtual predictions compared to the visual methods available. The predictions are also equally good compared to the recently available visual plus machine grading methods for each set. It was shown that one SCF parameter in combination with the virtual MoE_{dyn} is enough for the strength prediction of the good-quality boards. In contrast, an additional SCF_2 parameter improves the quality of the predictions for the lower-quality softwood and hardwood species considerably. Simulations are independent of the real density and stiffness values of the boards. However, using the actual density of the individual boards and modifying the determined MoE_{dyn} with actual densities improve the quality of the strength predictions considerably. Finally, all numerical parameters of the spruce, Douglas fir and beech samples were used together in a regression analysis, to analyze the correlation with the tensile strength. In this way, a mathematical equation is provided, which gives the opportunity to predict the strength of the samples independent of their species. Based on the provided equation, the strength of ash and maple boards was predicted. A relatively high correlation was found between the predicted and the experimental tensile strength values of these species. As a final step, the numerical parameters of all five samples were used together in a multiple regression analysis to generalize the developed model, and the results were compared to the experimental parameters (TKAR, DEB, DAB and MoE_{dyn}) for all these samples. Equally good correlations were observed in this case as well as between both sets of numerical and experimental parameters, presenting the robustness of the developed virtual method compared to any recently available grading methods

for the tensile strength prediction of timber. Additionally, any scanning technology allowing for the localization of knots can be combined with the developed method for reconstruction and better strength predictions.

Compliance with ethical standards

Conflict of interest On behalf of all authors, the corresponding author states that there is no conflict of interest.

References

Baño V, Arriaga F, Soilán A, Guaita M (2010) F.E.M. analysis of the strength loss in timber due to the presence of knots. In: World conference on timber engineering, Riva del Garda, pp 3–7. ISBN: 978-88-901660

Baudoin A, Skalli W, de Guise J, Mitton D (2008) Parametric subject-specific model for in vivo 3D reconstruction using bi-planar X-rays: application to the upper femoral extremity. Med Biol Eng Comput 46(8):799–805

Bodig J, Jayne BA (1993) Mechanics of wood and wood composites, 2nd edn. Krieger Publishing Company, New York. ISBN 13: 9780894647772

Bulleit WM, Falk RH (1985) Modeling stress wave passage times in wood utility. Wood Sci Technol 19:183–191

Cramer SM, Goodman JR (1982) Model for stress analysis and strength prediction of lumber. Wood Fiber Sci 15(4):338–349

Cramer SM, Goodman JR (1986) Failure modeling: a basis for strength prediction of lumber. Wood Fiber Sci 18:446–459

DIN 4074-1 (2012) Strength grading of wood—part 1: coniferous sawn timber. German Institute for Standardization, Berlin

Durelli AJ, Lake RL, Phillips E (1952) Stress distribution in plates under a uniaxial state of stress with multiple semi-circular and flat-bottom notches. In: Proceedings of the first national congress on applied mechanics. American Society of Mechanical Engineers, pp 309–315

EN 408 (2010) Timber structures—structural timber and glued laminated timber—determination of some physical and mechanical properties. CEN, Brussels

Foley C (2001) A three-dimensional paradigm of fibre orientation in timber. Wood Sci Technol 35:453–465

Giudeiceandrea F, Ursella E, Vicario E, Rais A (2018) Increasing the value of strength graded timber by industrial computer tomography. In: Wood conference in timber engineering, Vienna

Goodman JR, Bodig J (1978) Mathematical model of the tension behavior of wood with knots and cross grain. In: Proceedings from the first international conference on wood fracture, Banff

Goodman JR, Bodig J (1980) Tension behavior of wood—an anisotropic, inhomogeneous material. Structural research report No. 32. Colorado State University, Fort Collins

Graham RH, Raines M, Swift KG, Gill L (2005) Prediction of stress concentrations associated with interacting stress-raisers within aircraft design: methodology development and application. Proc Inst Mech Eng Part G J Aerosp Eng 219(3):193–203

Guindos P, Guaita M (2013) A three-dimensional wood material model to simulate the behavior of wood with any type of knot at the macro-scale. Wood Sci Technol 47:585–599

Hackspiel C, de Borst K, Lukacevic M (2014) A numerical simulation tool for wood grading model development. Wood Sci Technol 48(3):633–649. https://doi.org/10.1007/s00226-014-0629-0

Haddon RAW (1967) Stresses in an infinite plate with two unequal circular holes. Q J Mech Appl Math 20:277–291

Hazrati Marangalou J, Ito K, Cataldi M, Taddei F, van Rietbergen B (2013) A novel approach to estimate trabecular bone anisotropy using a database approach. J Biomech 46:2356–2362

Hu M, Briggert A, Olsson A, Johansson M, Oscarsson J, Säll J (2018) Growth layer and fiber orientation around knots in Norway spruce: a laboratory investigation. Wood Sci Technol 52(1):7–27. https://doi.org/10.1007/s00226-017-0952-3

Jenkel C (2016) Structural and material inhomogeneities in timber, modelling by means of the finite element method. Dissertation, Technische Universität Dresden

Jenkel C, Kaliske M (2013) Analyse von Holzbauteilen unter Berücksichtigung struktureller Inhomogenitäten (Analysis of timber components taking into account structural inhomogeneities). Bauingenieur 88:494–507 **(in German)**

Kandler G, Lukacevic M, Füssl J (2016) An algorithm for the geometric reconstruction of knots within timber boards based on fibre angle measurements. Constr Build Mater 124:945–960

Khaloian A, Gard WF, van de Kuilen JW (2017) 3D FE-numerical modelling of growth defects in medium dense European hardwoods. In: Proceedings of the sixth international scientific conference on hardwood processing, Lahti, pp 60–67

Kim JH, Anandakumar G (2010) Stress wave propagation in functionally graded solids under impact loading. In: Proceedings of the IMPLAST 2010 conference. Rhode Island

Kowalczyk P (2010) Simulation of orthotropic microstructure remodelling of cancellous bone. J Biomech 43:563–569. https://doi.org/10.1016/j.jbiomech.2009.09.045

Lang R, Kaliske M (2013) Description of inhomogeneities in wooden structures: modelling of branches. Wood Sci Technol 47:1051–1070

Ling CB (1948) On the stresses in a plate containing two circular holes. J Appl Phys 19:77–82

Lukacevic M, Füssl J (2014) Numerical simulation tool for wooden boards with a physically based approach to identify structural failure. Eur J Wood Prod 72:497–508

Lukacevic M, Füssl J, Eberhardsteiner J (2015) Discussion of common and new indicating properties for the strength grading of wooden boards. Wood Sci Technol 49:551–576

NASA (1975) Astronautic structures manual, vol 1. George C. Marshall Space Flight Center, Marshall Space Flight Center, Huntsville

Nath S (2013) Stress wave propagation in split Hopkinson pressure bar. Master's thesis, National Institute of Technology Rourkela

Nilsson C (2009) Modelling of dynamically loaded shotcrete. Master's thesis, Royal Institute of Technology, Stockholm. ISSN: 1103-4297

Olsson A, Oscarsson J, Johansson M, Källsner B (2012) Prediction of timber bending strength on basis of bending stiffness and material homogeneity assessed from dynamic excitation. Wood Sci Technol 46(4):667–683

Olsson A, Oscarsson J, Serrano E, Källsner B, Johansson M, Enquist B (2013) Prediction of timber bending strength and in-member cross-sectional stiffness variation on the basis of local wood fibre orientation. Eur J Wood Prod 71(3):319–333

Oscarsson J (2014) Strength grading of structural timber and EWP laminations of Norway spruce-development potentials and industrial applications. Doctoral thesis, Linnaeus University

Phillips GE, Bodig J, Goodman JR (1981) Flow-grain analogy. Wood Sci 14:55–65

Pilkey WD (1997) Peterson's stress concentration factors, 2nd edn. Wiley, New York

Pilkey WD, Pilkey DF (2008) Peterson's stress concentration factors, 3rd edn. Wiley, New York

Rais A, Poschenrieder W, Pretzsch H, van de Kuilen JWG (2014a) Influence of initial plant density on sawn timber properties for Douglas-fir (*Pseudotsuga menziesii* (Mirb.) Franco). Ann For Sci 71:617–626

Rais A, van de Kuilen JWG, Pretzsch H (2014b) Growth reaction patterns of tree height, diameter, and volume of Douglas-fir (*Pseudotsuga menziesii* [Mirb.] Franco) under acute drought stress in Southern Germany. Eur J For Res 133(6):1043–1056. https://doi.org/10.1007/s10342-014-0821-7

Shantharaja M, Sandeep GM (2014) Experimental and numerical analysis of propagation of stress wave in sheet metal. Int J Sci Technol Res 3(10):40–42. ISSN: 2277-8616

Stapel P, van de Kuilen JWG (2013) Effects of grading procedures on the scatter of characteristic values of European grown sawn timber. Mater Struct 46:1587–1598. https://doi.org/10.1617/s11527-012-9999-7

Stapel P, van de Kuilen JWG (2014a) Influence of cross-section and knot assessment on the strength of visually graded Norway spruce. Eur J Wood Prod 72(2):213–227. https://doi.org/10.1007/s00107-013-0771-7

Stapel P, van de Kuilen JWG (2014b) Efficiency of visual strength grading of timber with respect to origin, species, cross section, and grading rules: a critical evaluation of the common standards. Holzforschung 68(2):203–216. https://doi.org/10.1515/hf-2013-0042

Suiker ASJ, Metrikine AV, de Borst R (2001) Comparison of wave propagation characteristics of the Cosserat continuum model and corresponding discrete lattice models. Int J Solids Struct 38:1563–1583

Tabor Z, Rokita E (2007) Quantifying anisotropy of trabecular bone from gray-level images. Bone 40(4):966–972

Verner EA, Becket EB (1973) Finite element stress formulation for wave propagation. Int J Numer Methods Eng 7:441–459

Whitley DW (2013) Interacting stress concentration factors and their effect on fatigue of metallic aerostructures. Doctoral thesis, Missouri University of Science and Technology

Zandbergs JG, Smith FW (1987) Finite elements fracture prediction for wood with knots and cross grain. Wood Fiber Sci 20:97–106

Affiliations

A. Khaloian Sarnaghi[1] · J. W. G. van de Kuilen[1,2,3]

[1]   Department of Wood Technology, Technical University of Munich, Winzererstraße 45, 80797 Munich, Germany

[2]   Faculty of Civil Engineering and Geosciences, Delft University of Technology, Delft, The Netherlands

[3]   CNR-Ivalsa, Florence, Italy

Supplementary Material

Table 1s: Linear and exponential multiple regression analysis for spruce

	SCF 1	SCF 2	SCF 3	MOE 1[*1]	MOE 2[*2]	ρ	TKAR	DEB	DAB	MOE 3[*3]	R² Linear	R² Non-linear
					x						0.53	
				x							0.40	
										x	0.50	
	x	x	x	x							0.62	0.71
	x			x							0.61	0.69
	x	x		x							0.61	0.70
	x	x		x		x					0.71	0.76
	x	x	x	x		x					0.72	0.77
						x				x	0.52	0.49
	x	x	x		x	x					0.73	0.77
f_pred. spruce	x				x	x					0.71	0.75
					x	x					0.56	0.55
						x	x	x	x	x	0.6	0.60
						x					0.25	
							x				0.22	
								x			0.17	
									x		0.23	
	x										0.51	0.59
		x									0.33	0.4
			x								0.39	0.48
							x	x	x		0.31	0.35
	x	x	x								0.52	0.62

[*1] **Dynamic modulus of elasticity based on the average density**

[*2] **Dynamic modulus of elasticity based on the real density**

[*3] **Measured dynamic modulus of elasticity**

Table 2s: Linear and exponential multiple regression analysis for Douglas fir

	SCF 1	SCF 2	SCF 3	MOE 1[*1]	MOE 2[*2]	ρ	TKAR	DEB	DAB	MOE 3[*3]	R^2 Linear	R^2 Non-linear
					x						0.50	
				x							0.28	
										x	0.58	
	x	x	x	x							0.57	0.66
	x			x							0.52	0.58
	x	x		x							0.57	0.66
	x	x		x		x					0.66	0.72
	x	x	x	x		x					0.66	0.72
						x				x	0.63	0.59
f_{pred.}	x	x			x	x					0.67	0.72
douglas	x				x	x					0.64	0.67
fir					x	x					0.51	0.50
						x	x	x	x	x	0.67	0.64
						x					0.11	
							x				0.19	
								x			0.13	
									x		0.22	
	x										0.47	0.54
		x									0.39	0.49
			x								0.36	0.45
							x	x	x		0.27	0.27
	x	x	x								0.55	0.65

[*1] **Dynamic modulus of elasticity based on the average density**

[*2] **Dynamic modulus of elasticity based on the real density**

[*3] **Measured dynamic modulus of elasticity**

Table 3s: Linear and exponential multiple regression analysis for beech

	SCF 1	SCF 2	SCF 3	MOE 1[*1]	MOE 2[*2]	ρ	TKAR	DEB	DAB	MOE 3[*3]	R² Linear	R² Non-linear
					x						0.40	
				x							0.35	
										x	0.50	
	x	x	x	x							0.62	0.59
	x			x							0.55	0.51
	x	x		x							0.61	0.58
	x	x		x		x					0.64	0.61
	x	x	x	x		x					0.64	0.61
						x				x	0.50	0.49
fpred.	x	x			x	x					0.64	0.61
	x				x	x					0.58	0.53
beech					x	x					0.40	0.40
						x		x	x	x	0.52	0.51
						x					0.05	
											0.22	
								x			0.19	
									x		0.18	
	x										0.43	0.47
		x									0.46	0.50
			x								0.34	0.42
								x	x		0.18	0.15
	x	x	x								0.56	0.54

[*1] **Dynamic modulus of elasticity based on the average density**

[*2] **Dynamic modulus of elasticity based on the real density**

[*3] **Measured dynamic modulus of elasticity**

Table 4s: Coefficient of different linear multiple correlation analysis of the simulated parameters for spruce, Douglas fir and beech based on equation 7

	Case	SCF1	SCF2	SCF3	MOE_{dyn1}	MOE_{dyn2}	Density	Constant
		a	b	c	d	e	f	g
$f_{pred,spruce}$	1	-6.2294	-0.0288	-1.5554	0.0022	-	-	16.0581
	2	-7.6943	-	-	0.0023	-	-	14.4130
	3	-6.4373	-1.4847	-	0.0023	-	-	14.9383
	4	-5.4970	-1.5997	-	0.0021	-	0.0507	-7.1880
	5	-4.9625	1.8434	-3.6842	0.0019	-	0.0530	-5.5281
	6	-	-	-	-	0.0034	-0.0428	3.0561
	7	-4.9151	1.9402	-3.6815	-	0.0020	-0.0065	19.8019
	8	-6.7208	-	-	-	0.0021	-0.0135	19.7148
	9	-5.4685	-1.4885	-	-	0.0021	-0.0139	20.5780
	10	-5.7145	-1.4670	-	-	0.0019	-	18.3808
	11	-6.9423	-	-	-	0.0018	-	17.5927
$f_{pred,douglasfir}$	1	-3.6528	-2.3046	-0.3038	0.0013	-	-	19.5719
	2	-4.7647	-	-	0.0019	-	-	8.0921
	3	-3.6614	-2.7106	-	0.0013	-	-	19.2358
	4	-2.8675	-2.1717	-	0.0024	-	0.0680	-32.0906
	5	-2.8496	-1.5070	-0.4954	0.0024	-	0.0683	-31.7932
	6	-	-	-	-	0.0045	-0.0222	-30.1034
	7	-2.8133	-1.4500	-0.4898	-	0.0024	0.0046	-1.7889
	8	-3.6128	-	-	-	0.0029	-0.0038	-7.7438
	9	-2.8324	-2.1081	-	-	0.0024	0.0033	-1.5535
	10	-2.8157	-2.0832	-	-	0.0025	-	-0.9384
	11	-3.6437	-	-	-	0.0028	-	-8.5613
$f_{pred,beech}$	1	-2.9349	-12.2828	0.8054	0.0024	-	-	27.2257
	2	-4.1666	-	-	0.0035	-	-	-1.4057
	3	-2.8944	-11.2678	-	0.0024	-	-	27.6563
	4	-2.6608	-11.2157	-	0.0025	-	0.0567	-18.6575
	5	-2.6989	-12.1652	0.7534	0.0026	-	0.0566	-18.8992
	6	-	-	-	-	0.0054	-0.0228	-28.4682
	7	-2.6913	-12.0168	0.7649	-	0.0026	0.0058	19.6918
	8	-3.8905	-	-	-	0.0037	-0.0123	4.1540

| | 9 | -2.6526 | -11.0531 | - | - | 0.0026 | 0.0063 | 18.5819 |
| | 10 | -2.6568 | -10.9270 | - | - | 0.0027 | - | 22.1212 |
| | 11 | -3.9102 | - | - | - | 0.0035 | - | -3.2400 |

MOE$_{dyn1}$ is the simulated dynamic modulus of elasticity, using the average density in equation 5

MOE$_{dyn2}$ is the simulated dynamic modulus of elasticity, using the actual density in equation 5

Table 5s: Coefficient of different linear multiple correlation analysis of the measured parameters for spruce, Douglas fir and beech based on equation 8

	Case	TKAR	DEB	DAB	MOE$_{dyn}$	Density	Constant
		a	b	c	d	e	f
$f_{pred,spruce}$	1	-18.4359	-21.7498	-3.0950	0.0023	-0.0095	12.8304
	2	-34.4056	-32.8446	-4.9715	-	-	48.8899
	3	-	-	-	0.0033	-0.0387	0.9489
$f_{pred,douglasfir}$	1	-20.0228	-29.5413	10.0295	0.0032	-0.0325	8.4558
	2	-22.5075	-36.1036	-10.6911	-	-	39.9669
	3	-	-	-	0.0038	-0.0598	6.2608
$f_{pred,beech}$	1	-	-18.2578	-0.6857	0.0052	0.0049	-34.6314
	2	-	-43.7953	-11.2540	-	-	43.5367
	3	-	-	-	0.0058	-0.0044	-38.6822

MOE$_{dyn}$ is the measured dynamic modulus of elasticity from the tests
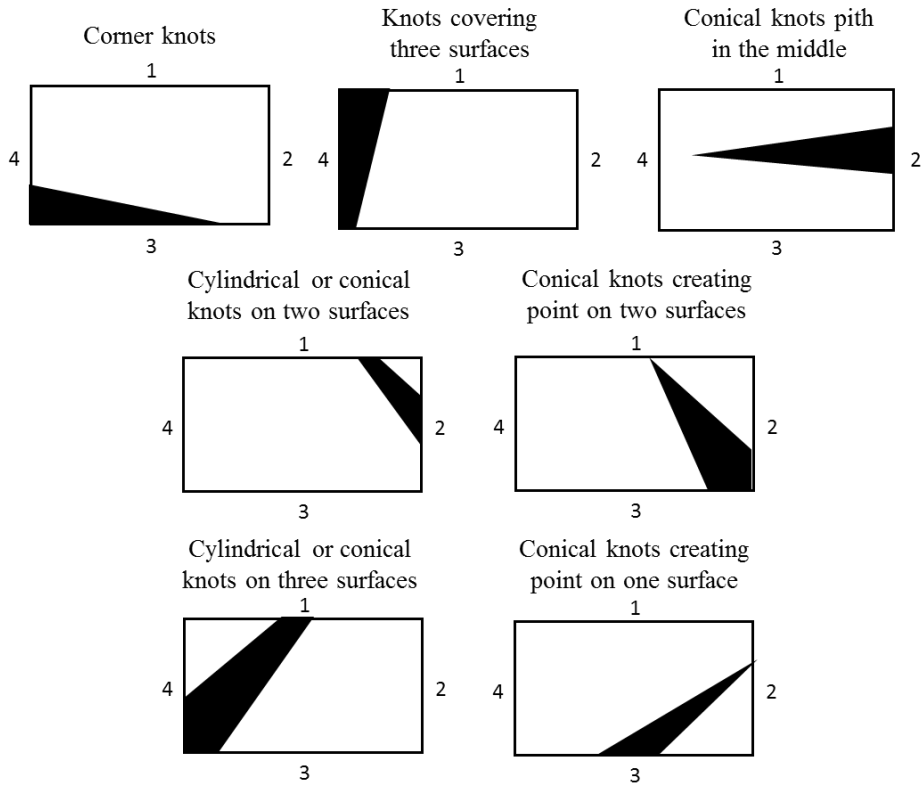
Knot position	Surface number that can be occupied by knot			
Knot on only one surface	1	2	3	4
Knot occupying two surfaces	1,2		1,3	1,4
	2,3			2,4
	3,4			
Knot occupying three surfaces	1,2,3		1,2,4	1,3,4
	2,3,4			
Knot occupying four surfaces	1,2,3,4			

Figure 1s: Knot shapes and configurations summarized in 7 subgroups and 15 surface combination possibilities